

Sander N. Wijnsma

Power-to-Biomethane Process Modelling

Master's thesis in Chemical Engineering

Supervisor: Magne Hillestad

July 2020

NTNU
Norwegian University of Science and Technology
Faculty of Natural Sciences
Department of Chemical Engineering



Norwegian University of
Science and Technology

Sander N. Wijnsma

Power-to-Biomethane Process Modelling

Master's thesis in Chemical Engineering
Supervisor: Magne Hillestad
July 2020

Norwegian University of Science and Technology
Faculty of Natural Sciences
Department of Chemical Engineering



Preface

This thesis was written as the final work for completing the international master's program in Chemical Engineering at the Norwegian University of Science and Technology during the spring of 2020.

I would like to thank supervisor Professor Magne Hillestad and co-supervisors Jacob J. Lamb and Associate Professor Kristian M. Lien for allowing me to work on a topic that is of personal interest and relevant for industry. I am also very grateful towards my supervisors for the feedback, support and guidance provided during my specialisation and master's project as part of the Environmental Engineering and Reactor Technology group. In addition, I would like to thank Sayed E. Hashemi for discussing ideas and to overcome difficulties within HYSYS.

This has been a challenging time for all of us due to the COVID-19 crisis and I am very appreciative that my family, friends and Anita kept on giving me support and motivated me to finish this master's degree the best I can.

Declaration of Compliance:

I declare that this is an independent work according to the exam regulations of the Norwegian University of Science and Technology (NTNU)

Trondheim, Norway

3rd of July, 2020

Summary

In this project the Power-to-Methane process will be designed and evaluated that consists of an alkaline electrolyser, multi-tubular methanation reactor and polyimide membrane. The feed gas CO₂ is modelled in accordance to specifications given from the amine absorber located at the Biokraft plant in Skogn and the product is required to be of liquefaction quality. By applying the Power-to-Methane process the productivity of the plant can be increased while decreasing the CO₂ emissions of the plant.

The process has been designed and evaluated in HYSYS V10. An advanced MATLAB (R2019a) code for the multi-tubular methanation reactor was connected by using a CAPE-OPEN unit operation. Such an advanced way of modelling the methanation reactor was required because of a high runaway temperature from the highly exothermic methanation reaction. As a consequence of this high runaway temperature, the catalyst can be deactivated which is strongly unwanted.

The design work and results are in accordance to similar work in literature. The Power-to-Methane process is rather novel and has become more interesting in industry over the last years. The process becomes more novel in this project since the thought is to include the liquefaction step to produce bio-LNG from the high quality biomethane that is produced.

The results of the model suggest that the Power-to-Methane process is favoured at high operating pressure. However, this results in a higher reaction rate which in turn increases the temperature runaway. To solve this challenge, it is possible to reduce the dilution factor to oppose the reaction rate. This suggests that there must be an optimum point at which the pressure can be maximised while maintaining a stable process.

The alkaline electrolyser for the production of hydrogen has a high investment cost and electrical energy demand. Therefore, it is the main contributor to the cost for the Power-to-Methane process. In fact, the electrical energy demand is found to be so high, that the cost for producing methane are almost as high as the production cost of hydrogen making the process not profitable for now. However, the electricity cost and investment cost electrolyser are expected to decrease in the next years before the plant is expected to be build.

Table of Contents

Preface	i
Summary	iii
1 Introduction	1
1.1 Previous Work	3
1.2 Project Objective	3
1.3 Limitations	4
1.4 Thesis Structure	4
2 Theoretical Background	5
2.1 Hydrogen Production	5
2.2 Electrolysis	6
2.3 Methanation	11
2.4 Gas Purification	19
2.5 Process Equipment	27
3 Design Basis	31
3.1 Battery Limit	31
3.2 Feed Specifications	32
3.3 Product Specifications	33
4 Process Description	35
4.1 Power-to-Methane	35
4.2 Alternative designs	37
5 Process Modelling	39
5.1 Alkaline Electrolyser	39
5.2 Multi-Tubular Methanator	42
5.3 Polyimide Membrane	49
5.4 Design Variables	51

TABLE OF CONTENTS

6	Simulation Results	53
6.1	Main Case Study	53
6.2	Influence of Temperature and Pressure	62
6.3	Influence of Catalyst Dilution Factor	66
6.4	Influence of H ₂ /CO ₂ Ratio	70
7	Cost Estimation	73
7.1	Capital Expenditures (CAPEX)	73
7.2	Operating Expenditures (OPEX)	77
8	Investment Analysis	79
8.1	Profitability Evaluation	79
8.2	Sensitivity Analysis	83
9	Discussion	85
9.1	Kinetics	85
9.2	Simulations	86
9.3	Economics	88
10	Conclusion	89
	Bibliography	91
A	List of Symbols	III
B	HYSYS Flowsheets	VII
C	HYSYS Workbooks	XI
D	Sizing and Costing	XVII
E	Methanation Model	XXVII
F	Operating Manual	LXVII

In the last decade, a strong demand has arisen to increase the share of renewable energy sources in the current energy mix. This energy transition from fossil fuels to renewable energy sources will make the production of electricity more dependent on the availability of wind turbines and solar panels. As a consequence of the intermittent nature of these energy sources, the electricity network will have to endure strong fluctuations over short to long periods of time. To decarbonise the energy sector while balancing the supply and demand and minimising energy losses, an attractive option is to store the surplus electricity. In this way the electricity can be used in periods with a high demand. Several technologies exist for electricity storage that can be classified based on their working principle as mechanical (flywheel, compressed air and pumped hydro - PHES), thermal (latent and sensible heat) and chemical (batteries, power-to-X, superconductors - SMES) [1]. Each of these storage technologies have a specific storage capacity, efficiency and discharge time where they can be applied for, as can be seen in Figure 1.1.

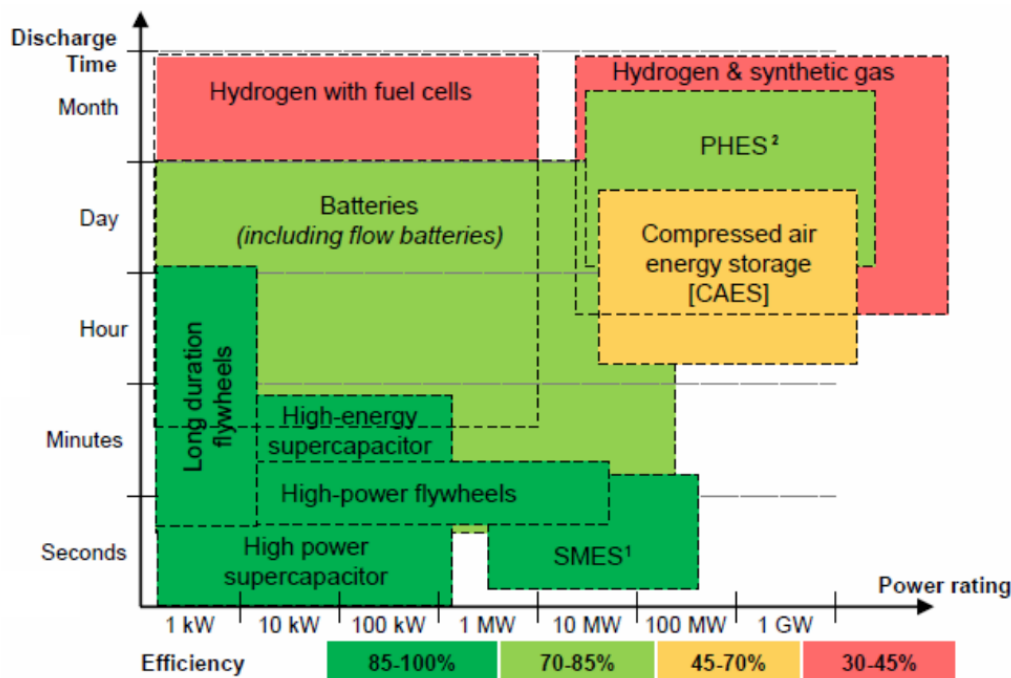


Figure 1.1: Comparing electricity storage technologies based on capacity and discharge time [2]

To store large quantities of electricity over long periods of time it has become more interesting to apply the Power-to-X concept. This concept is rapidly expanding in Europe in the last years [3] and utilises an electrolyser that converts electric energy into chemical energy in the form of hydrogen (H_2) gas. An advantage is that chemicals can be transported over long distances without large losses of energy compared to the transport of electricity. Hydrogen gas can be used as a base chemical in industry, as a transport fuel at high pressure levels or further converted to other chemicals that have a higher energy density such as methane, methanol, ammonia and even kerosene. There are several advantages of converting hydrogen into these higher energy density chemicals. For example, methane can be injected into the existing gas grid (H_2 limits of 0-12 vol%), compressed for CNG cars or liquefied for use in heavy duty transportation. Making it a possibility to make sustainable fuels for busses, trucks, trains, ships and planes [3, 4].

Many projects focus on the production of hydrogen gas (almost 70 %) but an increasing number of projects are initiated to produce methane [3]. Audi E-Gas by HZI EtoGas is one of the larger commercial plants ($325 \text{ Nm}^3 \text{ CH}_4$ per hour) applying the Power-to-Methane concept since 2013. CO_2 is captured from biogas by amine absorption and the H_2 is generated by alkaline electrolysers with a total capacity of 6 MW powered by an offshore wind park in the North sea [1]. More power-to-gas projects can be found in Wulf et al. [3] and Thema et al. [5].

One commercial plant producing this liquefied form of methane is Biokraft. Biokraft AS has built the world's largest production site of liquefied biomethane (LBM) in Skogn, Trondheim. At this location, numerous biomass sources such as fish waste and paper waste from the local Norske Skog newsprint factory are converted into biogas (gas mixture that contains mainly methane - CH_4 and carbon dioxide - CO_2) by an anaerobic digestion process.

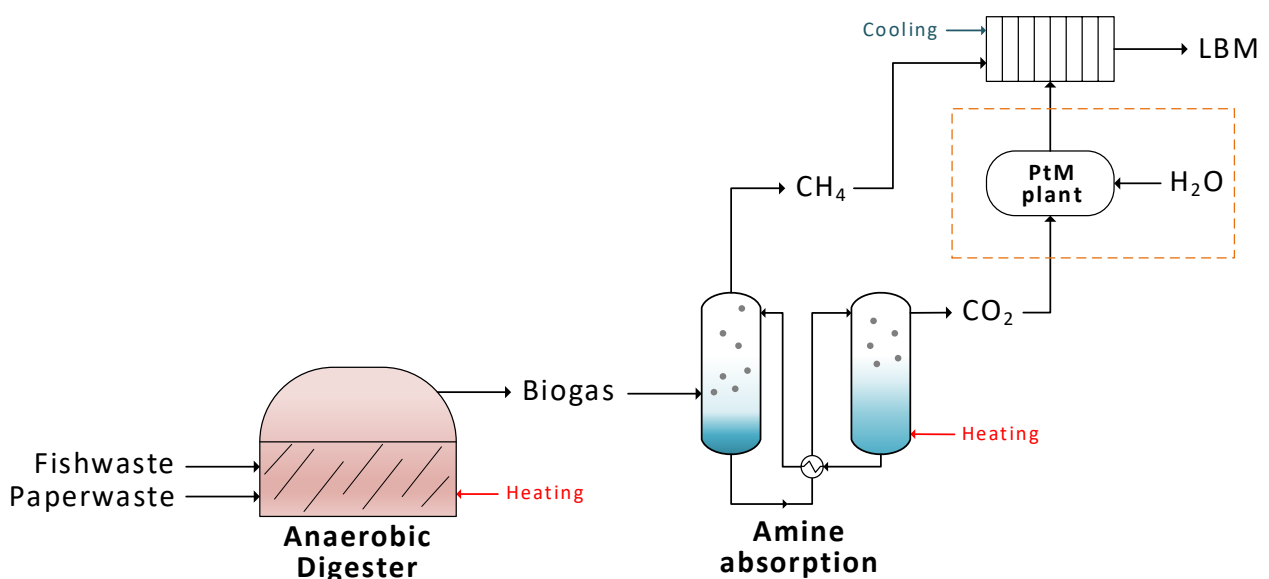


Figure 1.2: Simplified process flow diagram of the Biokraft plant in Skogn.

The biogas is then upgraded in an amine absorption column where an amine solvent chemically binds with the CO_2 in the gas mixture to selectively separate it from the other gasses. After the CO_2 is separated, the amine solvent is regenerated in a desorption column by increasing the temperature to around 120°C . This releases the CO_2 from the amine solvent where after it is emitted as a greenhouse gas to the environment as a flue gas. The now upgraded stream of nearly pure methane, called biomethane, is cooled to around -162°C to liquefy the gas into liquid form as biomethane (LBM). The process flow diagram of the plant is illustrated in Figure 1.2.

An option to reduce the greenhouse gas emission from the plant, balance the electricity network by applying the power-to-gas principle, and increasing the productivity of the plant by producing more biomethane for liquefaction, is presented in this work. This so called Power-to-Methane (PtM) process is shown in Figure 1.2 in the striped, orange square where H_2O and CO_2 are converted into CH_4 by use of energy.

1.1 Previous Work

This master's thesis is a continuation of the specialisation project performed in the autumn semester. Therefore, the theory described in the specialisation is used as a basis for the master's thesis and expanded upon. In the specialisation project the Power-to-Methane process was modelled in HYSYS and studied based on the main equipment being an alkaline electrolyser, equilibrium methanation reactor and a polyimide membrane. Here, the H_2/CO_2 ratio, methanation temperature and methanation pressure were varied while keeping the membrane area constant at a high value. From the results it became clear that the equilibrium model was not sufficient enough for an accurate determination of the outlet composition and temperature profile of the methanation reactor and thus to evaluate the process and cost [6]. Therefore, it was decided to model the process more rigorously.

1.2 Project Objective

The objective of this project is to simulate possible designs for the Power-to-Methane process based on a commercial alkaline electrolyser, a kinetic methanation reactor and a gas separation unit. The gas separation unit is constrained to recover a product that satisfies liquefaction quality requirements and the methanation reactor is limited by a maximum temperature to ensure safe and efficient operation. A techno-economic evaluation of the process will give an indication of the possibilities for integrating this process in a later phase at the bio-LNG plant in Skogn operated by Biokraft.

1.3 Limitations

To structure the project and make clear boundaries several limitations are stated below.

- The electrolyser model is based on commercial energy requirement data from NEL including rectifier/transformer losses for a newly activated electrolyser system.
- A HYSYS unit operation is implemented as membrane model (ChemBrane v7) operated without sweep in counter-current configuration and based on permeance data for similar gas mixtures.
- The methanation reaction is modelled kinetically based on experimental work including mass transfer limitations with averaged diffusion coefficients and a dilution factor to reduce temperature peaks from thermal runaway caused by the exothermic reaction.
- The product specifications are obtained from liquefaction specifications provided by Wärtsilä.
- Case studies are performed for the most important independent variables only.
- The price of biomethane, electricity cost and electrolyser cost is uncertain.

1.4 Thesis Structure

Chapter 2 gives a theoretical background on hydrogen production technologies, electrolysis, methanation, gas purification and other equipment used to model the plant. In **Chapter 3**, the design basis is given. Moreover, the limitations of the modelling and design work, and material specifications are given. After the Power-to-Methane process is described in **Chapter 4** and in **Chapter 5** it is explained how the main unit operations are modelled. **Chapter 6** illustrates and discusses the results obtained from the model and case studies. In **Chapter 7** and **Chapter 8**, an economic analysis is given for the main case study. Finally, the discussion, conclusion and recommendations of the project are stated in **Chapter 9** and **Chapter 10**. The report contains a bibliography and several appendix chapters to support the main report.

A theoretical background is given in this chapter to get an overview of which technologies are available for the power-to-methane process and how these technologies can be characterised. In this chapter the available hydrogen production methods are stated first. Thereafter, the main technologies, being electrolysis, methanation and gas purification, are explained in more detail. Lastly, other process equipment used in the plant is described.

2.1 Hydrogen Production

To convert carbon dioxide from an industrial plant like the Biokraft plant in Skogn it is required to mix hydrogen gas so that the Power-to-Methane process can take place. Nowadays, hydrogen can be produced by converting hydrocarbons, biomass, water and other feedstocks. An overview of the hydrogen production technologies is illustrated in Figure 2.1.

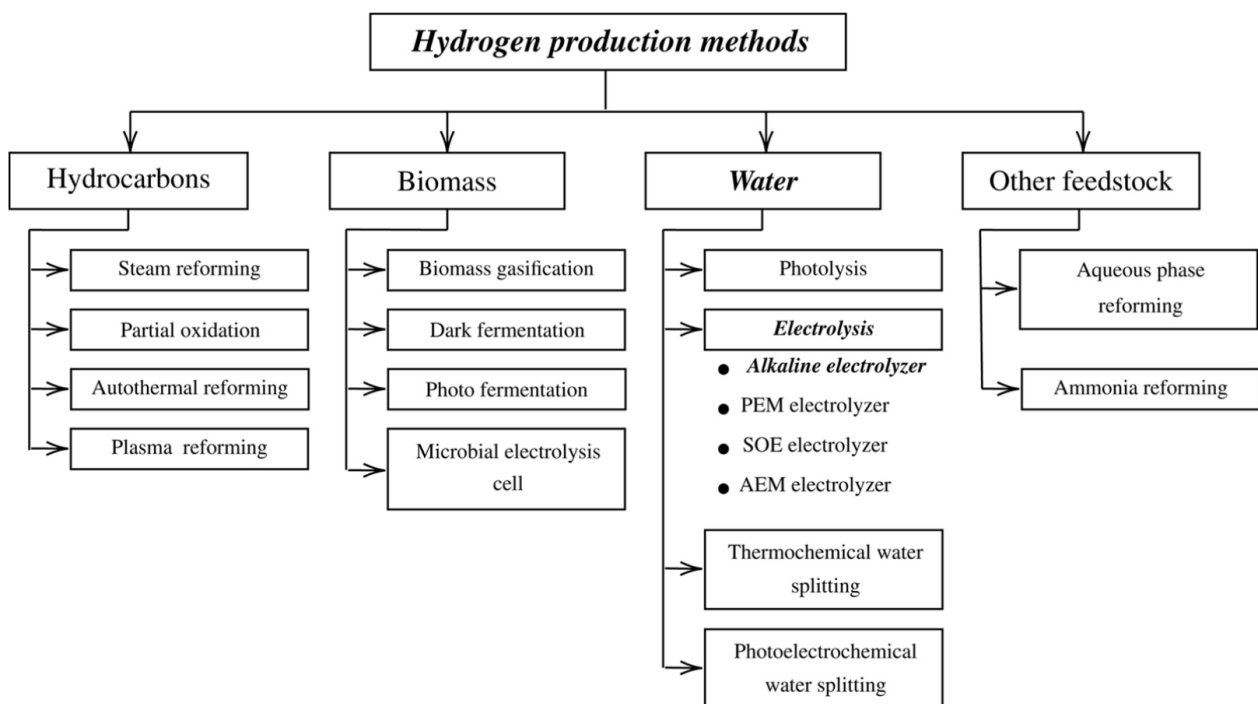


Figure 2.1: Hydrogen production technologies with emphasis on alkaline electrolysis (bold) [2].

Although electrolysis was the first commercial hydrogen production method, 95% of the hydrogen production in industry is based on fossil fuels. The main reason for this is that production from fossil fuels was shown to be cheaper due to the relatively high price of electricity used for electrolysis [2]. However, the cost of electricity is decreasing steadily in the last decade and in some countries, such as Norway, the electricity cost price is relatively low due to production allowance from hydropower.

The production of hydrogen by hydrocarbon based feedstocks including biomass gasification takes place at high temperatures and produces high amounts of CO₂, volatile organic compounds (VOC), nitrogen oxides (NO_x) and other air pollutants. An option to reduce air pollution is to incorporate renewable electricity produced from solar panels, hydropower and wind turbines in electrolysis technologies.

It is important to note that the environmental impact of electrolysis is highly dependent on how the electricity is produced. For example, production of electricity using coal or other fossil fuel sources will make the technique significantly less environmentally friendly [7].

Therefore, the hydrogen produced can be characterised by three colours, being:

- Grey hydrogen, produced by fossil fuels.
- Blue hydrogen, produced by fossil fuels including carbon capture and storage (CCS).
- Green hydrogen, produced by renewable energy sources.

In an ideal case, the hydrogen is produced locally by a renewable energy source to produce green hydrogen or is produced by utilisation of excess electricity from the grid to provide grid balancing.

2.2 Electrolysis

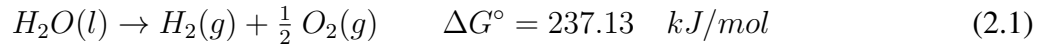
In this section, the fundamentals of electrolysis and the different electrolyser types are highlighted.

2.2.1 Fundamentals of Electrolysis

An electrolyser cell consist of an electrolyte, gas separator and electrodes (called the anode and cathode). When an electric current is applied to the cell, the electrons start to flow towards the cathode, making it negatively charged. The electrodes are immersed in an electrolyte which carries the charge as either OH⁻, H₃O⁺ or O²⁻ towards the positively charged anode to close the electron cycle. Because the charge carrying ion is selectively transported through the gas separator, oxygen is produced at the anode and hydrogen is produced at the cathode [4].

The main characteristic of electrolysis is electricity. When acquired from the electricity grid or directly from an intermittent energy source like wind, it has to be converted from AC to DC before electrolysis can take place. In addition, the water supplied to the electrolysis cell has to be purified in an ion exchanger to achieve the high purity requirements. Once both are supplied to the electrolyser,

the pure water is split into hydrogen and oxygen molecules [1] according to Equation 2.1.



From the Gibbs free energy at 25 °C (ΔG°) it is seen that the reaction is endothermic, meaning that energy has to be applied. Furthermore, according to Le Chatelier's principle, increasing temperatures positively influence the conversion whereas increasing pressures decrease the conversion of water [4].

Because electrolysis does not take place at standard conditions it is required to find ΔG (at specified conditions) from ΔG° . Nernst law can be applied to do this and is derived below.

$$\Delta G = \Delta G^\circ + RT \ln(K_{eq}) \quad \text{with} \quad \Delta G = -zFE \quad \text{and} \quad K_{eq} = \frac{p_{H_2O}}{p_{H_2} p_{O_2}^{1/2}} \quad (2.2)$$

where, R is the gas constant, K_{eq} is the equilibrium constant and P_i are the partial pressures for the components. Substitution and applying Dalton's law gives the total reversible cell voltage (E_{rev}).

$$E_{rev} = \frac{-\Delta G^\circ}{zF} - \frac{RT}{zF} \ln \left(\frac{y_{H_2O}}{y_{H_2} y_{O_2}^{1/2}} \frac{p_{tot}^{-1/2}}{p_{STD}} \right) \quad (2.3)$$

where y_i are the component molar fractions and p_{tot} and p_{STD} are the total- and standard pressures, respectively. At 25 °C, Equation 2.3 solves to find that the reversible cell voltage is 1.23 V; however, this is the minimum energy required to decomposition water and in practice this is never achieved as there is an overpotential that must be applied to overcome inefficiencies of the electrolysis system [8].

The actual cell voltage can be determined by adding all overpotential contributing factors.

$$E_{cell} = E_{rev} + \eta_{anode} + \eta_{cathode} + I \cdot R_{cell} \quad (2.4)$$

where, η_{anode} is the anode overpotential, $\eta_{cathode}$ is the cathode overpotential, I is the current and R_{cell} is the cell resistance that consist of resistances due to the circuit, electrolyte, bubbles and membrane. I and R_{cell} are referred to as ohmic losses [8].

Figure 2.2 shows the contributions in a typical plot used for electrolysis where the cell voltage is given for a specified current density. Here, the current density gives an indication of the production of hydrogen which is dependent on the DC-current into the cell and the number of cells in the cell, while the cell voltage gives an indication of the energy requirement to produce a specified amount of hydrogen.

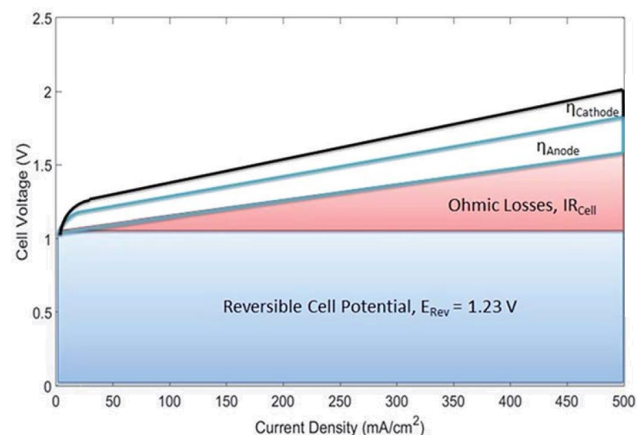


Figure 2.2: Contributions to actual cell voltage [8].

The voltage efficiency of the electrolyser cell is the ratio of the reversible and actual cell voltage [8].

$$\eta_{cell} = \frac{E_{rev}}{E_{cell}} = \frac{1.23V}{E_{cell}} \quad (2.5)$$

In Equation 2.5 the voltage efficiency is given on basis of the lower heating value (LHV - for water as a vapour product) but realistically seen the higher heating value (HHV - for water as a liquid product) would be more accurate (1.48V) for water electrolysis. These voltages are required for an electrolyser operating at 25°C without producing excess heat. In practice, it is more interesting to determine the overall efficiency based on the energy content of hydrogen produced and the energy (both electric and thermal) consumed by the electrolyser to produce that hydrogen.

$$\eta_{overall} = \frac{\text{Energy content of hydrogen}}{\text{Electric + thermal energy consumed}} = \frac{\text{HHV of } H_2}{E_{system}} \quad (2.6)$$

The higher heating value of hydrogen is often presented in units relating to the amount of hydrogen produced as 39.4 kWh/kg H₂ or 3.54 kWh/Nm³ H₂ since the energy consumption is usually given by suppliers in these units.

2.2.2 Electrolyser Types

Electrolysers can be categorised in two technology types. The first type is water electrolysis, which uses a liquid water feed below 100 °C to produce hydrogen. This type of electrolyser is commercially available and are called alkaline electrolysis (AE) and polymer electrolyte membrane electrolysis (PEME). The second type is steam electrolysis that uses steam up to 1000 °C to increase the electrical efficiency of the system and is called solid-oxide electrolysis (SOE). Although this electrolyser type has gained interests by industry in the last years, it is still in development [7]. The electrolysis technologies and their working principles are illustrated in Figure 2.3.

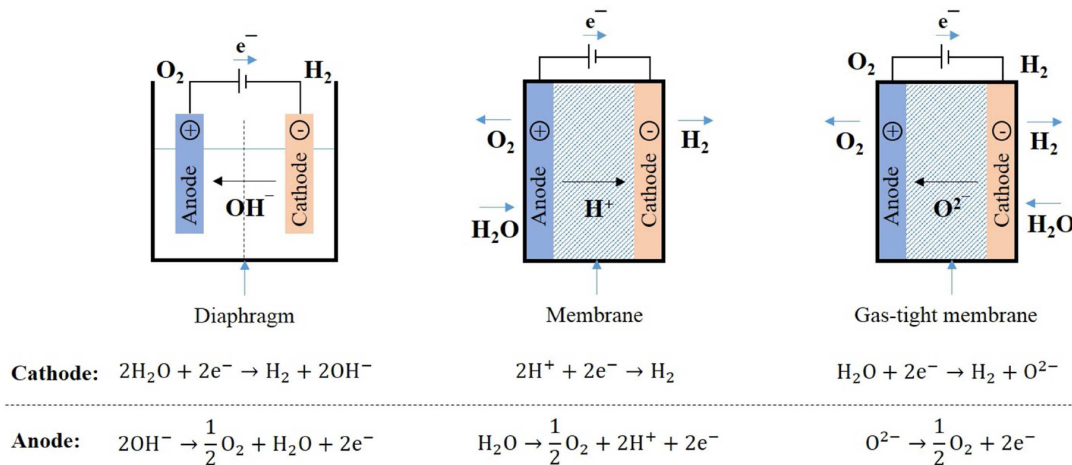


Figure 2.3: Principles of AE, PEME and SOE electrolysis technologies (from left) [7].

Alkaline electrolyzers are mature, have a high reliability and relatively low cost. However, according to Figure 2.4, the overall energy efficiency is much lower compared to PEME and SOE. In addition, the PEME can produce much larger amounts of hydrogen per amount of energy input [9].

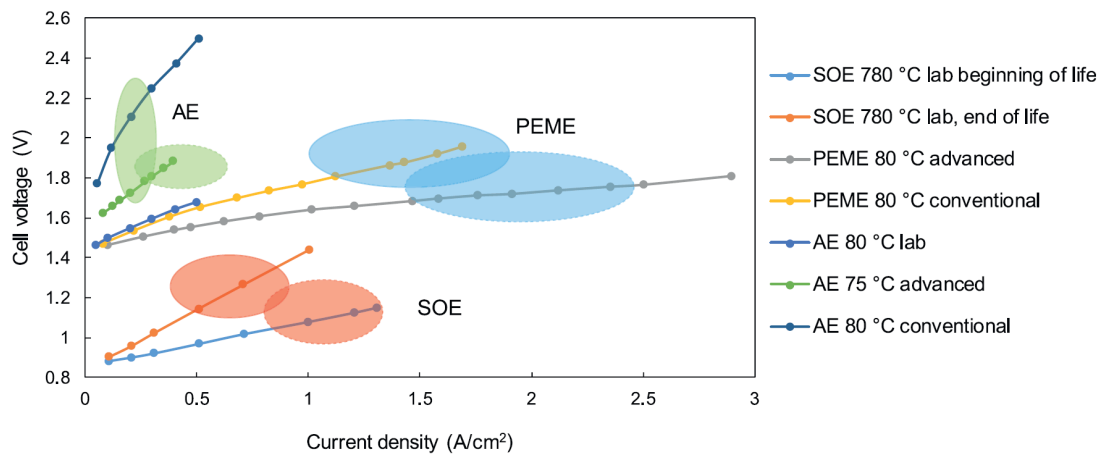


Figure 2.4: Comparison of electrolyser types with current and future operational conditions [9].

The reason for the higher production is that the PEME can operate at much higher current densities without large ohmic losses from gas evolution compared to the AE due to its zero-gap configuration (SOE also has this configuration as can be seen from the marked area between the electrodes in Figure 2.3). This configuration ensures that the gas bubbles produced close to the electrodes are transported from the electrodes on the opposite site as where the ion transport is taking place. This makes the ion transport not interfered with the gas evolution at the electrode [8].

Other important advantages of PEME for Power-to-Methane are the high flexibility and fast dynamic response which is critical for integrating renewable energy sources that are intermittent. However, the PEME consists of an acidic membrane making it a requirement to use noble metals for the electrodes to provide the necessary lifetime and activity. Platinum is most commonly used as active cathode catalyst and iridium oxide is most commonly used as the active anode catalyst. This makes the investment cost much higher compared to AE [1, 9]. Due to the greater durability of materials, higher chemical stability electrolyte and ease of interchangeable electrolyte it seems more suitable to apply AE for large-scale industrial water electrolysis [2].

One way to reduce the impact of gas bubbles is to increase the operational pressure of the electrolyser to reduce the gas fraction in the electrolyte. Alternatively, it is possible to configure the AE in the zero-gap configuration where the cathode and anode are placed near the diaphragm. When these two techniques are applied to AE, it is possible to significantly increase the current densities [8].

Solid-oxide electrolysis is the most recently developed technology. SOE has gained attention in recent years to be applied for Power-to-Methane processes because of the high electrical efficiency as well as the potential to heat integrate a strongly exothermic process such as methanation. Another advantage

of the SOE is the possibility to simultaneously split steam and CO₂ (called co-electrolysis) to produce syngas, containing mainly CO and H₂, which can also be converted in a methanator [9].

Although coupling with exothermic industrial processes can favour the SOE technique, the level of heat required is difficult to reach. The investment cost of SOE cells are currently also relatively high but is expected to go down in the future due to production scale up [9].

To get an overview of the key parameters for the different electrolyser types and summarise the advantages and disadvantages, a table has been illustrated below (Table 2.1).

Table 2.1: Summary of key operational parameters of AE, PEM and SOE [1, 2, 4, 9, 10]

Property	Alkaline electrolysis	PEM electrolysis	Solid-oxide electrolysis
Maturity	Mature	Commercial	Development
Electrolyte	25-30 wt% KOH	Polymer membrane	Solid-oxide (ZrO ₂ with Y ₂ O ₃)
Charge carrier	OH ⁻	H ₃ O ⁺	O ²⁻
Temperature [°C]	60-90	50-80	650-900
Pressure [bar]	< 30	< 100	1 (higher in future)
Voltage [V]	1.8-2.4	1.6-2.1	0.95-1.3
Efficiency [%]	62-82	67-82	> 80
Specific energy consumption [kWh/Nm ³ H ₂]	3.8-4.8	4.4-5.0	2.5-3.5
Current density [A cm ⁻²]	< 0.4	1.0-2.5	0.3-1.3
Cold start-up time	minutes-hours	seconds-minutes	hours
Eff. degradation [%/year]	0.25-1.5	0.5-2.5	N/A
System lifetime [year]	20-30	10-20	N/A
cell lifetime [year]	6-14	6-12	N/A
Transient operation	Min. 10-40% of load	Dynamic operation	Not well suited
Advantages	Mature technology	Dynamic operation	High system efficiency
	High reliability/robustness	High current density	Co-electrolysis possibility
	Low cost and long lifetime	Fast startup time	Heat integration possibility
Disadvantages	Low current density	Expensive materials	High investment cost
	High maintenance cost	Lower lifetime	High heating demand
	Large cell area		

* N/A, Not Available, means that no accurate enough value was not found in literature.

2.3 Methanation

Methanation is a process where hydrogen, in this case produced by electrolysis, is converted together with carbon dioxide as a carbon source to increase the energy density of hydrogen and reduce the CO₂ footprint. Methanation can either be carried out in a biological (biomethanation) or chemical (catalytic methanation) pathway. Both pathways can produce methane according to $\text{CO}_2 + 4 \text{H}_2 \leftrightarrow \text{CH}_4 + 2 \text{H}_2\text{O}$ but the main differences between the two are the catalyst type and employed operational conditions. In biomethanation the catalyst consists of methanogenic archaea that anaerobically metabolise CO₂ and H₂ at ambient conditions to produce CH₄ and energy to survive. On the other hand, the catalyst of catalytic methanation consists of metal particles that produce CH₄ at operational conditions between 200 to 550 °C and 1 to 40 bar. Catalytic methanation leads to higher efficiencies compared to biomethanation and, because of the operational conditions, a possibility arises to produce high pressure/temperature steam [4]. The rest of this section will be limited to the discussion of catalytic methanation since it was chosen to model the PtM process with this methanation pathway.

2.3.1 Thermodynamics

The reactions that can occur in catalytic methanation are dependent on the catalyst material and operational conditions of the system. Several side reactions can take place. The main reactions are specified in Table 2.2, where the independent reactions can be specified as the CO₂ methanation reaction (R1), CO methanation reaction (R2), the Boudouard reaction (R4) and the higher hydrocarbons reaction (R9-R10). The other reactions can be described as a linear combination [11].

Table 2.2: Main chemical reactions involved in catalytic methanation [11].

Nr.	Reaction formula	ΔH° [kJ mol ⁻¹]	ΔG° [kJ mol ⁻¹]	Reaction name
R1	$\text{CO}_2 + 4 \text{H}_2 \rightleftharpoons \text{CH}_4 + 2 \text{H}_2\text{O}$	-165.0	-113.2	CO ₂ methanation
R2	$\text{CO} + 3 \text{H}_2 \rightleftharpoons \text{CH}_4 + \text{H}_2\text{O}$	-206.1	-141.8	CO methanation
R3	$\text{CO}_2 + \text{H}_2 \rightleftharpoons \text{CO} + \text{H}_2\text{O}$	41.2	28.6	Reverse water-gas shift
R4	$2 \text{CO} \rightleftharpoons \text{C} + \text{CO}_2$	-172.4	-119.7	Boudouard reaction
R5	$2 \text{CO} + 2 \text{H}_2 \rightleftharpoons \text{CH}_4 + \text{CO}_2$	-247.3	-170.4	Rev. methane reforming
R6	$\text{CH}_4 \rightleftharpoons 2 \text{H}_2 + \text{C}$	74.8	50.7	Methane cracking
R7	$\text{CO} + \text{H}_2 \rightleftharpoons \text{C} + \text{H}_2\text{O}$	-131.3	-91.1	CO reduction
R8	$\text{CO}_2 + 2 \text{H}_2 \rightleftharpoons \text{C} + 2 \text{H}_2\text{O}$	-90.1	-62.5	CO ₂ reduction
R9	$n \text{CO} + (2n + 1) \text{H}_2 \rightleftharpoons \text{C}_n\text{H}_{2n+2} + n \text{H}_2\text{O}$	-	-	Higher hydrocarbons
R10	$n \text{CO} + 2 n \text{H}_2 \rightleftharpoons \text{C}_n\text{H}_{2n} + n \text{H}_2\text{O}$	-	-	

The Gibbs free energy for each methanation reaction can be calculated as

$$\Delta G = \Delta G^\circ + RT \ln(Q) \quad (2.7)$$

where, ΔG is the Gibbs free energy, ΔG° is the standard Gibbs free energy (see Table 2.2), R is the gas constant, T is the temperature and Q is the reaction quotient. As the reaction reaches equilibrium, ΔG becomes zero and Q can be exchanged for the equilibrium constant K_{eq} [12].

$$\ln(K_{eq}) = \frac{-\Delta G^\circ}{RT} \quad (2.8)$$

From the negative standard Gibbs free energy (ΔG°) and change in moles in Table 2.2 it can be seen that the main methanation reactions favour a low temperature (exothermic) and elevated pressures (negative mole change), as described by Le Chatelier's principle. To illustrate the behaviour of the methanation reactions from Table 2.2, the equilibrium constant as a function of the temperature is illustrated in Figure 2.5 taking into account the limited methanation operational range of 200-550 °C, marked in grey.

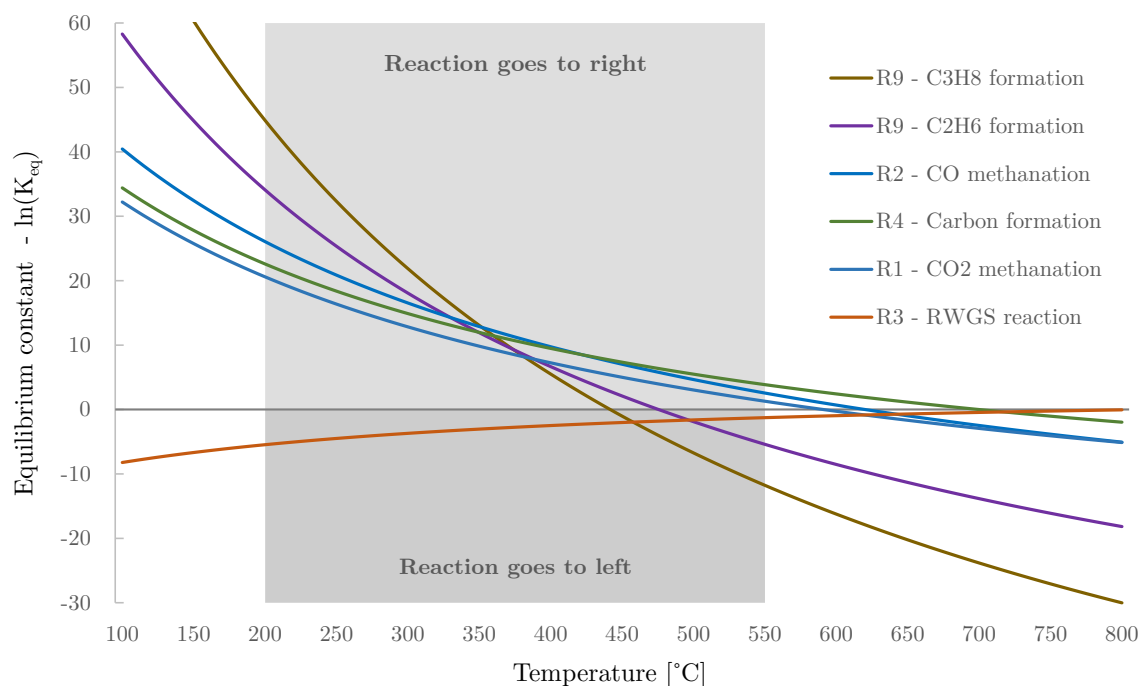


Figure 2.5: Equilibrium constant of methanation reactions as a function of temperature [11].

Figure 2.5 illustrates that the reaction equilibrium is shifted towards the reactants (shifted to the left side of the reaction) when $\ln(K_{eq}) < 0$. Alternatively, an $\ln(K_{eq}) > 0$ shifts the reaction equilibrium towards the products (shifted to the right side of the reaction). As can be seen, the formation of methane from the CO₂ methanation reaction (R1) and CO methanation (R2) is favoured by a positive equilibrium constant until around 600 °C. CO₂ is converted to CO by the reverse water-gas shift reaction (R3) above around 800 °C, meaning that below this temperature the contribution of CO₂

methanation to the formation of methane is larger than CO methanation due to CO₂ being the main carbon oxide present. In addition, CO is consumed by reactions R2, R3, R4, R5 which results in a nearly complete conversion of CO at relatively low temperatures. In contrast, CO₂ is more difficult to completely convert because reactions R3, R4, R5 produce it at decreasing temperatures. Coke formation is mainly caused by the boudouard reaction (R4) because of the high equilibrium constant value compared to the other coke forming reactions (R6, R7, R8) and occurs when the temperature is higher than 450 °C. According the profiles of the equilibrium constants, coke formation by the Boudouard reaction (R4) and formation of higher hydrocarbons (R9) is increasingly present when the temperature decreases [11].

The behaviour of the CO₂ methanation reaction (R1) at equilibrium as a function of temperature is indicated in Figure 2.6 (modelled by a simple equilibrium reactor in HYSYS during specialisation).

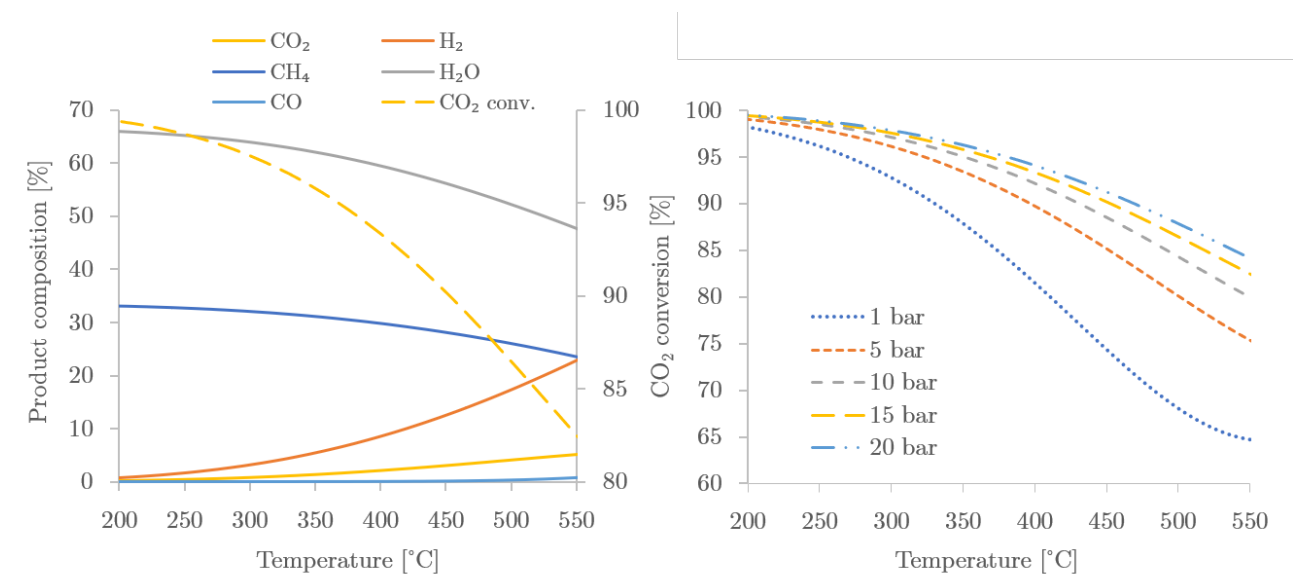


Figure 2.6: Equilibrium composition and CO₂ conversion at 15 bar (on left) and CO₂ conversion for pressure levels as a function of methanation temperature (on right) with 80 mol% H₂ and 20 mol% CO₂ initially [6].

Figure 2.6 illustrates that decreasing temperatures and increasing pressures influences the methanation reaction positively, as expected. It can be noted that the formation of CO is minimal but present at higher temperatures. Giving an indication that the one or multiple reactions in methanation (Table 2.2) produces CO. The equilibrium compositions illustrated are the maximum obtainable concentrations for the conditions (important for kinetic modelling).

The figure above is for a stoichiometric H₂/CO₂ ratio (4.0). In practice this is usually not done because of challenges in controlling the ratio and in some cases the ratio is increased/decreased to create a limiting component to minimise the concentration of that component in the product gas. In the case that the H₂/CO₂ ratio at the inlet of the reactor is lower than stoichiometric (4.0) carbon is expected to be present in the product gas mixture while a higher ratio suppresses the formation of carbon but leaves valuable hydrogen in the product stream [13].

2.3.2 Reactor Concepts

Since the methanation reaction is highly exothermic, thermal management is a key performance parameter in choosing a reactor concept to ensure high conversion of the reactants to methane. Better control of the temperature will result in a better conversion and safe operation of the system. The exothermic reaction is characterised by thermal runaway or hotspots. In these hotspots, the temperature increases rapidly because of the coherence between the reaction rate and temperature which can deactivate the catalyst if the limiting temperature is exceeded. To establish a good temperature control, different types of reactors have been developed namely fixed-bed, fluidised-bed, slurry reactors and structured reactors [4].

Most commercial of all the methanation reactor types are the multi-tubular fixed-bed reactor (sometimes called isothermal fixed-bed reactor) and the adiabatic fixed-bed reactor [1]. The main difference between the two reactor types is the cooling method applied. The first mentioned reactor type consists of a tube bundle with on the one side a cooling medium and on the other side the gas mixture while the other does not have a heat sink and is cooled externally from the reactor (intercooling).

The two reactor types are illustrated in Figure 2.7.

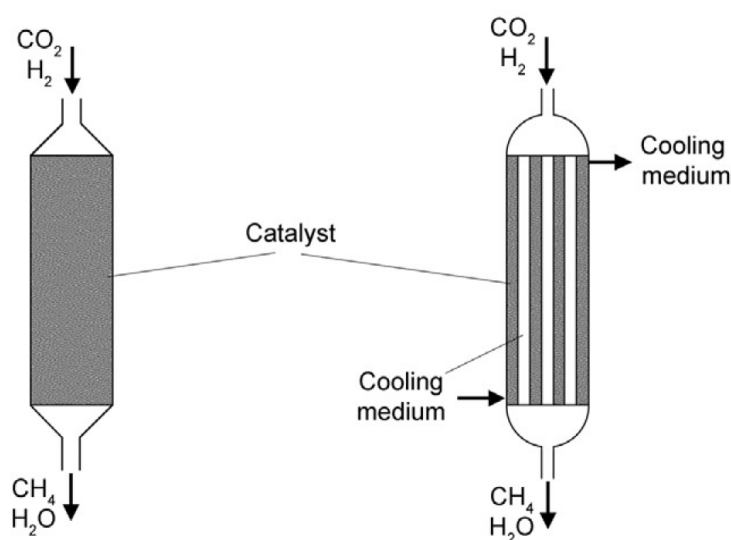


Figure 2.7: Commercial methanation reactor types, left: adiabatic, right: isothermal [1].

In an adiabatic methanation reactor, the temperature runaway often higher compared to the multi-tubular methanation reactor. This makes the conversion of CO_2 limited to around 40% in order to not reach a deactivation temperature of the catalyst. Therefore, the adiabatic reactor requires multiple stages with intercooling and a recycle loop (typically 2-5 stages). The disadvantages of this reactor type are the insufficient temperature control, high pressure drops and poor load flexibility [1].

The tubes of the multi-tubular methanation reactor are filled with catalyst particles on which the reaction takes place. Because of the coolant on the other side of the tubes, it is possible to control

the temperature runaway in a much better way. Typical coolants used in industry are water, molten salt or thermal oil. More efficient heat management of the multi-tubular methanator results in the requirement of only one reactor to reach the necessary conversion. However, this reactor type is more expensive in capital expenditures compared to the adiabatic methanation reactor[1].

Aside of the reactor type, it is possible to reduce the temperature runaway in several other ways. For example, it is possible to have a gas recirculating loop so that the concentration of inert (inert to the reaction) gasses is increased which increases the cold feed to the reactor inlet. Or it is possible to inject feed gas in stages from the side of the reactor so that not all the reaction takes place at once. Another interesting strategy is to dilute the catalyst by either dilution of the catalyst surface itself (less active material) or dilution of the bulk catalyst with inert particles made from for example SiC [14].

An advantage of the highly exothermic reaction is that high amounts of heat are produced at a relatively high temperature levels. This opens the possibility to create high temperature/pressure steam as a byproduct that can be used for heat integration with the process itself, other equipment already present at the location or a start-up of a new process with a high heat demand.

2.3.3 Catalyst

Although the methanation reactions are thermodynamically favourable (exothermic reactions), a catalyst is required to overcome the high kinetic barrier for reducing CO₂ (fully oxidised carbon = +4) to CH₄ (fully reduced carbon = -4). Thus an effective and efficient catalyst is needed to overcome the eight-electron process, obtain an appropriate reaction rate and high selectivity towards CH₄ [1, 13].

The active compounds for a methanation catalyst are mainly based on groups 8 to 10 of the periodic table and can be categorised related to their activity and selectivity as: [15]

Activity: Ru > Fe > Ni > Co > Mo

Selectivity: Ni > Co > Fe > Ru

Ruthenium (Re) is the most active metal for methanation, while Nickel (Ni) is the most commonly applied active metal for methanation in industry because it is the most selective, has a relatively high activity, good sulphur tolerance and a comparatively low price [15].

Often it is required to increase the surface area of the active metal so that more active sites are available to selectively convert CO₂ by the methanation reaction. To increase the surface area, a support like Al₂O₃, SiO₂ or TiO₂ is chosen. Most commonly Al₂O₃ in γ -modification is used commercially [15]. However, the main disadvantage of using Al₂O₃ as a support is sintering in presence of water (product in methanation) at high temperatures [11].

In addition, the catalyst must be able to withstand broad temperature ranges to avoid deactivation of

the catalyst [4], as stated before. The steeper the temperature change, the more catalyst is deactivated [13]. The thermal deactivation temperature is dependent on the catalyst, but in general, no volume element in the methanation reactor should exceed a temperature of 550 °C. Note that some speciality methanation catalysts are available on the market for operation between 600-700 °C [15, 14]. To withstand broad temperature ranges, the catalyst is in some cases promoted with for example MgO [15]. Other deactivating mechanisms are given in Table 2.3.

Generally speaking the choice of the catalyst its active material, support and promoter is dependent on the operational conditions of the system, presence of contamination in the feed, the required selectivity/activity of the catalyst and the price of the catalyst. Nevertheless, it has been revealed that a nickel based catalyst with alumina as support gave the most efficient catalytic systems [13].

Table 2.3: Catalyst deactivation mechanisms relevant for methanation [15, 14]

Type	Mechanism	Reversible	Description
Chemical	Poisoning	Sometimes	Chemisorption of species on active sites of catalyst - mainly caused by sulphur (H ₂ S, thiophenes)
	Vapor/solid reaction	Sometimes	Reaction of fluid/support/promoter with catalyst - mainly forms Ni(CO) ₄ at T < 230 °C
Thermal	Sintering	No	Thermal induced loss of catalytic surface area - mainly at T > 550°C (adiabatic reactors)
Mechanical	Fouling	Mostly	Blockage of active sites/pores by deposition of species - carbon deposition (Boudouard) or higher hydrocarbons
	Attrition/crushing	No	Loss of catalytic material due to abrasion or stresses - Start-up/shut-down, pressure fluctuations, fluidised bed

2.3.4 Reaction Mechanism and Kinetics

In general, the reaction mechanism for CO₂ methanation can be divided into an associative and dissociative scheme, as illustrated in Figure 2.8. The general difference seems to be that in some cases CO is present and reacting with the RWGS reaction, CO methanation reaction or an intermediate step while in others CO₂ is the main carbon component. The exact mechanism for methanation is still under debate [13].

In the CO₂ associative scheme, carbon dioxide adsorbs as a carbonate (CO_{3ad}) on the metal/oxide surface and gets hydrogenated in multiple steps to form methane while for the CO₂ dissociative scheme carbon dioxide adsorbs on the active site or metal/oxide surface as (CO_{2ad}) and can then be divided into an associative and dissociative scheme as well. In the CO associative scheme, the CO group reacts with hydrogen atoms to form intermediates such as formyl, carbonhydroxyl (COH_{ad}) and CHOH_{ad} which are subsequently reduced to C_{ad} groups that are hydrogenated to methane. For the CO dissociative scheme, the C-O bond is broken directly at an active site to form C_{ad} which is hydrogenated to methane in a similar way [13].

As discussed in Section 2.3.3, the catalyst type, and thus the activity and selectivity for CO₂ methanation differs (active metal/support/promoter type and metal content). Hence, the reaction mechanism is most likely linked to the catalyst type, making the reaction mechanism specific for each different methanation catalyst employed. For this reason, it is important to determine the reaction mechanism together with the kinetics in an experimental/pilot setup for the specific catalyst employed to accurately determine a rate expression for modelling the process [13].

Several reaction rate equations have been developed by Koschany [16] for their NiAl based CO₂ methanation catalyst. The reaction rate expressions are based on the power law with or without an adsorption term and on a Langmuir-Hinselwood-Hougen-Watson (LHHV) isotherm basis. The general form of these expressions is given in Equation 2.9.

$$\text{Power law: } r = k \prod_{i=1}^{i=1} c_i^{\alpha_i} \quad \text{and} \quad \text{LHHV: } r = \frac{k \prod_{i=1}^{i=1} c_i^{\alpha_i}}{(1 + \sum_i K_i c_i)^{\alpha_i}} \quad (2.9)$$

Where, r is the reaction rate, k is the rate constant, c is the concentration (sometimes pressure based), a is the activity and K is the adsorption constant. Because of the higher complexity of the LHHV reaction rate expression from taking the adsorption terms into account, the fit of the kinetic experiments is usually better.

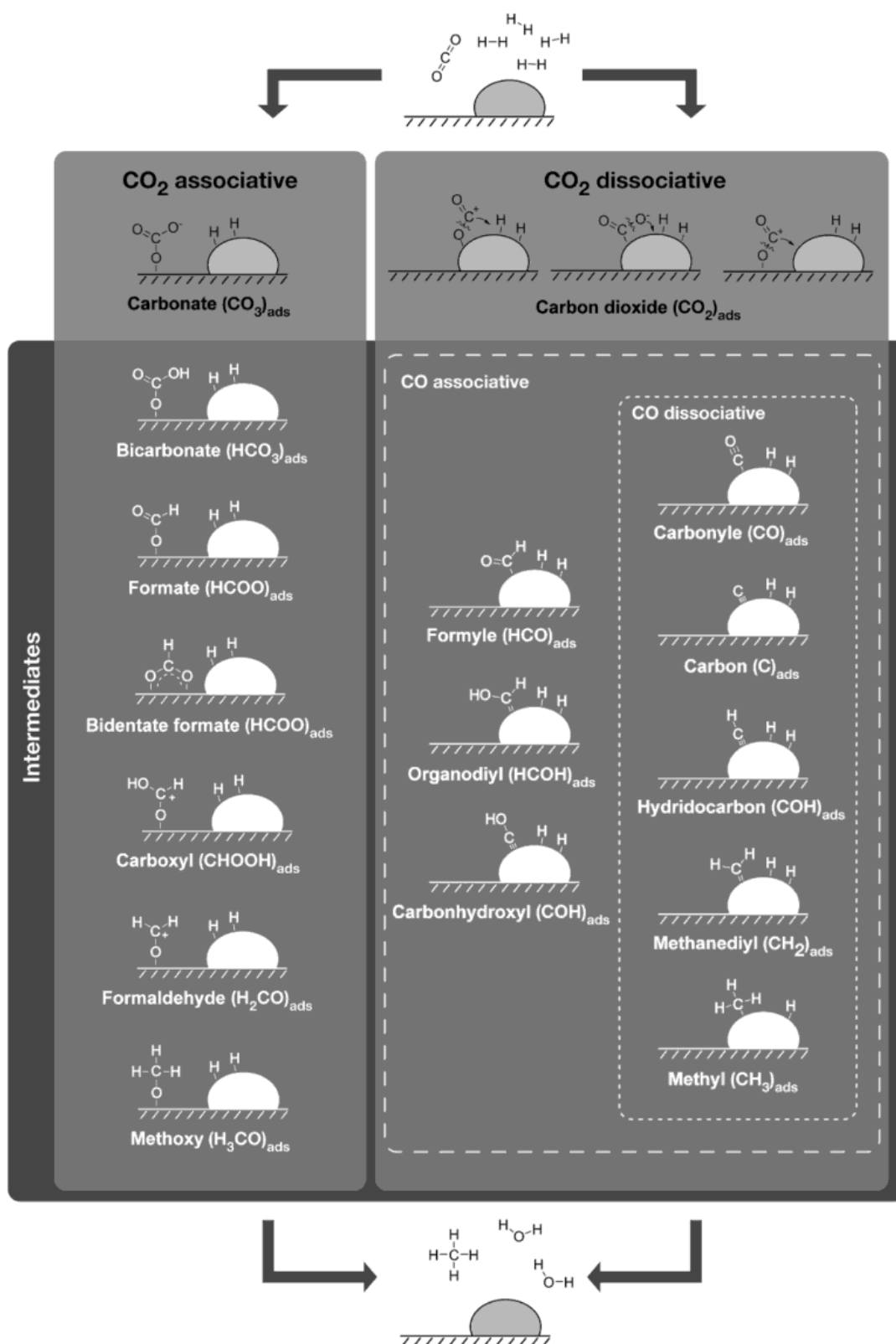


Figure 2.8: Methanation reaction mechanism according to associative and dissociative schemes [13].

2.4 Gas Purification

The gas mixture from the methanation reactor consists mainly of the methanation reaction products methane and water vapour. Additionally, part of the reactants (CO_2 and H_2) will be present since the conversion is not 100% due to thermodynamic equilibrium and will be even lower in the case that a kinetic model of the methanation process is considered. Furthermore, small quantities of other gasses such as nitrogen can be present. The water vapour can be separated from the gas mixture in a knock-out vessel but other gasses present must be separated using a different kind of gas purification method to reach the liquefaction quality requirement. The three major separation technologies discussed in this section are adsorption, membranes and cryogenic distillation.

2.4.1 Adsorption

Separation of gas mixtures is commonly performed by applying adsorption techniques due to simplicity, low operating costs and the allowance for high gas purity or high recovery of contaminants [17, 18].

Gas separation by adsorption is based on the difference in interaction strength between each component in the gas mixture and a porous solid called an adsorbent. The interaction strength between the gas molecule and the adsorbent depends on the adsorbent material (e.g. activated carbon and zeolites), partial pressure of the gas components in the gas mixture and operational temperature/pressure [18] and is roughly categorised in Figure 2.9. In the case that one component is more strongly adsorbed, then it accumulates on the adsorbent while the other components remain in the gas mixture. Eventually, the adsorbent bed becomes saturated with adsorbed gas components and a so called 'breakthrough' will take place where the product gas starts to become contaminated. At that moment, the adsorbent bed needs to be regenerated [17].

The adsorbent bed can be regenerated by either reducing the pressure (known as pressure swing adsorption - PSA) or increasing the temperature (known as temperature swing adsorption - TSA). Alternatively, it is possible to integrate a vacuum pump in the system to reduce the pressure even further (known as vacuum swing adsorption - VPSA). However, for most commercial separation systems PSA is applied as the adsorption technique. The main reason for this is that TSA has the disadvantage that heating and cooling of the columns is more time consuming compared to the (de-)pressurisation of PSA systems. The PSA process consequently allows for short cycles of desorption and adsorption

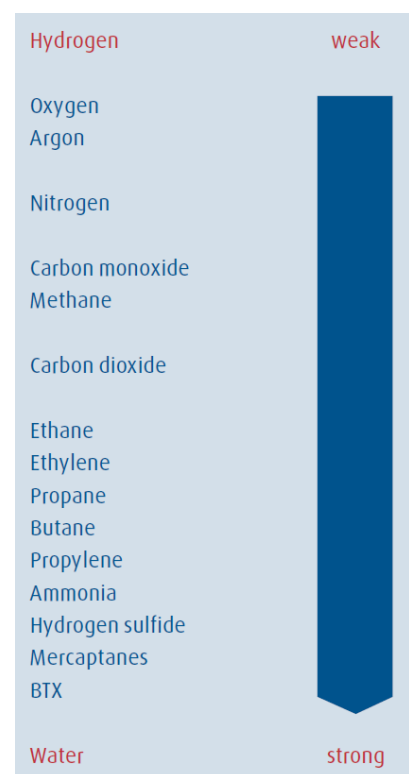


Figure 2.9: Relative interaction strength of adsorption [18].

within the range of minutes. Rapid cycling gives efficient use of adsorbent and leads to smaller vessel sizes and lower capital cost [18, 17].

To make the adsorption/desorption process continuous, it is required to apply multiple adsorption stages. Typical for PSA is the use of 4 to 12 adsorbent vessels that are sequenced to compensate for heating and cooling effects from the heat of adsorption and desorption. A four stage PSA is illustrated in Figure 2.10 for the separation of H_2 from a feed gas. The feed gas is pressurised to 10-40 bar over multiple adsorption stages by using a recycle of the H_2 product. Here, the weak H_2 passes through the adsorbent (keeping its high pressure) while others are adsorbed to the solid surface until the bed becomes saturated. For the regeneration a purge/sweep gas is used to clear away the desorbed components [17] to the PSA offgas stream (low pressure). A disadvantage of the PSA gas purification method is that the recovery of the product is not high when a limited amount of PSA columns is applied. In terms of the PtM plant this means that a large recycle stream would be required.

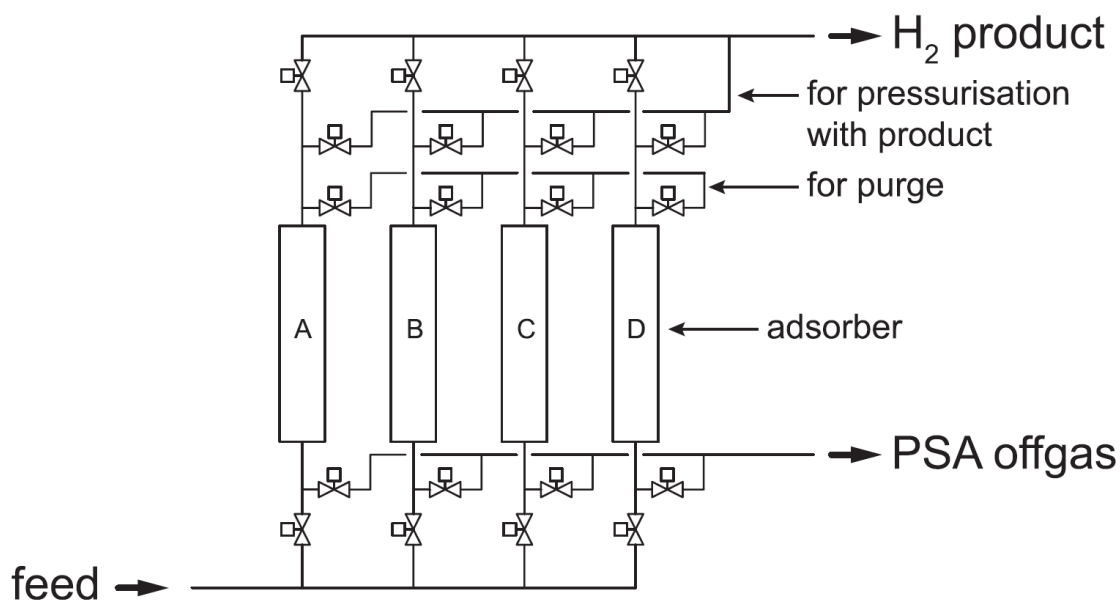


Figure 2.10: Pressure swing adsorption (PSA) with four adsorption columns [19].

The PSA process seen from a single adsorber can be divided into four general process steps being: adsorption, depressurisation, regeneration and re-pressurisation. However, each unit is integrated with the other units to make the process continuous and efficient as seen in Figure 2.11.

After the adsorption step (adsorber A) is completed, the column is depressurised in three steps. The first (E1) is called pressure equalisation, where the hydrogen stored in the void space is used to pressurise another adsorber (adsorber C) while minimising product losses and maximising the recovery rate. Secondly, the pressure is decreased further by using part of the product as a purge gas (PP) to regenerate another reactor (adsorber D). Lastly, the remaining pressure must be released or dumped (D) in counter-current direction to prevent break-through at the top of the adsorber. Now, the

regeneration step can take place using the purge (PP) of another adsorber (adsorber B) to desorb the final impurities to the PSA offgas. And finally, the re-pressurisation (R1) is done with the pressure equalisation step (E1) from another adsorber (adsorber C) together with the recycle for pressurisation with product (R0) to finalise the process which is repeated over and over again [18].

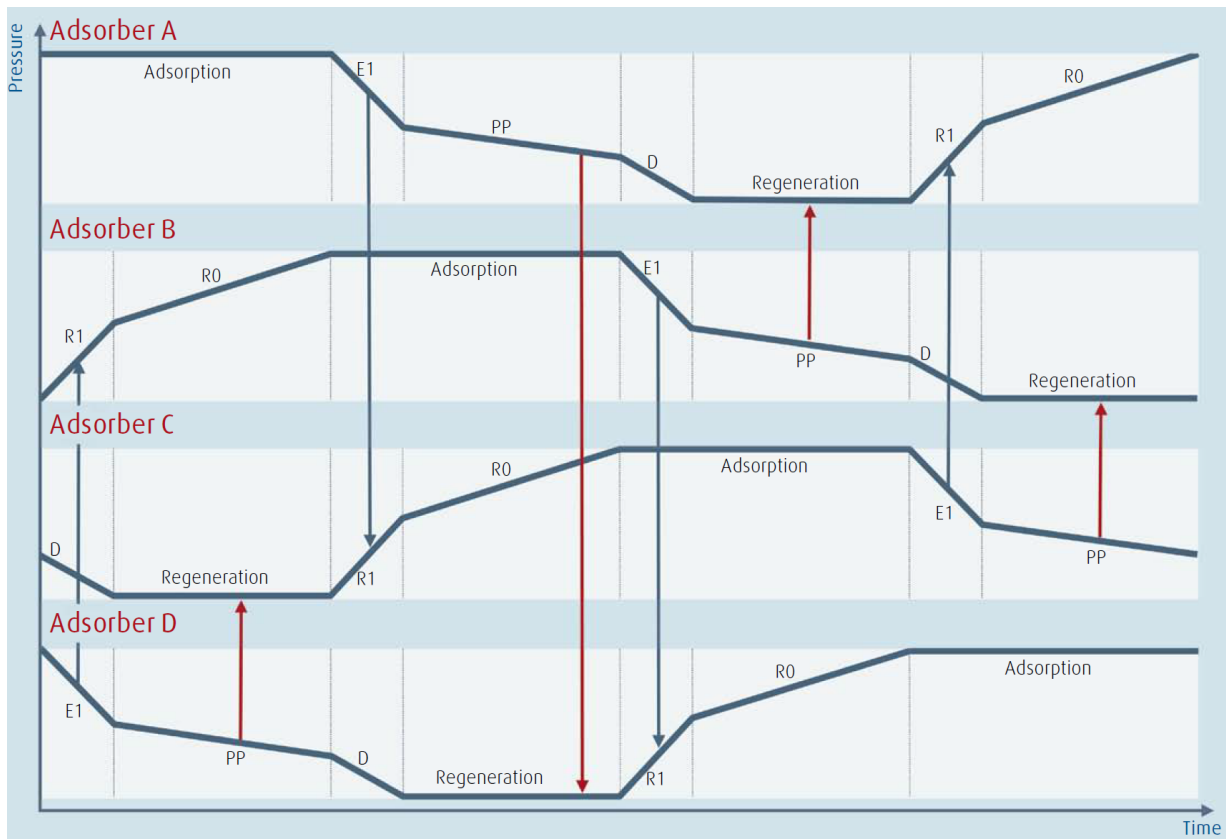


Figure 2.11: Dynamic pressure profile in four integrated PSA columns [18].

In literature, the uptake of gas on the adsorbent is often represented by adsorption isotherms for the individual components in the gas mixture. However, the adsorption capacity is influenced by the presence of other components in the gas mixture as some of them are more favoured. This makes it not possible to use individual gas isotherms (without interaction parameters) for the modelling of multi-component adsorption [19]. In addition, the process is dynamic and can be challenging to model accurately in a simple approach due to the large amount of interaction between the integrated PSA columns and lack of data for the gas mixture in question.

2.4.2 Membranes

Separation of gas components from a gas mixture can be done by using a membrane unit. Membranes can be classified into polymeric membranes that are readily available commercially, metallic membranes that are highly selective towards hydrogen and inorganic membranes that have a low cost and are chemically/thermally stable [20]. In this section the working principle, transport mechanism and design considerations are highlighted with a focus on the polymeric type.

Principles of Membrane Separation

The feed gas contains a mixture of gasses that is desired to be cleaned for one or more components to reach the required purity. A membrane purifies the feed gas mixture by allowing only a few species to permeate through the membrane barrier. The driving force for gas separation is based on the difference in chemical potential across the membrane and is for simplicity commonly described by a concentration or pressure difference, since these parameters can be empirically measured [21].

The component(s) that permeate through the membrane barrier are collected in the so called permeate stream, while the remaining, purified gas stream is called the retentate stream [17]. In Figure 2.12, a typical hollow-fibre membrane module is illustrated with indicated flow directions (counter-current).

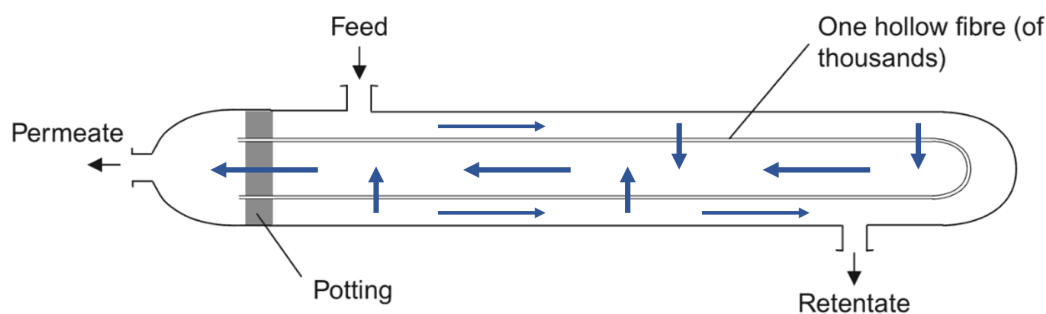


Figure 2.12: Schematic representation of a hollow-fibre membrane module [17].

To achieve a high retentate purity and recovery of the desired components it is important to choose a membrane material that has a high performance in terms of selectivity and physical strength. Still it can be challenging to achieve a high purity retentate or permeate recovery because of the decreasing driving forces during operation. If the driving forces become too small, then the flux of the to separate component becomes very low and an uneconomically large membrane area is required to achieve the desired purity [17]. To reduce the membrane area, it is possible to choose a multi-stage configuration, introduce a sweep gas (dilutes the species concentration in the permeate stream) and change the configuration or material of the membrane. Despite these suggestions, this can negatively influence the cost of the system and a clear trade-off between the membrane performance and the cost of the system is observed [21].

A singular membrane unit can be configured in different ways based on the flow direction of the permeate stream compared to the feed steam. In Figure 2.13 the three configurations are illustrated,

being (a) cross-flow or perfectly mixed flow, (b) co-current flow and (c) counter-current flow. The configuration is based on the design of the membrane and can be enhanced by adding a sweep gas stream. Figure 2.13 also shows the typical concentration profiles for each configuration over the membrane.

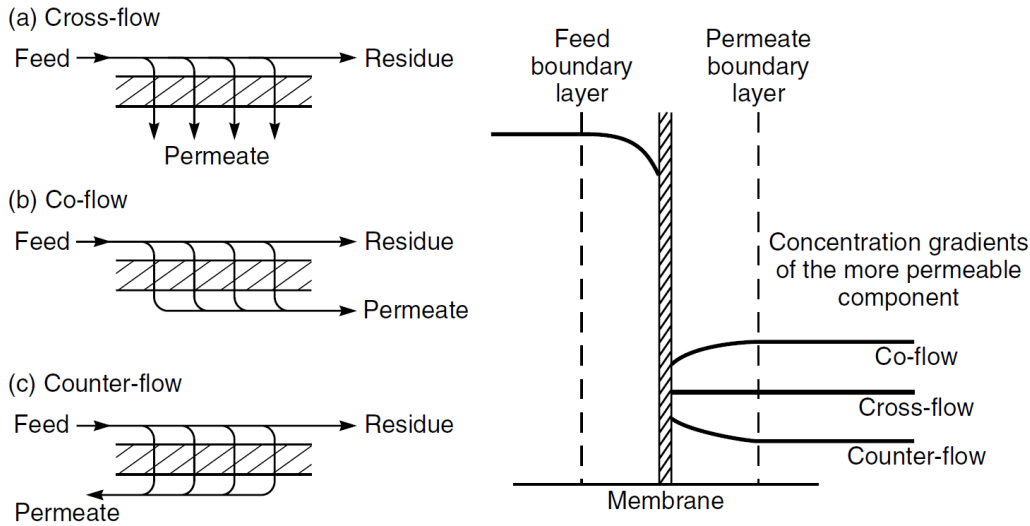


Figure 2.13: (a) Cross- (b) co- (c) counter-flow and concentration gradient across membrane [21].

The concentration gradient is the largest for counter-current flow. This means, that the counter-current configuration provides the largest molar flux through the membrane and thus the best separation efficiency. For modelling, the membrane is usually divided into membrane increments (equal area slices) that need to be solved. However, it is more difficult to model this configuration type since the permeate and feed concentrations are unknown at the same location and a concentration gradient in the permeate stream is present [22].

Transport Mechanism

Membranes can be divided into porous (inorganic) and dense (polymeric, metallic) membranes. For porous membranes the separation mechanism is based on molecular sieving, while for dense membranes this is solution-diffusion. The transport equations in this section are based on solution-diffusion mechanism since the dense membrane type is the most commercial technique [21].

A key parameter in membrane engineering is the flux (transport per unit area) through the membrane, that is usually described by the steady state Fick's law for binary diffusion [22] as in Equation 2.10.

$$J_{i,x} = -D_i \frac{dC_i}{dx} \quad \left[\frac{\text{mol}}{\text{m}^2 \text{ s}} \right] \quad (2.10)$$

Where, the flux of species i in x -direction ($J_{i,x}$) through the membrane is described as a function of the diffusivity proportionality constant (D_i) and the species concentration gradient. The minus sign indicates that diffusion occurs from a higher to lower concentration.

Dense solution-diffusion based membranes separate gasses because of differences in the solubility

and mobility of permeants in the membrane material [21]. Since that the pressure at the feed and permeate side can be measured relatively simply, the concentration gradient can be substituted with a partial pressure gradient by substituting either Henry's law for polymeric membranes or Sievert's law for metallic membranes (takes into account that diatomic hydrogen molecules dissociate on the metal surface before dissolution) [21].

$$S_i = \frac{C_i}{p_i^n} \quad \begin{array}{l} n = 1 \text{ for Henry's law} \\ n = 0.5 \text{ for Sievert's law} \end{array} \quad (2.11)$$

Where, C_i is the species concentration, p_i is the partial pressure for species i and S_i is the species solubility proportionality constant for Henry's law ($n = 1$) and Sievert's law ($n = 0.5$).

For metallic dense membranes, the separation mechanism occurs by dissociation of the hydrogen molecules into hydrogen atoms. This makes that a palladium membrane can selectively separate hydrogen gas since other molecules don't undergo this change. However, for the dissociation to take place, a high temperature ($> 300^\circ\text{C}$) is required so that the dissociation process is faster than the diffusion of atomic hydrogen through the metal lattice [21].

Rearranging Equation 2.11 and substituting into 2.10, as well as assuming that the concentration profile through the membrane is linear gives

$$J_{i,x} = -D_i S_i \frac{dp_i^n}{dx} \approx -D_i S_i \frac{\Delta p_i^n}{\Delta x} \quad (2.12)$$

Here, the Δp_i^n is the partial pressure difference between the feed and permeate sides of the membrane and Δx is the effective membrane thickness which is assumed to be equal over the whole membrane (x). The diffusivity (D_i) and solubility (S_i) constants are usually merged to give the so called permeability (\mathcal{P}) constant or merged together with the membrane thickness to give the so called permeance (P) constant. The result of this gives Equation 2.13.

$$J_{i,x} = -\frac{\mathcal{P}_i}{x} (p_{i_f}^n - p_{i_p}^n) = -P_i (p_{i_f}^n - p_{i_p}^n) \quad (2.13)$$

where $J_{i,x}$ is the flux across the membrane for species i , \mathcal{P}_i is the permeability (membrane's ability to permeate gas species), x is the membrane thickness, P_i is the permeance and p_{i_f} and p_{i_p} are the partial pressures of species i on the feed and permeance sides of the membrane, respectively.

The permeability and permeance are measured empirically and are dependent on the experimental temperature and pressure. The permeability is often reported in unit Barrer¹, while the permeance is often reported in gas permeation units (GPU)². Close watch on the units of the permeance/permeability and stated operational conditions of the experimental data is important for accurate modelling.

¹Barrer is defined as $10^{-10} \text{ cm}^3(\text{STP}) \text{ cm/cm}^2 \cdot \text{s} \cdot \text{cmHg}$ or $2.41 \cdot 10^{-3} \text{ mol/kPa} \cdot \text{h} \cdot \text{m}^2$ for $0.5 \mu\text{m}$ effective thickness

²GPU is defined as $10^{-6} \text{ cm}^3(\text{STP})/\text{cm}^2 \cdot \text{s} \cdot \text{cmHg}$

Design Considerations

Three indicative factors for the performance of a membrane are the selectivity (α), pressure ratio (φ) and stage-cut (θ). The selectivity is a measure of the membrane's ability to separate two gas species based on the ratio of their permeabilities, the pressure ratio gives the indication of the trade-off between energy requirement for compression of the feed gas and the retentate purity, while the stage-cut gives an indication of the trade-off between the retentate purity and product losses in the permeate stream (recovery) [21].

The expressions for the selectivity, pressure ratio and stage-cut are given in Equation 2.14 [21].

$$\alpha_{ij} = \frac{p_{p,i}/p_{p,j}}{p_{f,i}/p_{f,j}} = \frac{\mathcal{P}_i}{\mathcal{P}_j} \quad \varphi = \frac{P_f}{P_p} \quad \theta = \frac{\text{permeate flowrate}}{\text{feed flowrate}} \quad (2.14)$$

Where, $p_{p,i}$ and $p_{p,j}$ are the partial pressures of species i and j at the permeate side whereas $p_{f,i}$ and $p_{f,j}$ are the the partial pressures of species i and j at the feed side, \mathcal{P}_i and \mathcal{P}_j are the permeability of species i and j , and P_f and P_p are the total pressures at the feed and permeate sides.

At a high pressure ratio, the driving forces of the molecules (permeability) is higher compared to lower pressure ratio operation because the partial pressure difference over the membrane is larger. In the case that the selectivity is much larger than the pressure ratio ($\alpha \gg \varphi$), the performance of the membrane is determined by the pressure ratio only, while the opposite (a much larger pressure ratio) makes the performance determined by the selectivity only to reach a maximum purity for that membrane. At low stage-cuts, the retentate purity is low but the permeate is concentrated and contains has a relatively low flowrate, while at high stage-cuts the retentate purity is high but the permeate is only slightly more enriched than the feed and is of a relatively high flowrate [21]. Optimally, one would operate a highly selective membrane at a high pressure ratio to allow for maximum purity while maintaining a minimal stage-cut.

General effects of varying key operating factors [23]:

1. Increasing the pressure difference across the membrane increases the retentate purity.
2. Increasing the membrane area increases the retentate purity.
3. Increasing the retentate purity usually decreases the component recovery.
4. Increasing the feed flow rate decreases the retentate purity or increases the membrane area.
5. Increasing the temperature raises most permeabilities by about 10-15% per 10 °C.
6. Increasing the temperature has little effect on the selectivity.

Key requirements for a membranes used commercially [23]:

1. High permeability for the components to be removed.
2. high selectivity for the components to be removed in relation to other components.
3. High membrane stability against the present gas components.
4. Low effective thickness to ensure a high permeation rate.
5. High physical strength to withstand the required operating conditions.

2.4.3 Cryogenic Distillation

Cryogenic distillation is a widely used gas separation method for air separation, natural gas liquid recovery, ethylene recovery and propylene recovery [17]. The working principle of the process is based on the difference in boiling temperatures of the components present in the gas mixture so that selective components can be condensed/deposited out of the gas phase. Usually, the gas is cooled in stages similar to regular distillation technologies where one component is separated at the time until the contaminations are removed from the gas mixture. This leaves the possibility for integration of the gas separation technique and the liquefaction step required in the production of bio-LNG.

The boiling points of the components present in the this process its feed gas are:

Table 2.4: Boiling/melting points for components in the feed gas

Component	Boiling point @ 1.013 bar	Boiling point @ 10 bar
H ₂	-252.8	-241.8
N ₂	-195.8	-162.8
CO	-191.5	-157.3
CH ₄	-161.5	-124.0
CO ₂	-78.4 *	-40.1
H ₂ O	0 *	-0.1 *

* Temperatures represent melting points

In this case, the gas mixture needs to be cooled to -78.4 °C at atmospheric pressure or -40.1 °C at an elevated pressure of 10 bar to remove the CO₂ and H₂O components from the gas stream (* = removed as solids). Further enhancement of the purity by removing the other gas components would not be feasible since the low-temperature separation process will consume too much energy. Disadvantages of this separation technique is the high energy consumption and the fact that mechanical problems can arise from the deposition of CO₂ and H₂O in the equipment.

2.5 Process Equipment

Other equipment used to model the Power-to-Methane process is described in this section, and consists out of compressors, pumps, knock-out vessels and heat exchangers.

2.5.1 Compressors

Most systems that work on elevated pressures make use of multi-stage compressor layouts. The reason for this is that the temperature rise in a single-stage compressor working at high pressure ratios is too high, which results in inefficient operation. The increase in temperature due to compression is cooled by intercoolers between each stage of the multi-stage compressor unit [17].

The interstage pressure is normally selected to give equal work between each stage of the multi-stage compressor. The interstage pressure ratio can be calculated by Equation 2.15.

$$R = \sqrt[n]{\frac{P_{outlet}}{P_{inlet}}} \quad (2.15)$$

Where, R is the pressure ratio, P_{outlet} is the specified final pressure, P_{inlet} is the inlet pressure and n is the number of stages required for the multi-stage compressor unit. According to Sinnott & Towler [17], the normal maximum allowable pressure ratio of a single reciprocating/centrifugal compressor is 3.5. Therefore, the number of stages has been fitted with the maximum allowable pressure ratio.

The polytropic efficiency is often used to describe the real efficiency of compression for a compressor and varies with compressor type, size and throughput. A good estimate for the compressors in this plant is a polytropic efficiency of 70% as found in the Sinnott & Towler [17].

2.5.2 Pumps

To increase the pressure of a liquid stream it is often required to select a centrifugal pump (other types are used for special applications). The normal operating range of pumps is 0.25-1000 m³/hr [17]. In this process pumps are mostly used to increase the coolant its pressure up to the boiling point (this coolant is then called boiling feed water - BFW).

The power requirement for pumping \dot{E}_{Pump} a liquid is given in Equation 2.16.

$$\dot{E}_{Pump} = \frac{\Delta P \phi_v}{\eta_p} \quad (2.16)$$

Where, ΔP is the pressure difference [Pa], ϕ_v is the liquid volumetric flowrate [m³/s] and η_p is the pump efficiency [%]. The pump efficiency is dependent on the size of the pump but an adiabatic efficiency of 75% is used to model pumps.

2.5.3 Knock-Out Vessels

A knock-out vessel is applied when a gas stream is saturated with, or contains water vapours that need to be removed from the gas stream. The working principle of this technique is based on condensation of the water by cooling down the gas mixture at least until the dewpoint of water. For a higher separation efficiency, it is possible to cool the gas mixture further so that more H₂O is condensed. Usually, water is available in bulk and is used as the cheap coolant.

After cooling the gas mixture to the required temperature, the gas enters the (normally vertical) knock-out vessel, or two-phase separator, where the condensation starts. After a while, the two-phase separator is filled with water and controlled by a level controller. At the top of the vessel, a mist extractor section or demister pad is added to increase the efficiency of the separation.

2.5.4 Heat exchangers

A heat exchanger is used when a process stream is present that needs to be cooled down or heated up. Sometimes the reason for doing this is that high temperature (and pressure) streams contain valuable energy that can be usefully recovered. In the methanation process, most heat exchangers are used for cooling down the exothermic heat release or heat produced from the compression stages. The amount of energy that can be recovered depends on the temperature, flow, heat capacity and feasible temperature change of the stream [17].

Most important for modelling the process is to maintain a reasonable driving forces in the heat exchanger [17]. In the case that the temperature difference between two heat exchanging streams becomes too small, then the driving forces decreases which makes the required area of the heat exchanger unreasonable large (increasing the cost significantly). This means that the differential temperature between the hot and cold streams must be larger than a specified value so called ΔT_{\min} . In this model a ΔT_{\min} of 15 °C is maintained.

Many streams that need to be cooled in the process can be classified as waste-heat because the process has a very low heating demand compared to the cooling demand (when not counting other equipment present at the Biokraft plant in Skogn). Therefore, these streams are used to generate steam in a so called water-heat boiler. The pressure of the steam is dependent on the temperature of the hot stream. Normally, the lowest steam pressure used in process industry is 2.7 bar and is distributed at a header pressure of 8 bar [17].

The methanation reactor is cooled by high pressure and temperature boiling feed water that is evaporated in order to exchange the exothermic heat from the methanation reaction. This produces high pressure (HP) steam. The coolant temperature is chosen to be higher than the inlet temperature of the methanator to maintain driving forces for the methanation reaction. Therefore, the outlet temperature from the reactor is higher compared to the inlet temperature and is used to heat up the inlet streams by using a

so called feed-effluent heat exchanger.

In this chapter all the model aspects prior to making the model are clarified and consists of the battery limit, specifications of the raw materials and the required product purity.

3.1 Battery Limit

The battery limit is defined to limit the modelling and design work to the most important and interesting process components only. From Figure 1.2 it became clear which part of the plant has to be modelled. To be clear, this excludes the anaerobic digester, amine absorption column, liquefaction unit and other components present at Skogn since that equipment is already in use and its performance is known. The provided CO₂ properties are used in the model directly and the outlet of the Power-to-Methane process has to comply with the product quality of the liquefaction plant.

To model the Power-to-Methane process it is chosen to model an alkaline electrolyser, a multi-tubular methanation reactor and a single-stage polyimide membrane unit. The alkaline electrolyser produces the required hydrogen as one of the reactants for the methanation step and the polyimide membrane cleans the product gas to a sufficient purity. The choice of equipment is based on the most promising and commercial types of equipment that were described in the theoretical background (Section 2).

The CO₂ from the amine absorber column is contaminated with small quantities of CH₄, O₂, N₂, H₂O and H₂S as seen in Table 3.1. To reduce the number of components modelled, O₂ and H₂S are removed prior to entering the battery limit. The H₂S contamination is removed by a guard bed while the concentration of O₂ is accounted for by a higher N₂ concentration in the CO₂ stream. The flowrate of CO₂ specified in the model is assumed to be twice the capacity compared to the current capacity of the liquefaction unit (1500 Nm³ CH₄ per hour¹). This makes the model made in this project based on the second phase of the Biokraft plant at Skogn that is planned to be build in the near future, making the process possibly implemented for the third phase after that.

¹Nm³ is the volume at normal conditions specified at 0 °C and 101325 Pa

Currently, there is a 2 MW (electric) steam boiler available producing saturated steam of 6 bar(a) to satisfy the thermal demand of the plant. The thermal demand of the Biokraft plant in Skogn is also doubled in this case. This makes the thermal demand up to 4 MW that can be supplied with saturated steam of 6 bar(a). Furthermore, any left-over steam at high temperature (285 °C) or pressure (35 bar(a)) could be used for steam explosion as pre-treatment of the biomass for anaerobic digestion.

3.2 Feed Specifications

The composition, pressure and temperature of both the biogas from digestion and CO₂ from the amine absorption column are obtained from the supplier of the liquefaction process (Wärtsilä) [24]. By using the doubled capacity of the liquefaction unit (3000 Nm³ CH₄ per hour) it is possible to determine the feed specifications as given in Table 3.1. The calculation is shown below.

First, the doubled liquefaction capacity is used to find the volumetric flowrate of the CO₂ stream with its contaminations (ϕ_{v,CO_2}) from the specified composition of the biogas assuming that 32 vol% of the biogas ends up in the CO₂ stream.

$$\phi_{v,CO_2} = \frac{3000 \text{ Nm}^3/\text{hr} \cdot 32 \text{ vol}\% \text{ CO}_2}{68 \text{ vol}\% \text{ CH}_4} = 1412 \left[\frac{\text{Nm}^3}{\text{hr}} \right] \quad (3.1)$$

Then, the volumetric flowrate needs to be corrected for the actual process conditions of the CO₂ stream from the amine absorber that are 45°C and 1.025 bar(a). This is done with a manipulated version of the ideal gas law, as stated in Equation 3.2.

$$PV = nRT \quad \rightarrow \quad \phi_{v,2} = \phi_{v,1} \frac{T_1 P_2}{T_2 P_1} \approx 1.15 \cdot \phi_{v,1} \quad (3.2)$$

Where, $\phi_{v,2}$ is the volumetric flowrate at process conditions, $\phi_{v,1}$ is the initial volumetric flowrate, P and T are the pressure and temperature for the corresponding volumetric flowrates. For specification in HYSYS it is required to convert the volumetric flowrate to the molar flowrate. To do this, the molar density of the CO₂ steam with contaminations at the process conditions is extracted from HYSYS.

$$\phi_{M,2} = \phi_{v,2} \cdot 3.893 \times 10^{-2} \left[\frac{\text{kmol}}{\text{m}^3} \right] = 63.28 \left[\frac{\text{kmol}}{\text{hr}} \right] \quad (3.3)$$

The result of Equation 3.3 can be inserted into the molar flowrate cell in HYSYS to converge the CO₂ stream. Note, that the molar flowrate of component CO₂ is 62.14 kmol/m³.

The specifications of the biogas, CO₂ and CO₂ used in the model are given in Table 3.1.

Table 3.1: Feed specifications of biogas and CO₂ from Skogn and CO₂ model specifications [24].

Parameter	Biogas [%vol]	CO ₂ [%vol]	Model CO ₂ [%mol]
CO ₂	< 32	97.6 - 98.6	98.2
CH ₄	68	0.05 - 0.15	0.10
O ₂	< 0.5	< 0.1	N/A
N ₂			0.10
H ₂ O	saturated	1.2 - 1.8 (sat.)	1.6
H ₂ S	< 300 ppmv	< 3 ppmv	N/A
Pressure	101825 - 105325 Pa	102325 - 103325 Pa	102500 Pa
Flowrate	4411.76 Nm ³ /hr	1411.76 Nm ³ /hr	63.28 kmol/hr
Temperature	25 °C	38 - 50 °C	45 °C

3.3 Product Specifications

The product specifications are also adapted from the supplier specifications and are shown in Table 3.2. As can be seen, the product stream must be purified of almost all contaminations present. The main reason for the high purity requirement is that the liquefaction step after the PtM process takes place at cryogenic temperatures that cause CO₂, H₂S and H₂O to solidify (results in mechanical damage to the equipment).

Table 3.2: Product specifications of biomethane [24].

Parameter	Biomethane	Unit
CH ₄	99.9	%mol
CO ₂	≤ 50	ppm(mol)
H ₂ S	≤ 4	ppm(mol)
H ₂ O	≤ 1	ppm(mol)
Pressure	20	bar(g)
Temperature	≤ 40	°C

At the Biokraft plant in Skogn, the product is liquefied to bio-LNG at an elevated pressure of 20 bar(g) and subcooled to a temperature of -155 to -162 °C by a mixed refrigerant in a cryogenic heat exchanger where after it is stored in an insulated tank before transportation takes place.

In this chapter the Power-to-Methane process is described that is modelled in this project. Some other unit operations for this process are also discussed.

4.1 Power-to-Methane

In the Power-to-Methane process, carbon dioxide is converted to methane by use of hydrogen produced from electrolysis. If green hydrogen is mixed together with the biologically obtained CO₂ then the production process becomes sustainable and reasonably novel to be applied commercially. Moreover, the high energy content product CH₄ provides a recycle for the greenhouse gas CO₂ that is otherwise emitted to the environment, reducing the CO₂ emission and increasing the productivity of the plant.

The main process units considered for modelling the Power-to-Methane process are an alkaline electrolyser to convert (renewable) electricity to hydrogen gas, a multi-tubular methanation reactor to convert the reactants CO₂ and H₂ into CH₄ and H₂O and a single-stage polyimide membrane to purify the gas to the liquefaction quality requirements as specified in Table 3.2.

The process flow diagram of the Power-to-Methane process is illustrated in Figure 4.1.

There are two inlet material streams for the Power-to-Methane process that is modelled. These are the CO₂ and H₂O streams. Relatively clean H₂O is required for the alkaline electrolyser while seawater can be used for the heat exchangers. The CO₂ stream originates from the amine absorption unit located at the Biokraft plant in Skogn, which makes it slightly contaminated with other impurities, as stated previously in Table 3.1. Furthermore, energy streams are required. The electricity demand of the plant is high, which is mainly due to the electrolyser and for some extent caused by the compression stage. In addition, high amounts of heat are released in the form of steam.

The process flow diagram in Figure 4.1 is divided in the Power-to-Methane process that is modelled and the placement of this process within the already present equipment at the location (highlighted in grey). This makes it possible for the reader to get a good overview of the process as a whole, including the possible integration position at the Biokraft plant in Skogn.

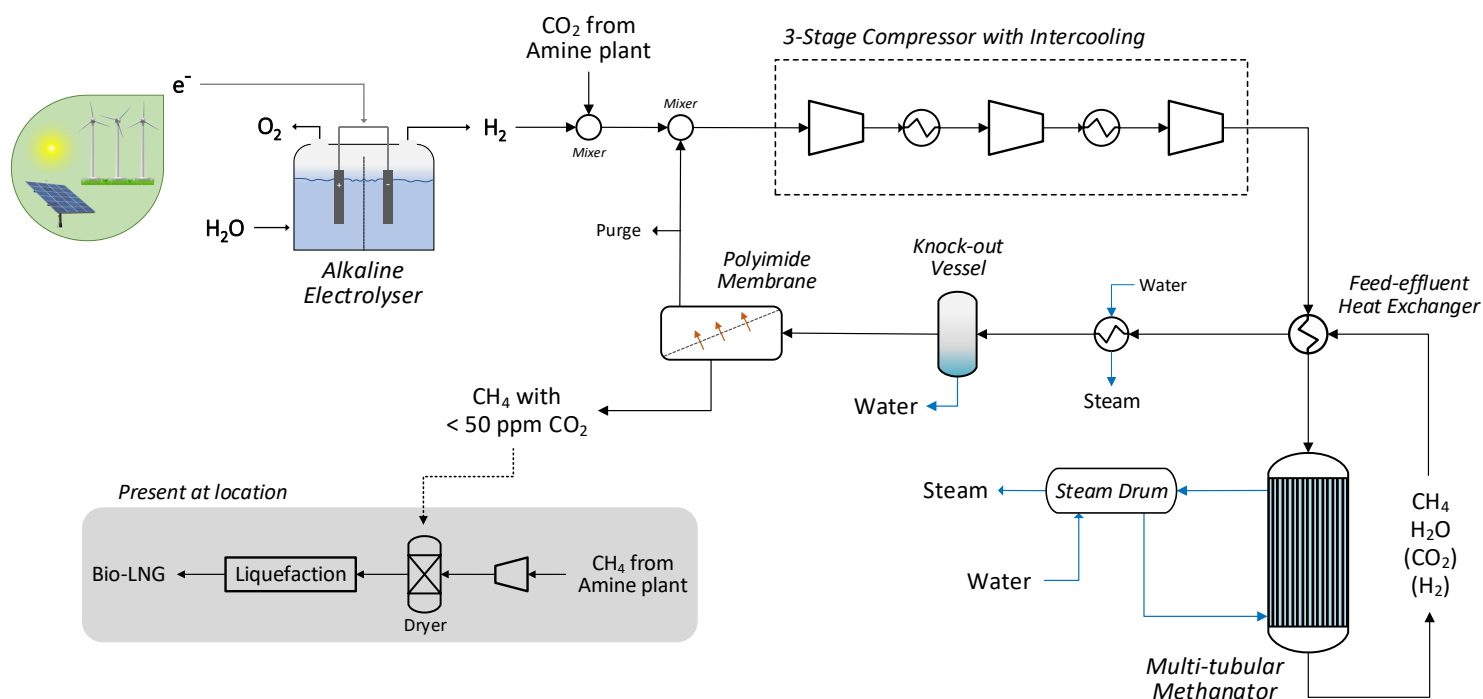


Figure 4.1: Process flow diagram for the Power-to-Methane process (made in Microsoft Visio).

As can be seen, the hydrogen produced from electrolysis is mixed firstly with CO_2 from the amine plant where after it is mixed with the gas from the recycle loop. The material stream after the first mixer is called the make-up gas (MUG) and is send to a three-stage compressor unit together with the recycle stream. In the three-stage compressor, the feed gas is compressed to a pressure between 12.5 and 20 bar(a) with interstage cooling to maintain a desirable temperature for efficient operation of the latter compressor unit. The compressed feed is then send through a feed-effluent heat exchanger to preheat the gas for the methanation reactor. In the multi-tubular methanation reactor, the methanation reaction ($\text{CO}_2 + 4 \text{H}_2 \rightleftharpoons \text{CH}_4 + 2 \text{H}_2\text{O}$) takes place over a catalyst to convert the reactants CO_2 and H_2 into the methanation products. As the methanation reaction is highly exothermic and has a limited temperature operating range there is a need for a heat sink with a high heat transfer coefficient. In this case, the choice has been made for water that is evaporated to steam to extract the heat of the reaction by evaporative cooling. The steam is then collected in a steam drum to produce high pressure steam while closing the mass balance of the coolant loop by refilling the water. The products material stream from the methanation reactor contains a high concentration of the methanation products CH_4 and H_2O but is contaminated with N_2 from the amine CO_2 stream as well as part of the methanation reactants due to incomplete conversion of the reactants in the methanation reactor. In addition, this stream is of a higher temperature than the inlet stream (coolant temperature is kept higher to ensure reaction driving forces) making it possible to preheat the inlet which reduces the duty of the cooler later. The methanation product stream consists of a high concentration of gaseous H_2O that needs to be separated by a knock-out vessel operating at a temperature of 20°C , so that most of the water in the process is removed. The heat exchanger before the knock-out vessel and the intercoolers of

compression all produce low pressure (LP) steam. Now, the gas mixture mostly consists of CH_4 with minor contaminations of H_2 , CO_2 , N_2 , H_2O . Because of the high (expected) electricity cost for electrolysis, a gas separation technique is required to minimise hydrogen losses and ensure a high product quality. As a gas separation unit, a polyimide membrane type is chosen where the permeate is recycled and the retentate is the product of the Power-to-Methane plant with a CO_2 concentration of less than 50 ppm. This is where the battery limit ends, but for process understanding, the retentate product is send to a dryer that is present at the Biokraft plant in Skogn to further polish the stream before it can be send to the liquefaction unit to produce bio-LNG as final product.

4.2 Alternative designs

The main process equipment for the Power-to-Methane process consist of an electrolyser, methanation reactor and gas separation unit. Some variations to the process described above can be made by exchanging one or more of these units. In Figure 4.2 three options are given for each unit operation that are the most suitable to be implemented as an alternative in the Power-to-Methane process.

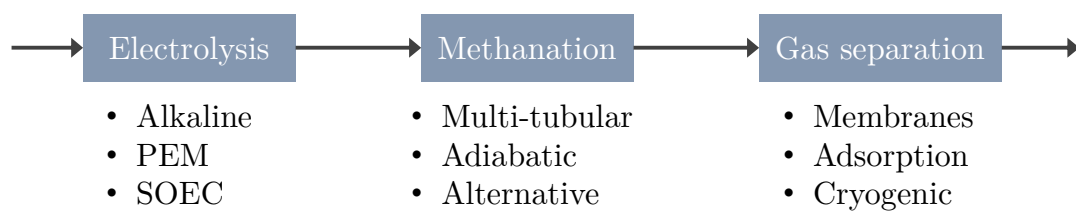


Figure 4.2: Block diagram containing the main process techniques for Power-to-Methane.

Instead of operating the process with a alkaline electrolyser, it is possible to implement an PEM (high current density) or SOEC electrolyser (steam or co-electrolysis). Each technique has its own advantages but the choice for alkaline is based on the maturity and cost of the technology compared to the other two electrolysis types, and for the reason that this electrolyser type is planned to be build.

The methanation reactor could have been an interstage cooled adiabatic reactor or alternative (fluidised bed, slurry or structured) type but due being a commercial technique and an excellent heat management technique the multi-tubular reactor is chosen to be modelled for the Power-to-Methane process.

Choosing the gas separation unit is less straightforward. In this case a polymeric (polyimide) membrane operating in one-stage is chosen, but testing the Power-to-Methane process for different gas separation techniques can be interesting as well. An option is to operate a membrane unit with multiple stages (to improve product quality and recovery) and/or a different type of material (e.g. polysulfone, palladium or carbon with higher selectivity for the gas mixture). Furthermore, an adsorption technique can be applied such as PSA although it is more challenging to model as discussed in Section 2.4. And a cryogenic gas separation unit is thought to be very interesting for this process as integration with the liquefaction plant is efficient to keep the pinch temperature of the process low.

In this chapter, a description will be given of how the main components (alkaline electrolyser, multi-tubular methanator and polyimide membrane) have been modelled and which assumptions are applied. Finally, the most important (in)dependent design variables and constraints are stated.

5.1 Alkaline Electrolyser

The alkaline electrolyser has been modelled by implementing available data for a similar type electrolyser from the supplier NEL Hydrogen. The data is uncertain but gives a much better fit to reality compared to the electrolyser model made in the specialisation project (*component splitter*). As seen in Figure 5.1, the HYSYS unit operation for the alkaline electrolyser is a *User Unit Operation* with attached material/energy streams.

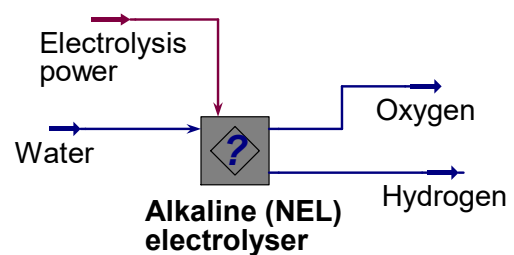


Figure 5.1: Electrolyser model from HYSYS.

One independent variable specified in the model is the H_2/CO_2 ratio in the MUG material stream. Because the molar flowrate of CO_2 in the CO_2 amine stream is known (see 3.1), it is possible to calculate the H_2 molar flowrate required to ensure this ratio. From this value, the O_2 molar flowrate is calculated according to the reaction equation:



So that the molar flowrate becomes half that of O_2 . Now, it is possible to calculate the H_2O molar flowrate using a similar method but this is not done because NEL specified the water consumption to be 0.9 L H_2O per $Nm^3 H_2$ (see Table 5.2). This can be transformed to 4326 kg/hr which is lower than the reaction stoichiometric allows for.

The most interesting to determine is the energy requirement to produce this much hydrogen. This is determined from the power consumption at the stack data as found in their brochure [25]. The value ranges from 3.8-4.4 kWh/ Nm^3 , therefore, the average value is used for determining the energy

requirement. Note, that it has been assumed that the rectifier and transformer make the power consumption increase with 5%.

Table 5.1: A3880 alkaline electrolyser data specifications [25].

Specifications	A3880
Capacity range per unit	2400-3800 Nm ³ /hr
Dynamic production range	3.75-100 % of flow range
Power consumption at stack	3.8-4.4 kWh/Nm ³
H ₂ purity possibility	99.99%
Possible outlet pressure	1-200 bar(g)
Feed water consumption	0.9 L/Nm ³
Footprint	≈ 770 m ²
Electrolyte	25% KOH aqueous solution

The main results from modelling the electrolyser are shown in Table 5.2.

Table 5.2: Important results for the electrolyser.

Parameter	Value
Energy requirement	47.88 kWh/kg H ₂
LHV efficiency	69.56%
HHV efficiency	82.35%
Hydrogen requirement	5573 Nm ³ /hr
Feed water consumption	4326 kg/hr

The found hydrogen requirement of 5573 Nm³/hr gives an indication that two units A3880 alkaline electrolysers are required. An image of this 8-cluster electrolyser is shown in Figure 5.2.

Applied assumptions for the electrolysis model are:

- The material streams have a purity of 100%.
- H₂ and O₂ are produced at 20 °C and 101325 Pa.
- The average power consumption at stack is applicable for modelling the process.
- The losses from the rectifier and transformer are 5% of the power consumption.

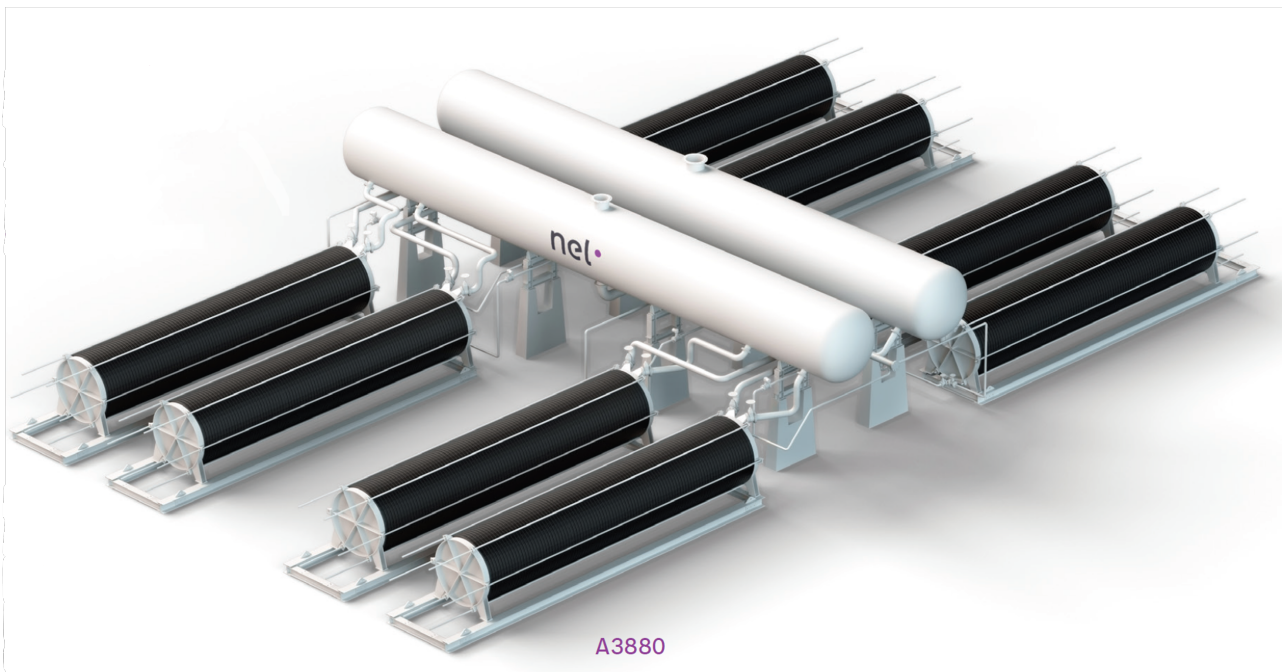


Figure 5.2: 8-cluster alkaline electrolyser model A3880 [25].

5.2 Multi-Tubular Methanator

The model for the multi-tubular methanation reactor is quite advanced compared the equilibrium model in HYSYS from the specialisation project. The kinetic rate expression from Koschany [16] was firstly implemented in a plug-flow reactor model in HYSYS but after completing the model it was noted that the temperature runaway was much higher than what is allowed for the methanation catalyst employed. Therefore, a more advanced MATLAB model was made to take into account radial variations and implement a more accurate heat and mass transfer model to try to minimise the temperature peaks. The MATLAB model code and a highly detailed description is given in Appendix E. Only the more important details are given in this section. After the MATLAB model was completed it was connected to HYSYS by using a CAPE-OPEN unit operation, as seen in Figure 5.3.

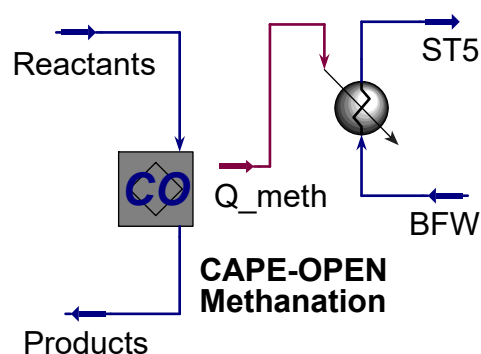


Figure 5.3: Methanation model from HYSYS.

In project 2 of the Reactor Technology (TKP4145) course from the master's program at NTNU a steam methane reforming (SMR) model was made. This code was used as a starting point to model the multi-tubular methanation reactor in this project. The steam methane reforming model needed to be adjusted mainly in the following aspects:

- Exchange reaction rate equations to Koschany [16] rate expressions.
- Implement expressions for the equilibrium, rate and adsorption constants.
- Implement new derived governing equation expressions for the process.
- Determine the heat flow from the tubes to the coolant.
- Add a new heat transfer model to take the coolant into account (SMR).
- Take interparticle mass transport limitations into account.

5.2.1 Methanation Model in Matlab

A stationary, two-dimensional pseudo-homogeneous (reaction takes place in bulk space of the tube) model is made where interparticle mass transport limitations are taken into account by an effectiveness factor (η) and the methanation runaway temperature can be controlled by a so called dilution factor. The model is relatively similar to Bremer et al. [26] and Fache et al. [14]. The choice for the pseudo-homogeneous model is to reduce the computational effort (and convergence time) as compared to a heterogeneous model. This is important since the HYSYS model needs to be easily converged even after implementing the MATLAB code into the CAPE-OPEN unit operation.

The multi-tubular methanation model is made by considering a single cylindrical tube, as seen in Figure 5.4. The methanation feed gas consisting mostly of the methanation reactants enters the tube from the top of the reactor and flows in the axial direction (z) over the length (L) of the reactor. Here, the gas comes in contact with a homogeneous mixture of catalyst particles that execute the methanation reaction. The heat of reaction (Q) is transported towards the cooling channel in the radial direction (r). In the cooling channel, water is evaporated at constant temperature and pressure to form steam. In theory, the processes taking place are similar for each tube in the multi-tubular methanation reactor (in practice there will also be a temperature variation from the centre of the reactor to the edge, but this is not taken into account).

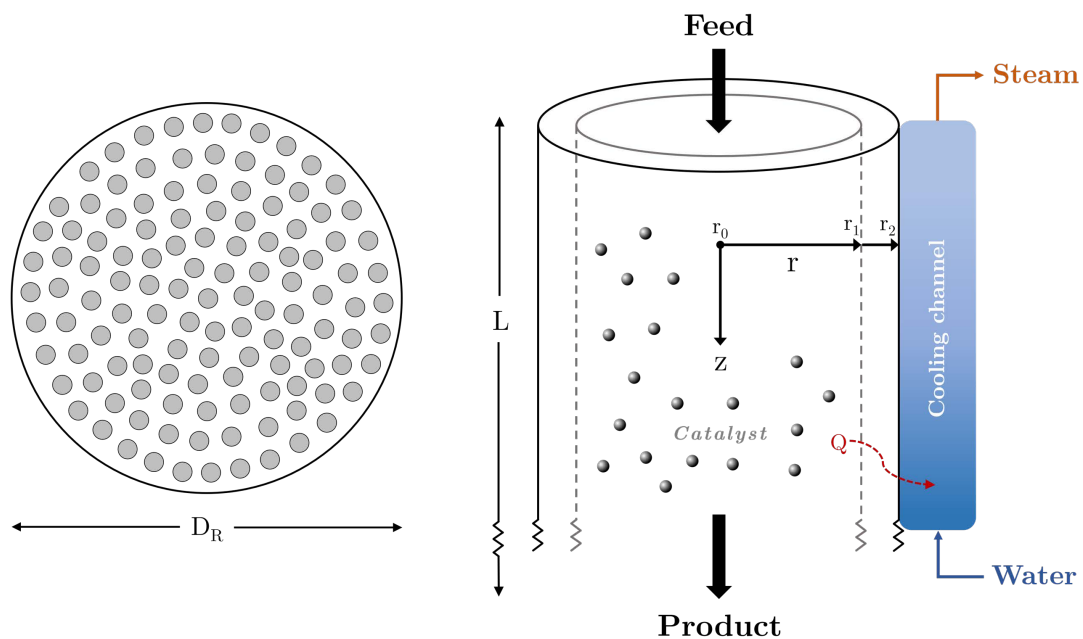


Figure 5.4: Illustration of the multi-tubular methanation reactor as seen from top and side.

The assumptions for the methanation model are:

- Catalyst particles are homogeneously mixed in the reactor.
- The profiles in each tube are independent of the other tubes.
- Fluid properties are not influenced by dilution factor.
- The coolant temperature is kept constant over the length of the tube.
- Heat transfer limitations in the particles are neglectable.
- Heat transfer to the environment is neglectable.
- Process is at steady-state and ideal gas mixture.
- Other assumptions stated in Appendix E.

To model this reactor, several expressions have been derived in Appendix E and the final result of the most important expressions is shown below. The expressions are derived in mass basis instead of molar basis since mass is conserved. A better explanation of the derivation and symbols used is given in Appendix E.

Axial velocity derivative (continuity equation) to conserve mass in the reactor tube.

$$\frac{du_z}{dz} = \frac{u_z}{T} \frac{dT}{dz} - \frac{u_z}{p} \frac{dp}{dz} - \frac{u_z}{M} \frac{dM}{dz} \quad (5.2)$$

Axial mass fraction derivative of component i in the gas mixture.

$$\frac{\partial \omega_i}{\partial z} = \frac{D_r}{u_z} \left(\frac{1}{r} \frac{\partial \omega_i}{\partial r} + \frac{\partial^2 \omega_i}{\partial r^2} - \frac{1}{r} \frac{\partial T}{\partial r} \frac{\partial \omega_i}{\partial r} \right) + \frac{R_i M_i \zeta \rho_{cat} (1 - \varepsilon) \eta}{\rho_g u_z} \quad (5.3)$$

Where, $i = \text{CH}_4, \text{CO}, \text{H}_2, \text{H}_2\text{O},$ and N_2 . The sum of the species mass fractions is one, making it possible to determine the component mass fraction of CO_2 (chosen because it has the highest overall concentration) from the other components, determined by Equation 5.4.

$$\omega_{\text{CO}_2} = 1 - \left(\omega_{\text{CH}_4} + \omega_{\text{CO}} + \omega_{\text{H}_2} + \omega_{\text{H}_2\text{O}} + \omega_{\text{N}_2} \right) \quad (5.4)$$

Axial temperature derivative in the tube.

$$\frac{\partial T}{\partial z} = \frac{1}{\rho_g C_p u_z} \left(\lambda_{er} \left(\frac{1}{r} \frac{\partial T}{\partial r} + \frac{\partial^2 T}{\partial r^2} \right) + R_{meth} \zeta \rho_{cat} (1 - \varepsilon) \eta (-\Delta H_{R_{meth}}) \right) \quad (5.5)$$

Heat transport from gas to coolant as function of the axial direction.

$$\frac{dQ}{dz} = 2\pi r_1 N_t U (T|_{r=r_1} - T_{coolant}) \quad (5.6)$$

Pressure drop in axial direction by Ergun equation.

$$-\frac{dp}{dz} = u_z \frac{1 - \varepsilon}{\varepsilon^3} \left[1.75 \frac{u_z \rho_g}{D_p} + 4.2 R e_p^{5/6} \frac{(1 - \varepsilon) \mu}{D_p^2} \right] \quad (5.7)$$

Implemented reaction rate expression according to Koschany [16].

$$R_{meth} = k p_{\text{CO}_2}^{0.5} p_{\text{H}_2}^{0.5} \left(1 - \frac{p_{\text{CH}_4} p_{\text{H}_2\text{O}}^2}{K_{eq} p_{\text{CO}_2} p_{\text{H}_2}^4} \right) / \text{DEN}^2 \quad [kmol kg_{cat}^{-1} s^{-1}] \quad (5.8)$$

With,

$$\text{DEN} = 1 + K_{OH} p_{\text{H}_2\text{O}} p_{\text{H}_2}^{-0.5} + K_{\text{H}_2} p_{\text{H}_2}^{0.5} + K_{mix} p_{\text{CO}_2}^{0.5} \quad (5.9)$$

Interparticle mass transport expression.

$$\eta = \frac{3}{\phi_{meth}} \left[\frac{1}{\tanh(\phi_{meth})} - \frac{1}{\phi_{meth}} \right] \quad [-] \quad (5.10)$$

The interparticle mass transport influences the reaction rate and is mostly dependent on the reaction rate, species concentration and diffusion coefficient. In the case that the reaction rate is high, the exothermic heat production is high this makes the effectiveness factor low (<0.1). Since this factor is multiplied with the reaction rate in the temperature and mass fraction differential, it opposes the high reaction rate and thus the temperature runaway peak. However, the magnitude of the effectiveness factor is not large enough to decrease the temperature runaway sufficiently in all cases. This is where the dilution factor comes into place.

The dilution factor influences the catalyst density (and/or bulk density) by reducing the amount of active material on the catalyst particle itself or by the use of inert particles. Dependent on the magnitude chosen of the dilution, it is possible to control the temperature for the process within the temperature limits. As discussed in [14], the catalyst dilution can increase the steady state efficiency and stability of the reactor but can have a negative impact on the transient efficiency and stability by increasing the reactor start-up time which is important for the Power-to-Methane process (dynamic operation required with intermittent energy sources). A good option would be to have a staged dilution over the length of the methanation reactor [14].

To solve all the expressions, a MATLAB code has been made (Attached in Appendix E) that is connected to HYSYS by a CAPE-OPEN unit operation (Manual given in Appendix F). A schematic representation of the model is given in Figure 5.5.

In HYSYS it is possible to adjust the values of the most important independent variables and the initial conditions (temperature, pressure, flowrate). These values are sent to the MATLAB *main.m* script that is embedded in the CAPE-OPEN unit operation. This script integrates all the differential equations and boundary conditions that are specified in the other scripts/functions such as *deriv.m* by using a so called mass matrix (is used since to solve algebraic-differential equations) together with the ode15s solver in MATLAB. The radial differential terms in the transport equations are discretised by the Finite Difference Method (in functions *dss020* and *dss042*) so that the ode15s solver only has to solve for the axial coordinates.

In this model, the tube diameter and number of tubes are adjusted in such a way that the velocity in the tube is in the operation range similar to that for methanol production (which is 0.5-1.0 m/s). The tube length is chosen to be 2m since this gave sufficient CO₂ conversion in most cases while limiting the capital expenditures of the plant. Other values were set equal to that of Bremer et al. [26].

Because of the CAPE-OPEN unit operation, it is required to use a CAPE-OPEN compliant fluid package in HYSYS for the streams attached to this unit. Therefore, a CAPE-OPEN fluid package

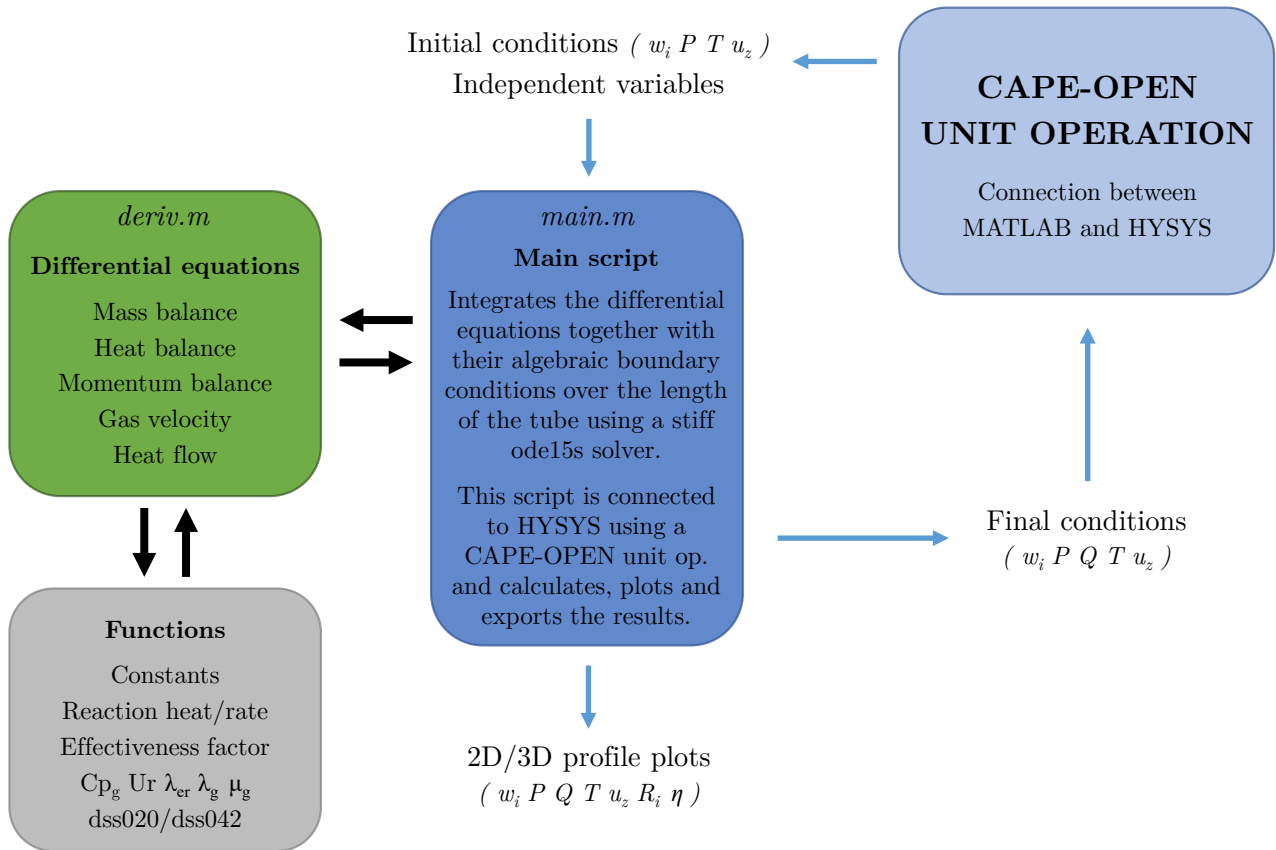


Figure 5.5: Schematic representation of the MATLAB model implementation.

according to the Peng-Robinson thermodynamics is made (Explained in Appendix F). A *steam cutter* is usually required when exchanging different fluid packages in the HYSYS simulation environment to convert the thermodynamic data. Nevertheless, it was chosen to operate all the steams with the CAPE-OPEN fluid package (except for the BFW coolant steams that operate on the ASME Steam fluid package).

5.2.2 Kinetic Validation of Methanation Model

The kinetics are validated using the plots from fig. 8 from Koschany [16] where the CO₂ conversion obtained from their experiments is illustrated as a function of the temperature, pressure and concentration. To validate the kinetics, several variables in the model have to be adjusted to ensure isothermal operation and intrinsic kinetics. Additionally, a similar inlet flowrate of $\phi_v^\circ = 0.12 \text{ Nm}^3/(\text{g}_{\text{cat}} \cdot \text{hr})$, catalyst mass of $m_{\text{cat}} = 25 \text{ mg}$ and inlet composition needs to be specified. From the given inlet flowrate and catalyst mass, the inlet velocity and catalyst density are determined, respectively. This is according to Equation 5.11 and 5.12 using the conditions stated in Table 5.3.

$$\rho_{\text{cat}} = \frac{m_{\text{cat}}}{V_{\text{cat}}} = \frac{25 \cdot 10^{-6}}{\pi R_{t,i}^2 L \cdot \varepsilon} \left[\frac{\text{kg}_{\text{cat}}}{\text{m}^3} \right] \quad (5.11)$$

$$u_{z,in} = \frac{\phi_v^\circ}{\pi R_{t,i}^2} = \frac{\phi_v^\circ}{3600 \pi R_{t,i}^2} \frac{T_{in} P_{Nm_3}}{P_{in} T_{Nm_3}} \left[\frac{\text{m}}{\text{s}} \right] \quad (5.12)$$

In Equation 5.12 the P_{Nm_3} and T_{Nm_3} are the pressure (101325 Pa) and temperature (273.15 K) at normal conditions, respectively, to convert the inlet flowrate to the conditions in the stream by the ideal gas law. T_{in} and P_{in} are specified manually in the model to find the corresponding CO₂ conversion (at specified inlet composition). This allows to recreate the figures from the article, as can be seen in Figures 5.6, 5.7a and 5.7b. In the experiments, Ar is used as an inert to sum the ratio to 100 (40 H₂/10 CO₂/50 Ar) but is replaced with N₂ as inert in the model.

Table 5.3: Kinetic validation model conditions.

Variable	Value
$R_{t,i}$	0.0127 m
L	4.0 m
ε	0.45
n_t	1.0
ζ	1.0
λ_{cat}	100 W/(m.K)
D_p	1e-5 m
ρ_{cat}	0.0274

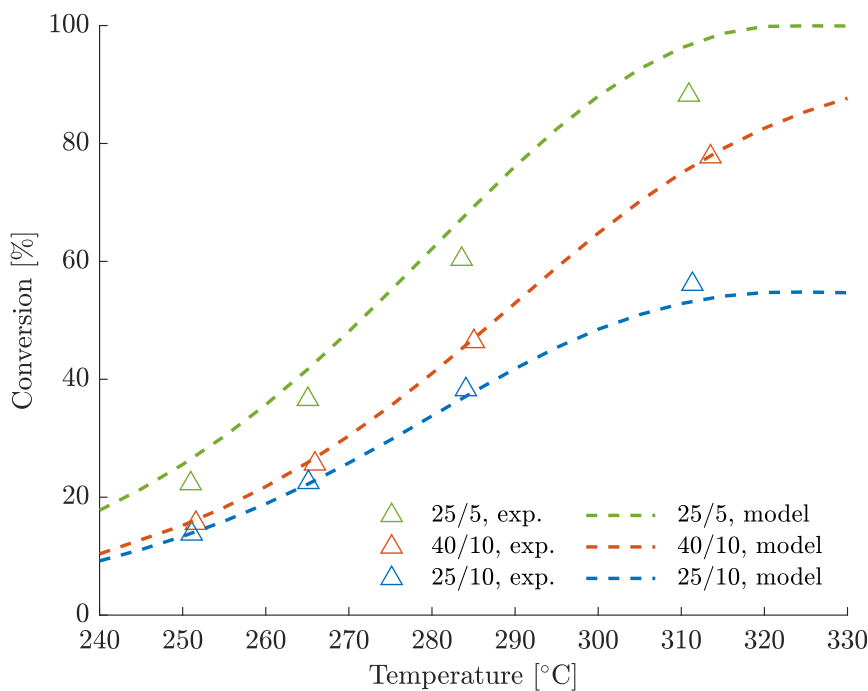


Figure 5.6: Kinetic validation, the effect of feed composition on CO₂ conversion for different H₂/CO₂ ratios at 6 bar.

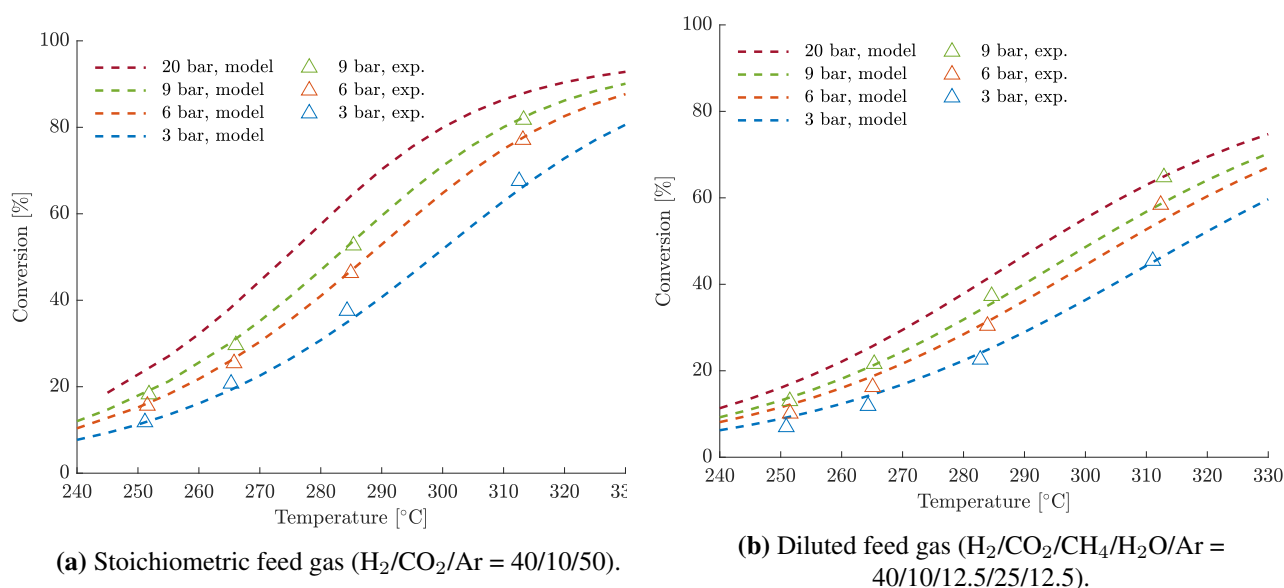


Figure 5.7: Kinetic validation, the effect of total pressure on CO_2 conversion for different H_2/CO_2 ratios.

In figures 5.6, 5.7a and 5.7b the CO_2 conversion is illustrated for the experiments from the article (triangle points) and model (striped line) as a function of the methanation temperature. In general, it can be seen that the CO_2 conversion is limited by chemical equilibrium at high temperatures (slope decreases) and limited by kinetics at low temperatures (reaction rate becomes zero, no CO_2 conversion). For Figure 5.6, three different H_2/CO_2 ratios are plotted to get an indication of the influence on the CO_2 conversion at a constant operational pressure of 6 bar. In Figure 5.7a and 5.7b the pressure is varied for the stoichiometric H_2/CO_2 ratio and for a feed that consists of the methanation reactants and product gasses. This gives an indication of the influence of the operational pressure as well as the influence of product gasses at the feed.

Figure 5.6 indicates that the model is capable of reflecting the H_2/CO_2 ratio of the feed very accurately for a stoichiometric/understoichiometric feed ratio. However, at an overstoichiometric ratio the model starts to slightly overestimate the CO_2 conversion at higher temperatures compared to the experiments.

Figure 5.7a shows that the dependence of total pressure on the reaction rates is rather low compared to the temperature dependence. The model seems to fit the experimental data very accurately over the whole temperature range for a stoichiometric ratio. In addition to the CO_2 conversion profiles at 3/6/9 bar where literature data is given, the CO_2 conversion is plotted for a pressure of 20 bar. This is for the reason that the Power-to-Methane process is operated at a higher pressure level than 9 bar. The higher pressure seems to give a reasonable profile as compared to the experimental data profiles.

Figure 5.7b illustrates that feeding water and methane in the feed gas slows down the reaction rate considerably. In addition, the model seems to be slightly more deviated from the experimental data mainly for higher pressure levels.

5.3 Polyimide Membrane

A polyimide membrane is modelled to separate the contaminations present after the methanation reactor and knock-out vessel. The goal of the separation is to reach <50 ppm(mol) CO_2 in the retentate material stream while minimising the amount of hydrogen lost in the retentate stream as well as the amount of methane recycled.

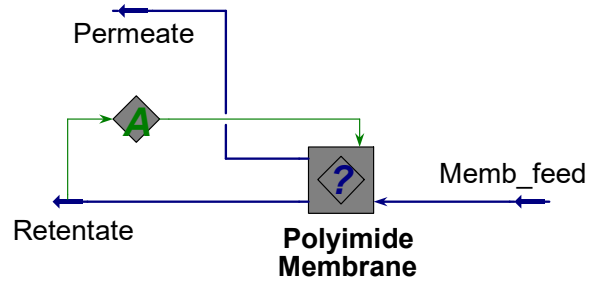


Figure 5.8: Membrane model from HYSYS.

In the specialisation project, the membrane was first modelled by a *component splitter* in HYSYS, but this does not take the mass transfer coefficient into account for each component present in the gas mixture and does not determine the membrane area requirement. Therefore, a more rigorous model, as seen in Figure 5.8, was applied to improve the model accuracy. For the master project, an adjust was added to manipulate the concentration of CO_2 in the retentate stream by variation of the membrane area to reach the quality requirement for liquefaction as specified in Table 3.2.

The more rigorous membrane model implemented is a membrane module called *ChemBrane* (v7.1). This is a *Unit User Op* in HYSYS created by Grainger [22] using Visual Basic® compatible code. The code generates the concentration profiles in the permeate and retentate stream by dividing the membrane into m equal area, perfectly mixed increments. To solve the module, the model requires the input of mass transfer coefficients (on permeance basis in $\text{mol}/(\text{kPa}\cdot\text{h}\cdot\text{m}^2)$ units), membrane type (co-current, mixed or counter-current), membrane increments and the membrane area. The model was validated by Grainger [22] by comparing model results with published data and it was found that the technique produced results with reasonable processing time and stability..

In the Power-to-Methane process, the *ChemBrane* unit operation is applied as a single polyimide membrane module that is operated without a sweep gas and in counter-current configuration since this provides the greatest separation efficiency and least membrane area [22].

What makes the *ChemBrane* module so interesting is that it solves counter-current membrane models using a novel 'start-up' algorithm where the initial guess of the permeate pressure is found by vacuum operation. There after, the non-linear system of equations is solved iteratively using a 4th-order Runge-Kutta method until the steady-state permeate pressure is found [22].

The mole flux for component i on the feed and permeate sides is given in Equation 5.13.

$$\begin{aligned} dF_{if} &= P_i (P_h \cdot y_{if} - P_l \cdot y_{ip}) dA \\ dF_{if,j} &= dF_{ip,j} \end{aligned} \quad (5.13)$$

Where, F_{if} and F_{ip} are the molar flow of i in the feed and permeate, P_i is the permeance for i , P_h is the feed pressure, P_l is the permeate pressure, y_{if} is the molar fraction of i in the feed increment, y_{ip}

is the molar fraction of i in the permeate increment and A is the membrane area [22]. A schematic representation of the model is given in Figure 5.9.

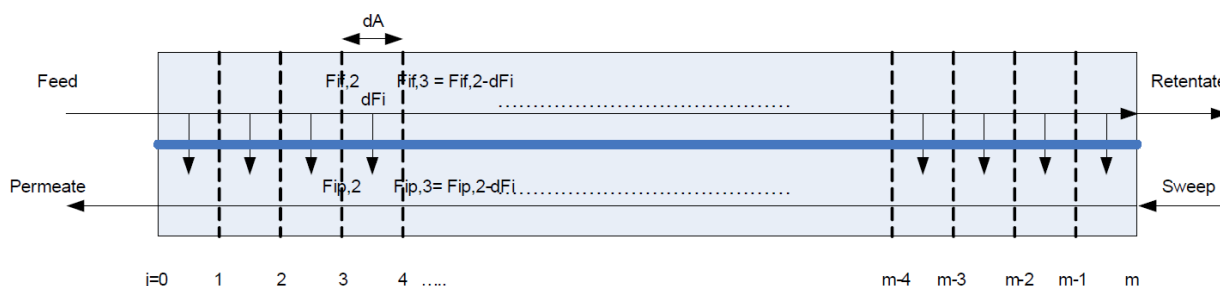


Figure 5.9: Counter-current ChemBrane model, membrane module representation [22].

A pressure drop of 5 psi is specified over the feed-retentate side of the membrane that is taken into account in the model by a log-mean average to calculate the partial pressures for each increment.

The assumptions for the ChemBrane model are [22]:

1. The permeability is independent of pressure and temperature (must be corrected accordingly).
2. Negligible dispersion in the axial direction.
3. No concentration polarisation.
4. Negligible pressure drop on the feed and permeate side.
5. Deformation of the hollow fibres under pressure is neglectable.

The permeance data implemented in ChemBrane unit operation in HYSYS originates from Baker [21] for a polyimide membrane from Ube Industries at $60\text{ }^\circ\text{C}$ with $T_g > 250\text{ }^\circ\text{C}$. The pure-gas permeability is given in Barrer which is converted permeance data by assuming that the membrane has an effective thickness of $0.5\text{ }\mu\text{m}$ ($5.0 \cdot 10^{-7}\text{ m}$). The raw permeability data and calculated permeance data is given in Table 5.4. The not specified components (H_2O and CO) are specified in ChemBrane as $10^{-9}\text{ mol}/(\text{kPa}\cdot\text{h}\cdot\text{m}^2)$ so that they do not cross the membrane and contaminate the retentate stream.

Table 5.4: Permeability data (Barrer) and permeance data $\text{mol}/(\text{kPa}\cdot\text{h}\cdot\text{m}^2)$

Component	Source data [21]	Implemented data
CH_4	0.40	$9.639 \cdot 10^{-4}$
H_2	50.0	0.1205
CO_2	13.0	$3.133 \cdot 10^{-2}$
N_2	0.60	$1.446 \cdot 10^{-3}$
O_2	3.00	$7.230 \cdot 10^{-3}$
H_2/CH_4 selectivity	125.0	
CO_2/CH_4 selectivity	32.50	

5.4 Design Variables

In this section the variables are most important independent and dependent variables are stated for the Power-to-Methane model made. These selected parameters are going to be used to do case studies in HYSYS and the results of the case studies are plotted and discussed in Chapter 6.

The selected independent variables to be varied in the case studies are the H_2/CO_2 ratio in the MUG material stream, the methanation temperature, methanation pressure and dilution factor. The settings for the case studies are given in Table 5.5.

Table 5.5: Independent variables for the sensitivity analysis with bounds.

Independent variables	Low	High	#Steps	Unit
H_2/CO_2 ratio	3.990	4.020	10	-
Methanation temperature	200	270	16	°C
Methanation pressure	12.5	20	17	bar(a)
Dilution factor	0.6	1.0	3	-

The model is solved by adjusting the area until the CO_2 concentration is 50 ppm(mol) in the retentate stream. This makes the model more challenging to converge because of the *adjust* block. The *Adjust* block is very sensitive and requires some help now and then. The *Secant* method that is used seems to be very sensitive to the initial guess. In the case that the area of the membrane is too large (making the concentration of CO_2 very low) it decides to increase the membrane area further while it should go the opposite way. It is thought, that this is caused by the interaction between the *recycle* and *adjust* block or because of the calculation method of the *adjust* block to converge the model. In order to overcome the challenges described previously, it is chosen to manually put the HYSYS solver on *On Hold* and accordingly change the membrane area back to a value that seemed to be working before. This is done while running the case studies in HYSYS.

After the case studies have been performed, the data needs to be checked for case studies that have a methanation runaway temperature above 550 °C. Both of the constraints need to be fulfilled and are given in Table 5.6.

Table 5.6: Constraints for the sensitivity analysis with bounds.

Constraint	Value	Unit
CO_2 concentration	< 50	ppm(mol)
Runaway temperature	550	°C

This chapter demonstrates the results of the Power-to-Methane process with an alkaline electrolyser, multi-stage compressor, methanation reactor and polyimide membrane modelled at steady-state. The chapter first gives the results from the main case study, and thereafter, demonstrates the sensitivity of temperature, pressure, catalyst dilution and H₂/CO₂ ratio on the dependent variables.

6.1 Main Case Study

The most important independent (top of tables) and dependent variables (bottom of tables) of the main case study are shown in Tables 6.1, 6.2, 6.3, 6.4.

The independent variables are specified in such a way that the methanation runaway temperature is maintained within its limits, the 50 ppm(mol) CO₂ concentration is reached and is in near optimal operation for this model (most settings specified after performing case studies). The methanation reactor and catalyst are designed based on a velocity requirement of around 0.5-1.0 m/s and literature data.

In Table 6.1 general variables are given for the Power-to-Methane process. Most interesting is that because of the high quality requirements of the product, a near 100% material efficiency (mol CO₂ inlet/mol CH₄ outlet) is achieved with around 55% energy efficiency based on the gas produced (LHV) and electricity requirement of the process. The main energy

Table 6.1: General variables of PtM process.

Variable	Value	Unit
MUG H ₂ /CO ₂ ratio	4.000	-
Membrane thickness	0.5	µm
Permeate pressure	1.013	bar(a)
Knock-out temperatures	20	°C
LOOP H ₂ /CO ₂ ratio	4.005	-
Recycle/MUG ratio	24.90	%
Membrane area	21755.7	m ²
Material efficiency	99.96	%
Energy efficiency (LHV)	54.58	%
CH ₄ vol. flowrate	1417.8	Nm ³ hr ⁻¹
CH ₄ mass flowrate	997.7	kg hr ⁻¹
CO ₂ concentration	49.85	ppm(mol)
CO ₂ after dehydration	50.03	ppm(mol)
Electrolysis power	23993.9	kW
Compressor work	1371.1	kW
Pump work	24.0	kW
Heating demand	2517.1	kW
Cooling demand	5770.5	kW

consumer of the process is the electrolyser (around 24 MW). Since the process has not been heat integrated, there is a possibility for heat integration, as can be noted from the heating/cooling demand.

the CO₂ concentration in ppm(mol) in the product stream is given twice in Table 6.1. The first is the concentration extracted from the material stream of the product in HYSYS while the other is the calculated CO₂ concentration when assuming that the product gas from the Power-to-Methane process can be send to the dehydration unit located at the Biokraft plant in Skogn. In that case the H₂O is removed and the CO₂ concentration increases. For the case-studies later in this chapter the dehydrated CO₂ concentration is taken as the constraint instead of the output concentration in the model.

The CH₄ volumetric flowrate of the product is determined at normal conditions (Nm³) but given by HYSYS properties in standard conditions (Sm³). Since the pressure and temperature have a large influence on the volume of gasses, it is needed to do a conversion. Normal cubic meter (Nm³) is at 0 °C and 1.01325 bar(a) while standard cubic meter (Sm³) is at 15 °C and 1.01325 bar(a). To convert these two volume definitions the ideal gas law can be used Equation 6.1.

$$PV = nRT \rightarrow \frac{V_1}{V_2} = \frac{T_1 P_2}{T_2 P_1} \quad (6.1)$$

Solving this equation gives that the ratio between the two definitions is equal to 1.05491287. Meaning that one Sm³ is around 5.5% larger than one Nm³. Equation 6.1 is used further on.

Methanation plays an important role in the system since it converts the byproducts from amine absorption at the Biokraft plant in Skogn to methane and water. Because it is rigorously modelled, the estimation of component concentrations for each material steam can be determined more accurately but is strongly dependent on the independent variables specified in Tables 6.2 and 6.3. A good estimation of the variables is taken from literature data [26, 14] that also modelled the methanation process.

Table 6.2: Methanation reactor variables.

Variable	Value	Unit
Tube length	2.0	m
Tube inner diameter	0.0254	m
Tube thickness	0.003	m
Tube inner distance	0.005	m
Number of tubes	1000	-
Tube heat coefficient	54.0	$\text{W m}^{-1} \text{K}^{-1}$
Reactor volume	2.295	m^3
Reactor diameter	1.209	m

Table 6.3: Methanation catalyst variables.

Variable	Value	Unit
Dilution factor	0.6	-
Void fraction	0.45	-
Catalyst diameter	0.003	m
Catalyst pore diameter	1e-8	m
Catalyst tortuosity	2.0	-
Catalyst porosity	0.6	-
Catalyst conductivity	0.2430	$\text{W m}^{-1} \text{K}^{-1}$
Catalyst density	2300	kg m^{-3}
Bulk density	759	kg m^{-3}

Next to the methanation variables of the methanation reactor itself, the inlet conditions are important for the accurate determination of the methanation process. As can be seen in Table 6.4, the main independent variables are the reactants temperature, reactants pressure and coolant temperature.

The gas-hourly space velocity (GHSV) is commonly used in reaction engineering and is determined by equation 6.2 [27].

$$GHSV = \frac{v_0|_{STP}}{V_{reactor}} \quad (6.2)$$

Where, $v_0|_{STP}$ is the inlet gas volumetric flowrate at standard conditions (Sm^3) and $V_{reactor}$ is the reactor volume. The GHSV is a measure of the time for one reactor volume to be put through the reactor. A higher GHSV means that the velocity through the reactor is fast. Thus the contact time is low [27].

In methanation it is important how much the reactants are converted to their products. A measure of this is to calculate the CO_2 conversion. The CO_2 conversion is determined from Equation 6.3 [17].

$$CO_2 \text{ conversion} = \frac{\text{inlet } CO_2 \text{ moles} - \text{outlet } CO_2 \text{ moles}}{\text{inlet } CO_2 \text{ moles}} \quad (6.3)$$

Because of the highly exothermic reaction and work of compression, there is a need for cooling in the process. The coolers use boiling feed water (BFW) that is evaporated to produce useful steam that can be used for heat integration with process equipment at the Biokraft plant in Skogn or other heat demanding units.

Table 6.4: Methanation general variables.

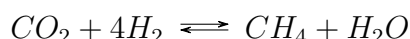
Variable	Value	Unit
Reactants temperature	250	$^{\circ}\text{C}$
Coolant temperature	300	$^{\circ}\text{C}$
Reactants pressure	16.0	bar(a)
CO_2 conversion	80.63	%
Products temperature	314.6	$^{\circ}\text{C}$
Runaway temperature	517.6	$^{\circ}\text{C}$
Pressure drop	0.13	bar(a)
Cooling duty	2832	kW
Inlet tube velocity	0.58	m s^{-1}
Min/Max tube velocity	0.44/0.74	m s^{-1}
GHSV	4013	h^{-1}

Table 6.5: Steam generation from the process coolers.

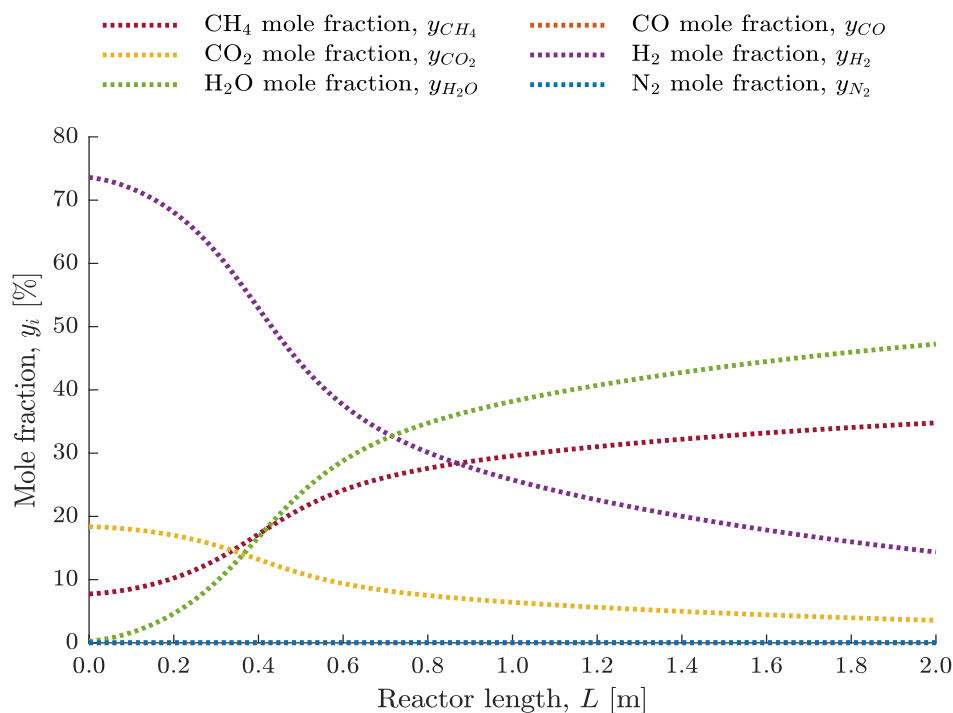
Parameter	Compressor intercoolers (ST1/ST2)	Methanator coolant (ST4)	Knock-out cooler (ST5)
Cooling demand [kW]	442/500	2832	1997
Steam temperature [°C]	135/151	300	181
Steam pressure [bar]	3/5	86	10
Steam flowrate [kg/h]	588/660	7249	2609

The figures given in the remainder of this section are collected from the methanation reactor operated at the main case study settings. This means that the profiles given here represent the operation of the methanation reactor only and do not represent the whole process. However, these results are interesting to show since the methanation model made is quite advanced compared to other models for this process found in literature. In addition, the results give a more fundamental understanding about the process as a whole that can help to understand the profiles in Sections 6.2, 6.3 and 6.4.

In the multi-tubular methanation reactor only the CO₂ methanation reaction takes place:



Therefore, the composition varies only for the molecules present in this chemical reaction.



	CO ₂ mol%	H ₂ mol%	CH ₄ mol%	H ₂ O mol%
Inlet	18.4	73.6	7.7	0.3
Outlet	3.6	14.4	34.8	47.2

Figure 6.1: Molar fraction of the individual components over the tube length.

Figure 6.1 illustrates the composition profiles over the length of the methanation reactor/tube. Because of the recycle loop, some of the reaction its products (CH₄ and H₂O) are present at the inlet. As seen in Figure 5.7b before, this reduces the CO₂ conversion (Here 80.6%). At the outlet of the methanation reactor the gas mixture consists mostly of CH₄ and H₂O but has a slight reactants contamination.

The composition change is however not equal to the change of the molar flowrates of the individual components because the CO_2 methanation reaction has a negative mole change as seen in Figure 6.2.

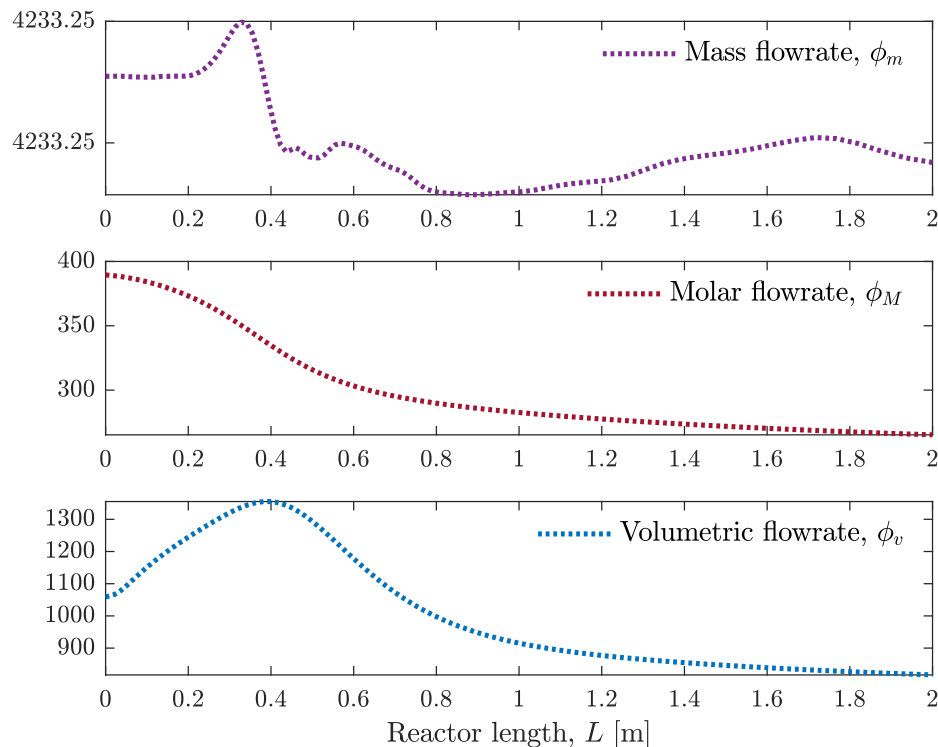


Figure 6.2: Mass/molar/volumetric flowrate over the tube length.

From Figure 6.2 it can be seen that the mass flowrate is considerably constant (as expected since mass is conserved, the variation is caused by numerical accuracy). In addition, the volumetric flowrate seems to have a peak close to the inlet of the reactor where and decreases to a lower point than the inlet condition. The lower outlet volumetric flowrate is caused by the molar flowrate decrease and slightly counteracted by the temperature/pressure changes. The peak close to the inlet is caused by temperature runaway.

Because of the two dimensional model for the multi-tubular methanation reactor, the figures on the next page(s) are given as surface plots where the profile is shown as a function of the tube length and tube radius (only half of the cylindrical tube diameter needs to be plotted since it is mirrored). The tube radius is at the centre point at 0 cm and at the wall at 1.27 cm.

The temperature runaway is caused by the highly exothermic methanation reaction. As a consequence, this makes it challenging to maintain the temperature within the specified limit of $550\text{ }^\circ\text{C}$ to prevent catalyst deactivation. In addition, the highly active catalyst implemented from Koschany [16] increases the reaction rate further making the CO_2 converted mostly in the beginning of the reactor (between 0-1 m) which in turn enhances the temperature release. The methanation runaway temperature and reaction rate are illustrated in Figures 6.3 and 6.4. To reduce temperature runaway, reduce the reaction rate by diluting the catalyst particles (inert particles or less active material) or gas mixture (inert gas,

product in feed or overstoichiometric H_2/CO_2 ratio) as well as increasing the heat transfer rate.

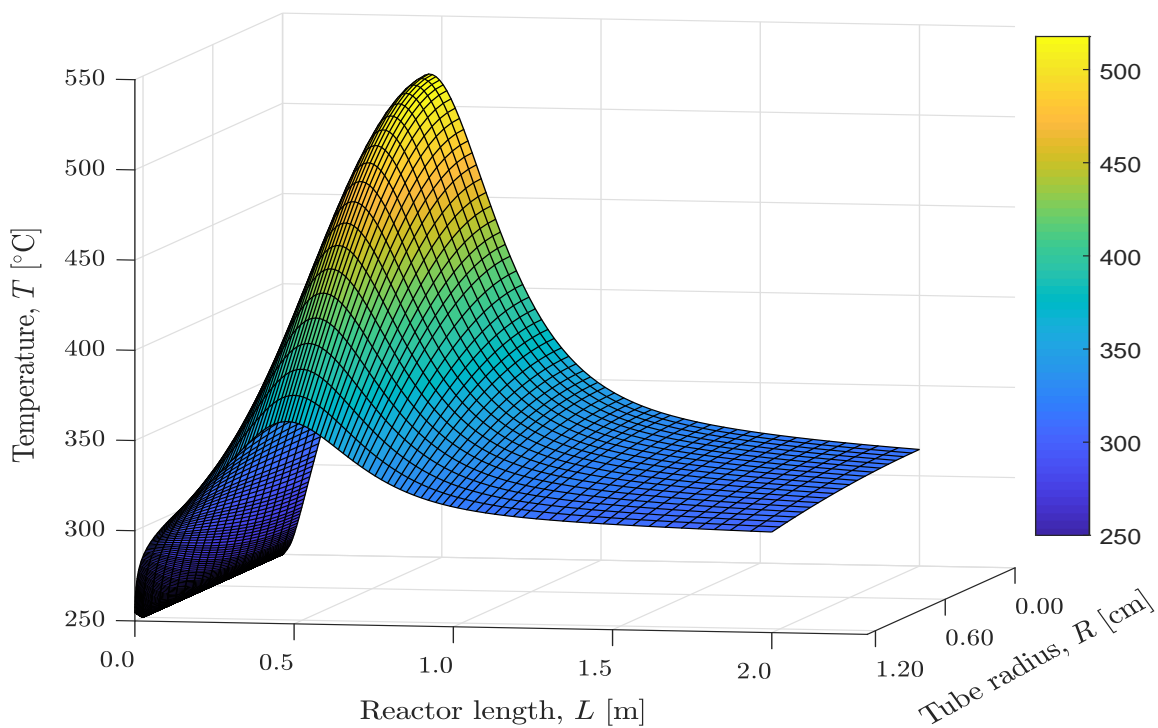


Figure 6.3: Temperature in the reactor tube.

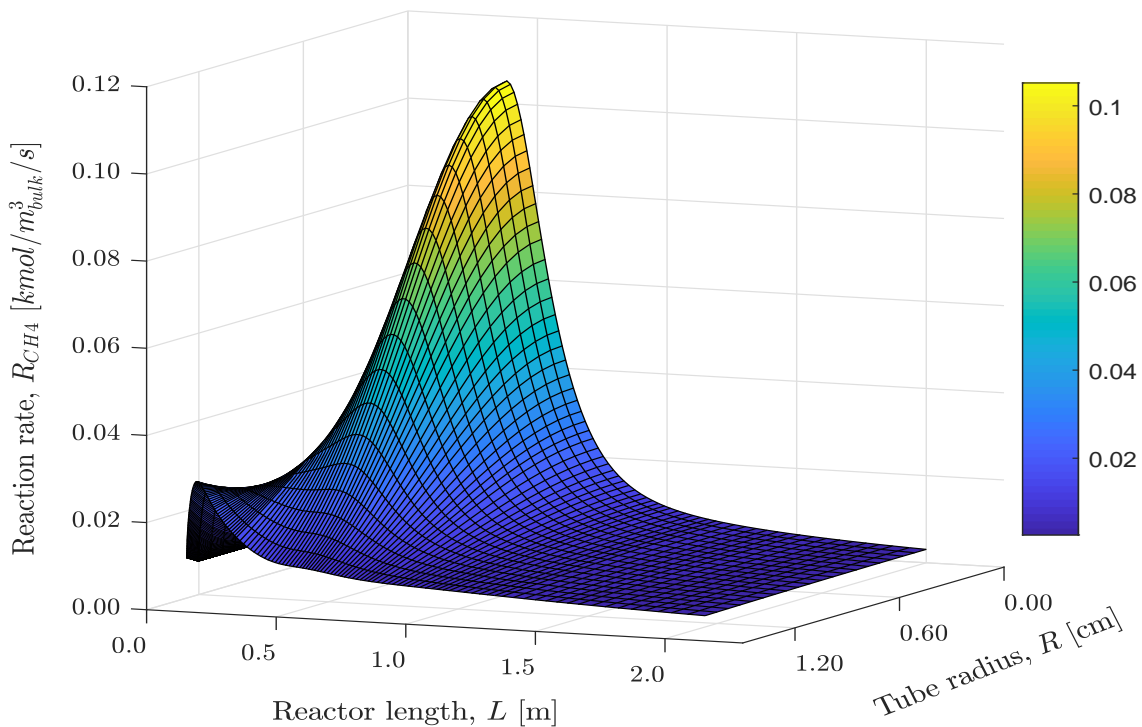


Figure 6.4: Reaction rate of CO_2 methanation in the reactor tube.

Another variable taken into account with the two dimensional methanation model is the effectiveness factor. The effectiveness factor includes the mass transfer limitations from the catalyst particles in the pseudo-homogeneous model to approach a heterogeneous model. As can be seen in figure 6.5, the effectiveness approaches zero when the reaction rate and temperature are high. Since the reaction rate is highly dependent on the effectiveness factor, this causes a natural decrease of the temperature runaway compared to a pseudo-homogeneous model without effectiveness factor.

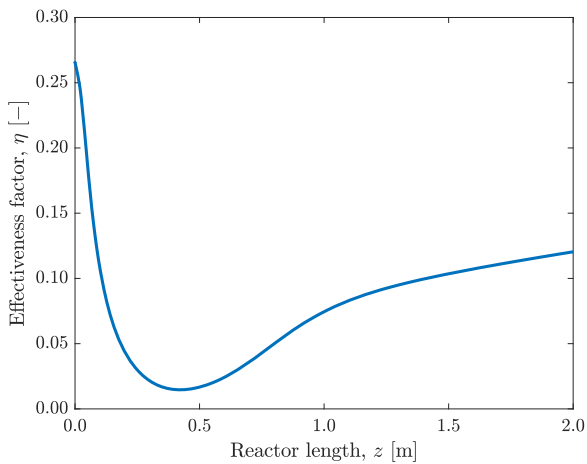


Figure 6.5: Effectiveness factor over the tube length.

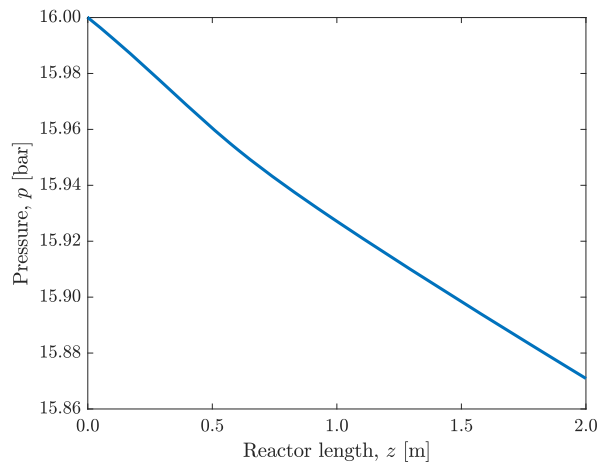


Figure 6.6: Pressure over the tube length.

Figures 6.6 and 6.7 illustrated the pressure and velocity profiles through the reactor, respectively. The pressure drop is approximately $\Delta P = 0.23$ bar(a) as determined by Ergun equation and seems to decrease in a rather linear trend. The velocity profile is similar to the volumetric flowrate and related to the temperature, pressure and composition from continuity, as discussed in Appendix E.

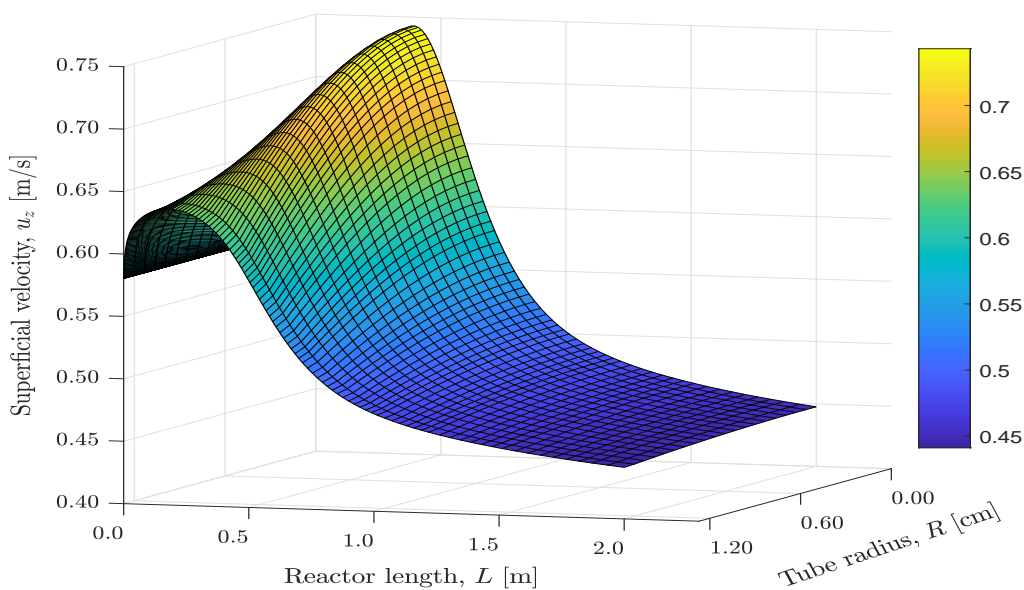


Figure 6.7: Superficial velocity in the reactor tube.

6.2 Influence of Temperature and Pressure

The temperature and pressure are shown to be very important independent variables for the PtM process. On the one hand, lower temperatures favour the highly exothermic methanation reaction but is limited to kinetics in terms of driving forces of the reaction. On the other hand, increasing pressures favour the methanation reaction due to the negative change in moles. Additionally, higher operating pressures results in higher driving forces for the membrane separation unit while a too low pressure level results in difficulties of converging the model to the high product quality demands. Altogether, this suggests there is a limited operating range where the process can be operated in. In this section, the methanation temperature and pressure are varied between 200-270 °C and 12.5-20 bar, respectively. The other independent variables are kept constant to the main case study.

The influence of temperature and pressure on the CO₂ conversion is illustrated in Figure 6.8.

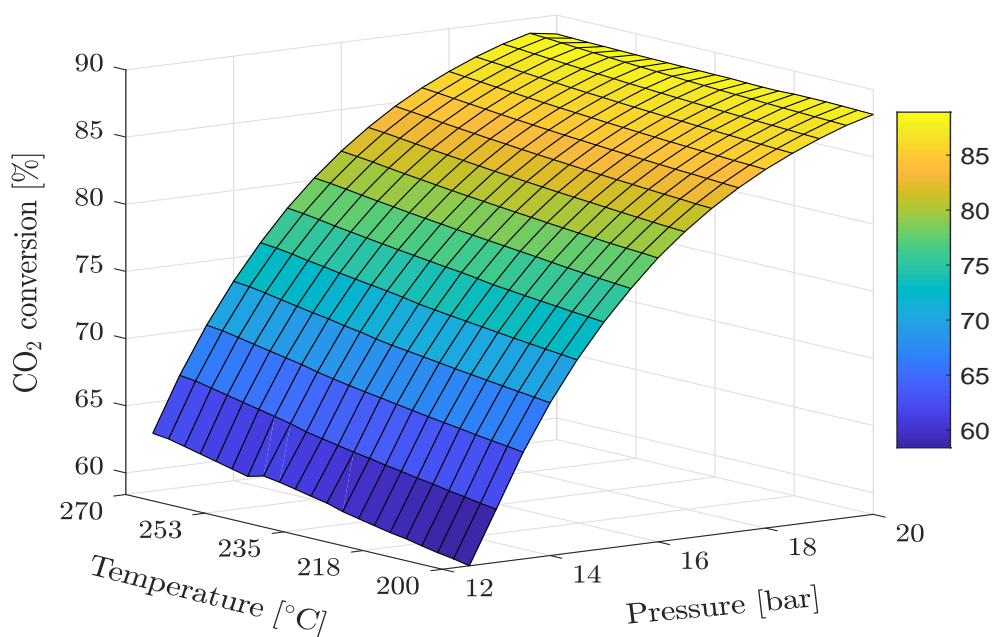


Figure 6.8: CO₂ conversion as a function of methanation temperature and pressure.

As can be seen from the surface plot, an increasing temperature and pressure gives a higher conversion of the reactant CO₂ in the methanation reactor. Moreover, it can be noted that pressure influences the CO₂ conversion more than temperature. At high pressure, the methanation reaction starts to approach equilibrium as can be seen from the decreasing slope of the profile (92.5% conversion at 40 bar).

From Figure 6.8 it seems that operating at a high pressure is favourable in terms of the CO₂ conversion. Logically speaking this also means that less CO₂ needs to be separated by the membrane to reach the product quality requirements. However, the operational pressure of the system is limited. As can be seen in Figure 6.9, at 19 bar(a) operational pressure, the temperature runaway in the methanation reactor is higher than the constraint of 550 °C.

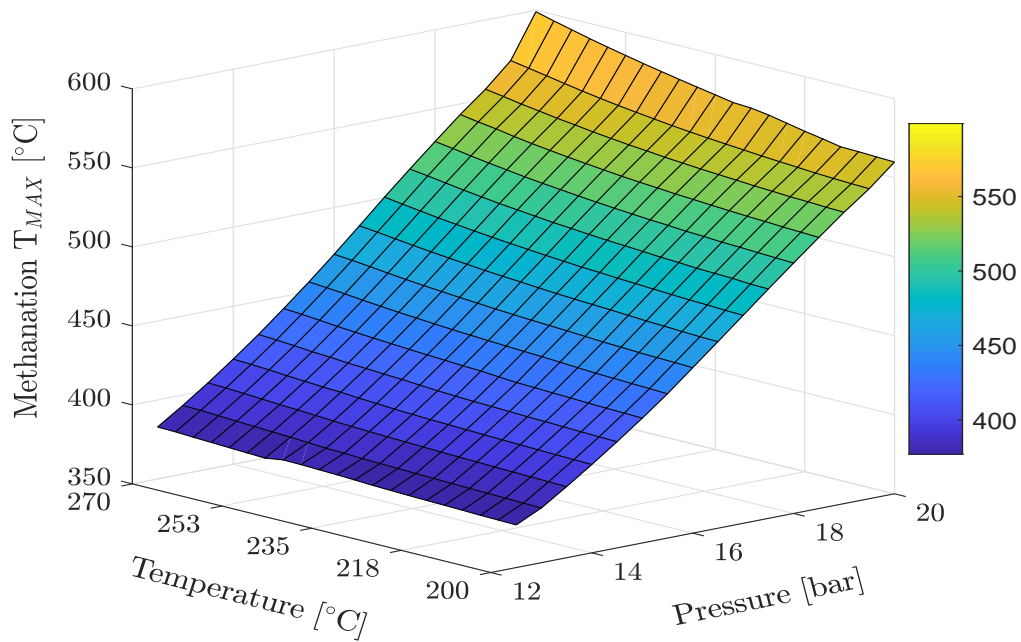


Figure 6.9: Runaway temperature as a function of methanation temperature and pressure.

The membrane area decreases with increasing pressure as expected from the higher separation selectivity. Additionally, it is barely influenced by the operational temperature and seems to have an inverse relation to the CO_2 conversion. Less CO_2 converted means more CO_2 to be separated by the membrane. At 12.5 bar the membrane area is more than twice as high as when operated at 20 bar, as can be seen in Figure 6.10.

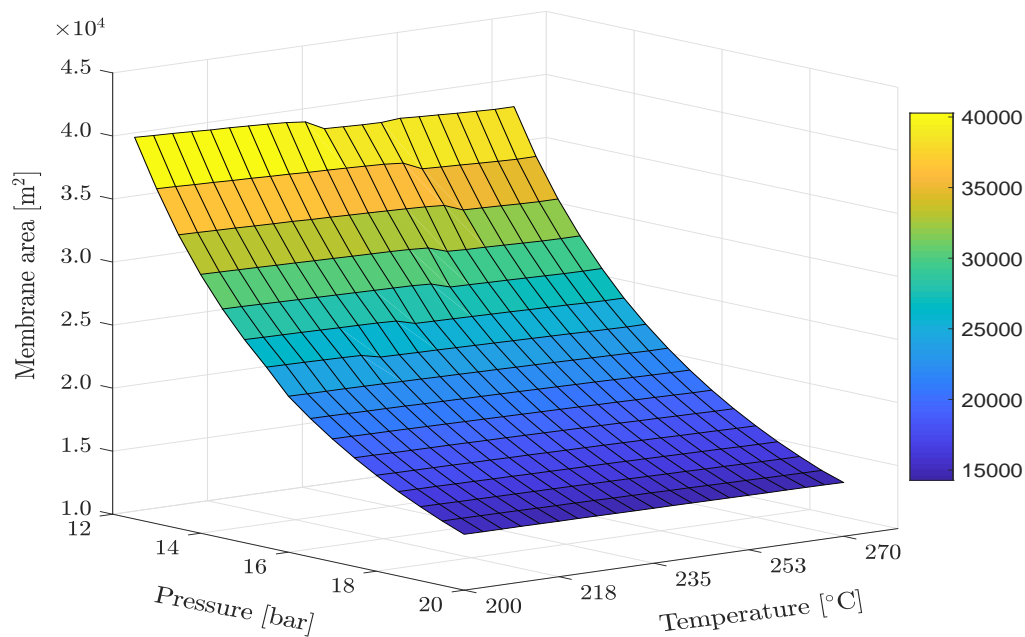


Figure 6.10: Membrane area as a function of methanation temperature and pressure.

In Figure 6.11, the recycle flowrate (columns) and CH₄ concentration in the recycle steam (line) are illustrated for three pressure levels and two temperature levels. Furthermore, each column is separated into parts that represent the individual component molar flowrates.

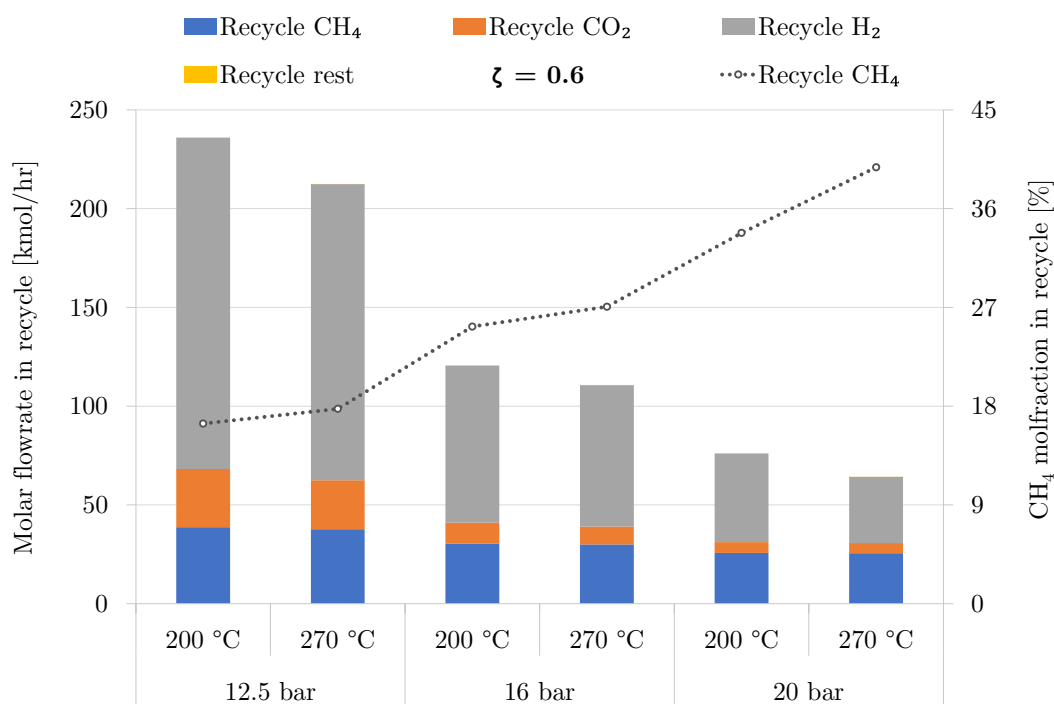


Figure 6.11: Recycle flowrate (column) and composition (line) as function of temperature and pressure.

As can be seen from Figure 6.11, the molar flowrate of the recycle stream is relatively high at a low pressure. In fact, the recycle stream becomes 70-80% of the MUG material stream and this is unwanted. At a higher pressure, there is less recycle requirement. However, at a high pressure, the concentration of CH₄ in the recycle steam becomes high as seen from the dotted line. However, this does not mean that the CH₄ concentration at the inlet of the methanation reactor is higher since the CH₄ molar flowrate is reducing (blue columns) and the H₂/CO₂ ratio in the MUG is the same. It can also be noted that there is a decrease in moles recycled of H₂ and CO₂.

The recycled H₂ and CO₂ do have an influence on the H₂/CO₂ ratio in the loop since the H₂/CO₂ ratio in MUG is constant. Interestingly, when the pressure is 12.5 bar the H₂/CO₂ ratio in the loop increases up to 4.5.

One of the more interesting variables is the energy efficiency of the process. A high energy efficiency means that an amount of the product is produced at the cost of a low amount of energy. However, no unit is 100% efficient and combined this results in large energy losses. For this process, the (electrical) energy efficiency of the PtM process is calculated since no heat integration case has been performed but seems fairly promising due to the large quantities of steam produced.

The (electrical) energy efficiency is calculated in Equation 6.4.

$$\eta_{total} = \frac{\text{Energy produced}}{\text{Electricity consumed}} = \frac{\phi_{m,CH_4} \cdot LHV_{CH_4}}{\left(\dot{E}_{Electrolysis} + \dot{E}_{Compression} + \dot{E}_{Pumps} \right)} \quad (6.4)$$

Where, ϕ_{m,CH_4} is the mass flowrate of CH_4 in the retentate product [kg/s], LHV_{CH_4} is the lower heating value of CH_4 being 50.0 MJ/kg (HHV = 55.5 MJ/kg) [28], $\dot{E}_{Electrolysis}$ is the electricity demand for electrolysis [MW] and $\dot{E}_{Compression}$ and \dot{E}_{Pumps} are work for compression [MW] and the pumps [MW], respectively.

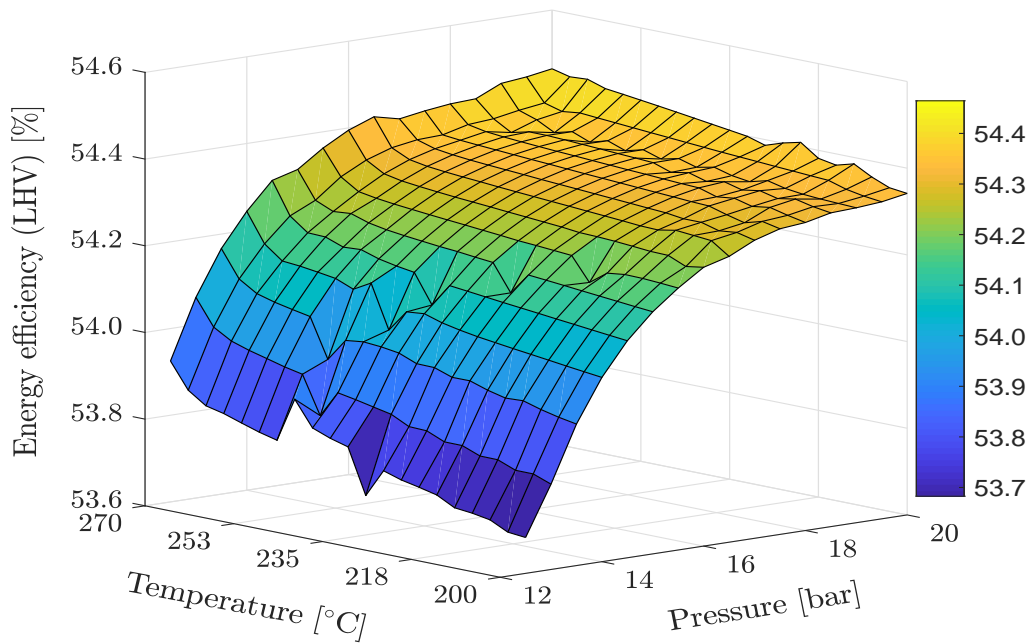


Figure 6.12: Energy efficiency (LHV) as a function of methanation temperature and pressure.

Figure 6.12 illustrates the electrical energy efficiency of the Power-to-Methane process as a function of temperature and pressure. Higher pressure has a positive influence on the efficiency. This is related to the lower pressure requiring more recycle which in turn increases the work for compression. The power consumption of the plant is dominated by the electrolyser as stated before.

6.3 Influence of Catalyst Dilution Factor

In this section, the catalyst dilution factor will be varied to find the sensitivity towards the model. The catalyst dilution factor applied before was 0.6, which can be seen as 60% being active catalyst and 40% inert catalyst. Since the methanation temperature limit of 550 °C is a challenging factor for operating at high pressure levels this influence of the dilution factor has become significantly important. Therefore, three dilution factors are being tested.

In Figure 6.13 the CO₂ conversion is plotted against pressure for a dilution factor of 0.6, 0.8 and 1.0. Each dilution factor is illustrated at 200 °C (circle) and 270 °C (triangle).

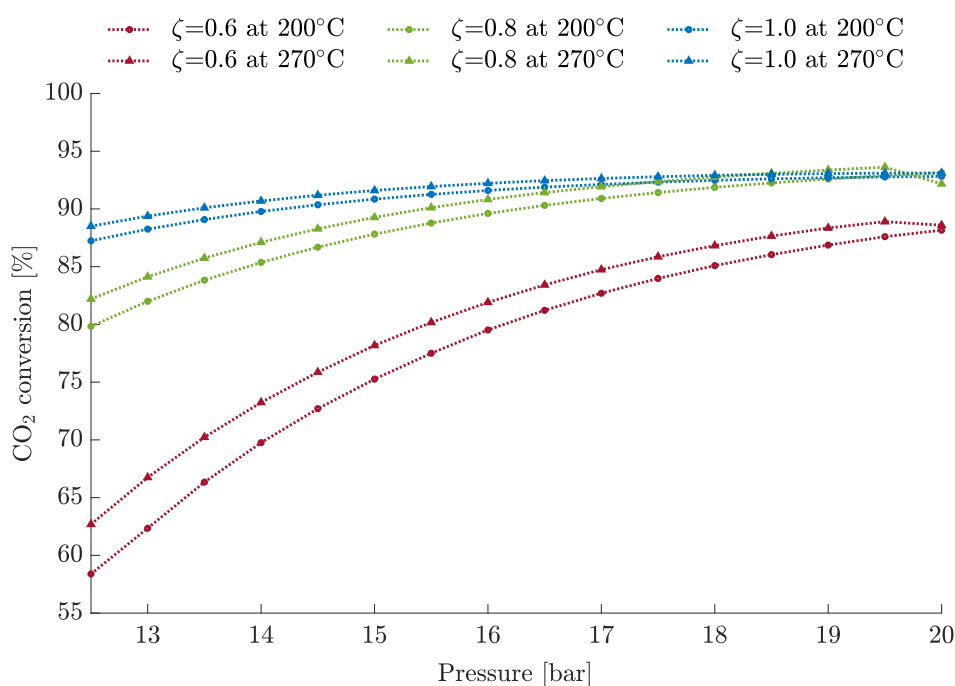


Figure 6.13: CO₂ conversion at 200 °C (circle) and 270 °C (triangle) as function of pressure and dilution factor.

From Figure 6.13 it is seen that for high pressures the CO₂ conversion starts to become limited to equilibrium conversion. The dilution factor has a strong influence on the CO₂ conversion since it directly influences the reaction rate. The closer the dilution factor (more active catalyst) is to 1.0 the higher the CO₂ conversion becomes. A decreasing dilution factor influences the CO₂ conversion strongly as the CO₂ conversion for $\zeta = 0.6$ is far away from $\zeta = 0.8$ or 1.0, mainly at lower pressure levels. In addition, the influence of temperature becomes smaller the higher the dilution factor is.

As discussed in section 6.2, the high CO₂ conversion comes at a price of a high runaway temperature in the methanation reactor. In order to operate at high pressure the dilution factor has to be reduced to reduce the reaction rate and thus the CO₂ conversion. See Figure 6.14 for the runaway temperature in the methanation reactor for three levels of the dilution factor (and two levels of methanation temperature) as a function of pressure.

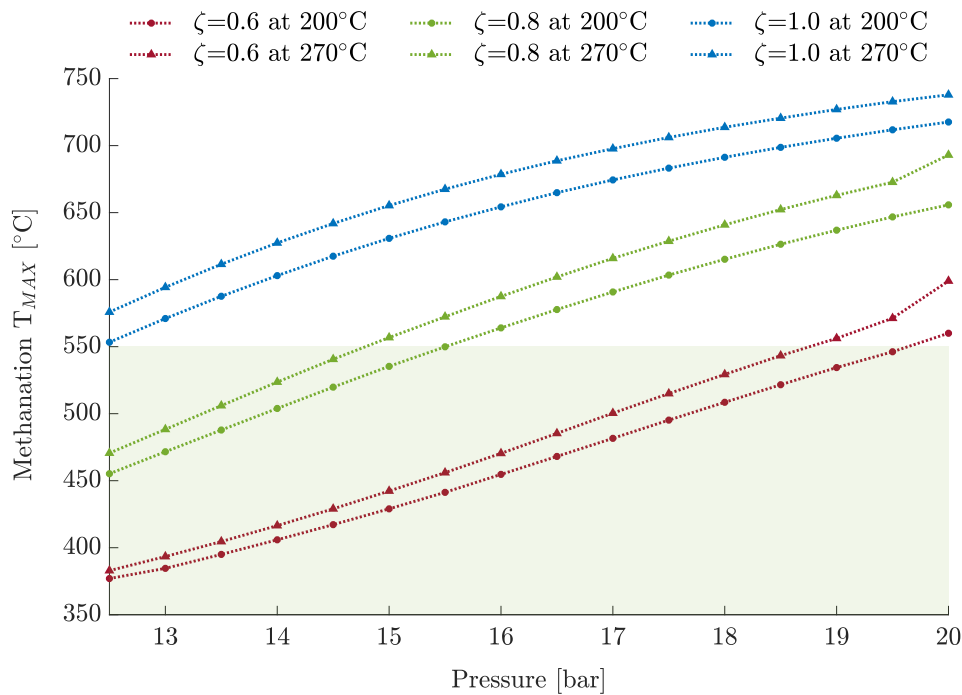


Figure 6.14: Runaway temperature at 200°C (circle) and 270°C (triangle) as function of pressure and dilution factor.

Figure 6.14 gives an indication of the required dilution factor for methanation to ensure that the temperature is kept within limits. For a dilution factor of 1.0 the runaway temperature is above the limits even at low pressure while a dilution factor of 0.6 opens up the possibility to operate at pressures close to 20 bar. From this figure it becomes evident that the main case study in Section 6.1 could have been operated at 19 bar while maintaining the temperature limit or the dilution factor could have been increased to around 0.7 while keeping the other operating conditions similar. This would have increased the CO₂ conversion with almost 10%. As a consequence, the gas purification demand is decreased which in turn would decrease the membrane area and recycle flowrate making the energy efficiency increase. Although this would be a good option to improve the system further, operating at higher temperatures makes the operability of the process more critical.

In addition, the runaway temperature is dependent on the coolant temperature (here 300 °C) too. Decreasing the methanation temperature could be interesting to reduce methanation runaway further.

The membrane area as a function of pressure for three dilution factors is illustrated in Figure 6.15.

As discussed earlier, a lower dilution makes the CO₂ conversion decrease which increases the gas purification requirement of the polyimide membrane. At a pressure of 12.5 bar the membrane area is around 40000 m² at a dilution factor of 0.6 while only 30000 m² is required at a dilution factor of 1.0 at the same pressure. The operational pressure has a higher impact on the membrane area requirement than the dilution factor and as was noted before, it seems to have an inverse relation to the CO₂ conversion for varying pressure.

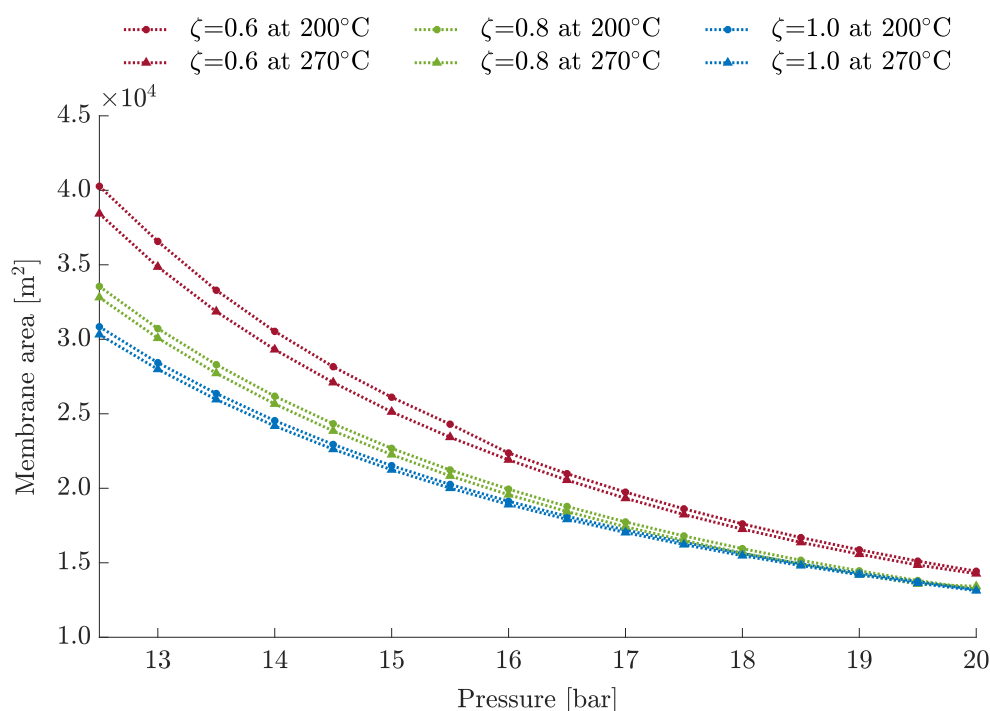


Figure 6.15: Membrane area at 200°C (circle) and 270°C (triangle) as function of pressure and dilution factor.

Figure 6.16 illustrates the recycle molar flowrate (columns) and CH₄ molar fraction (dotted lines) for three pressure levels and dilution factors and two temperature levels.

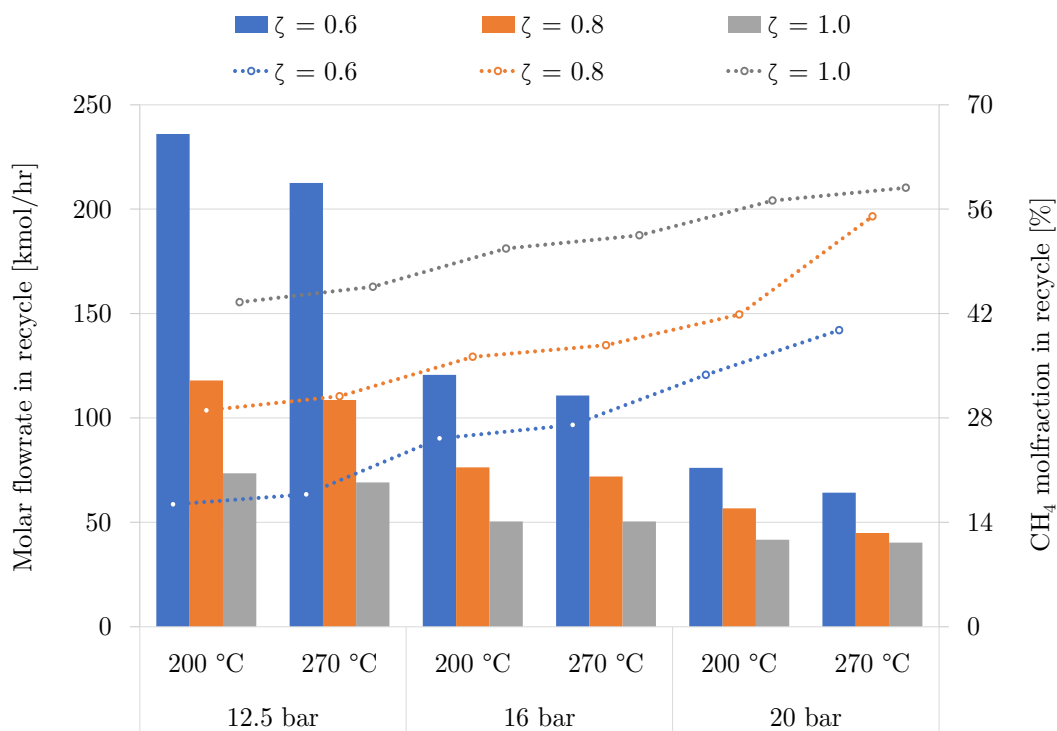


Figure 6.16: Recycle flowrate (column) and composition (line) as function of the catalyst dilution factor for different pressure and temperature levels.

The recycle molar flowrate is dependent on the pressure and dilution factor more than the temperature level and decreases strongly with an increasing pressure and dilution factor. This can be related back to the CO₂ conversion of the methanation process. At $\zeta = 0.6$ and 12.5 bar, the recycle molar flowrate is around 70-80% of MUG. As stated before this is unwanted because the equipment size needs to be larger to incorporate the higher volumes and more compressor work is required. The mol% of CH₄ in the recycle is increasing with pressure as well as the dilution factor.

Figure 6.17 illustrates the energy efficiency based on the LHV for the process as a function of pressure, temperature and dilution factor.

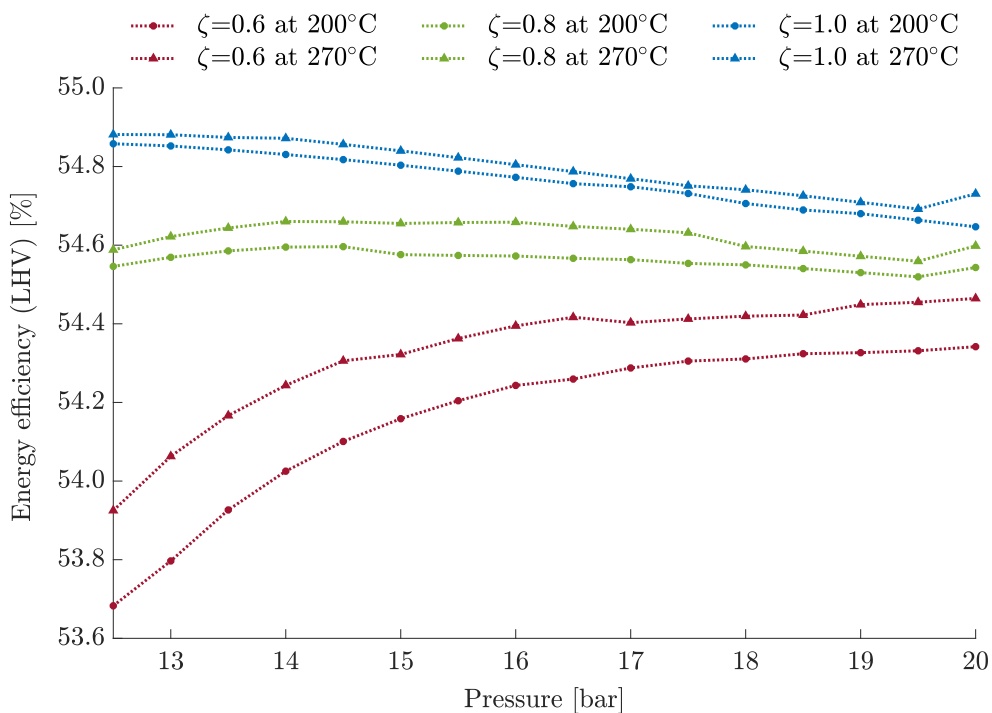


Figure 6.17: Energy efficiency at 200°C (circle) and 270°C (triangle) as function of pressure and dilution factor.

The electrical energy efficiency increases for a $\zeta = 0.6$ with increasing pressure because a higher amount of gas (from the recycle stream) needs to be recompressed. However, the higher $\zeta = 0.8$ and $\zeta = 1.0$ show a decreasing trend with pressure. Since the CO₂ ratio is similar at a high dilution factor, almost the same amount is to be recycled for each pressure level. Most likely, this decreasing trend in the energy efficiency is caused by the higher compressor work required to compress a feed gas to a higher pressure level.

6.4 Influence of H₂/CO₂ Ratio

in this section, the H₂/CO₂ ratio in the MUG is varied between 3.99 and 4.02 while keeping the methanation temperature and pressure at 250 °C and 16 bar for a dilution factor of 0.6. The reason for the small range of varying the H₂/CO₂ ratio in the MUG is the difficulty in convergence of the model further away from a stoichiometric H₂/CO₂ ratio in MUG. For all the studies before, the H₂/CO₂ ratio in MUG was kept at a stoichiometric ratio of 4.0.

The influence of the H₂/CO₂ ratio in the MUG is illustrated in Figure 6.18 on the H₂/CO₂ ratio in the recycle (calculated from reactants material stream) and the electrolysis power requirement.

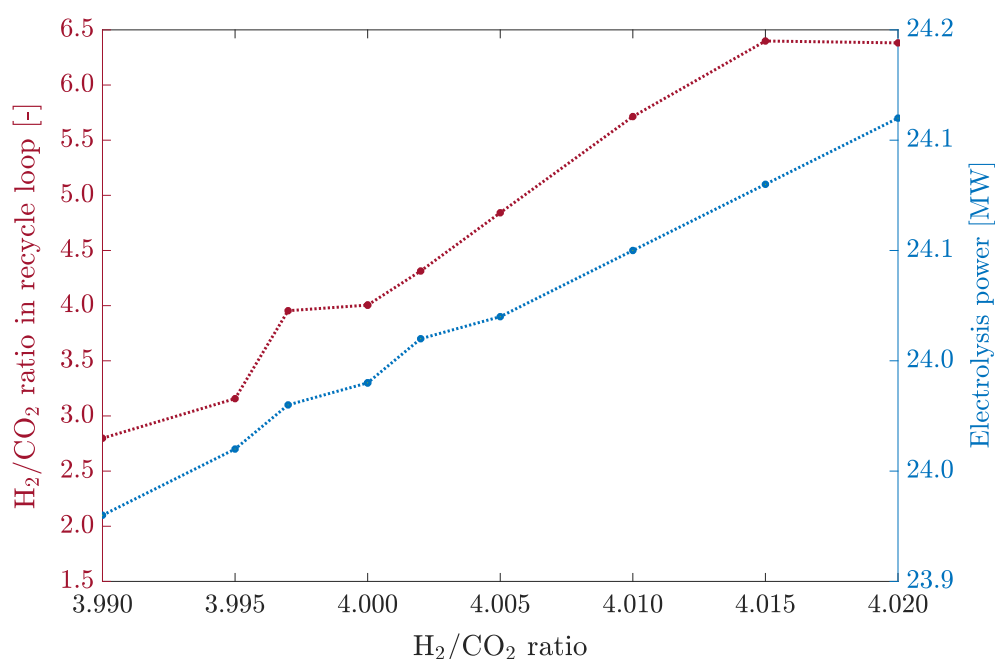


Figure 6.18: H₂/CO₂ in recycle loop and electrolysis power as function of the H₂/CO₂ ratio.

The influence of the H₂/CO₂ ratio in the MUG on the H₂/CO₂ ratio in the recycle is evident from Figure 6.18. Changing the H₂/CO₂ ratio in the MUG to 4.005 already increases the H₂/CO₂ ratio in the recycle to 4.84 which makes the reactants material stream highly overstoichiometric for the methanation reaction. Lower H₂/CO₂ ratio in the MUG also results in a highly understoichiometric ratio for the methanation reaction. Increasing the H₂/CO₂ ratio in the MUG stream will increase the electrolysis power demand because more H₂ has to be produced.

The CO₂ conversion in Figure 6.19 seems to show an optimum around 4.000 and 4.002 for the specified operational conditions. A higher H₂/CO₂ ratio in the recycle will make CO₂ the limiting component making the CO₂ conversion increase in theory. However, a dilution of the reactants feed will counteract the CO₂ conversion increase because of the decreasing reaction rate, shown in the kinetic validation Figure 5.7b. The temperature runaway decreases with an increasing H₂/CO₂ ratio in MUG which is related to the increase of the recycle molar flowrate at higher ratios since the leftover

H_2 has to be recycled and the decrease of CO_2 conversion.

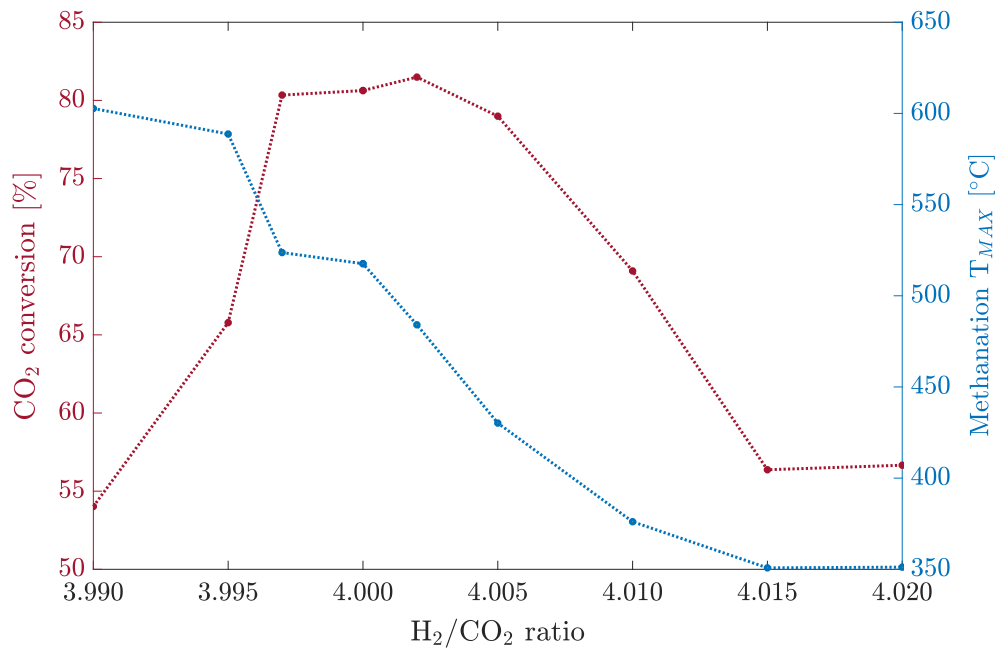


Figure 6.19: CO_2 conversion and runaway temperature as function of the H_2/CO_2 ratio.

Figure 6.20 illustrates the energy efficiency based on LHV and the compressor work as a function of the H_2/CO_2 ratio in the MUG. The variables seem to have an inverse relationship to each other which means that the compressor work amplifies the increase of electricity more than the increase of electrolysis power required due to the larger recycle flowrate.

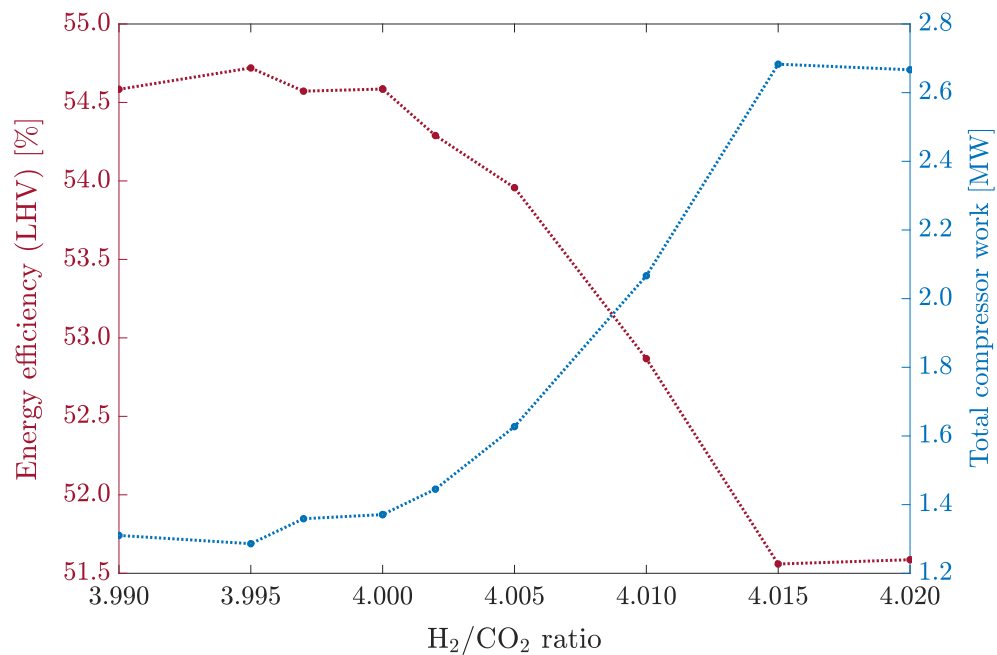


Figure 6.20: Energy efficiency and total compressor work as function of the H_2/CO_2 ratio.

The higher recycle flowrate required at higher H_2/CO_2 ratio in the MUG can be found back in Figure 6.21. Here, an overstoichiometric ratio causes both the membrane area to increase in order to obtain the quality requirements as well as an increase of the stage-cut of the membrane (Moles at membrane inlet/Moles at permeate outlet).

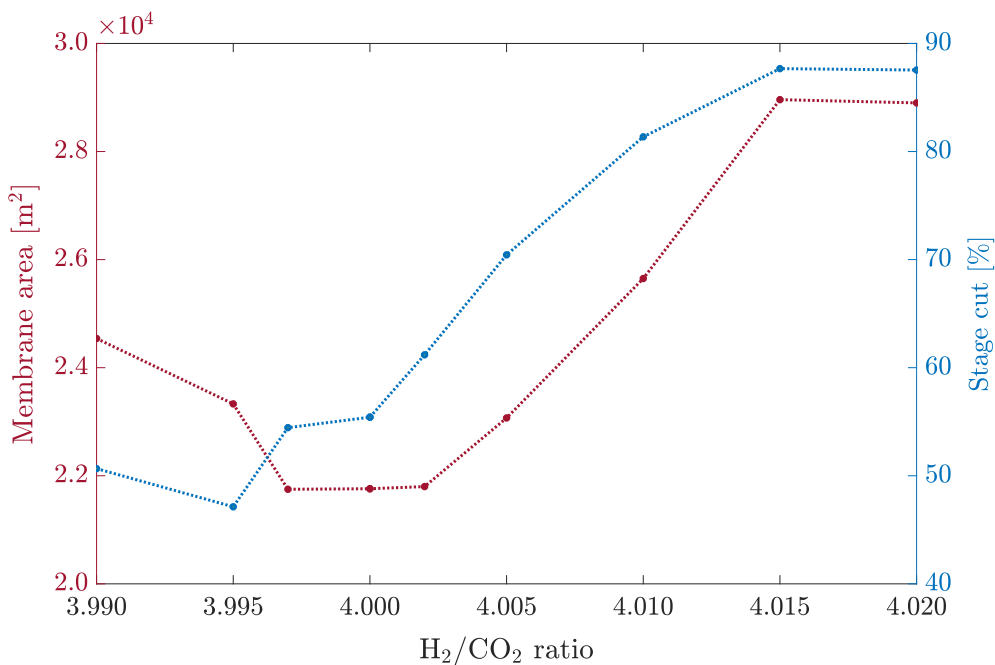


Figure 6.21: Membrane area and stage-cut as function of the H_2/CO_2 ratio.

Figure 6.21 indicates that the optimal H_2/CO_2 ratio in the MUG is close to 4.0 since the membrane area is minimised and the stage-cut relatively low.

The cost involved in a project are classified into capital expenditures (CAPEX) and operating expenditures (OPEX). The CAPEX are cost associated with the construction of a new plant and is estimated, in this case, based on capital cost estimates for similar process equipment retrieved from Sinnott & Towler [17] and Woods [29]. In combination with cost factors, the CAPEX or total investment cost is found with an accuracy of around 30-50%. Whereas OPEX are cost associated with the production that consists of fixed (e.g. operation) and variable (e.g. utilities) cost [17]. In this chapter, a cost estimation will be performed for the main case study as discussed in Section 6.1 and is noted in both United States Dollars (USD) and Norwegian Kroner (NOK) with an exchange rate of 0.11 USD/NOK.

7.1 Capital Expenditures (CAPEX)

The capital expenditures of the Power-to-Methane plant are estimated with the factorial method as described in Sinnott & Towler [17]. The method steps can be presented as:

1. Simulate the plant and prepare material and energy balances.
2. Size equipment units and select materials of construction.
3. Estimate the equipment cost from similar equipment using historic data.
4. Relate historic equipment cost to current equipment cost.
5. Estimate the installed (ISBL - inside battery limit) cost using cost factors.
6. Estimate the offsite (OSBL - outside battery limit), engineering and contingency cost.
7. Calculate the fixed capital investment cost (C_{FC}) as the sum of 5) and 6).
8. Estimate the working capital as a percentage of C_{FC} .
9. Sum the fixed and working capital cost to find the total investment cost (CAPEX).

7.1.1 Equipment Cost

The equipment cost (C_e) are determined in carbon steel using mainly Sinnott & Towler [17] as a data source. However, in the case that the type of equipment is not available or the size is outside the limits of data from Sinnott & Towler [17] it is possible to extract correlations from Woods [29] instead.

When Sinnott & Towler [17] data source is used, the equipment cost are estimated by Equation 7.1.

$$C_e = a + B \cdot S^n \quad (7.1)$$

Where, a and b are the cost correlation constants, S is a size parameter with equipment specific units, and n is the exponent determining the economy-of-scale effect. Here, a , b and S are given values from literature [17] for the specific equipment type while S is retrieved from the simulation. Typically n is less than one, meaning that the cost/size ratio decreases with increasing size of the equipment. Making it relatively more expensive to buy small units compared to large units [29].

The equipment cost estimation using the data from Woods [29] is based on the cost of a reference unit and is related to a size ratio as well as exponent n . Here, the reference cost is usually noted in free-on-board (FOB) cost. The equipment cost data from Woods is estimated by Equation 7.2.

$$C_e = \text{Reference cost} \left(\frac{\text{Equipment size}}{\text{Reference size}} \right)^n \quad (7.2)$$

To find out how the equipment costs are estimated for each process component, see Appendix D.

However, the estimated equipment cost in both cases uses historical data that are subject to inflation and need to be updated to relate the historic cost to present cost [17]. This is done on the basis of the Chemical Engineering Plant Cost Index (CEPCI), as in Equation 7.3.

$$C_e \text{ in year } A = C_e \text{ in year } B \left(\frac{\text{CEPCI value of year } A}{\text{CEPCI value of year } B} \right) \quad (7.3)$$

Where, the CEPCI values can be seen in Table 7.1.

Table 7.1: CEPCI values for Sinnott & Towler (2007), Woods and current day

Cost index	CEPCI value	Year	Source
Woods	1000	-	[29]
Sinnott & Towler	509.7	2007	[17]
Current day	607.5	2019	[30]

7.1.2 Installed Cost

From the inflation corrected equipment cost obtained from Equation 7.3 the ISBL or installed cost can be estimated. This cost includes equipment erection, piping, instrumentation and control, electrical, civil, structures and buildings, lagging and paint and material [17]. The contribution of each item is calculated by multiplying the equipment cost by several factors as seen in Equation 7.4 and 7.5.

$$C = \sum_{i=1}^{i=M} C_{e,i,CS} \left[(1 + f_p) f_m + (f_{er} + f_{el} + f_i + f_c + f_s + f_l) \right] \quad (7.4)$$

$$C = \sum_{i=1}^{i=M} C_{e,i,SS} \left[(1 + f_p) + (f_{er} + f_{el} + f_i + f_c + f_s + f_l) / f_m \right] \quad (7.5)$$

Where $C_{e,i,CS}$ is the cost of equipment i in carbon steel, $C_{e,i,SS}$ is the cost of equipment i in stainless steel, M is the number of equipment units and the f factors and their typical values are given in Table 7.2. Factor f_m is not equal to the ratio of the metal price itself but also includes labour cost, overheads, etc. that do not scale directly with the metal price [17]. Therefore, two expressions are used to calculate the installed cost.

Table 7.2: Typical installation factors for fluid type processes [17].

Cost factor	Installation factor description	Value
f_p	Installation factor for piping	0.8
f_m	Installation factor for material type	1.0/1.3*
f_{er}	Installation factor for equipment erection	0.3
f_{el}	Installation factor for electrical work	0.2
f_i	Installation factor for instrumentation and process control	0.3
f_c	Installation factor for civil engineering work	0.3
f_s	Installation factor for structures and buildings	0.2
f_l	Installation factor for lagging, insulation or paint	0.1

* 1.0 for carbon steel (c/s) and 1.3 for stainless steel (s/s).

After calculating the individual equipment cost as done in Appendix D, the cost is multiplied with the cost installation factors to find the installed cost of the equipment. To avoid corrosion, the process is designed in stainless steel type 304. The results are summarised in Table 7.3.

Table 7.3: Equipment cost (C_e) and installed cost (C) for main process components.

	Equipment cost		Installed cost			
	MUSD	MNOK	MUSD	MNOK		
Alkaline electrolyser	10.80	98.16	40.38	367.11		
Centrifugal compressors	2.54	23.12	9.51	86.47		
Polyimide membrane	0.44	3.96	1.63	14.79		
Heat exchangers	0.38	3.41	1.40	12.76		
Multi-tubular methanator	0.07	0.67	0.27	2.49		
Centrifugal pumps	0.03	0.31	0.13	1.14		
Knock-out vessel	0.03	0.30	0.09	0.86		
	C_e	14.29	129.91	C	53.42	485.62

A graphical representation of the installed cost (C_e) is given in Figure 7.1.

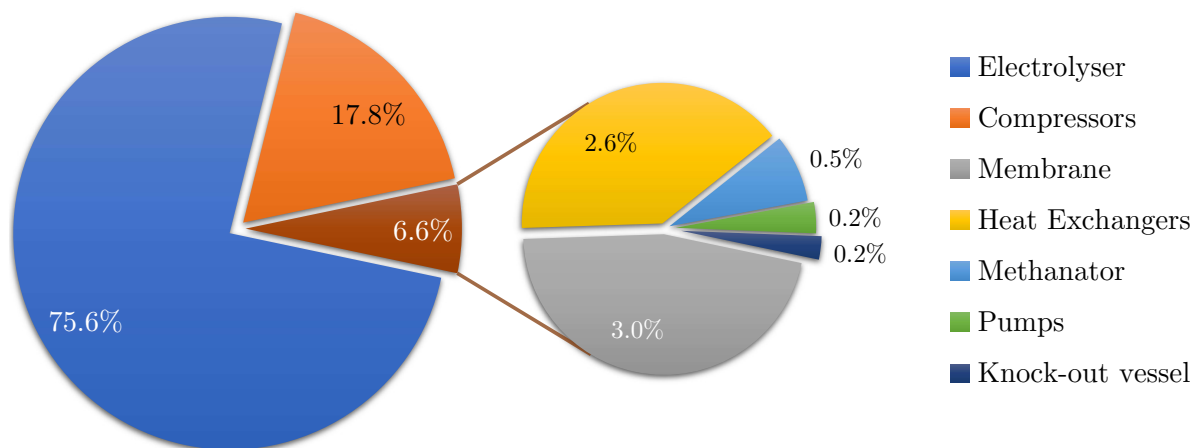


Figure 7.1: Installed equipment cost (ISBL - for stainless steel 304).

Figure 7.1 clarifies that the equipment/installed cost is dominated by the capital expenditures for the alkaline electrolyser unit. More than 3/4 part is the cost for the electrolyser. Interesting is that the methanation unit, pumps and knock-out vessel equipment cost is practically neglectable.

7.1.3 Fixed Capital Cost

After the equipment is sized and cost estimated with the above expressions and cost factors, the fixed capital cost of the PtM plant can be determined. The fixed capital investment cost (C_{FC}) is given in Equation 7.6.

$$C_{FC} = C(1 + OSBL)(1 + D\&E + X) \tag{7.6}$$

Where, C is the installed equipment cost (often referred to as ISBL) obtained from Equation 7.4 and 7.5, $OSBL$ is the cost factor for offsites (the cost of additions that must be made to the site infrastructure to accommodate the new plant), $D\&E$ is the cost related to design and engineering of the plant and X is contingency cost which are extra cost added into the budget to allow for variation from the cost estimate [17].

Because of the well developed infrastructure at the Skogn plant, the fixed capital cost factors $OSBL$ (normally between 10-50% of ISBL) and $D\&E$ (normally between 10-30% of OSBL+ISBL) are reasonably lower compared to building a new plant. In this case 10% of ISBL and 15% of ISBL+OSBL, respectively. However, because of techno-economical uncertainties in estimating the electrolyser, methanator and membrane process components accurately the contingency factor is taken to be relatively high (normally between 10-50% of OSBL+ISBL). In this case 25% of OSBL+ISBL [17].

The total fixed capital cost (CAPEX) results are given in MUSD and MNOK in Table 7.4. Note that the CAPEX is around 5.7 times higher than the equipment cost calculated.

Table 7.4: CAPEX of the PtM plant for the main case study.

Cost parameter	MUSD	MNOK
Equipment cost in 2019 (C_e)	14.29	129.91
Installed cost or ISBL (C)	53.42	485.62
Offsites or OSBL	5.34	48.56
Engineering or D&E	8.81	80.13
Contingency or X	14.69	133.55
Fixed capital cost (CAPEX)	82.26	747.85

7.2 Operating Expenditures (OPEX)

The operational expenditures or production cost are associate with the production of the plant and can be divided into the variable cost that are proportional to the plant output or production rate of the plant and fixed cost that are present regardless of the plant output or production rate [17]. It is assumed that the plant is operational 96% of the time (8409.6 hour/year).

7.2.1 Variable Cost of Production

The variable cost for this process consist only of utilities. The electricity price is the average of the last 5 year in Norway [31] taken as 319 NOK/MWh and the price for water for cooling and the electrolyser from Sinnott & Towler [17] taken as 0.53 USD/m³.

Table 7.5: Variable cost of production for the main case study.

Equipment	Size of equipment	MUSD/year	MNOK/year
Pumps	24.0 kW	0.01	0.06
Compressors	1371.0 kW	0.40	3.62
Electrolysers	23993.9 kW	6.97	63.36
Fresh water	16.7 m ³ /hr	0.07	0.68
Utility cost		7.45	67.72

7.2.2 Fixed Cost of Production

To operate the new part of the plant, it is assumed that one more operator is required for each shift (4 shifts per day) next to the already present shift operators. The salaries for operators varies by region and experience level, but for an initial estimate an average salary of 60000 USD/(shift operator-year) is taken. The supervision of the operator and direct salary overhead (cost of benefits, payroll taxes, health insurance, etc.) are excluded from this salary. In addition, the fixed cost of production for this plant there are cost for maintenance (electrolyser stack replacement, catalyst replacement, membrane replacement, general maintenance), taxes and insurance and a general plant overhead cost for functions such as human resources, research and development, finance, etc. The fixed cost of production is summarised in Table 7.6.

Table 7.6: Fixed cost of production for the main case study.

Cost parameter	Estimate based on	MUSD/year	MNOK/year
1) Operating labour	One operator per shift	0.24	2.18
2) Supervision	25% of 1)	0.06	0.55
3) Direct salary overhead	50% of 1) + 2)	0.15	1.35
4) Maintenance	3% of ISBL cost	1.60	14.57
5) Taxes and Insurance	1% of ISBL cost	0.53	4.86
6) General plant overhead	50% of 1) + 2) + 3)	1.03	9.33
Fixed cost of Production		3.61	32.85

8.1 Profitability Evaluation

8.1.1 Revenues

The revenues of the process consist out of the product that consists of biomethane of high purity and the byproduct steam. The steam produced from the exothermic heat release and compression can be used for heat integration of the PtM process, equipment present at the Biokraft plant in Skogn, or used for steam explosion. The steam gives an indirect revenue and is therefore taken into account for calculating the total revenue of the plant.

The value of the biomethane of liquefaction quality is uncertain. A five-year average of the LNG price gives a cost price of around 2 NOK/Sm³ [32]. However, an estimated value was given by my supervisor that is in contact with the plant in Skogn. The value of steam is dependent on the pressure of the steam but is taken as an average [17]. In this process, there is low level steam (<10 bar) as well as high level steam (86 bar) produced. The value of the steam and biomethane produced from the process is given in Table 8.1.

Table 8.1: Variable cost of production for the main case study.

Product	Size of product	Value	MUSD/year	MNOK/year
Biomethane	1417.8 Sm ³ /hr	8 NOK/Sm ³	10.49	95.39
LP/HP Steam	11.11 tonnes/hr	7.31 USD/tonne	0.68	6.21
Total revenue			11.18	101.59

The total revenue of biomethane and steam in Table 8.1 is 11.18 MUSD/year while the sum of the variable cost and fixed cost of production is 11.06 MUSD/year. This is a good indication that the process is not profitable since the fixed capital cost of 82.26 MUSD must also be financed over the lifetime of the plant.

8.1.2 Production Cost per kg

An interesting variable for the profitability is the cost for the production of one kilogram of biomethane. In that case the variable cost of production (VCOP), fixed cost of production (FCOP) and fixed capital investment (FC) must be taken into account. To do this, the annualised cost method can be used. First, the annual capital charge ratio (ACCR) must be determined with Equation 8.1.

$$ACCR = \frac{[i(1+i)^n]}{[(1+i)^n - 1]} \quad (8.1)$$

Where, i is the interest rate of 6% and n is the lifetime of the plant in years (assumed to be 20 years). The ACCR determines the fraction of interest that must be paid each year for the equipment over the lifetime, so that the capital cost can be related to VCOP and FCOP. After determining ACCR, the total annualised cost (TAC) can be found with Equation 8.2.

$$TAC = (VCOP + FCOP) + ACCR \cdot FC \quad (8.2)$$

With TAC, it is possible to determine the production cost of one kilogram of biomethane. The results are summarised in Table 8.2.

Table 8.2: Production cost based on plant capacity and TAC.

	Value	Unit
Production capacity	8390258	kg/yr
Production cost (VCOP + FCOP)	11.06	MUSD/yr
Fixed capital cost (FC)	82.26	MUSD
Total annual cost (TAC)	18.23	MUSD/yr
Production cost per unit	2.17	USD/kg CH ₄
Production cost per unit	19.8	NOK/kg CH ₄
Production cost per unit	1.53	USD/Sm ³ CH ₄
Production cost per unit	13.9	NOK/Sm ³ CH ₄

The cost price for producing methane with this configuration seems not to be profitable. The total revenues per year are 11.06 MUSD/year while the TAC is 18.23 MUSD/year. In addition, the production cost per unit of methane is much higher than the before specified cost price of 8 NOK/Sm³.

8.1.3 Net Present value and Cash Flow

To understand the profitability better and find the economic feasibility, the net present value (NPV) is determined. The NPV is a measure of the economic performance of the plant. If NPV is positive,

then the project is profitable while a negative NPV indicates that the plant has an economic loss and can be determined from Equation 8.3.

$$NPV = \sum_{n=1}^{n=t} \frac{CF_n}{(1+i)^n} \quad (8.3)$$

Where, CF_n is the cash flow in year n , t is the plant lifetime in years (assumed to be 20 years) and i is the interest rate (is assumed to be 6%). Furthermore, a tax rate of 22% [33] and a straight-line depreciation is taken in account over a 10 years period after receiving revenues. The straight-line depreciation (calculated in Equation 8.4) is an allowance for "wear and tear, deterioration or obsolescence of the property" which is a result from its use [17].

$$D_i = \frac{C_{FC}}{n} \quad (8.4)$$

Where D_i is the depreciation charge in year i , C_{FC} is the capital investment cost and n is the period of depreciation in years. All calculations are done in an `Excel` sheet from Sinnott & Towler [17].

In Section 8.1.2 it became clear that the current cost price of 8 NOK/Sm³ to produce methane is too high for a profitable project. Therefore, Figure 8.1 illustrates the NPV for higher product cost prices to give an indication of the cost price needed to make the plant profitable. A current and future scenario is given.

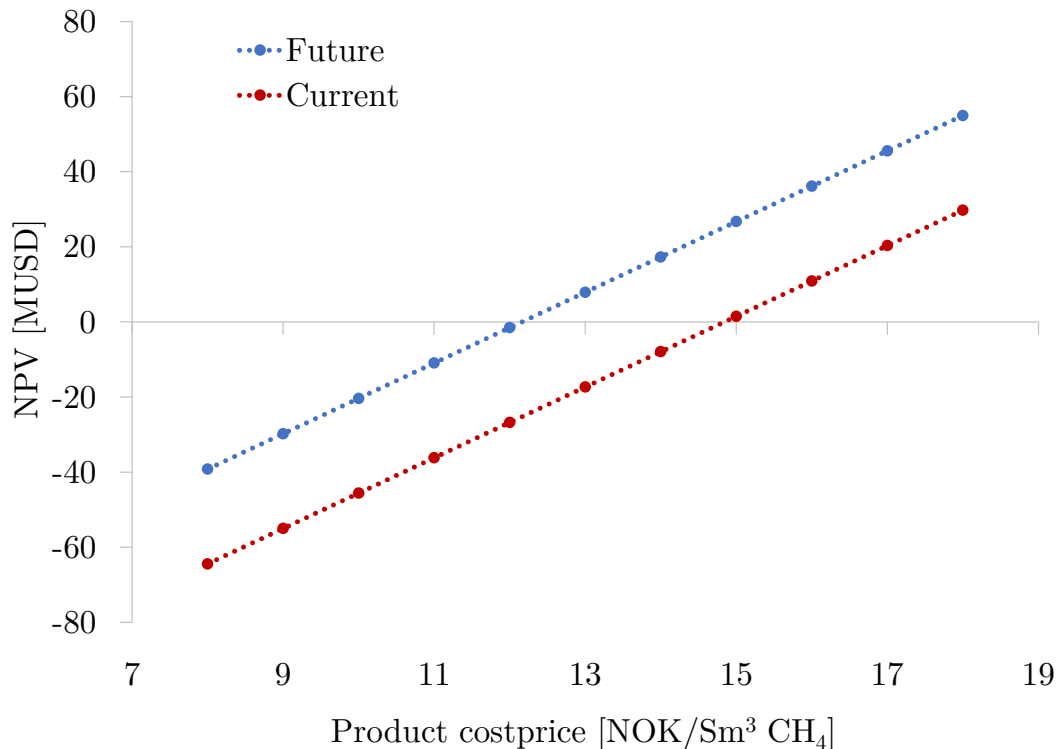


Figure 8.1: Net present value (NPV) for current and future electrolysis cost.

The current scenario (red dotted line) illustrates the product cost price from the cost estimation done in Chapter 7. Here, the electrolyser unit costs 450 USD per kW installed and the electricity price is 314 NOK per MWh. For this scenario 15 USD/Sm³ CH₄ is required to reach a profitable case. However, the actual model of the plant made is for the production capacity of a new phase of the Biokraft plant in Skogn possibly started up in 5-10 years. Over the years, it is expected that these prices will decrease, and therefore, a future scenario is estimated (blue dotted line). In that case, the electrolyser cost is expected to go down to 350 USD/kW installed and the cost for electricity becomes 250 NOK/MWh. This makes the project profitable at a price of 12.5 NOK/Sm³ CH₄ (which is still relatively high compared to 8 NOK/Sm³). The analysis of both scenarios is described in Appendix D.

For this future scenario case, the economic analysis can be further displayed. From the start of the investment, there will be cash flows going in and out to realise the project. This cash flow can be visualised in a cash-flow diagram showing the cumulative cash flow over the plant lifetime [17].

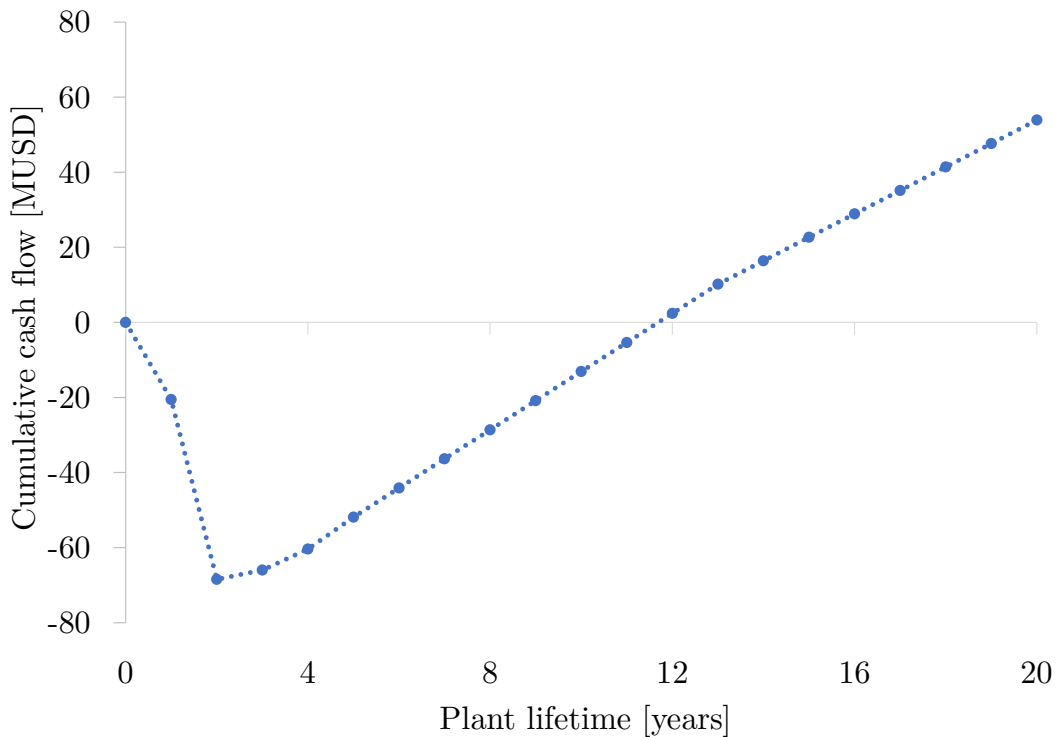


Figure 8.2: Cumulative cash flow for future electrolysis cost process at 12.5 USD/Sm³ CH₄.

Figure 8.2 illustrates that the the future scenario becomes break-even at around 12 years after the initial investment with an NPV of 3.2 MUSD and cumulative cash flow of 55.0 MUSD after a lifetime of 20 years. Although this is an profitable case, the prices used for the future scenario are uncertain.

8.2 Sensitivity Analysis

Because of the uncertainty in prices, a sensitivity analysis is performed by varying the base values with a percentage to see the effect on the NPV of the plant. The base case values for the sensitivity analysis are taken for the future scenario discussed previously where the value of methane produced at the plant is 12.5 USD per $\text{Sm}^3 \text{CH}_4$, the electrolysis cost is 350 USD per kW installed capacity and the electricity price is 250 NOK per MWh (27.5 USD/MWh). The interest rate (6%), tax rate (22%), lifetime (20 years, 8410 hours/year), depreciation period as well as the other capital and operating expenditures are kept equal. The sensitivity analysis changes the base values with 40%.

	-40%	-20%	0%	20%	40%	Unit
Value of Methane	7.5	10.0	12.5	15.0	17.5	NOK/ Sm^3
NPV	-43.9	-20.3	3.2	26.7	50.3	MUSD
Electrolysis cost	210	280	450	420	490	USD/kW installed
NPV	23.5	13.3	3.2	-6.9	-17.0	MUSD
Electricity cost	150	200	250	300	350	NOK/MWh
NPV	20.1	11.6	3.2	-5.2	-13.7	MUSD

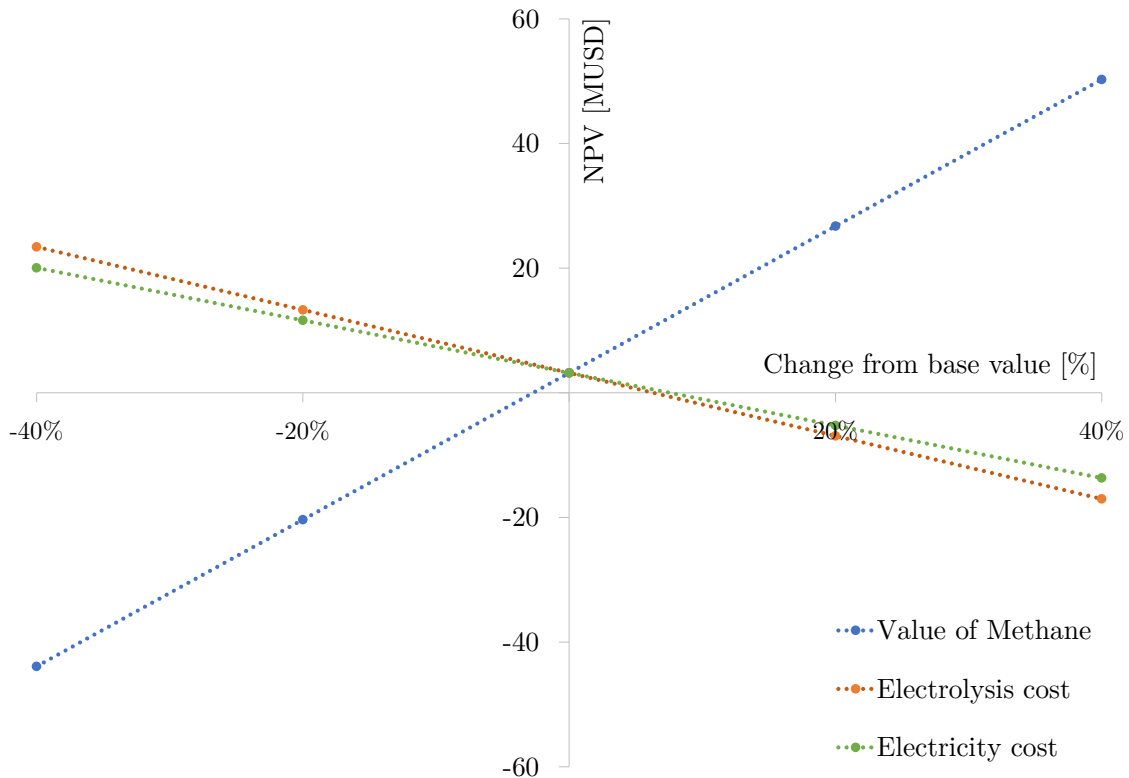


Figure 8.3: NPV sensitivity as a function of product value, electrolyser cost and electricity cost.

Figure 8.3 shows that the value of methane has the largest effect on the NPV of the plant while the electrolysis cost and electricity cost are relatively similar to each other (electrolyser capital cost

slightly larger effect). Furthermore, the NPV value of the base case (future scenario) is close to origin where a small change from the base value makes the profitability negative.

The electricity price is of large importance for the profitability of the process. In Figure 8.4 the monthly averaged electricity price for Norway is illustrated.

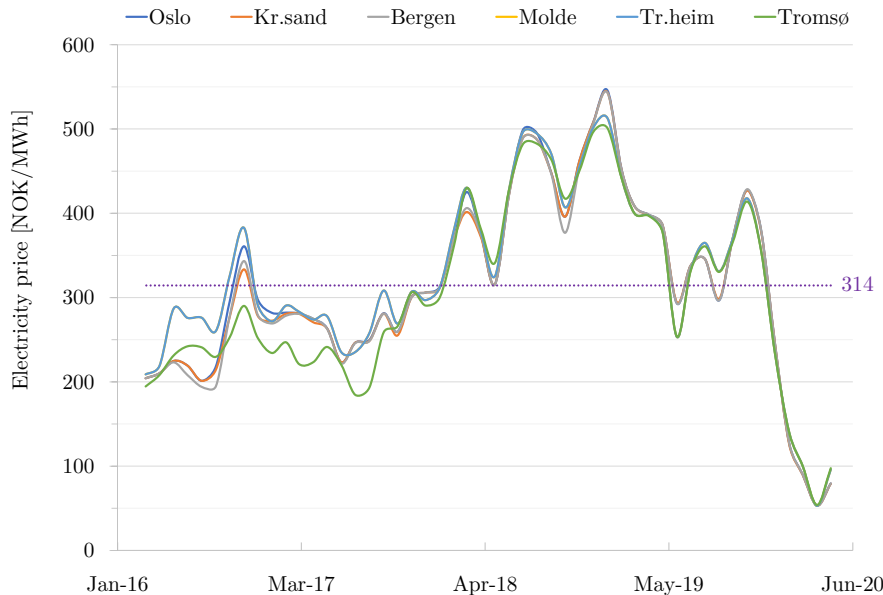


Figure 8.4: Norwegian day-ahead electricity prices for five locations (monthly averaged) [31].

The electricity price in Norway is relatively low compared to other European countries due to the large scale electricity production from hydropower. In the last months, the electricity price has decreased significantly from the four year average shown in purple due to COVID-19.

However, even with the low price of 100 NOK/MWh the plant can not become profitable if the value of methane is kept on 8 USD/Sm³ CH₄.

In this chapter the findings and assumptions of the simulation and economics chapters are discussed for the Power-to-Methane process including an alkaline electrolyser, multi-tubular methanation reactor and polyimide membrane.

9.1 Kinetics

The kinetics implemented in the MATLAB methanation model are for a nickel-aluminium catalyst with a considerably fast reaction rate compared to other literature. The reaction rate expression for the CO₂ methanation reaction was fitted by Koschany [16] based on intrinsic reaction kinetics and a CO₂ dissociative reaction mechanism. The parameter estimation for the LHHW rate equation showed a relatively large standard deviation. However, their plug-flow methanation model estimated the experimental results accurately.

Because of the uncertainty in the reaction mechanism as discussed in Section 2.3.4 and relatively high parameter estimation uncertainty, the results obtained by using this kinetic model is limited to an extent. Other literature has suggested to model the CO₂ methanation reaction based on the CO methanation reaction together with the reverse water-gas shift (RWGS) reaction. However, these are often based on steam reforming catalysts and not specifically designed for methanation. From the thermodynamics of the methanation process it has been seen that the RWGS is not favourable at lower temperatures, and therefore, it was chosen to model the CO₂ methanation reaction on a methanation catalyst from Koschany.

Because of the relatively fast reaction rate of the NiAl catalyst from Koschany the CO₂ conversion will be higher compared to other possible methanation catalysts. As a result, the methanation runaway temperature is more critical for this catalyst and a slow reaction rate catalyst could help reduce the challenging heat management in the multi-tubular methanation reactor.

9.2 Simulations

The independent variables chosen for the main case study in Section 6.1 were based on a more optimal setting obtained from the case studies for the influence of temperature/pressure, dilution factor and H_2/CO_2 ratio in MUG from Sections 6.2, 6.3 and 6.4. However, most of the independent variables for the methanation reactor and catalyst were kept constant at similar values to literature or to limit the temperature runaway. Keeping these variables constant could have a great influence on the more optimal setting found from the simulation results. Especially the length, diameter and number of tubes as well as the void fraction, membrane thickness, permeance data and coolant temperature would be interesting to study in more detail. Therefore, the results are indicative but give a good first impression of the process modelled.

In the case that one of the before mentioned independent variables is varied the results will change. By varying the dimensions of the methanation reactor (length, diameter, number) changes are seen for the CO_2 conversion and internal temperature. A larger tube diameter or higher number of tubes decreases the superficial velocity in the tubes. As long as a sufficient velocity is reached, the CO_2 conversion is higher if not limited to equilibrium. However, this is at the cost of a higher and steeper temperature runaway which is to be prevented. Furthermore, increasing the tube length can improve the conversion but can be unnecessary since most of the reaction takes place close to the inlet of the reactor. A disadvantage of increasing the methanation reactor dimensions is the higher capital cost.

The coolant of the methanation reactor is evaporated to steam at constant high temperature and pressure. At the moment 300 °C is chosen to limit the methanation temperature runaway while maintaining sufficient driving forces to initiate the CO_2 methanation reaction and have a possibility for high pressure steam production. However, a lower temperature can definitively help reduce the methanation runaway temperature. Because of the feed-effluent heat exchanger, the inlet temperature was limited to 270 °C to maintain a sufficient ΔT_{min} . Increasing the coolant temperature increases the pressure of steam produced and allows the inlet temperature to be higher than 270 °C but will result in a higher runaway temperature (which is already limited even when the catalyst is diluted). Decreasing the coolant temperature below the inlet temperature would require an extra heat exchanger after the feed-effluent heat exchanger to have the inlet temperature high enough to initiate the reaction. A lower coolant temperature compared to the reactants temperature will increase the heat transfer between the gas and coolant at the inlet making the runaway decrease but decreases the pressure of steam generated. This indicates there might be an optimal point for the coolant temperature.

The area of the membrane is strongly dependent on the permeance data (selectivity of gas components), permeate pressure and thickness of the membrane. When the thickness of the membrane or permeate pressure is reduced then less area is required to achieve the required purity.

The results of the temperature/pressure case study indicate that the process parameters are highly

dependent on the pressure of the system but barely change for variations in temperature. Although the methanation reaction favours low temperatures, it is limited by kinetics and should result in a decrease of the CO₂ conversion at some point. The reason for not seeing the decrease of CO₂ conversion can be linked to the relatively high coolant temperature that together with the exothermic heat ensures a high conversion. This hypothesis was confirmed since the CO₂ conversion became 46.5% by changing the coolant temperature to 280 ° with an inlet temperature of 250 °C, pressure of 16 bar(a) and $\zeta = 0.6$. Suggesting that the coolant temperature can be reduced slightly from 300° to reduce methanation runaway. Leaving the possibility of operating at a higher dilution factor when the coolant temperature is decreased. Nevertheless, a strong decrease in the CO₂ conversion is seen from 80.6% to 46.5% by decreasing the coolant temperature from 300 to 280 °C, respectively.

From the results it can also be noted that the system favours a high operating pressure to maximise the CO₂ conversion and energy efficiency while minimising the membrane area and recycle requirements. The main challenge of operating at high pressure is the temperature runaway. From the dilution factor case study, it became clear that the temperature runaway can be maintained by decreasing the dilution factor. These observations indicate that a more diluted catalyst (lower dilution factor) is required to limit the reaction rate and thus the CO₂ conversion and temperature runaway when the goal is to operate at high pressure levels.

The results for the H₂/CO₂ ratio case study indicates that the optimal operating point is near a stoichiometric ratio of H₂/CO₂ = 4.0. Operating above or below this ratio contaminates the product with either CO₂ (above) or H₂ (below) and reduces the reaction rate. On the one hand, an overstoichiometric ratio in the recycle causes H₂ to be in excess at the reactants material stream, making CO₂ the limiting component in the CO₂ methanation reaction so that the CO₂ can be converted up to 100%. This will result in the requirement for a higher H₂ production, separation and compression but makes it less challenging to reach the 50 ppm CO₂ product quality requirement, as can be seen in Figure 6.19 for a H₂/CO₂ ratio of 4.002. On the other hand, increasing the H₂/CO₂ ratio in the MUG will increase the electrolysis power demand because more H₂ has to be produced which in turn also decreases the energy efficiency of the process.

The energy efficiency based on the LHV illustrated in Figures 6.12, 6.17 and 6.20 is around 54-55% and can be increased by taking into account the turbine cycle. In that case around 1MW can be recovered from the steam generation. To more accurately determine the energy efficiency, the exergy needs to be determined after performing a heat integration to include the energy consumption from heating/cooling the system. Doing a heat integration also improves the knowledge about the different pressure levels of steam produced in the plant.

The profiles in Sections 6.2, 6.3 and 6.4 indicate that the model might have some inconsistency and a limited accuracy because the profiles are not smooth. This can mainly be seen in Section 6.4 because these case studies were done by hand due to difficult convergence of the model to reach the specified

H_2/CO_2 ratio in MUG. Since the H_2/CO_2 ratio was adjusted less than one percent from its base (only from 3.99 to 4.02), the discussions and conclusions have to be approached with care. In practice, it is difficult to control the H_2/CO_2 ratio with less than 1% accuracy because of measurement difficulties and errors related to composition control.

When renewable electricity is used to support the production of green hydrogen for the plant, it is not only required that the electrolyser is able to operate dynamically with a varying load but also the rest of the plant. This makes it extra challenging to operate the plant. One option to maintain a steady operation of the plant is to use electricity from the grid even if it is not produced in a renewable way. Another option is to adjust the amount of CO_2 entering the Power-to-Methane process so that the H_2/CO_2 ratio is maintained or have storage of H_2 and CO_2 at the location.

9.3 Economics

The economic evaluation is based on a costing approach from Sinnott & Towler [17], Woods [29] and literature data for specialised equipment and utility cost. Especially the uncertainty about the cost for electrolyser equipment, product revenues and installation factors for equipment might explain an inaccurate determination of the cost of the process. In addition, the sensitivity analysis shows that the value of methane (not known exactly and dependent on the location) is very important for the profitability of the plant. Nevertheless, the cost evaluation gives a good first impression of the overall economics of the plant.

Since the equipment cost is strongly related to the scale as indicated in Equation 7.1, small units will be relatively expensive in capital cost compared to large scale units [17]. The uncertainty is therefore large in the sizing and costing for the heat exchangers because the process was not heat integrated with the process itself and other equipment present at the Biokraft plant in Skogn. For a more accurate cost estimation it is necessary to make a heat exchanger network (HEN) design where both the heat exchangers of the PtM plant and the Biokraft plant in Skogn are heat integrated.

The results indicate that the Power-to-Methane process with an alkaline electrolyser, multi-tubular methanation reactor and polyimide membrane is possible to be implemented to produce methane of liquefaction quality. Because of the high quality requirement, nearly all the CO₂ that enters the plant modelled is converted to CH₄. In fact, for a 1411.8 Nm³/hr flowrate from the amine absorption column CO₂ stream, it is possible to produce 1417.8 Nm³/hr which is nearly the same volume as the inlet. Therefore, by applying the Power-to-Methane process the productivity can be increased significantly while decreasing the CO₂ emissions of the plant without a requirement to expand the anaerobic digesters for the new phase of the Biokraft plant in Skogn.

The process models made in this work are similar to other work. The uncertainties are mainly located in the permeability data from of the membrane unit and the energy requirement for liquefaction. The MATLAB model made for the methanation reactor is of high interest for researchers in this area since the CO₂ methanation process was not often modelled in as much detail as done in this thesis.

The influence of temperature/pressure case study suggests that the Power-to-Methane process is favoured at higher operating pressure. However, this results in a higher reaction rate which in turn increases the temperature runaway. To solve this problem, it is possible to reduce the dilution factor to oppose the reaction rate as was found from the dilution factor case studies. This suggests that there must be an optimum that can be found at which the pressure can be maximised while maintaining a stable process.

Although the results indicate that the Power-to-Methane process can be stable operated and in a way that the quality requirements can be obtained, the cost analysis shows the negative side of the process. The production cost per Sm³ CH₄ is 13.9 NOK/Sm³ while the product is only worth 8 NOK/Sm³ CH₄. For this reason, the process is shown to not be profitable for now. However, as shown in the future case where the electrolysis cost goes down to 350 NOK/kW installed, the electricity price becomes 250 NOK/MWh and the value of methane becomes 12.5 NOK/Sm³ the NPV becomes positive. The cost estimation is based on the method described in Sinnott & Towler. The cost factors used and other estimated values for the capital and operational expenditures make the investment analysis uncertain and must be interpreted with care.

Further work on this topic can be done on the following points:

- Model the gas separation technique with more reliable permeance data.
- Model a different gas separation technique such as PSA or cryogenic.
- Model the Power-to-Methane process using a SOEC electrolyser to reduce the electricity demand and allow for an interesting heat integration case study.
- Request data for modelling the electrolyser more accurately.
- Model the interesting steam electrolysis and co-electrolysis techniques.
- Perform a heat integration of the Power-to-Methane process and equipment present at the location in Skogn to minimise the heating/cooling demand of the full plant.
- Find an optimal operating point from the pressure, temperature (coolant and inlet) and dilution factor using the heat integrated model.
- Perform more case studies with the MATLAB methanation model for limiting the runaway temperature by catalyst dilution and staged feed gas injection and possibly publish an article.

Bibliography

- [1] Karim Ghaib and Fatima-Zahrae Ben-Fares. Power-to-methane: A state-of-the-art review. *Renewable and Sustainable Energy Reviews*, 81:433–446, 2018.
- [2] Martín David, Carlos Ocampo-Martínez, and Ricardo Sánchez-Peña. Advances in alkaline water electrolyzers: a review. *Journal of Energy Storage*, 23:392–403, 2019.
- [3] Christina Wulf, Jochen Linßen, and Petra Zapp. Review of power-to-gas projects in europe. *Energy Procedia*, 155:367–378, 2018.
- [4] Manuel Götz, Jonathan Lefebvre, Friedemann Mörs, Amy McDaniel Koch, Frank Graf, Siegfried Bajohr, Rainer Reimert, and Thomas Kolb. Renewable power-to-gas: A technological and economic review. *Renewable energy*, 85:1371–1390, 2016.
- [5] M. Thema, F. Bauer, and M. Sterner. Power-to-gas: Electrolysis and methanation status review. *Renewable and Sustainable Energy Reviews*, 112:775–787, 2019.
- [6] Sander N. Wijnsma. Power-to-biomethane process simulation. Technical report, Norwegian University of Science and Technology (NTNU), 2019.
- [7] Bruna Rego de Vasconcelos and Jean-Michel Lavoie. Recent advances in power-to-x technology for the production of fuels and chemicals. *Frontiers in chemistry*, 7, 2019.
- [8] Robert Phillips and Charles Dunnill. Zero gap alkaline electrolysis cell design for renewable energy storage as hydrogen gas. *RSC Adv.*, 6:100643–100651, 10 2016.
- [9] Ligang Wang, Mar Pérez-Fortes, Hossein Madi, Stefan Diethelm, François Maréchal, et al. Optimal design of solid-oxide electrolyser based power-to-methane systems: A comprehensive comparison between steam electrolysis and co-electrolysis. *Applied energy*, 211:1060–1079, 2018.
- [10] Alexander Buttler and Hartmut Spliethoff. Current status of water electrolysis for energy storage, grid balancing and sector coupling via power-to-gas and power-to-liquids: A review. *Renewable and Sustainable Energy Reviews*, 82:2440–2454, 2018.
- [11] Jiajian Gao, Qing Liu, Fangna Gu, Bin Liu, Ziyi Zhong, and Fabing Su. Recent advances in methanation catalysts for the production of synthetic natural gas. *Rsc Advances*, 5(29):22759–22776, 2015.
- [12] Peter Atkins and Julio De Paula. *Atkins' Physical Chemistry*. W.H. Freeman and Company, 8th edition, 2006.

- [13] Chalachew Mebrahtu, Florian Krebs, Salvatore Abate, Siglinda Perathoner, Gabriele Centi, and Regina Palkovits. CO₂ methanation: principles and challenges. In *Studies in Surface Science and Catalysis*, volume 178, pages 85–103. Elsevier, 2019.
- [14] Axel Fache, Frederic Marias, Vincent Guerré, and Stephane Palmade. Optimization of fixed-bed methanation reactors: Safe and efficient operation under transient and steady-state conditions. *Chemical Engineering Science*, 192:1124–1137, 2018.
- [15] Stefan Rönsch, Jens Schneider, Steffi Matthischke, Michael Schlüter, Manuel Götz, Jonathan Lefebvre, Praseeth Prabhakaran, and Siegfried Bajohr. Review on methanation—from fundamentals to current projects. *Fuel*, 166, 2016.
- [16] Franz Koschany, David Schlereth, and Olaf Hinrichsen. On the kinetics of the methanation of carbon dioxide on coprecipitated nial (o) x. *Applied Catalysis B: Environmental*, 181:504–516, 2016.
- [17] Ray Sinnott and Gavin Towler. *Chemical Engineering Design: SI edition*. Elsevier, 5th edition, 2009.
- [18] Linde. Hydrogen recovery by pressure swing adsorption. Brochure, 2009.
- [19] Werner Liemberger, Markus Groß, Martin Miltner, and Michael Harasek. Experimental analysis of membrane and pressure swing adsorption (psa) for the hydrogen separation from natural gas. *Journal of Cleaner Production*, 167:896–907, 2017.
- [20] K. Atsonios, K. Panopoulos, A. Doukelis, A. Koumanakos, E. Kakaras, T. Peters, and YC. van Delft. Introduction to palladium membrane technology. *Palladium Membrane Technology for Hydrogen Production, Carbon Capture and Other Applications*. Elsevier, pages 1–21, 2015.
- [21] Richard W. Baker. *Membrane Technology and Applications*. John Wiley & Sons, 3rd edition edition, 2012.
- [22] David Grainger. *Development of carbon membranes for hydrogen recovery*. PhD thesis, Norwegian University of Science and Technology, September 2007. Department of Chemical Engineering.
- [23] Arthur L. Kohl and Richard Nielsen. *Gas purification*. Elsevier, 1997.
- [24] Anders Siggberg. Biogas liquefaction technology workshop. In *Samsø LBM - 6 TPD LBM plant presentation*, page 10. Wärtsilä, June 2017.
- [25] NEL Hydrogen. NEL Hydrogen Electrolysers. Brochure, 2019. The World’s Most Efficient and Reliable Electrolysers.
- [26] Jens Bremer and Kai Sundmacher. Operation range extension via hot-spot control for catalytic CO₂ methanation reactors. *Reaction Chemistry & Engineering*, 2019.

-
- [27] Scott H. Fogler. *Essentials of Chemical Reaction Engineering*. Pearson International Edition, 4th edition, 2006.
- [28] Engineering ToolBox. Convective heat transfer online. <https://www.engineeringtoolbox.com/>.
- [29] Donald R Woods. *Rules of thumb in engineering practice*. John Wiley & Sons, 2007.
- [30] Chemical Engineering, Essentials for the CPI Professionals. Chemical Engineering Plant Cost Index (CEPCI) - Annual Average for year 2019. Accessed in June 2020. <https://www.chemengonline.com/2019-chemical-engineering-plant-cost-index-annual-average/>.
- [31] Nord Pool. Day-ahead electricity prices for different locations in Norway (monthly averaged). Website, 2020. www.nordpoolgroup.com/Market-data1/Dayahead/Area-Prices/NO/Monthly.
- [32] Bluegold Research. Regional lng prices (monthly average), where a 5-year average value for europe was estimated. Website, 2020. bluegoldresearch.com/regional-lng-prices.
- [33] KPMG. Corporate tax rates table. Website, 2020. kpmg.com/tax-rates-online/corporate-tax-rates-table.
- [34] Davide Parigi, Emanuele Giglio, Alicia Soto, and Massimo Santarelli. Power-to-fuels through carbon dioxide re-utilisation and high-temperature electrolysis: A technical and economical comparison between synthetic methanol and methane. *Journal of cleaner production*, 226:679–691, 2019.
- [35] Everett Anderson. Pathways to Green Hydrogen, NEL Hydrogen. Presentation, Hannover Fair, April 2018.
- [36] Shamim Haider, Arne Lindbråthen, and May-Britt Hägg. Techno-economical evaluation of membrane based biogas upgrading system: A comparison between polymeric membrane and carbon membrane technology. *Green Energy & Environment*, 1(3):222–234, 2016.
- [37] Hugo A. Jakobsen. *Chemical reactor modeling*. Springer, 2008.
- [38] Yunus A. Cengel and Afshin J. Ghajar. *Heat and Mass Transfer, Fundamentals & Applications*. McGraw-Hill, 2015.
- [39] A. Kayode Coker. *Ludwig's Applied Process Design for Chemical and Petrochemical Plants (Fourth Edition) - Chapter 4 - FLUID FLOW*, volume Volume 1. ScienceDirect, 2007.
- [40] Robert J. Kee, Michael E. Coltrin, and Peter Glarborg. *Chemically Reacting Flow, Theory and Practice*. John Wiley & Sons, 2003.
- [41] AspenTech. Aspen HYSYS v10, 2019/2020.
- [42] Gilbert F. Froment, Kenneth B. Bischoff, and Juray De Wilde. *Chemical reactor Analysis and Design*, volume 3rd Edition. John Wiley & Sons, 2011.
-

BIBLIOGRAPHY

- [43] Mohammad Ostadi. MATLAB as a CAPE-OPEN unit operation in HYSYS. Presentation, February 2017. Department of Chemical Engineering, NTNU.

Appendices

Table of Contents

A	List of Symbols	III
B	HYSYS Flowsheets	VII
C	HYSYS Workbooks	XI
D	Sizing and Costing	XVII
D.1	Multi-tubular Methanator	XVII
D.2	Polyimide Membrane	XVIII
D.3	Alkaline Electrolyser	XIX
D.4	Centrifugal Compressors	XIX
D.5	Knock-out Vessel	XIX
D.6	Heat Exchangers	XXI
D.7	Centrifugal Pumps	XXII
D.8	Steam-turbine Cycle	XXIV
D.9	Economic Analysis	XXV
E	Methanation Model	XXVII
E.1	Continuity Equation	XXVII
E.2	Species Mass Balance	XXVIII
E.3	Energy Balance	XXIX
E.4	Momentum Balance	XXXI
E.5	Boundary Conditions	XXXII
E.6	Reaction Rate	XXXIII
E.7	Heat Coefficients	XXXVIII
E.8	Model Equations	XL
E.9	MATLAB Model Code	XLIV
F	Operating Manual	LXVII
F.1	Open the HYSYS simulation from Hand-in Files	LXVII
F.2	Create CAPE-OPEN Fluid Package in HYSYS	LXVIII
F.3	Operate the CAPE-OPEN Unit Operation	LXVIII

Appendix A

List of Symbols

The list of symbols displayed here state the symbols used for the methanation model.

Symbol	Description	Units
a	Coefficient for friction factor	-
A	Area	m^2
A_i	Prefactor for species i	
b	Coefficient for friction factor	-
b_i	Viscosity coefficient for species i	$\text{kg m}^{-1} \text{s}^{-1} \text{K}^{-0.5}$
B_i	Prefactor for species i	
C	Concentration	kmol m^{-3}
C_i	Prefactor for species i	
D_e	Effective diffusion coefficient	$\text{m}^2 \text{s}^{-1}$
D_{ij}	Binary diffusion coefficient	$\text{m}^2 \text{s}^{-1}$
D_m	Molecular diffusion coefficient	$\text{m}^2 \text{s}^{-1}$
D_{Kn}	Knudsen diffusion coefficient	$\text{m}^2 \text{s}^{-1}$
D_p	Diameter of catalyst particle	m
D_{pore}	Diameter of catalyst pore	m
D_r	Effective radial dispersion coefficient	$\text{m}^2 \text{s}^{-1}$
D_i	Prefactor for species i	
Cp_g	Gas mixture heat capacity	$\text{J kmol}^{-1} \text{K}^{-1}$
Cp_i	Component heat capacity	$\text{J kmol}^{-1} \text{K}^{-1}$
f	Friction factor	-
\mathbf{g}	Gravity vector	m s^{-2}
h	Convection heat transfer coefficient	$\text{W m}^{-2} \text{K}^{-1}$
k_w	Tube heat conductivity coefficient	$\text{W m}^{-1} \text{K}^{-1}$
L	Length of tube	m
\bar{M}	Average molar mass of gas mixture	kg kmol^{-1}
M_i	Molar mass for species i	kg kmol^{-1}

Continued on next page

LIST OF SYMBOLS

Continued from previous page

Symbol	Description	Units
n	Mole	mol
N	Number of species in gas mixture	-
Nu	Nusselt number	-
Pe	Peclet number	-
\mathbf{j}_i	diffusive flux vector	$\text{kg m}^{-1} \text{s}^{-1}$
p	Pressure	Pa
Pr	Prandtl number	-
r	Radial coordinate	m
R	Gas constant	$\text{J kmol}^{-1} \text{K}^{-1}$
R_i	Rate of reaction of species i	$\text{kmol kg}^{-1} \text{s}^{-1}$
Re	Reynolds number	-
Re_p	Particle Reynolds number	-
S_i	Viscosity coefficient for species i	K
r_{meth}	Rate of methanation reaction	$\text{kmol kg}^{-1} \text{s}^{-1}$
r_0	Centre of tube	m
r_1	Inner tube radius	m
r_2	Outer tube radius	m
u_z	Superficial velocity	m s^{-1}
U	Overall heat transfer coefficient	$\text{W m}^{-2} \text{K}^{-1}$
\mathbf{u}	Velocity vector	m s^{-1}
t	Time	s
T	Temperature	K
$T _{r=r_1}$	Temperature at centre of the tube	K
$T _{r=r_2}$	Temperature at wall inside the tube	K
$T_{coolant}$	Temperature outside the tube (coolant)	K
i	species i e.g. CH_4	-
\mathbf{q}	Heat flux vector	W m^{-1}
V	Volume	m^3
\dot{Q}	Heat flowrate	W
y	Mole fraction	-
z	Axial coordinate	m
λ_{er}	Effective radial conductivity	$\text{W m}^{-1} \text{K}^{-1}$

Continued on next page

Continued from previous page

Symbol	Description	Units
λ_g	Gas mixture conductivity	$\text{W m}^{-1} \text{K}^{-1}$
λ_i	Component conductivity	$\text{W m}^{-1} \text{K}^{-1}$
μ_g	Gas mixture viscosity	$\text{kg m}^{-1} \text{s}^{-1}$
ω_i	Mass fraction of species i	-
ε	Void fraction	-
ε_p	Porosity	-
ϕ_{meth}	Thiele modulus for methanation reaction	-
ν	Stoichiometric coefficient	-
ν_k	Diffusion volume coefficient	-
η	Effectiveness factor	-
ρ	Density	kg m^{-3}
ρ_g	Gas mixture density	kg m^{-3}
σ	Stress tensor	N m^{-2}
ΔH_R	Heat of reaction	J kmol^{-1}

Appendix B

HYSYS Flowsheets

In the specialisation project, the CO₂ methanation reaction was simulated by a Gibbs reactor unit operation in HYSYS as seen in Figure B.1. Some of the results from this were illustrated in the theory chapter in figure 2.6. However, for the master's thesis it was required to make a kinetic model. At first, this was done by modelling using a plug-flow reactor unit operation in HYSYS incorporating the Koschany [16] kinetics as seen in Figure B.1.

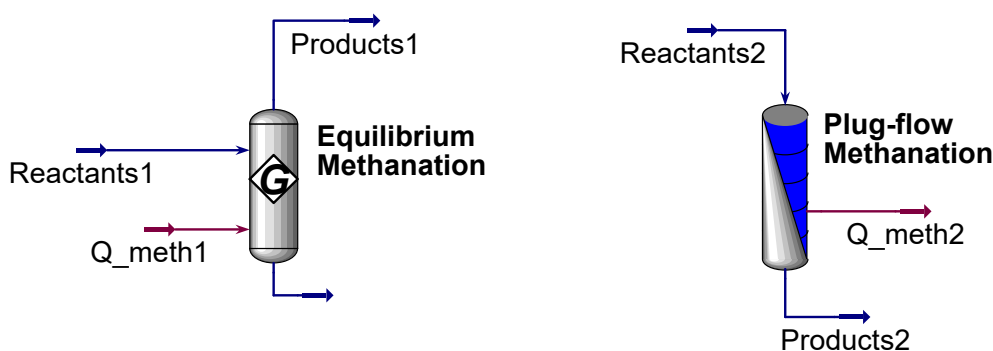


Figure B.1: Left: Gibbs unit operation for equilibrium methanation modelling.
Right: Plug-flow unit operation for kinetic methanation modelling.

Nonetheless, this model was still not sufficiently detailed mainly because of the temperature runaway in the beginning of the reactor from the exothermic reaction. To reduce the temperature runaway and thus catalyst deactivation a two dimensional model was made including an effectiveness and dilution factor in MATLAB. This model also uses the Koschany [16] kinetics and was coupled with HYSYS using a CAPE-OPEN unit operation.

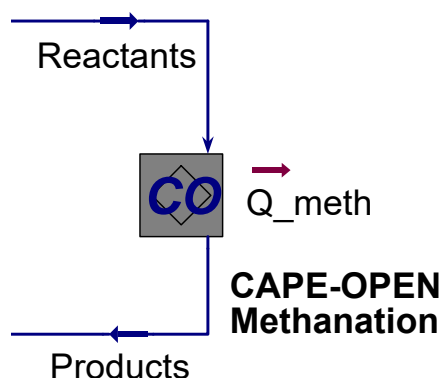


Figure B.2: CAPE-OPEN unit operation for kinetic methanation modelling.

The exothermic heat from the methanation reactor is in the form of steam evaporated from high pressure boiling feed water (BFW). The steam can either be used directly for heat integration with other processes or it can be expanded in a steam turbine to produce electricity. The steam turbine is rather costly in this so called steam cycle and has an high temperature heat demand (in the economiser) but

can produce up to 1 MW of electricity that can be used for the electrolysis process. The steam cycle is illustrated in Figure B.3 while the steam generation itself is illustrated in Figure B.5.

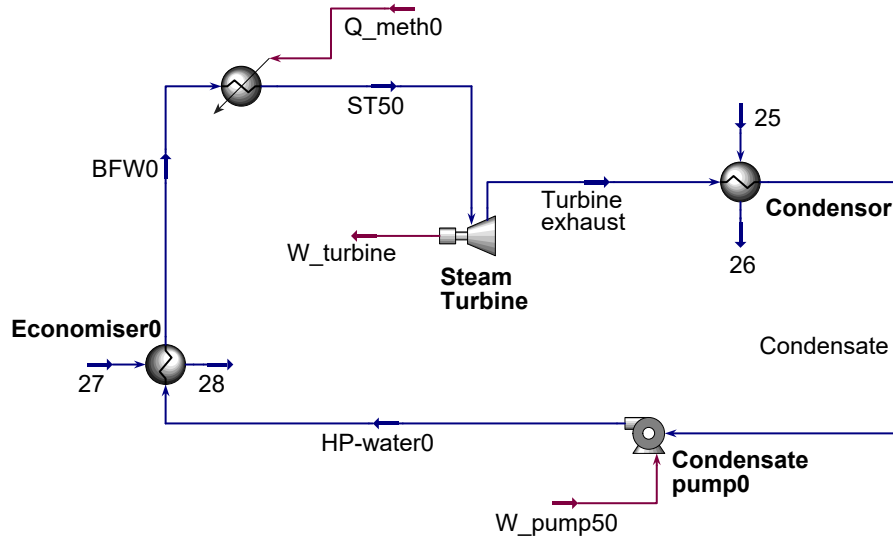


Figure B.3: Steam turbine cycle for local electricity production, alternative to steam cycle.

The Power-to-Methane process is shown in Figures B.4 and B.5. First the electrolyser produces H_2 which is mixed with CO_2 from the amine plant located at the Biokraft plant in Skogn. This make-up-gas (*MUG*) stream is mixed with the *recycle*. The *Feed* is then compressed in either a two-stage (Figure B.4) or three-stage compressor unit dependent on the operational pressure of the plant. The *compressed* stream goes to the CAPE-OPEN methanation reactor where the exothermic heat is converted to steam (ST_5) and heat is exchanged in a feed-effluent heat-exchanger between the *reactants* and *products* of the methanator. The gas mixture is now purified in a Knock-out vessel and Polyimide membrane to obtain the *Retentate* of liquefaction quality specifications and *Permeate* for the *recycle* stream.

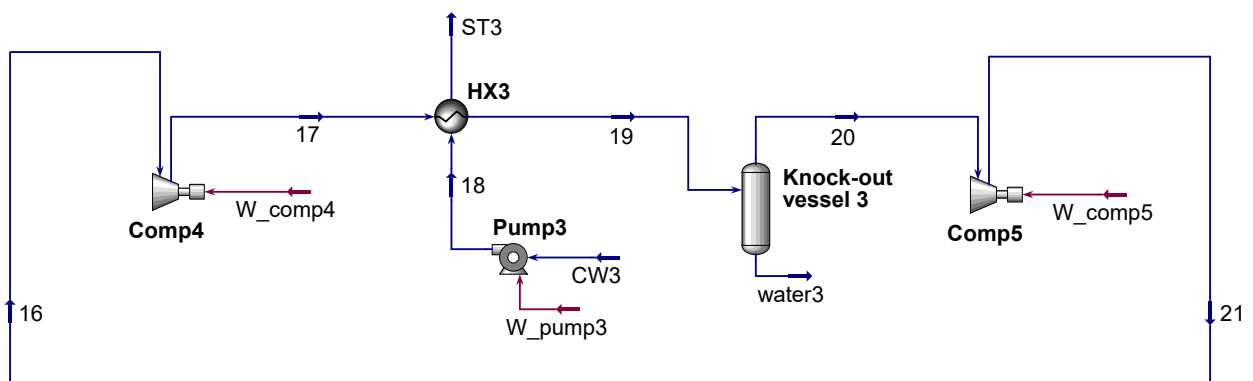


Figure B.4: Top part from HYSYS flowsheet of the Power-to-Methane process simulated.

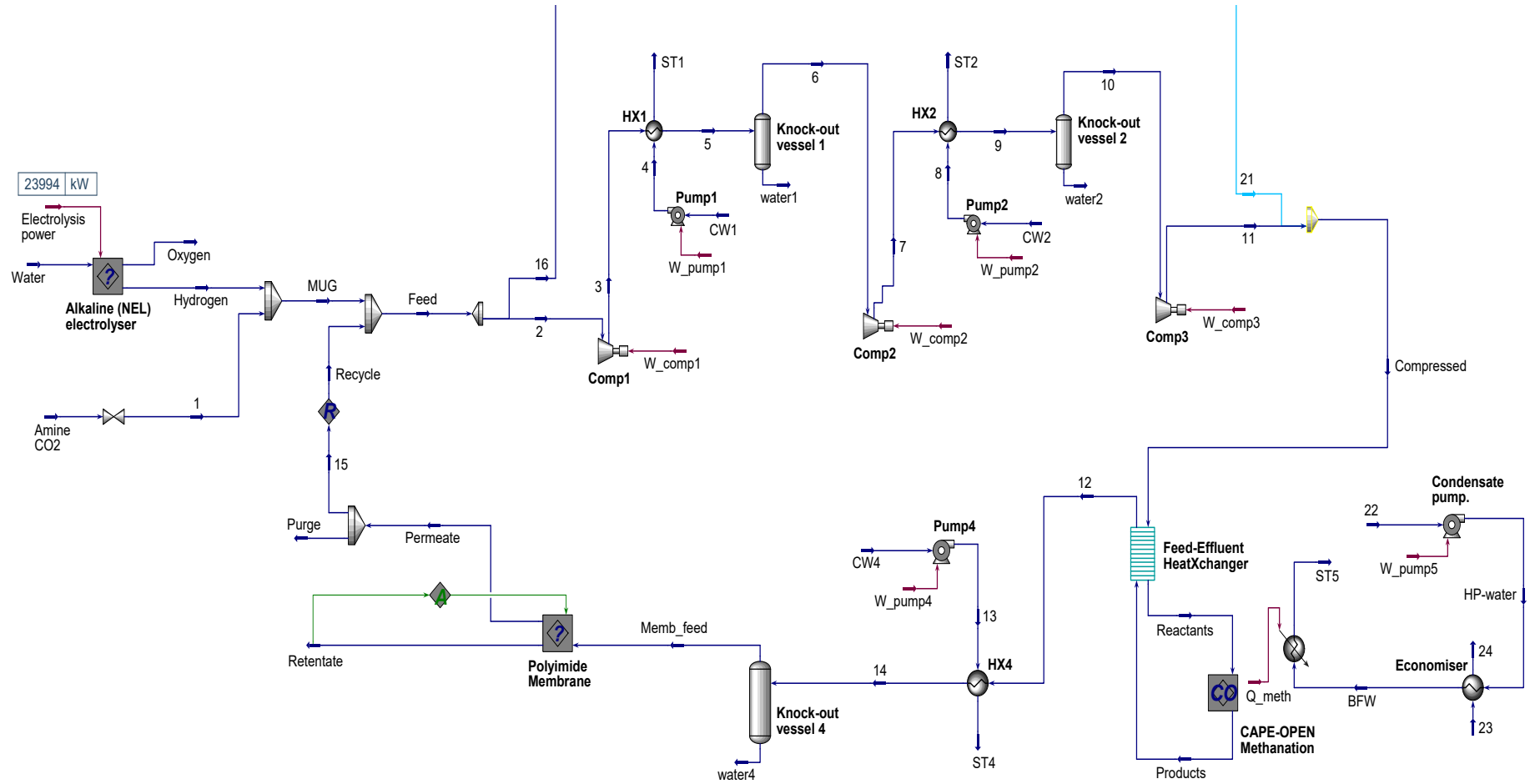


Figure B.5: Main HYSYS flowsheet of the Power-to-Methane process simulated.

Appendix C

HYSYS Workbooks

The values specified in this appendix are for the main case study as discussed in Section 6.1. The energy streams and membrane unit in tables C.1, C.2 and C.3 are extracted from HYSYS spreadsheets. The material steam workbook and composition workbook are imported from HYSYS directly.

Table C.1: Variables of polyimide membrane and permeance data.


Variable	Value	Unit
Membrane thickness	0.5	μm
Permeate pressure	1.013	bar(a)
Membrane area	21755.74	m^2
Pressure ratio	14.98	-
Stage-cut	55.42	%
CH ₄ permeance	9.63936e-4	$\text{mol kpa}^{-1} \text{hr}^{-1} \text{m}^{-2}$
H ₂ permeance	1.204920e-1	$\text{mol kpa}^{-1} \text{hr}^{-1} \text{m}^{-2}$
CO ₂ permeance	3.132792e-2	$\text{mol kpa}^{-1} \text{hr}^{-1} \text{m}^{-2}$
CO/H ₂ O permeance	1.0e-009	$\text{mol kpa}^{-1} \text{hr}^{-1} \text{m}^{-2}$
N ₂ permeance	1.445904e-3	$\text{mol kpa}^{-1} \text{hr}^{-1} \text{m}^{-2}$
O ₂ permeance	7.229520e-3	$\text{mol kpa}^{-1} \text{hr}^{-1} \text{m}^{-2}$

Table C.2: Energy streams excl. methanation.

Variable	Value	Unit
Electrolysis power	23993.85	kW
Comp1 work	425.19	kW
Comp2 work	497.76	kW
Comp3 work	448.12	kW
Pump1 work	0.053	kW
Pump2 work	0.102	kW
Pump4 work	0.917	kW
HX1 duty	441.67	kW
HX2 duty	499.73	kW
HX4 duty	1997.13	kW


Table C.3: Steam generation (top) and turbine cycle (bottom) alternatives.

Variable	Value	Unit
Pump5 duty	22.93	kW
Economiser duty	2517.08	kW
Pump50 duty	23.90	kW
Economiser0 duty	1841.17	kW
Condenser duty	3710.47	kW
Steam turbine work	986.44	kW

1		Case Name: Model_final_22062020.hsc
2	 NORWEGIAN UNIVERSITY OF Bedford, MA USA	Unit Set: SI+
3		Date/Time: Tue Jun 23 12:15:59 2020
4		
5		

Workbook: Case (Main)


Material Streams							Fluid Pkg:	All
11	Name	Amine CO2	Memb_feed	water4	Retentate	Permeate		
12	Vapour Fraction	1.0000	1.0000	0.0000	0.9980	1.0000		
13	Temperature (C)	45.00 *	20.00	20.00	20.00	19.14		
14	Pressure (bar)	1.025 *	15.18	15.18	14.84	1.013		
15	Molar Flow (kgmole/h)	63.28	140.2	125.1	62.48	77.68		
16	Mass Flow (kg/h)	2756	1979	2253	1004	975.6		
17	Liquid Volume Flow (m3/h)	3.338	6.555	2.258	3.339	3.216		
18	Heat Flow (kW)	-6854	-2980	-9957	-1319	-1661		
19	Name	Sweep	Recycle	Purge	15	MUG		
20	Vapour Fraction	1.0000	1.0000	1.0000	1.0000	1.0000		
21	Temperature (C)	30.00 *	19.14 *	19.14	19.14	26.28		
22	Pressure (bar)	1.013 *	1.013 *	1.013	1.013	1.013		
23	Molar Flow (kgmole/h)	0.0000 *	77.65 *	0.0000	77.68	311.9		
24	Mass Flow (kg/h)	0.0000	975.5	0.0000	975.6	3257		
25	Liquid Volume Flow (m3/h)	0.0000	3.215	0.0000	3.216	10.51		
26	Heat Flow (kW)	0.0000	-1661	-0.0000	-1661	-6864		
27	Name	Water	1	14	Reactants	Products		
28	Vapour Fraction	0.0000	1.0000	0.5285	1.0000	1.0000		
29	Temperature (C)	15.00 *	44.99	20.00 *	250.0 *	314.6		
30	Pressure (bar)	1.013 *	1.013 *	1.013	16.00 *	15.87		
31	Molar Flow (kgmole/h)	248.6	63.28	265.2	389.5	265.2		
32	Mass Flow (kg/h)	4478	2756	4233	4233	4233		
33	Liquid Volume Flow (m3/h)	4.487	3.338	8.813	13.73	8.813		
34	Heat Flow (kW)	-1.982e+004	-6854	-1.294e+004	-7745	-1.059e+004		
35	Name	12	13	ST4	CW4	Feed		
36	Vapour Fraction	1.0000	0.0000	1.0000 *	0.0000	1.0000		
37	Temperature (C)	195.6	5.000 *	180.6	4.924	24.77		
38	Pressure (bar)	15.53	10.51	10.16	1.013 *	1.013		
39	Molar Flow (kgmole/h)	265.2	144.8	144.8	144.8	389.5		
40	Mass Flow (kg/h)	4233	2609	2609	2609	4233		
41	Liquid Volume Flow (m3/h)	8.813	2.615	2.615	2.615	13.73		
42	Heat Flow (kW)	-1.094e+004	-1.153e+004	-9530	-1.153e+004	-8525		
43	Name	Compressed	ST1	ST2	16	21		
44	Vapour Fraction	1.0000	1.0000 *	1.0000 *	1.0000	---		
45	Temperature (C)	151.6	134.5	150.8	24.77	---		
46	Pressure (bar)	16.34	3.086	4.857	1.013	16.34		
47	Molar Flow (kgmole/h)	389.5	32.62	36.64	0.0000	0.0000		
48	Mass Flow (kg/h)	4233	587.7	660.1	0.0000	-0.0000		
49	Liquid Volume Flow (m3/h)	13.73	0.5889	0.6614	0.0000	0.0000		
50	Heat Flow (kW)	-8096	-2155	-2416	-0.0000	---		
51	Name	ST5	BFW	Condensate	HP-water0	Turbine exhaust		
52	Vapour Fraction	1.0000 *	0.0000 *	0.0000 *	0.0000	0.8086		
53	Temperature (C)	300.0	300.0	100.0	101.3	108.4		
54	Pressure (bar)	85.93	85.93	1.013 *	86.27	1.358		
55	Molar Flow (kgmole/h)	402.4	402.4	402.4	402.4	402.4		
56	Mass Flow (kg/h)	7249	7249	7249	7249	7249		
57	Liquid Volume Flow (m3/h)	7.264	7.264	7.264	7.264	7.264		
58	Heat Flow (kW)	-2.653e+004	-2.936e+004	-3.122e+004	-3.120e+004	-2.751e+004		
59	Name	ST50	ST3	Oxygen	Hydrogen	17		
60	Vapour Fraction	1.0000 *	1.0000 *	1.0000	1.0000	---		
61	Temperature (C)	300.0	---	15.00 *	20.00 *	---		
62	Pressure (bar)	85.93	---	1.013 *	1.013	4.069		
63	Molar Flow (kgmole/h)	402.4	---	124.3	248.6	0.0000		
64	Mass Flow (kg/h)	7249	---	3977	501.1	0.0000		
65	Liquid Volume Flow (m3/h)	7.264	---	3.496	7.174	0.0000		
66	Heat Flow (kW)	-2.653e+004	---	-10.40	-9.821	---		

1		Case Name: Model_final_22062020.hsc
2	 NORWEGIAN UNIVERSITY OF Bedford, MA USA	Unit Set: SI+
3		Date/Time: Tue Jun 23 12:15:59 2020
4		
5		

Workbook: Case (Main) (continued)

Material Streams (continued)							Fluid Pkg:	All
11	Name	19	20	water3	18	CW3		
12	Vapour Fraction	1.0000	1.0000	0.0000	---	---		---
13	Temperature (C)	20.00 *	20.00	20.00	5.000 *	---		---
14	Pressure (bar)	3.724	3.724	3.724	---	1.013 *		---
15	Molar Flow (kgmole/h)	0.0000	0.0000	0.0000	---	---		---
16	Mass Flow (kg/h)	0.0000	0.0000	0.0000	---	---		---
17	Liquid Volume Flow (m3/h)	0.0000	0.0000	0.0000	---	---		---
18	Heat Flow (kW)	-0.0000	-0.0000	-0.0000	---	---		---
19	Name	11	2	3	5	7		
20	Vapour Fraction	1.0000	1.0000	1.0000	1.0000	1.0000		1.0000
21	Temperature (C)	151.6	24.77	149.5	20.00 *	165.8		165.8
22	Pressure (bar)	16.34	1.013	2.560	2.215	6.468		6.468
23	Molar Flow (kgmole/h)	389.5	389.5	389.5	389.5	389.5		389.5
24	Mass Flow (kg/h)	4233	4233	4233	4233	4233		4233
25	Liquid Volume Flow (m3/h)	13.73	13.73	13.73	13.73	13.73		13.73
26	Heat Flow (kW)	-8096	-8525	-8100	-8542	-8044		-8044
27	Name	9	6	water1	10	water2		
28	Vapour Fraction	1.0000	1.0000	0.0000	1.0000	0.0000		0.0000
29	Temperature (C)	20.00 *	20.00	20.00	20.00	20.00		20.00
30	Pressure (bar)	6.124	2.215	2.215	6.124	6.124		6.124
31	Molar Flow (kgmole/h)	389.5	389.5	0.0000	389.5	0.0000		0.0000
32	Mass Flow (kg/h)	4233	4233	0.0000	4233	0.0000		0.0000
33	Liquid Volume Flow (m3/h)	13.73	13.73	0.0000	13.73	0.0000		0.0000
34	Heat Flow (kW)	-8544	-8542	-0.0000	-8544	-0.0000		-0.0000
35	Name	4	8	CW1	CW2	BFW0		
36	Vapour Fraction	0.0000	0.0000	0.0000	0.0000	0.0000 *		0.0000 *
37	Temperature (C)	5.000 *	5.000 *	4.981	4.967	300.0		300.0
38	Pressure (bar)	3.431	5.202	1.013 *	1.013 *	85.93		85.93
39	Molar Flow (kgmole/h)	32.62	36.64	32.62	36.64	402.4		402.4
40	Mass Flow (kg/h)	587.7	660.1	587.7	660.1	7249		7249
41	Liquid Volume Flow (m3/h)	0.5889	0.6614	0.5889	0.6614	7.264		7.264
42	Heat Flow (kW)	-2596	-2916	-2596	-2916	-2.936e+004		-2.936e+004
43	Name	HP-water	22	23	24	25		
44	Vapour Fraction	0.0000	0.0000	0.0000 *	0.0000 *	0.0000		0.0000
45	Temperature (C)	20.82	20.00 *	325.0 *	324.8	15.00 *		15.00 *
46	Pressure (bar)	86.27	1.013 *	122.1	121.7	1.013 *		1.013 *
47	Molar Flow (kgmole/h)	402.4	402.4	2.783e+005	2.783e+005	2322		2322
48	Mass Flow (kg/h)	7249	7249	5.014e+006	5.014e+006	4.184e+004		4.184e+004
49	Liquid Volume Flow (m3/h)	7.264	7.264	5024	5024	41.92		41.92
50	Heat Flow (kW)	-3.188e+004	-3.190e+004	-2.002e+007	-2.002e+007	-1.852e+005		-1.852e+005
51	Name	26	27	28				
52	Vapour Fraction	0.0000 *	0.0000 *	0.0000 *				
53	Temperature (C)	88.74	325.0 *	324.8				
54	Pressure (bar)	0.6685	122.1	121.7				
55	Molar Flow (kgmole/h)	2322	2.036e+005	2.036e+005				
56	Mass Flow (kg/h)	4.184e+004	3.668e+006	3.668e+006				
57	Liquid Volume Flow (m3/h)	41.92	3675	3675				
58	Heat Flow (kW)	-1.814e+005	-1.464e+007	-1.464e+007				

59								
60								
61								
62								
63								
64								
65								
66								
67								
68								

1		Case Name: Model_final_22062020.hsc
2	 NORWEGIAN UNIVERSITY OF Bedford, MA USA	Unit Set: SI+
3		Date/Time: Tue Jun 23 12:16:14 2020
4		
5		

Workbook: Case (Main)

Compositions Fluid Pkg: All

11	Name	Amine CO2	Memb_feed	water4	Retentate	Permeate
12	Comp Mole Frac (Methane)	0.0010 *	0.6582	0.0000	0.9953	0.3871
13	Comp Mole Frac (H2O)	0.0160 *	0.0016	0.9999	0.0037	0.0000
14	Comp Mole Frac (Hydrogen)	0.0000 *	0.2721	0.0000	0.0000	0.4909
15	Comp Mole Frac (CO2)	0.9820 *	0.0673	0.0001	0.0000	0.1213
16	Comp Mole Frac (CO)	0.0000 *	0.0000	0.0000	0.0000	0.0000
17	Comp Mole Frac (Nitrogen)	0.0010 *	0.0008	0.0000	0.0010	0.0006
18	Comp Mole Frac (Oxygen)	0.0000 *	0.0000	0.0000	0.0000	0.0000

19	Name	Sweep	Recycle	Purge	15	MUG
20	Comp Mole Frac (Methane)	1.0000 *	0.3871 *	0.3871	0.3871	0.0002
21	Comp Mole Frac (H2O)	0.0000 *	0.0000 *	0.0000	0.0000	0.0032
22	Comp Mole Frac (Hydrogen)	0.0000 *	0.4908 *	0.4909	0.4909	0.7971
23	Comp Mole Frac (CO2)	0.0000 *	0.1215 *	0.1213	0.1213	0.1993
24	Comp Mole Frac (CO)	0.0000 *	0.0000 *	0.0000	0.0000	0.0000
25	Comp Mole Frac (Nitrogen)	0.0000 *	0.0006 *	0.0006	0.0006	0.0002
26	Comp Mole Frac (Oxygen)	0.0000 *	0.0000 *	0.0000	0.0000	0.0000


27	Name	Water	1	14	Reactants	Products
28	Comp Mole Frac (Methane)	0.0000 *	0.0010	0.3478	0.0773	0.3478
29	Comp Mole Frac (H2O)	1.0000 *	0.0160	0.4724	0.0026	0.4724
30	Comp Mole Frac (Hydrogen)	0.0000 *	0.0000	0.1438	0.7360	0.1438
31	Comp Mole Frac (CO2)	0.0000 *	0.9820	0.0356	0.1838	0.0356
32	Comp Mole Frac (CO)	0.0000 *	0.0000	0.0000	0.0000	0.0000
33	Comp Mole Frac (Nitrogen)	0.0000 *	0.0010	0.0004	0.0003	0.0004
34	Comp Mole Frac (Oxygen)	0.0000 *	0.0000	0.0000	0.0000	0.0000

35	Name	12	13	ST4	CW4	Feed
36	Comp Mole Frac (Methane)	0.3478	***	***	***	0.0773
37	Comp Mole Frac (H2O)	0.4724	1.0000	1.0000	1.0000 *	0.0026
38	Comp Mole Frac (Hydrogen)	0.1438	***	***	***	0.7360
39	Comp Mole Frac (CO2)	0.0356	***	***	***	0.1838
40	Comp Mole Frac (CO)	0.0000	***	***	***	0.0000
41	Comp Mole Frac (Nitrogen)	0.0004	***	***	***	0.0003
42	Comp Mole Frac (Oxygen)	0.0000	***	***	***	0.0000

43	Name	Compressed	ST1	ST2	16	21
44	Comp Mole Frac (Methane)	0.0773	***	***	0.0773	0.0773
45	Comp Mole Frac (H2O)	0.0026	1.0000	1.0000	0.0026	0.0026
46	Comp Mole Frac (Hydrogen)	0.7360	***	***	0.7360	0.7360
47	Comp Mole Frac (CO2)	0.1838	***	***	0.1838	0.1838
48	Comp Mole Frac (CO)	0.0000	***	***	0.0000	0.0000
49	Comp Mole Frac (Nitrogen)	0.0003	***	***	0.0003	0.0003
50	Comp Mole Frac (Oxygen)	0.0000	***	***	0.0000	0.0000

51	Name	ST5	BFW	Condensate	HP-water0	Turbine exhaust
52	Comp Mole Frac (Methane)	***	***	***	***	***
53	Comp Mole Frac (H2O)	1.0000	1.0000 *	1.0000 *	1.0000	1.0000
54	Comp Mole Frac (Hydrogen)	***	***	***	***	***
55	Comp Mole Frac (CO2)	***	***	***	***	***
56	Comp Mole Frac (CO)	***	***	***	***	***
57	Comp Mole Frac (Nitrogen)	***	***	***	***	***
58	Comp Mole Frac (Oxygen)	***	***	***	***	***

59	Name	ST50	ST3	Oxygen	Hydrogen	17
60	Comp Mole Frac (Methane)	***	***	0.0000 *	0.0000 *	0.0773
61	Comp Mole Frac (H2O)	1.0000	1.0000	0.0000 *	0.0000 *	0.0026
62	Comp Mole Frac (Hydrogen)	***	***	0.0000 *	1.0000 *	0.7360
63	Comp Mole Frac (CO2)	***	***	0.0000 *	0.0000 *	0.1838
64	Comp Mole Frac (CO)	***	***	0.0000 *	0.0000 *	0.0000
65	Comp Mole Frac (Nitrogen)	***	***	0.0000 *	0.0000 *	0.0003
66	Comp Mole Frac (Oxygen)	***	***	1.0000 *	0.0000 *	0.0000

1	 NORWEGIAN UNIVERSITY OF Bedford, MA USA	Case Name: Model_final_22062020.hsc
2		Unit Set: SI+
3		Date/Time: Tue Jun 23 12:16:14 2020
4		
5		

Workbook: Case (Main) (continued)

Compositions (continued) Fluid Pkg: All

11	Name	19	20	water3	18	CW3
12	Comp Mole Frac (Methane)	0.0773	0.0773	0.0773	***	***
13	Comp Mole Frac (H2O)	0.0026	0.0026	0.0026	1.0000	1.0000 *
14	Comp Mole Frac (Hydrogen)	0.7360	0.7360	0.7360	***	***
15	Comp Mole Frac (CO2)	0.1838	0.1838	0.1838	***	***
16	Comp Mole Frac (CO)	0.0000	0.0000	0.0000	***	***
17	Comp Mole Frac (Nitrogen)	0.0003	0.0003	0.0003	***	***
18	Comp Mole Frac (Oxygen)	0.0000	0.0000	0.0000	***	***
19	Name	11	2	3	5	7
20	Comp Mole Frac (Methane)	0.0773	0.0773	0.0773	0.0773	0.0773
21	Comp Mole Frac (H2O)	0.0026	0.0026	0.0026	0.0026	0.0026
22	Comp Mole Frac (Hydrogen)	0.7360	0.7360	0.7360	0.7360	0.7360
23	Comp Mole Frac (CO2)	0.1838	0.1838	0.1838	0.1838	0.1838
24	Comp Mole Frac (CO)	0.0000	0.0000	0.0000	0.0000	0.0000
25	Comp Mole Frac (Nitrogen)	0.0003	0.0003	0.0003	0.0003	0.0003
26	Comp Mole Frac (Oxygen)	0.0000	0.0000	0.0000	0.0000	0.0000
27	Name	9	6	water1	10	water2
28	Comp Mole Frac (Methane)	0.0773	0.0773	0.0773	0.0773	0.0773
29	Comp Mole Frac (H2O)	0.0026	0.0026	0.0026	0.0026	0.0026
30	Comp Mole Frac (Hydrogen)	0.7360	0.7360	0.7360	0.7360	0.7360
31	Comp Mole Frac (CO2)	0.1838	0.1838	0.1838	0.1838	0.1838
32	Comp Mole Frac (CO)	0.0000	0.0000	0.0000	0.0000	0.0000
33	Comp Mole Frac (Nitrogen)	0.0003	0.0003	0.0003	0.0003	0.0003
34	Comp Mole Frac (Oxygen)	0.0000	0.0000	0.0000	0.0000	0.0000
35	Name	4	8	CW1	CW2	BFW0
36	Comp Mole Frac (Methane)	***	***	***	***	***
37	Comp Mole Frac (H2O)	1.0000	1.0000	1.0000 *	1.0000 *	1.0000
38	Comp Mole Frac (Hydrogen)	***	***	***	***	***
39	Comp Mole Frac (CO2)	***	***	***	***	***
40	Comp Mole Frac (CO)	***	***	***	***	***
41	Comp Mole Frac (Nitrogen)	***	***	***	***	***
42	Comp Mole Frac (Oxygen)	***	***	***	***	***
43	Name	HP-water	22	23	24	25
44	Comp Mole Frac (Methane)	***	***	0.0000 *	0.0000	0.0000 *
45	Comp Mole Frac (H2O)	1.0000	1.0000	1.0000 *	1.0000	1.0000 *
46	Comp Mole Frac (Hydrogen)	***	***	0.0000 *	0.0000	0.0000 *
47	Comp Mole Frac (CO2)	***	***	0.0000 *	0.0000	0.0000 *
48	Comp Mole Frac (CO)	***	***	0.0000 *	0.0000	0.0000 *
49	Comp Mole Frac (Nitrogen)	***	***	0.0000 *	0.0000	0.0000 *
50	Comp Mole Frac (Oxygen)	***	***	0.0000 *	0.0000	0.0000 *
51	Name	26	27	28		
52	Comp Mole Frac (Methane)	0.0000	0.0000 *	0.0000		
53	Comp Mole Frac (H2O)	1.0000	1.0000 *	1.0000		
54	Comp Mole Frac (Hydrogen)	0.0000	0.0000 *	0.0000		
55	Comp Mole Frac (CO2)	0.0000	0.0000 *	0.0000		
56	Comp Mole Frac (CO)	0.0000	0.0000 *	0.0000		
57	Comp Mole Frac (Nitrogen)	0.0000	0.0000 *	0.0000		
58	Comp Mole Frac (Oxygen)	0.0000	0.0000 *	0.0000		

59
60
61
62
63
64
65
66
67
68

Appendix D

Sizing and Costing

In this appendix, the sizing and costing performed of each individual component is explained. The costing/sizing is done for the multi-tubular methanator [29, 34], alkaline electrolyser [25, 35], polyimide membrane [36], three-stage centrifugal compressor unit with intercooling, knock-out vessel, heat exchangers, centrifugal pumps and the steam-turbine cycle [17]. The equipment cost specified for each equipment is where needed corrected for cost escalation.

D.1 Multi-tubular Methanator

The multi-tubular methanation reactor is a fixed-bed reactor that consists in this case of 1000 tubes with a inner diameter of 2.54 cm and a length of 2 m filled with a NiAl catalyst. To determine the cost it was required to assume that the methanator can be cost estimated as a fixed-tube heat-exchanger from carbon steel using data from Woods [29]. The catalyst, is determined similar as Parigi et al. [34] that also determined the methanation catalyst cost.

For the equipment cost determination, it is required to find the catalyst volume inside the tubes. This is done by first finding the total inner volume of the tubes with Equation D.1.

$$V_{tubes,i} = \frac{\pi}{4} D_i^2 \cdot L \cdot n_t \quad (D.1)$$

and accordingly to find the total catalyst volume by Equation D.2.

$$V_{catalyst,total} = V_{tubes,i} (1 - \varepsilon) \quad (D.2)$$

Since there are active catalyst particles present as well as inert particles present, the total catalyst volume is multiplied with the dilution factor (ζ) to find the active catalyst volume. The remainder the inert catalyst volume. The equations are given in Equation D.3.

$$\begin{aligned} V_{catalyst,active} &= V_{catalyst,total} \cdot \zeta \\ V_{catalyst,inert} &= V_{catalyst,total} (1 - \zeta) \end{aligned} \quad (D.3)$$

The cost is divided into the cost for the multi-tubular reactor itself and the catalyst present inside the tubes of the reactor. The multi-tubular methanation reactor is approximated to be a fixed-tube heat-exchanger from carbon steel where the FOB cost are given to be 350000 USD per 3 m³ catalyst

with $n = 0.68$ [29]. These data are inserted in Equation 7.2 to find the equipment cost without catalyst. The catalyst cost is determined from the volume of active and inert catalyst. Here, the cost of the methanation catalyst is given to be 15539 USD per m^3 active catalyst and the inert catalyst is assumed to cost 1554 USD per m^3 (10% of active catalyst cost) [34]. The calculated cost are given in Table D.1.

Table D.1: Important sizing/costing data from the methanation reactor

Parameter	Value	Unit
$V_{catalyst,total}$	0.557	m^3
$V_{catalyst,active}$	0.334	m^3
$V_{catalyst,inert}$	0.223	m^3
Equipment cost	67695	USD
Catalyst cost	5543	USD
C_e	73238	USD

The sizing of the reactor has been checked by calculating the reactor cost with a different approach. In that case, the methanation reactor was sized as a vertical pressure vessel (304 s/s) for the reactor shell mass and tube shell mass (similar to Section D.5). This gave a similar results.

Sizing of the methanation reactor is done in the MATLAB model. First, the cross-sectional area of the reactor including the tubes and coolant space is found based on the inner-tube distance (D_{it}) according to Fache et al. [14]. Then, the cross-sectional area is multiplied with the tube length to find the volume of the reactor.

$$V_{reactor} = n_t (2R_{t,o} + D_{it})^2 \frac{\sqrt{3}}{2} \cdot L \quad (\text{D.4})$$

The diameter of the reactor is determined from the reactor volume.

$$D_{reactor} = \sqrt{\frac{4 V_{reactor}}{\pi L}} \quad (\text{D.5})$$

D.2 Polyimide Membrane

A cost estimate for the polyimide membrane is made based on estimate for a polymeric membrane from Haider [36]. The equipment cost is 20 USD per m^2 installed.

The membrane area is extracted from the HYSYS ChemBrane model as 21755.7 m^2 .

The equipment cost for the polyimide membrane is:

$$C_e = 21755.7 \text{ kW} \cdot 20 \frac{\text{USD}}{\text{m}^2} = 435114 \text{ USD} \quad (\text{D.6})$$

D.3 Alkaline Electrolyser

The methanation reactant H_2 is produced from electricity. The alkaline electrolyser is cost estimated based on 8-cluster commercial NEL electrolysers with a benchmark capital expenditure ratio of 450 USD/kW [35]. This is equal to 4.09 NOK/W.

The amount of hydrogen required for the H_2/CO_2 ratio of 4.0 is calculated in HYSYS based on the energy requirement in kWh/kg H_2 given by NEL [25]. To produce this amount of hydrogen, a it is calculated that a 23994 kW (24MW) electrolyser is required. The cost for the electrolyser is determined from multiplication of the energy requirement of 23994 kW with the benchmark cost.

$$C_e = 23994 \text{ kW} \cdot 450 \frac{\text{USD}}{\text{kW}} = 10797230 \text{ USD} = 10.8 \text{ MUSD} \quad (\text{D.7})$$

D.4 Centrifugal Compressors

The MUG and recycle material streams are initially at atmospheric pressure but have to be pressurised in order to increase the methanation reaction rate and give sufficient driving forces for separating the gas mixture in a polyimide membrane. For the main case study, the differential pressure is around 16 bar requiring a three-stage compressor unit.

The equipment cost for each compressor is determined from [17] by assuming the cost relation for centrifugal compressors to be valid. Equation D.8 is used to determine the equipment cost in c/s based on the driver power in kW as a unit for size.

$$C_e = (490000 + 16800 \cdot W_{comp.}^{0.6}) \cdot \left(\frac{607.5}{509.7} \right) \quad (\text{D.8})$$

The expression is valid between 75-30000 kW, driver power. The results are summarised in Table D.2.

D.5 Knock-out Vessel

To separate water vapour from the product gas it is required to have a knock-out vessel. The equipment cost of the knock-out vessel can be determined from [17] as a vertical pressure vessel based on the

Table D.2: Compressor sizing and costing results.

Compressor	Power [kW]	Cost [USD]
comp1	425.13	814631
comp2	497.76	889692
comp3	448.12	838906
	C_e	2543229

shell mass (m_s) of the column. The shell mass is found from:

$$m_s = \pi D_v H_v t_w \rho_s \quad (\text{D.9})$$

Where, D_v is the vessel diameter, H_v the vessel height, t_w is the wall thickness and ρ_s is the density of the material. In this case, the vessel is build using stainless steel having a density of 8000 kg/m³.

The minimum vessel diameter (D_v) can be determined by Equation D.10.

$$D_v = \sqrt{\frac{4 \phi_v}{\pi u_s}} \quad (\text{D.10})$$

Where, ϕ_v is the gas volumetric flowrate (extracted from HYSYS as 272.98 m³/h) and u_s is the settling velocity (u_s) for the given gas stream. The settling velocity describes the velocity in which liquid droplets settle out from the gas mixture. Therefore, the vertical separator must have a sufficient diameter to slow down the gas sufficiently [17]. The settling velocity (u_s) for a vertical separator without demister pad is given in Equation D.11.

$$u_t = 0.07 ((\rho_L - \rho_v)/\rho_v)^{0.5} \quad (\text{D.11})$$

$$u_s = 0.15 u_t$$

Where, u_t is the settling velocity with a demister pad, ρ_v is the vapour density and ρ_L is the liquid density. The values for ρ_v and ρ_L are extracted from HYSYS to be 7.4969 and 852.07 kg/h, respectively.

The height of the vessel (H_v) can be determined by Equation D.12.

$$H_v = D_v + \frac{D_v}{2} + H_L + 0.4 \quad (\text{D.12})$$

Where, the terms except H_L should be minimal 2m and H_L is the required height of the liquid in the vessel calculated by Equation D.13.

$$H_L = \frac{\text{Volume hold-up}}{\text{Vessel cross-sectional area}} = \frac{4 \phi_L}{\pi D_v^2} \cdot \text{hold-up time} \quad (\text{D.13})$$

Where, ϕ_L is the liquid volumetric flowrate (extracted from HYSYS as 2.643 m³/h) and a minimum of 10 minutes hold-up time is assumed to allow for smooth operation and control [17].

The minimum vessel wall thickness is given by Equation D.14 as specified by ASME BPV Code [17].

$$t_w = \frac{P_d D_v}{2SE + 1.2P_d} \quad (\text{D.14})$$

Where, P_d is the design pressure which is assumed to be 10% above the normal operation pressure (15.17 bar(a)), S is the maximum allowable stress which is 15000 psi for stainless steel type 304 (ss) at 300 °F and E is the weld efficiency that is assumed to be 1.0 for fully radiographed welds [17].

With the shell mass of the pressure vessel the cost can be determined from [17] (for 304 s/s):

$$C_e = (15000 + 68 \cdot m_s^{0.85}) \cdot \left(\frac{607.5}{509.7} \right) \quad (\text{D.15})$$

That is valid for a lower and upper shell mass of 120 and 250 000 kg, respectively. The results are summarised in Table D.3

Table D.3: Knock-out vessel sizing and costing results.

Variable	Value
u_s	0.1114 m/s
D_v	0.9308 m
H_L	0.6474 m
H_v	2.6474 m
t_w	0.0074 m
m_s	460.56 kg
C_e	32755.8 USD

D.6 Heat Exchangers

The equipment cost of the heat exchangers is determined from Sinnott & Towler [17] using the area as the unit for size. The area of the heat exchangers is estimated using Equation D.16.

$$A = \frac{Q}{U \Delta T_{LM}} \quad (\text{D.16})$$

Where, the duty (Q) is extracted from the HYSYS simulations for each heat exchanger and the log mean temperature difference (ΔT_{LM}) is calculated by Equation D.17 (can be found in HYSYS as the LMTD).

$$\Delta T_{LM} = \frac{\Delta T_1 - \Delta T_2}{\ln(\Delta T_1/\Delta T_2)} \quad \begin{aligned} \Delta T_1 &= T_{hot,out} - T_{cold,in} \\ \Delta T_2 &= T_{hot,in} - T_{cold,out} \end{aligned} \quad (\text{D.17})$$

Since all the heat exchangers cool the gas mixture by evaporation of water to steam, the heat transfer coefficient (U) can be estimated as 200 W/(m²·°C) for a steam/gas shell and tube exchanger [17]. The heat transfer coefficient (U) for the feed-effluent heat exchanger (FEHX - gas/gas heat exchanger) can be estimated as 30 W/(m²·°C).

From the determined area, the equipment cost can be determined from Equation D.18 [17] for c/s .

$$C_e = (24000 + 46 \cdot A^{1.2}) \cdot \left(\frac{607.5}{509.7} \right) \quad (\text{D.18})$$

Equation D.18 is valid between 10-1000 m². The results are summarised in Table D.4.

Table D.4: Heat exchanger sizing and costing results.

Exchanger	Duty [kW]	ΔT_{LM} [°C]	Area [m ²]	Cost [USD]
HX1	441.7	15.0	147.2	50510
HX2	499.7	15.0	166.6	54010
FEHX	350.92	53.7	218.0	63691
HX4	1997.1	15.0	665.7	162552
Economiser	2517.1	111.8	112.5	44473
			C_e	375237

D.7 Centrifugal Pumps

Since most heat exchangers in the process cool the gas mixture by using boiling feed water, pumps are required to compress the cooling water up to the boiling point of water. These pumps are cost estimated based on single-stage centrifugal pumps according to Sinnott & Towler [17].

The unit of size for the cost estimation is the liquid volumetric flowrate ($\phi_{v,L}$) in L/s. From HYSYS the liquid volumetric flowrate is extracted in m³/h and converted. The equipment cost can be determined from Equation D.19 for c/s .

$$C_e = (6900 + 206 \cdot \phi_{v,L}^{0.9}) \cdot \left(\frac{607.5}{509.7} \right) \quad (\text{D.19})$$

Equation D.19 is valid between 0.2-126 L/s. The results are given in Table D.5.

As can be seen in Table D.5, the volumetric flowrate for pump1 and pump2 are too low for Equation D.19 to be valid. However, the cost is still calculated according to this since the equipment cost for the centrifugal pumps is neglectable.

Table D.5: Centrifugal pumps costing results.

Pump	$\phi_{v,L}$ [L/s]	Cost [USD]
Pump1	0.16	8273
Pump2	0.18	8278
Pump4	0.73	8411
Pump5	2.02	8692
	C_e	33654

D.8 Steam-turbine Cycle

An alternative to producing high pressure steam from the methanation reactor is to convert the steam to electricity by using a steam-turbine cycle. The steam-turbine cycle consists of a steam turbine, condenser, condensate pump and economiser.

The equipment cost for a steam-turbine is calculated based on Sinnott & Towler [17] as a "condensing steam-turbine" using the power (W_{st}) in kW as a unit of size which can be extracted from HYSYS. Equation D.20 is used to calculate the equipment cost for the steam-turbine.

$$C_e = (-12000 + 1630 \cdot W_{st}^{0.75}) \cdot \left(\frac{607.5}{509.7}\right) \quad (\text{D.20})$$

The equipment cost for the condenser and economiser are based on heat exchangers as calculated in Section D.6 and the condensate pump equipment cost is according to Section D.7.

The equipment costing results are given in Tables D.6 and D.7.

Table D.6: Steam cycle pump and turbine cost.

	$\phi_{v,L}$ [L/s]	Cost [USD]
Pump50	2.02	8692

	W_{st} [kW]	Cost [USD]
Turbine	986.44	327655

Table D.7: Steam cycle heat exchanger sizing and costing results.

Exchanger	Duty [kW]	ΔT_{LM} [°C]	Area [m ²]	Cost [USD]
Economiser1	1841.1	90.7	101.5	42633
Condenser	3710.5	41.9	442.4	110642

D.9 Economic Analysis

In this section the economic analysis results will be discussed and illustrated. The fixed capital cost (FC), variable cost of production (VCOP), fixed cost of production (FCOP) and revenues are determined in Chapters 7 and 8. The results of this are then imported into an Excel spreadsheet provided by Sinnott & Towler [17] to find the cumulative cash flow and net present value (NPV).

It is assumed that the plant is in operation 96% of the time (8410 hours/year) for a lifetime of 20 years, has an interest rate of 6% [17], with a tax rate of 22% [33] and is using the straight line depreciation method [17] in the first 10 years after production is start-up and revenues are made.

The economic analysis for 'current' prices (450 USD per kW installed electrolysis capacity, 314 NOK per MWh electricity and 8 NOK per Sm³ CH₄ produced) is given below. Not profitable.

REVENUES AND PRODUCTION COSTS		CAPITAL COSTS		CONSTRUCTION SCHEDULE						
Main product revenue <u>10.49</u> Byproduct revenue 0.68 Raw materials cost Utilities cost 7.45 Consumables cost VCOP <u>6.77</u> Salary and overheads 1.48 Maintenance 1.60 Interest 0.53 Royalties FCOP <u>3.61</u>		ISBL Capital Cost 53.4 OSBL Capital Cost 5.3 Engineering Costs 8.8 Contingency 14.7 Total Fixed Capital Cos 82.3 Working Capital 0.0		Capital Cost Basis Year 2007 to 2019 Units <input type="radio"/> English <input type="radio"/> Metric On Stream 8,410 hr/yr 350.40 day/yr						
\$MM/yr		\$MM		Year	% FC	% WC	% FCOP	% VCOP		
				1	30.00%		0.00%	0.00%		
				2	70.00%		0.00%	0.00%		
				3	0.00%		100.00%	50.00%		
				4	0.00%		100.00%	70.00%		
				5	0.00%		100.00%	100.00%		
				6	0.00%		100.00%	100.00%		
				7+	0.00%		100.00%	100.00%		
ECONOMIC ASSUMPTIONS										
Cost of equity	Debt ratio			Tax rate	22%					
Cost of debt				Depreciation method	Straight line					
Cost of capital 6%				Depreciation period	10 years					
CASH FLOW ANALYSIS										
All figures in \$MM unless indicated										
Project year	Cap Ex	Revenue	CCOP	Gr. Profit	Deprcn	Taxbl Inc	Tax Paid	Cash Flow	PV of CF	NPV
1	24.7	0.0	0.0	0.0	0.0	0.0	0.0	-24.7	-23.3	-23.3
2	57.6	0.0	0.0	0.0	0.0	0.0	0.0	-57.6	-51.3	-74.5
3	0.0	5.2	7.0	-1.7	8.2	-10.0	0.0	-1.7	-1.5	-76.0
4	0.0	7.3	8.3	-1.0	8.2	-9.2	-2.2	1.2	0.9	-75.1
5	0.0	10.5	10.4	0.1	8.2	-8.1	-2.0	2.1	1.6	-73.5
6	0.0	10.5	10.4	0.1	8.2	-8.1	-1.8	1.9	1.3	-72.1
7	0.0	10.5	10.4	0.1	8.2	-8.1	-1.8	1.9	1.3	-70.9
8	0.0	10.5	10.4	0.1	8.2	-8.1	-1.8	1.9	1.2	-69.7
9	0.0	10.5	10.4	0.1	8.2	-8.1	-1.8	1.9	1.1	-68.5
10	0.0	10.5	10.4	0.1	8.2	-8.1	-1.8	1.9	1.1	-67.5
11	0.0	10.5	10.4	0.1	8.2	-8.1	-1.8	1.9	1.0	-66.5
12	0.0	10.5	10.4	0.1	8.2	-8.1	-1.8	1.9	0.9	-65.5
13	0.0	10.5	10.4	0.1	0.0	0.1	-1.8	1.9	0.9	-64.6
14	0.0	10.5	10.4	0.1	0.0	0.1	0.0	0.1	0.0	-64.6
15	0.0	10.5	10.4	0.1	0.0	0.1	0.0	0.1	0.0	-64.6
16	0.0	10.5	10.4	0.1	0.0	0.1	0.0	0.1	0.0	-64.5
17	0.0	10.5	10.4	0.1	0.0	0.1	0.0	0.1	0.0	-64.5
18	0.0	10.5	10.4	0.1	0.0	0.1	0.0	0.1	0.0	-64.5
19	0.0	10.5	10.4	0.1	0.0	0.1	0.0	0.1	0.0	-64.4
20	0.0	10.5	10.4	0.1	0.0	0.1	0.0	0.1	0.0	-64.4
ECONOMIC ANALYSIS										
Average cash flow	1.1	\$MM/yr	NPV	10 years	-67.5	\$MM	IRR	10 years	-27.2%	
Simple pay-back period	73.073	yrs		15 years	-64.6	\$MM		15 years	-17.7%	
Return on investment (10 yrs)	-8.25%			20 years	-64.4	\$MM		20 years	-16.6%	
Return on investment (15 yrs)	-6.79%		NPV to yr	12	-65.5	\$MM				

APPENDIX D. SIZING AND COSTING

In the *Cash Flow Analysis*, several parameters are calculated. The first, second and third columns are based upon the *Revenues and Production Costs*, *Capital Costs* and *Construction Schedule*. The cash cost of production (CCOP) is the sum of the fixed (FCOP) and variable production cost (VCOP). The others are based on these parameters and *Economic Assumptions*. Most interesting are the cash flow, payback time, net present value (NPV) and internal rate of return (IRR).

The economic analysis for 'future' prices (350 USD per kW installed electrolysis capacity, 250 NOK per MWh electricity and 12.5 NOK per Sm³ CH₄ produced) is given below. Profitable.

		Capital Cost Basis Year 2007 to 2019								
		Units	English Metric							
		On Stream	8,410 hr/yr 350.40 day/yr							
REVENUES AND PRODUCTION COSTS		CAPITAL COSTS		CONSTRUCTION SCHEDULE						
	\$MM/yr		\$MM	Year	% FC	% WC	% FCOP	% VCOP		
Main product revenue	16.39	ISBL Capital Cost	44.4	1	30.00%		0.00%	0.00%		
Byproduct revenue	0.68	OSBL Capital Cost	4.4	2	70.00%		0.00%	0.00%		
Raw materials cost		Engineering Costs	7.3	3	0.00%		100.00%	50.00%		
Utilities cost	5.95	Contingency	12.2	4	0.00%		100.00%	70.00%		
Consumables cost		Total Fixed Capital Cos	68.4	5	0.00%		100.00%	100.00%		
VCOP	5.26	Working Capital	0.0	6	0.00%		100.00%	100.00%		
Salary and overheads	1.34			7+	0.00%		100.00%	100.00%		
Maintenance	1.33									
Interest	0.44									
Royalties										
FCOP	3.12									
ECONOMIC ASSUMPTIONS										
Cost of equity		Debt ratio		Tax rate	22%					
Cost of debt				Depreciation method	Straight line					
Cost of capital	6%			Depreciation period	10 years					
CASH FLOW ANALYSIS										
All figures in \$MM unless indicated										
Project year	Cap Ex	Revenue	CCOP	Gr. Profit	Deprcn	Taxbl Inc	Tax Paid	Cash Flow	PV of CF	NPV
1	20.5	0.0	0.0	0.0	0.0	0.0	0.0	-20.5	-19.4	-19.4
2	47.9	0.0	0.0	0.0	0.0	0.0	0.0	-47.9	-42.6	-62.0
3	0.0	8.2	5.8	2.4	6.8	-4.4	0.0	2.4	2.1	-60.0
4	0.0	11.5	6.8	4.7	6.8	-2.2	-1.0	5.6	4.5	-55.5
5	0.0	16.4	8.4	8.0	6.8	1.2	-0.5	8.5	6.3	-49.1
6	0.0	16.4	8.4	8.0	6.8	1.2	0.3	7.8	5.5	-43.7
7	0.0	16.4	8.4	8.0	6.8	1.2	0.3	7.8	5.2	-38.5
8	0.0	16.4	8.4	8.0	6.8	1.2	0.3	7.8	4.9	-33.7
9	0.0	16.4	8.4	8.0	6.8	1.2	0.3	7.8	4.6	-29.1
10	0.0	16.4	8.4	8.0	6.8	1.2	0.3	7.8	4.3	-24.7
11	0.0	16.4	8.4	8.0	6.8	1.2	0.3	7.8	4.1	-20.6
12	0.0	16.4	8.4	8.0	6.8	1.2	0.3	7.8	3.9	-16.8
13	0.0	16.4	8.4	8.0	0.0	8.0	0.3	7.8	3.6	-13.2
14	0.0	16.4	8.4	8.0	0.0	8.0	1.8	6.2	2.8	-10.4
15	0.0	16.4	8.4	8.0	0.0	8.0	1.8	6.2	2.6	-7.8
16	0.0	16.4	8.4	8.0	0.0	8.0	1.8	6.2	2.5	-5.3
17	0.0	16.4	8.4	8.0	0.0	8.0	1.8	6.2	2.3	-3.0
18	0.0	16.4	8.4	8.0	0.0	8.0	1.8	6.2	2.2	-0.8
19	0.0	16.4	8.4	8.0	0.0	8.0	1.8	6.2	2.1	1.2
20	0.0	16.4	8.4	8.0	0.0	8.0	1.8	6.2	1.9	3.2
ECONOMIC ANALYSIS										
Average cash flow	7.1	\$MM/yr		NPV	10 years	-24.7	\$MM	IRR	10 years	-3.9%
Simple pay-back period	9.703	yrs			15 years	-7.8	\$MM		15 years	4.0%
Return on investment (10 yrs)	0.06%				20 years	3.2	\$MM		20 years	6.6%
Return on investment (15 yrs)	2.61%			NPV to yr	12	-16.8	\$MM			

Appendix E

Methanation Model

In this section the conservation equations, being the mass-, energy-, and momentum balances, are simplified to describe the gas within the tube. These differential equations together with several algebraic equations and chemical data are required for simulation of the temperature profile, gas velocity profile, pressure profile, and mass fraction profiles of the components in both the axial and radial direction of the fixed bed reactor tube. A stationary pseudo-homogeneous (reaction takes place in bulk space of the tube) model is made where interparticle mass transport limitations are taken into account by an effectiveness factor (η). The choice for the pseudo-homogeneous model was to reduce the computational effort so that the convergence time remains minimal.

E.1 Continuity Equation

The continuity or total mass balance is given in Equation E.1. This equation is provided as the governing equation in vector notation [37] for the bulk phase inside the cylindrical tube.

$$\frac{\partial \rho}{\partial t} + \nabla \cdot (\rho \mathbf{u}) = 0 \quad (\text{E.1})$$

Since the process is stationary, the first term on the LHS can be neglected to get the stationary three-dimensional continuity equation as

$$\nabla \cdot (\rho \mathbf{u}) = 0 \quad (\text{E.2})$$

By assuming that the radial and angular convective terms are neglectable¹ and applying the product rule the equation reduces to

$$\frac{\partial}{\partial z}(\rho_g u_z) = \rho_g \frac{\partial u_z}{\partial z} + u_z \frac{\partial \rho_g}{\partial z} = 0 \quad (\text{E.3})$$

Further rearrangement gives

$$\frac{du_z}{dz} = -\frac{u_z}{\rho_g} \frac{d\rho_g}{dz} \quad (\text{E.4})$$

The density derivative is substituted by Equation E.56 assuming ideal gas to reduce the number of derivatives to be solved.

$$\frac{du_z}{dz} = -\frac{u_z}{\rho_g} \left(\frac{\rho_g}{M} \frac{dM}{dz} + \frac{\rho_g}{p} \frac{dp}{dz} - \frac{\rho_g}{T} \frac{dT}{dz} \right) \quad (\text{E.5})$$

Finally, above equation can be rearranged to obtain the axial velocity profile.

$$\boxed{\frac{du_z}{dz} = \frac{u_z}{T} \frac{dT}{dz} - \frac{u_z}{p} \frac{dp}{dz} - \frac{u_z}{M} \frac{dM}{dz}} \quad (\text{E.6})$$

¹To avoid solving the momentum balance, boundary conditions for the radial velocity are introduced.

E.2 Species Mass Balance

The species i mass balance in terms of flux \mathbf{j}_i is given in Equation E.7. This equation is provided as the governing equation in vector notation [37] of the species mass balances for the bulk phase inside the cylindrical tube.

$$\frac{\partial(\rho\omega_i)}{\partial t} + \nabla \cdot (\rho\mathbf{u}\omega_i) = -\nabla \cdot \mathbf{j}_i + R_i \quad (\text{E.7})$$

(1) (2) (3) (4)

Where, (1) is the mass accumulation which is zero for a stationary process, (2) is the transport due to convection/advection, (3) is the transport due to molecular diffusion that can be described by Fick's first law as $\mathbf{j}_i = -\rho_g D_r \nabla \omega_i$ and (4) is the species reaction rate described by $R_i = R_i M_i \zeta \rho_{cat} (1 - \varepsilon) \eta$ for having reaction rate units in mass basis per reactor volume [$kg_{cat} m_{bulk}^{-3} s^{-1}$] taking a catalyst dilution factor (ζ) in account to limit the reaction rate and temperature hotspot.

Implementing the molecular diffusion and reaction terms and removing the negligible terms, gives the stationary three-dimensional species mass balance as

$$\nabla \cdot (\rho_g \mathbf{u} \omega_i) = \nabla \cdot (\rho_g D_r \nabla \omega_i) + R_i M_i \zeta \rho_{cat} (1 - \varepsilon) \eta \quad (\text{E.8})$$

By assuming that the radial and angular convective terms can be neglected, that the effective radial dispersion coefficient (D_r) is constant throughout the cross-section and that angular and axial dispersion terms are negligible, equation E.8 reduces to

$$\frac{\partial}{\partial z} (\rho_g u_z \omega_i) = D_r \frac{1}{r} \frac{\partial}{\partial r} \left[r \rho_g \frac{\partial \omega_i}{\partial r} \right] + R_i M_i \zeta \rho_{cat} (1 - \varepsilon) \eta \quad (\text{E.9})$$

Applying the product rule and rearrangement gives the species mass balance as

$$\frac{\partial \omega_i}{\partial z} = \frac{1}{u_z \rho_g} \left(D_r \left[\frac{\partial \rho_g}{\partial r} \frac{\partial \omega_i}{\partial r} + \frac{\rho_g}{r} \frac{\partial \omega_i}{\partial r} + \rho_g \frac{\partial^2 \omega_i}{\partial r^2} \right] - u_z \omega_i \frac{\partial \rho_g}{\partial z} - \rho_g \omega_i \frac{\partial u_z}{\partial z} + R_i M_i \zeta \rho_{cat} (1 - \varepsilon) \eta \right) \quad (\text{E.10})$$

Finally, the axial and radial density derivatives (Equations E.57 and E.59) as well as the axial velocity derivative (Equation E.6) are substituted to reduce the number of derivatives to be solved by the ode15s solver. Note, that by doing this, the two RHS convective terms cancel out. This gives the axial mass fraction profiles for the gas mixture components.

$$\boxed{\frac{\partial \omega_i}{\partial z} = \frac{D_r}{u_z} \left(\frac{1}{r} \frac{\partial \omega_i}{\partial r} + \frac{\partial^2 \omega_i}{\partial r^2} - \frac{1}{r} \frac{\partial T}{\partial r} \frac{\partial \omega_i}{\partial r} \right) + \frac{R_i M_i \zeta \rho_{cat} (1 - \varepsilon) \eta}{\rho_g u_z}} \quad (\text{E.11})$$

$$i = \text{CH}_4, \text{CO}, \text{H}_2, \text{H}_2\text{O}, \text{ and } \text{N}_2$$

To reduce the number of species mass balance equations to be solved and thus reducing the computational effort, component CO₂ is calculated by the fact that the sum of the species mass fractions is equal to one. Therefore, the mass fractions of CH₄, CO, H₂, H₂O, and N₂ are the only components that are solved by the differential solver while the mass fraction of CO₂ for all z is solved by

$$\omega_{CO_2} = 1 - \left(\omega_{CH_4} + \omega_{CO} + \omega_{H_2} + \omega_{H_2O} + \omega_{N_2} \right) \quad (E.12)$$

Component CO₂ is chosen because it has the highest overall concentration, therefore, the residuals are less significant compared to when another components is chosen.

E.3 Energy Balance

The governing equation in terms of temperature T and flux \mathbf{q} is given in Equation E.13 and is referred to as the energy balance. This equation is provided as a governing equation in vector notation [37] to find the temperature profile of the bulk phase inside the cylindrical tube.

$$\rho C_p \frac{\partial T}{\partial t} + \rho C_p \mathbf{u} \cdot \nabla T = -\nabla \cdot \mathbf{q} - \frac{T}{\rho} \left(\frac{\partial \rho}{\partial T} \right)_{p,w} \frac{Dp}{Dt} - \sigma : \nabla \mathbf{u} + \sum_{r=1}^R \frac{h_r}{M_r} \nabla \cdot \mathbf{j}_r + \sum_{r=1}^R \frac{R_r}{M_r} (-\Delta H_{R_r}) \quad (E.13)$$

(1) (2) (3) (4) (5) (6) (7)

Where, (1) is the change of heat content with time which is zero for a stationary process, (2) is the convective/advective transport, (3) is the heat transport by conduction within the bulk phase, that can be described by Fourier's law as $\mathbf{q} = -\lambda_{er} \nabla T$, (4) is the change of heat content with time due to compression which is negligible for a stationary process, (5) is the viscous heat dissipation term which is negligible, (6) is the radiation heat flux in the fluid, which is negligible and (7) is the energy production/consumption caused by the number of chemical reactions (R) in this process, being only the CO₂ methanation reaction, can be described in correct units as $R_{meth} = R_{meth} M \zeta \rho_{cat}(1 - \varepsilon) \eta$.

Implementing Fourier's law, the reaction rate expression and reducing negligible terms gives the stationary three dimensional energy balance as

$$\rho_g C_p \mathbf{u} \cdot \nabla T = \nabla \cdot (\lambda_{er} \nabla T) + R_{meth} \zeta \rho_{cat}(1 - \varepsilon) \eta (-\Delta H_{R_{meth}}) \quad (E.14)$$

By assuming that the radial and angular advective terms can be neglected, that the effective radial conductivity (λ_{er}) is constant throughout the cross-section and that angular and axial conduction terms are negligible, equation E.14 reduces to find the axial temperature profile as

$$\frac{\partial T}{\partial z} = \frac{1}{\rho_g C_p u_z} \left(\lambda_{er} \left(\frac{1}{r} \frac{\partial T}{\partial r} + \frac{\partial^2 T}{\partial r^2} \right) + R_{meth} \zeta \rho_{cat}(1 - \varepsilon) \eta (-\Delta H_{R_{meth}}) \right) \quad (E.15)$$

In addition to the axial temperature profile, it is necessary to find the heat flow from the gas inside the tubes towards the coolant. This heat flow can be described according to the heat transfer rate equation commonly used for heat exchanger unit operations [38].

$$Q = U A \Delta T \quad [W] \tag{E.16}$$

To find the heat transfer per unit length of a single cylindrical reactor tube, it is possible to integrate E.16 over the area of a tube ($A = \pi D L = 2\pi r L$).

$$Q = \int_0^A (U \Delta T) dA = \int_0^L \int_0^{2\pi r} (U \Delta T) dc dz = 2\pi r \int_0^L (U \Delta T) dz \tag{E.17}$$

The heat transfer per unit length for the tube bundle consisting of N_t tubes becomes

$$\boxed{\frac{dQ}{dz} = 2\pi r_1 N_t U (T|_{r=r_1} - T_{coolant})} \tag{E.18}$$

where,

$$\frac{1}{U} = \frac{1}{h_{gas}} + \frac{r_1}{k_w} \ln\left(\frac{r_2}{r_1}\right) + \frac{r_1}{r_2 h_{coolant}} \quad [W^{-1} m^2 K^1] \tag{E.19}$$

Note, that three thermal resistances are present in the determination of the heat transfer coefficient (U). One is the thermal resistance of the tube wall (conduction - k_w) and the others are the thermal resistances from the fluids on each side of the wall (convection - h_{gas} & $h_{coolant}$).

The overall heat transfer coefficient is dominated by the smallest heat convection coefficient, since the inverse of a large number gives a small number. In this case, the gas in the tube has the smallest heat convection coefficient and dominates the overall heat transfer coefficient [38].

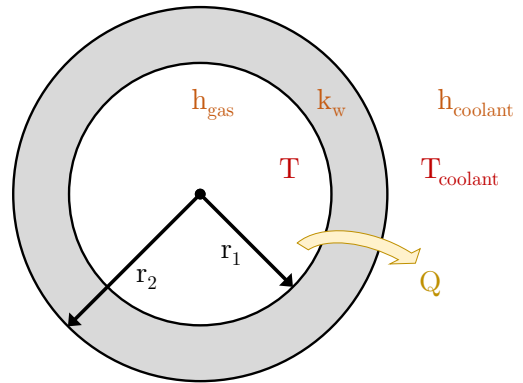


Figure E.1: Heat transfer coefficients for reactor tube.

The heat transfer coefficients are determined in Appendix E.7.

E.4 Momentum Balance

The Equation of Motion is given in Equation E.20. This equation is provided as a governing equation in vector notation [37] and is the basis to find the pressure profile within the cylindrical tube.

$$\frac{\partial(\rho\mathbf{u})}{\partial t} + \nabla \cdot (\rho\mathbf{u}\mathbf{u}) = -\nabla p - \nabla \cdot \sigma + \rho\mathbf{g} \quad (\text{E.20})$$

With regard to pressure changes within the fixed-bed reactor, it has been assumed that the momentum balance is dominated by friction (f). This allows to rely on Ergun equation for flow through porous media to model the axial pressure drop. Therefore, the simplified momentum balance becomes

$$-\frac{dp}{dz} = f \frac{u_z^2 \rho_g}{D_p} \quad (\text{E.21})$$

Where, the friction factor is described by

$$f = \frac{1 - \varepsilon}{\varepsilon^3} \left[a + b \frac{1 - \varepsilon}{Re_p} \right] \quad (\text{E.22})$$

The constants a and b are not true constants and are limited for specified Reynolds numbers (Re). For the original Ergun equation $a = 1.75$ and $b = 150$, but it has been found that Ergun's equation is limited at $Re/(1 - \varepsilon) < 500$. Therefore, Tallmange suggested $a = 1.75$ and $b = 4.2 Re_p^{5/6}$ to increase the valid operational range [39]. Tallmange's coefficients are therefore applied in this model, making the friction factor as

$$f = \frac{1 - \varepsilon}{\varepsilon^3} \left[1.75 + 4.2 Re_p^{5/6} \frac{1 - \varepsilon}{Re_p} \right] \quad (\text{E.23})$$

Inserting the friction factor and particle Reynolds number (Re_p) into equation E.24 gives the axial pressure profile over the reactor length (axial direction).

$$\boxed{-\frac{dp}{dz} = u_z \frac{1 - \varepsilon}{\varepsilon^3} \left[1.75 \frac{u_z \rho_g}{D_p} + 4.2 Re_p^{5/6} \frac{(1 - \varepsilon) \mu}{D_p^2} \right]} \quad (\text{E.24})$$

Ergun's equation is applicable to all types of flow (laminar, transition, turbulent) and gives the total energy loss due to motion as the sum of the viscous energy loss (first RHS term) and the kinetic/turbulent energy loss (second RHS term). For gas phase systems, approximately 80% of the energy loss is dependent on turbulence and thus the second RHS term is contributing stronger to the pressure drop [39].

The radial changes of the density, velocity and Reynolds number are area averaged.

E.5 Boundary Conditions

The system equations derived before are solved by Neumann (value as a derivative of the solution) and Dirichlet type (value of the solution itself) boundary conditions. These boundary conditions are provided for the cylindrical reactor tube and consist of inlet ($z = z_0$), centre ($r = r_0$) and wall ($r = r_1$) definitions for the to be solved parameters: mass fractions (ω_i), temperature (T), heat flow (Q) and superficial velocity (u_z). All inlet boundary conditions are specified directly into the ode15s solver while the radial boundary conditions are inserted into the dss020 and dss042 discretisation schemes.

Mass fractions:
$$\omega_i \Big|_{z=z_0} = \omega_{in,i} \quad \text{for } r_0 \leq r \leq r_1$$

$$\frac{d\omega_i}{dr} \Big|_{r=r_0} = 0 \quad \text{for } z_0 \leq z \leq L$$

$$\frac{d\omega_i}{dr} \Big|_{r=r_1} = 0 \quad \text{for } z_0 \leq z \leq L$$

Temperature:
$$T \Big|_{z=z_0} = T_{in} \quad \text{for } r_0 \leq r \leq r_1$$

$$\frac{dT}{dr} \Big|_{r=r_0} = 0 \quad \text{for } z_0 \leq z \leq L$$

$$\frac{dT}{dr} \Big|_{r=r_1} = -\frac{U}{\lambda_{er}} (T \Big|_{r=r_1} - T_{coolant}) \quad \text{for } z_0 \leq z \leq L$$

Heat flow:
$$Q \Big|_{z=z_0} = 0 \quad \text{for } r_0 \leq r \leq r_1$$

Superficial gas velocity:
$$u_z \Big|_{z=z_0} = u_{z,in} \quad \text{for } r_0 \leq r \leq r_1$$

$$\frac{du_z}{dr} \Big|_{r=r_0} = 0 \quad \text{for } z_0 \leq z \leq L$$

$$\frac{du_z}{dr} \Big|_{r=r_1} = 0 \quad \text{for } z_0 \leq z \leq L$$

E.6 Reaction Rate

Determination of the reaction rate properties is performed by applying the reaction kinetics from Koschany et al. [16] for the CO₂ methanation reaction, obtaining the reaction enthalpy for the operational temperature range from `HSC chemistry` and taking interparticle mass transfer expressions from Bremer et al. [26] together with Robert et al. [40] to improve the accuracy of the model.

Reaction Kinetics

The CO₂ methanation reaction kinetics from Koschany et al. (2016) have been implemented in a MATLAB model as a two-dimensional pseudo-homogeneous reactor connected to the HYSYS worksheet using `CAPE-OPEN`. To verify the model results obtained from the MATLAB model, these kinetics have also been implemented in a HYSYS model as a plug flow reactor unit operation.

The nickel-based catalyst (Ni/Al₂O₃) studied in their article is a state-of-art methanation catalyst with a relatively high activity (compared to practical steam reforming catalysts) having a Ni/Al ratio of 1. The reaction kinetics of this catalyst depends on a Langmuir-Hinshelwood Hougen-Watson (LHHW) type rate equation, measured and parameterised for conditions between 180-340 °C and 1-9 bar for both a stoichiometric and non-stoichiometric feed. For operational conditions outside of the temperature range the usage of this rate equation is valid since the reaction rate is limited by chemical equilibrium for higher temperatures (thermodynamic limitation) and approaches zero for lower temperatures (kinetic limitation) [16, 26]. Higher operational pressures increase uncertainties.

The reaction mechanism to derive the LHHW kinetic rate equation is based on the so-called hydrogen assisted pathway in CO methanation where first hydrogen reacts with CO to form the formyl HCO before carbon is split from oxygen [16] and is shown in Table E.1.

Table E.1: Reaction mechanism for CO₂ methanation for derivation of LHHW rate equation [16].

Step	Reaction	Note
1	$\text{CO}_2 + 2 * \rightleftharpoons \text{CO}^* + \text{O}^*$	
2	$\text{H}_2 + 2 * \rightleftharpoons 2 \text{H}^*$	
3	$\text{CO}^* + \text{H}^* \rightleftharpoons \text{CHO}^* + *$	Rate determining step
4	$\text{CHO}^* + * \rightleftharpoons \text{CH}^* + \text{O}^*$	
5	$\text{CH}^* + 3 \text{H}^* \rightleftharpoons \text{CH}_4^* + 3 *$	
6	$\text{CH}_4^* \rightleftharpoons \text{CH}_4 + *$	
7	$\text{O}^* + \text{H}^* \rightleftharpoons \text{OH}^* + *$	Irreversible
8	$\text{OH}^* + \text{H}^* \rightleftharpoons \text{H}_2\text{O}^* + *$	} Equilibrium
9	$\text{H}_2\text{O}^* \rightleftharpoons \text{H}_2\text{O} + *$	

The kinetic rate equation is derived from this reaction mechanism assuming that the process is in steady state (SSA), step 3 is the rate determining step, step 7 is irreversible, step 8 and 9 are in equilibrium and that hydrogen, carbon monoxide and the hydroxyl are the most abundant surface intermediates (MASI) so that [16]

$$R_{meth} = k p_{CO_2}^{0.5} p_{H_2}^{0.5} \left(1 - \frac{p_{CH_4} p_{H_2O}^2}{K_{eq} p_{CO_2} p_{H_2}^4} \right) / DEN^2 \quad [kmol \text{ kg}_{cat}^{-1} \text{ s}^{-1}] \quad (E.25)$$

$$DEN = 1 + K_{OH} p_{H_2O} p_{H_2}^{-0.5} + K_{H_2} p_{H_2}^{0.5} + K_{mix} p_{CO_2}^{0.5} \quad (E.26)$$

The corresponding rate (k) and adsorption constants (K_x) in parameterised form given as [16]

$$k = k_{ref} \cdot \exp \left(\frac{E_A}{R} \left(\frac{1}{T_{ref}} - \frac{1}{T} \right) \right) \quad [kmol \text{ bar}^{-1} \text{ kg}_{cat}^{-1} \text{ s}^{-1}] \quad (E.27)$$

$$K_x = A_{x,ref} \cdot \exp \left(\frac{\Delta H_x}{R} \left(\frac{1}{T_{ref}} - \frac{1}{T} \right) \right) \quad [bar^{-0.5}] \quad (E.28)$$

Where, the kinetic parameter estimation at the reference temperature (T_{ref}) of 555K gives the following values for the pre-exponential factors (k_{ref} and $A_{x,ref}$), activation energy (E_A) and adsorption enthalpy (ΔH_x) as [16]

Parameter	Value	Unit
k_{555K}	$3.46 \cdot 10^{-4}$	$kmol \text{ bar}^{-1} \text{ kg}_{cat}^{-1} \text{ s}^{-1}$
E_A	$77.5 \cdot 10^6$	$J \text{ kmol}^{-1}$
$A_{OH,555K}$	0.50	$bar^{-0.5}$
ΔH_{OH}	$22.4 \cdot 10^6$	$J \text{ kmol}^{-1}$
$A_{H_2,555K}$	0.44	$bar^{-0.5}$
ΔH_{H_2}	$-6.2 \cdot 10^6$	$J \text{ kmol}^{-1}$
$A_{mix,555K}$	0.88	$bar^{-0.5}$
ΔH_{mix}	$-10.0 \cdot 10^6$	$J \text{ kmol}^{-1}$

The negative term in Equation E.25 indicates the chemical equilibrium concentration for the CO₂ methanation reaction and is characterised by its equilibrium constant (K_{eq}) which is expressed as

$$K_{eq} = A_q T^\beta \cdot \exp \left(\frac{E_q}{RT} \right) \quad [bar^{-2}] \quad (E.29)$$

Here, the factors (A_q , β and E_q) are determined for the temperature range of 150-450 °C by using data from HSC chemistry and verified by HYSYS.

For the MATLAB model, the form of the rate equations above is valid. However, for the HYSYS model implementation it is required to rearrange the expressions to their non-parameterised form and further

fit them to the HYSYS format as

$$R_{meth} = \left(k p_{CO_2}^{0.5} p_{H_2}^{0.5} - k' \frac{p_{CH_4} p_{H_2O}^2}{p_{CO_2}^{0.5} p_{H_2}^{3.5}} \right) / DEN^2 \quad [kmol m_{bulk}^{-3} s^{-1}] \quad (E.30)$$

$$DEN = 1 + K_{OH} p_{H_2O} p_{H_2}^{-0.5} + K_{H_2} p_{H_2}^{0.5} + K_{mix} p_{CO_2}^{0.5}$$

Where,

$$k = k_{ref} \cdot \exp\left(\frac{-E_A}{RT}\right) \quad [kmol bar^{-1} m_{bulk}^{-3} s^{-1}] \quad (E.31)$$

$$k' = \frac{k}{K_{eq}} = \frac{k_{ref} \cdot \exp(-E_A/RT)}{A_q \cdot T^\beta \cdot \exp(E_q/RT)} = A' \cdot T^{-\beta} \cdot \exp\left(\frac{-E'}{RT}\right) \quad (E.32)$$

$$K_x = A_{x,ref} \cdot \exp\left(\frac{-\Delta H_x}{RT}\right) \quad [bar^{-0.5}] \quad (E.33)$$

so that,

$$A' = \frac{k_{ref}}{A_q} \quad E' = E_A - E_q \quad (E.34)$$

In addition, it is required to convert k and k' to reactor volume basis and taking into account the effectiveness factor as well as the dilution factor directly to get

$$k_{ref,new} = k_{ref,old} \cdot \zeta \rho_{cat} (1 - \varepsilon) \eta \quad [kmol bar^{-1} m_{bulk}^{-3} s^{-1}] \quad (E.35)$$

Reaction Enthalpy

To determine the reaction enthalpy for the CO₂ methanation reaction accurately for the process temperature range between 150-600 °C, data has been extracted by HSC Chemistry and fitted by a polynomial to find the factors required.

$$\Delta H_R = \left(-1.47040 \cdot 10^2 - 6.59812 \cdot 10^{-2} T + 2.31450 \cdot 10^{-5} T^2 + 1.51675 \cdot 10^{-10} T^3 \right) \cdot 10^6 \quad [J kmol^{-1}] \quad (E.36)$$

Intraparticle Mass Transport Limitations

The pseudo-homogeneous model assumes that the diffusion and reaction of species takes place in the bulk phase. In practice, this takes place mainly inside the catalyst. Therefore, the pseudo-homogeneous model does not explicitly take the mass transport limitations in the catalyst particles into account which leads to an unreal representation of the methanation process. To include intraparticle mass transport limitations, an effectiveness factor (η) is introduced that associates the mass transport limitations as obtained in the pseudo-homogeneous model to a heterogeneous model. The choice to not model the process with a heterogeneous model is to minimise the computational efforts and thus limit the convergence time.

$$\eta = \frac{\text{Actual rate of reaction (including mass transfer limitations)}}{\text{Predicted rate of reaction (of pseudo-homogeneous model)}} \quad (\text{E.37})$$

The effectiveness factor implemented in the pseudo-homogeneous model is based on the Thiele modulus for spherical particles assuming that the CO_2 methanation reaction is a first order reaction (ϕ_{meth}) and is given as

$$\eta = \frac{3}{\phi_{meth}} \left[\frac{1}{\tanh(\phi_{meth})} - \frac{1}{\phi_{meth}} \right] \quad [-] \quad (\text{E.38})$$

To determine the Thiele modulus it is assumed that the rate of the CO_2 methanation reaction is limited by species CO_2 (because it has the highest overall mass fraction in the gas mixture). This makes CO_2 the key component in determining the mass transfer limitations. In addition, the concentration of CO_2 (C_{CO_2}) is found with the ideal gas law to be $C_{\text{CO}_2} = p x_{\text{CO}_2} / RT$ and the stoichiometric constant of CO_2 (ν_{CO_2}) is -1 according to the CO_2 methanation reaction.

The Thiele modulus can in this case be expressed as

$$\phi_{meth} = \frac{D_p}{2} \sqrt{\frac{\nu_{\text{CO}_2} R_{meth}}{D_{e,\text{CO}_2} C_{\text{CO}_2}}} = \frac{D_p}{2} \sqrt{\frac{-R_{meth} RT}{D_{e,\text{CO}_2} p x_{\text{CO}_2}}} \quad [-] \quad (\text{E.39})$$

where, the effective diffusion coefficient of CO_2 (D_{e,CO_2}) for mass transport within the catalyst is determined from the Bosanquet equation with molecular diffusion (D_{m,CO_2}) for gas-gas collisions and Knudsen diffusion (D_{Kn,CO_2}) for gas-wall collisions. In addition, the effective diffusion coefficient takes into account the particle configuration by the particle porosity (ε_p), tortuosity (τ_p) and the average pore diameter (D_{pore}) as well as interactions between the different gas species and is given as [26]

$$\frac{1}{D_{e,\text{CO}_2}} = \frac{\tau_p}{\varepsilon_p} \left[\frac{1}{D_{m,\text{CO}_2}} + \frac{1}{D_{Kn,\text{CO}_2}} \right] \quad [m_p \text{ s } m_b^{-3}] \quad (\text{E.40})$$

where, the Knudsen diffusion, independent of the other species in the gas mixture, is [26]

$$D_{Kn,CO_2} = \frac{D_{pore}}{3} \sqrt{\frac{8RT}{\pi M_{CO_2}}} \quad (E.41)$$

and the molecular diffusion, dependent on the other gas species, is determined from a simplified form of the Maxwell-Stefan formula called the mixture-averaged diffusion coefficient [40]

$$\frac{1}{D_{m,CO_2}} = \sum_{i \neq j}^{N-1} \frac{y_i}{D_{ij}} + \frac{y_j}{1 - w_j} \sum_{i \neq j}^{N-1} \frac{w_i}{D_{ij}} \quad (E.42)$$

where, $i = CH_4, CO, H_2, H_2O$ and N_2 , $j = CO_2$, N is the number of components in the gas mixture (6), y is mole fraction, w is mass fraction and D_{ij} are the binary diffusion coefficients that are determined by an equation developed by Fuller et al. (1966) [17]

$$D_{ij} = \frac{1.013 \cdot 10^{-7} T^{1.75} \left(\frac{1}{M_i} + \frac{1}{M_j} \right)^{\frac{1}{2}}}{p \left[\left(\sum_i \nu_k \right)^{\frac{1}{3}} + \left(\sum_j \nu_k \right)^{\frac{1}{3}} \right]^2} \quad [m_b^3 m_p^{-1} s^{-1}] \quad (E.43)$$

It has to be noted that the mixture-averaged diffusion coefficient only requires calculation for interactions between $j = CO_2$ and the $i \neq j$ species (resulting D_{ij} vector: $[CH_4;CO_2, CO;CO_2, H_2;CO_2, H_2O;CO_2, N_2;CO_2]$) and assumes that the velocities of species $i \neq j$ are equal, diffusion takes place according to Fick's law and that the Maxwell-Stefan formula is isothermal, isobaric, equimolar and in steady state. This approach gives a limited accuracy due to the selection of one key component and a mixture-averaged diffusion coefficient for the molecular diffusion, but gives a relatively good approach to the general solution according to Bremer (2019).

Intraparticle Heat Transport Limitations

The mass transfer limitations have been taken into account by applying the effectiveness factor (η) to increase model accuracy. However, it is assumed that the particle temperature is equal to the fluid temperature for all positions in the cylindrical tube. This assumption is reducing the modelling accuracy, but is in practice often found neglectable. The heat and concentration profiles within a single catalyst particle is illustrated in Figure E.2.

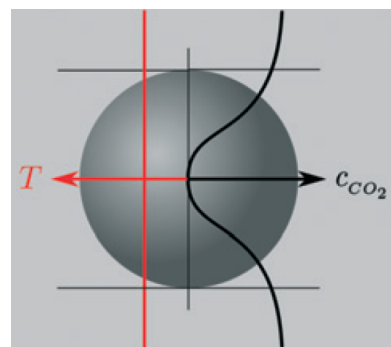


Figure E.2: Heat/Mass transport limitations within catalyst particle.

E.7 Heat Coefficients

The heat transfer coefficients for conduction (k_w) in the cylinder material and convection (h_{gas} and $h_{coolant}$) of the fluids inside and outside of the tube need to be determined for an accurate determination of the overall heat transfer coefficient (U). In addition, the effective radial conductivity (λ_{er}) for the gas mixture inside the tube must be determined.

It is assumed that the tubes in the reactor are made from 0.5% carbon steel with an outer diameter of one inch ($r_2 = 1.47$ cm) and a thickness of 2mm ($r_1 = 1.27$ cm). According to Sinnott & Towler [17] the corresponding heat transfer coefficient (k_w) for this material is 54 W/m/K and is used with the assumption that it does not vary with temperature.

On the inside of the tube a single gas phase is present consisting of several gas species. While on the outside of the tube a phase change from liquid to gas (flow boiling) of water takes place. The heat transfer coefficient for the fluids on both sides of the tube can be determined from the fluid's conductivity (λ) and dimensionless groups. However, the outside heat coefficient is approximated equal to 5000 W/m²/K as a model simplification which value is extracted from [28].

As discussed previously, the heat transfer coefficient for the gas inside the tube gives the largest contribution to the overall heat transfer coefficient. The heat transfer coefficient for the gas mixture inside the tube close to the wall is [38]

$$h_{gas} = \frac{Nu \lambda_g}{D_p} \quad [W \ m^{-2} \ K] \quad (E.44)$$

Where, the Nusselt number expression for a cylindrical tube with $Re = 40-4000$ is [38]

$$Nu = 0.683 Re^{0.466} Pr^{0.3333} \quad (E.45)$$

It is also possible to calculate Nusselt based on the particle Reynolds number as [41]

$$Nu = 1.6 Re_p^{0.5} Pr^{0.3333} \quad (E.46)$$

Here, the Reynolds and Prandtl number are [37]

$$Re = \frac{\rho_g u_z D_{T,i}}{\mu_g} \quad Re_p = \frac{\rho_g u_z D_p}{\mu_g} \quad (E.47)$$

$$Pr = \frac{\mu_g C_{p_g}}{\lambda_g} \quad (E.48)$$

The effective radial conductivity is a parameter that is modelled considering the presence of two contributions, the first is dependent on the flow conditions while the second is in the absence of flow [42].

$$\lambda_{er} = \lambda_{er}^0 + \lambda_{er}^t \quad (E.49)$$

The static term (λ_{er}^0) is according to Yagi, Kunii and Smith (1960) caused by transport through fluid in the void space of the reactor as well as transport through the void space of the catalyst particles and can be described by Jakobsen [42].

$$\frac{\lambda_{er}^0}{\lambda_g} = \varepsilon \left(1 + \beta \frac{D_p \alpha_{rv}}{\lambda_g} \right) + \frac{\beta(1 - \varepsilon)}{\left[\frac{1}{\phi} + \frac{D_p \alpha_{rs}}{\lambda_g} \right]^{-1} + \gamma \frac{\lambda_g}{\lambda_{cat}}} \quad (E.50)$$

Where,

$$\alpha_{rv} = \frac{0.227 \cdot 10^{-3}}{1 + \frac{\varepsilon}{2(1 - \varepsilon)} \frac{1 - p}{p}} \left(\frac{T}{100} \right)^3 \quad (E.51)$$

$$\alpha_{rs} = 0.227 \cdot 10^{-3} \frac{1 - p}{p} \left(\frac{T}{100} \right)^3 \quad (E.52)$$

Where, the β coefficient depending on the particle geometry and packing density is between 0.9 and 1.0 (1.0 is selected), $p = 1.0$, $\gamma = \frac{2}{3}$ and $\phi = 0.3$ [42].

The dynamic term (λ_{er}^t) is based on solely on the heat transport in the fluid and is in analogy with the mass transfer through the fluid. The dynamic contribution is [42]

$$\frac{\lambda_{er}^t}{\lambda_g} = \Psi Pr Re_p \quad (E.53)$$

Where, Ψ for a cylindrical packing is given as 0.14.

E.8 Model Equations

The other algebraic and differential equations used to solve the model are presented in this chapter. This includes the axial and radial profiles for the gas density from ideal gas assumption, conversion from mole to mass fractions, mass dispersion coefficient and expressions that describe the chemical and physical properties in the model.

Density Gradient in Axial and Radial Direction

The gas mixture density is found from the ideal gas law as

$$pV = nRT, \quad , \text{ with } \rho_g = \frac{m}{V} = \frac{pM}{RT} \quad \longrightarrow \quad \rho_g = \frac{pM}{RT} \quad (\text{E.54})$$

Differentiating both sides of equation E.54 with respect to the axial direction gives

$$\frac{d}{dz}(\rho_g) = \frac{d}{dz}\left(\frac{pM}{RT}\right) \quad (\text{E.55})$$

Applying the product rule and reciprocal rule on Equation E.55 while assuming that R is constant gives

$$\frac{d\rho_g}{dz} = \frac{p}{RT} \frac{dM}{dz} + \frac{M}{RT} \frac{dp}{dz} - \frac{pM}{RT^2} \frac{dT}{dz} \quad (\text{E.56})$$

This expression can be further simplified by substituting equation E.54 into each of the terms to give the gas mixture density in axial direction as

$$\boxed{\frac{d\rho_g}{dz} = \frac{\rho_g}{M} \frac{dM}{dz} + \frac{\rho_g}{p} \frac{dp}{dz} - \frac{\rho_g}{T} \frac{dT}{dz}} \quad (\text{E.57})$$

For the radial derivative, differentiating both sides of equation E.54 gives

$$\frac{d}{dr}(\rho_g) = \frac{d}{dr}\left(\frac{pM}{RT}\right) \quad (\text{E.58})$$

Applying the reciprocal rule and assuming that the radial pressure (p), molar mass (M) and gas constant (R) are constant gives the gas mixture density in radial direction as

$$\boxed{\frac{d\rho_g}{dr} = \frac{-pM}{RT^2} \frac{dT}{dr} = \frac{-\rho_g}{T} \frac{dT}{dr}} \quad (\text{E.59})$$

The gas mixture density is now dependent on the temperature derivative for the radial direction and dependent on the temperature, pressure and molar mass for the axial direction. Conservation equations for the velocity, temperature, pressure and mass fraction derivatives have been found. However, the axial molar mass derivative is not, and therefore, a new expression is introduced.

The so called average molar mass is used to calculate the molar mass of the gas mixture from the molar mass of the pure species as

$$\bar{M} = \frac{1}{\sum_{i=1}^N \left(\frac{w_i}{M_i} \right)} \quad (\text{E.60})$$

Differentiating both sides of equation E.60 gives

$$\frac{d\bar{M}}{dz} = \frac{-1}{\bar{M}^2} \sum_{i=1}^N \left(\frac{1}{M_i} \frac{dw_i}{dz} \right) \quad (\text{E.61})$$

Mole Fraction Conversion

To determine the chemical properties such as the conductivity, viscosity and heat capacity, to plot the mole fraction profiles, and calculate other parameters it is necessary to convert the mass fractions into mole fractions or opposite.

To convert mass fractions to mole fractions use Equation E.62 below.

$$y_i = \frac{\frac{\omega_i}{M_i}}{\sum_{i=1}^N \frac{\omega_i}{M_i}} \quad (\text{E.62})$$

To convert mole fractions to mass fractions use Equation E.63 below.

$$w_i = \frac{\frac{y_i}{M_i}}{\sum_{i=1}^N \frac{y_i}{M_i}} \quad (\text{E.63})$$

To convert fractions, it is required to take all components in the gas mixture into account in contrary to the species mass balance. Also, the mole fractions have to be calculated for all points in the axial and radial direction of the tube.

Mass Dispersion Coefficient

The mass dispersion coefficient determination was taken for a two dimensional steam methane reforming model [37, 42] and is given as

$$D_r = \frac{u_z r_1}{Pe} \quad (E.64)$$

Where, the Peclet number is given to be [37, 42]

$$Pe = 8.8 \left[2 - \left(1 - \frac{D_p}{r_1} \right)^2 \right] \quad (E.65)$$

Conductivity of Components and Gas Mixture

This calculation is performed in MATLAB with a function called *heatcoef.m*.

The conductivities of the individual components (λ_i) present (CH₄, CO, CO₂, H₂, H₂O, N₂) can be calculated as

$$\lambda_i = A_i + B_i T + C_i T^2 + D_i T^3 \quad (E.66)$$

Where, the coefficients are given as:

i	A	B	C	D
CH ₄	$-1.869 \cdot 10^{-3}$	$8.727 \cdot 10^{-5}$	$1.179 \cdot 10^{-7}$	$-3.614 \cdot 10^{-11}$
CO	$5.067 \cdot 10^{-4}$	$9.1025 \cdot 10^{-5}$	$-3.524 \cdot 10^{-8}$	$8.199 \cdot 10^{-12}$
CO ₂	$-7.215 \cdot 10^{-3}$	$8.015 \cdot 10^{-5}$	$5.477 \cdot 10^{-9}$	$-1.053 \cdot 10^{-11}$
H ₂	$8.099 \cdot 10^{-3}$	$6.689 \cdot 10^{-4}$	$-4.158 \cdot 10^{-7}$	$1.562 \cdot 10^{-10}$
H ₂ O	$7.341 \cdot 10^{-3}$	$-1.013 \cdot 10^{-5}$	$1.801 \cdot 10^{-7}$	$-9.100 \cdot 10^{-11}$
N ₂	$3.919 \cdot 10^{-4}$	$9.816 \cdot 10^{-5}$	$-5.067 \cdot 10^{-8}$	$1.504 \cdot 10^{-11}$

The individual component conductivities determined in equation E.66 are used to determine the gas mixture conductivity (λ_g) by assuming a linear dependency.

$$\lambda_g = \sum_{i=1}^N (y_i \lambda_i) \quad [W \ m^{-1} \ K^{-1}] \quad (E.67)$$

Viscosity of Components and Gas Mixture

This calculation is performed in MATLAB in the function called *yderiv.m*.

The viscosities of the individual components (μ_i) can be computed from

$$\mu_i = \frac{b_i T^{1.5}}{T + S_i} \quad (E.68)$$

Where, the coefficients are given as:

i	b_i	S_i
CH_4	$1.00 \cdot 10^{-6}$	168
CO	$1.50 \cdot 10^{-6}$	220
CO_2	$1.50 \cdot 10^{-6}$	220
H_2	$0.65 \cdot 10^{-6}$	67
H_2O	$1.75 \cdot 10^{-6}$	625
N_2	$1.40 \cdot 10^{-6}$	108

The individual component viscosities determined in equation E.68 are used to determine the gas mixture viscosity (μ_g) by assuming a linear dependency.

$$\mu_g = \sum_{i=1}^N (y_i \mu_i) \quad [kg \ m^{-1} \ s^{-1}] \quad (E.69)$$

Heat Capacity of Components and Gas Mixture

This calculation is performed in MATLAB in the function called *yderiv.m*.

The heat capacity of the individual components (C_{p_i}) can be calculated with

$$C_{p_i} = A_i + B_i T + C_i T^2 + D_i T^3 \quad (E.70)$$

Where, the coefficients are given as:

i	A	B	C	D
CH_4	$1.925 \cdot 10^4$	$5.213 \cdot 10^1$	$1.197 \cdot 10^{-2}$	$-1.132 \cdot 10^{-5}$
CO	$3.087 \cdot 10^4$	$-1.285 \cdot 10^1$	$2.789 \cdot 10^{-2}$	$-1.272 \cdot 10^{-5}$
CO_2	$1.980 \cdot 10^4$	$7.344 \cdot 10^1$	$-5.602 \cdot 10^{-2}$	$1.715 \cdot 10^{-5}$
H_2	$2.714 \cdot 10^4$	$0.927 \cdot 10^1$	$-1.381 \cdot 10^{-2}$	$0.764 \cdot 10^{-5}$
H_2O	$3.224 \cdot 10^4$	$0.1924 \cdot 10^1$	$1.055 \cdot 10^{-2}$	$-0.3596 \cdot 10^{-5}$
N_2	$3.115 \cdot 10^4$	$-1.357 \cdot 10^1$	$2.680 \cdot 10^{-2}$	$-1.168 \cdot 10^{-5}$

The individual component heat capacities determined in equation E.70 are used to determine the gas mixture heat capacity (C_{p_g}) by assuming a linear dependency.

$$C_{p_g} = \sum_{i=1}^N (y_i C_{p_i}) \quad [J \ kg^{-1} \ K^{-1}] \quad (E.71)$$

E.9 MATLAB Model Code

In this appendix, the MATLAB code is listed that was used to model the methanation reactor with kinetics from Koschany (2016) for the CO₂ methanation reaction. Several scripts and functions have been implemented to make the model converge and communicate with HYSYS, as seen in figure 5.5.

Main Script

The main script, `main.m`, uses `ode15s` to solve the mass matrix with algebraic-differential equations consisting of the continuity equation, species mole balance, energy balance, heat balance, momentum balance with their boundary conditions as a function of z . The script also initiates plotting of the profiles and communication through the CAPE-OPEN unit operation. The `getFeedProp` property imports the inlet properties from the HYSYS feed stream, the `getParameter` property imports the specified parameter setpoint from the HYSYS spreadsheet and the `setProduct` property exports the result from the MATLAB script to the HYSYS product stream.

```

1  %%%%%%%%%%%%%%%%%%%%%%%%%%%%%%%%%%%%%%%%%%%%%%%%%%%%%%%%%%%%%%%%%%%%%%%%%%
2  %                                                                                               %
3  %      PSEUDO-HOMOGENEOUS, TWO-DIMENSIONAL MODEL OF CO2 METHANATION      %
4  %      REACTION IN A FIXED BED REACTOR WITH IMPLEMENTED                    %
5  %      KINETICS ACCORDING TO KOSCHANY2016                                   %
6  %                                                                                               %
7  %%%%%%%%%%%%%%%%%%%%%%%%%%%%%%%%%%%%%%%%%%%%%%%%%%%%%%%%%%%%%%%%%%%%%%%%%%
8
9  % main.m
10 % This script solves the component mass fractions (2D), Pressure (1D),
11 % Superficial velocity (2D) and the temperature (2D) and plots the result.
12 % x = variables, y = mole fraction, w = mass fraction.
13
14 clc          % clear text in command window
15 clear       % clear variables created in Workspace
16 close all   % close all opened plots
17 warning off % disable warnings in command window
18
19 tic         % Begin timer for simulation
20
21
22 %% DATA EXTRACTION
23 % -----
24
25 run('constant.m') % Run constant file
26
27 global LENGTH RADIUSi Tubes Rwall EPS EPSp tau Dpore Dp RHOcat zeta ...
28         LAMBDAcat kwall Tcoolant RP Ncomp Mmass GASCONST RADIUSo Dit
29
30
31 %% FEED PROPERTIES IMPORTED FROM HYSYS
32 % -----
33
34 Tin = getFeedProp(1, 'temperature'); % [K]
35 Pin = getFeedProp(1, 'pressure');    % [Pa]
36 Fin = getFeedProp(1, 'totalFlow');  % [mol/s]
37 yin = getFeedProp(1, 'fraction');   % [molfrac]
38
39
40 %% PARAMETERS IMPORTED FROM HYSYS
41 % -----

```

```

42
43 LENGTH = getParameter('Length'); % [m]
44 RADIUSi = getParameter('Inner tube diameter')/2; % [m]
45 Tubes = getParameter('Number of tubes'); % [-]
46 Rwall = getParameter('Wall thickness'); % [m]
47 Dit = getParameter('Inner tube distance'); % [m]
48 EPS = getParameter('Void fraction'); % [-]
49 EPSp = getParameter('Catalyst porosity'); % [-]
50 tau = getParameter('Catalyst tortuosity'); % [-]
51 Dpore = getParameter('Catalyst pore diameter'); % [m]
52 Dp = getParameter('Catalyst diameter'); % [m]
53 RHOCat = getParameter('Catalyst density'); % [kg/m3]
54 zeta = getParameter('Catalyst dilution factor'); % [-]
55 LAMBDAcat = getParameter('Catalyst conductivity'); % [W/(m.K)]
56 kwall = getParameter('Tube heat coefficient'); % [W/(m.K)]
57 Tcoolant = getParameter('Coolant temperature')+273.15; % [K]
58 RP = getParameter('Radial discr. points'); % [-]
59
60 RADIUSo = RADIUSi+Rwall; % Outer tube radius [m]
61 rp = Dp/2; % Catalyst radius [m]
62 av = 3/rp.*(1-EPS); % Catalyst specific surface area [m2/m3]
63
64
65 %% NUMERICAL GRID
66 % -----
67
68 zspan = [0, LENGTH]; % Axial integration span
69 r = linspace(0, RADIUSi, RP)'; % Radial points for plots
70
71
72 %% INITIAL CONDITIONS
73 % -----
74 % The inlet conditions are used as an initial guess to solve the model
75 % Chosen to not include CO2 since it has the highest overall mass fraction
76
77 Tin = Tin*ones(RP,1); % Inlet Temperature vector [K]
78
79 Uin = 4*Fin*GASCONST*Tin/(pi*(RADIUSi^2)*2*Tubes*Pin*1000); % Superficial
80 % velocity
81 % [m/s]
82
83 % Convert mole fractions (y) to mass fractions (w)
84 % expression: w(i) = y(i)*Mw(i)/(sum(y(i)*Mw(i)))
85 %%%%%%%%%%%%%%%%%%%%%%%%%%%%%%%%%%%%%%%%%%%%%%%%%%%%%%%%%%%%%%%%%%%%%%%%%%
86 Yin = [yin(1) yin(5) yin(4) yin(3) yin(2) yin(6)]; % new component order
87 comps = [1 2 4 5 6]; % excluding CO2, only 5 components are determined
88 Win = zeros(1,RP*(Ncomp-1)); % Preallocation
89 for j = 1:Ncomp-1
90     i = comps(j);
91     Win((j-1)*RP+1:j*RP) = Yin(i).*MMASS(i)./( ...
92         Yin(1).*MMASS(1) + ... % CH4
93         Yin(2).*MMASS(2) + ... % CO
94         Yin(3).*MMASS(3) + ... % CO2
95         Yin(4).*MMASS(4) + ... % H2
96         Yin(5).*MMASS(5) + ... % H2O
97         Yin(6).*MMASS(6) ); % N2
98
99 end %for
100
101 Qin = 0; % Inlet heat flow [W]
102
103
104 x0 = [Win'; Uin; Tin; Pin; Qin]; % initial guess in x0 vector
105
106 %% MASS MATRIX (IN RADIAL DIRECTION)
107 % -----
108 % Makes a 72x72 matrix where each 10th and 11th point on the diagonal is

```

APPENDIX E. METHANATION MODEL

```
107 % a BC point (centre of tube, wall of tube) to solve the in algebraic form
108 % boundary conditions together with the radial direction ODEs.
109
110 massmatrix = eye(RP*7+2,RP*7+2); % Ones on diagonal and zeros on rest
111 % +2 for the 2D pressure and heat flow
112 for i = 1:7
113     massmatrix((i-1)*RP+1,(i-1)*RP+1) = 0; % Each 11th diag. point =0 (BC)
114     massmatrix(i*RP,i*RP) = 0; % Each 10th diag. point =0 (BC)
115 end
116
117
118 %% ODE SOLVER
119 % -----
120 % Solves the ordinary differential equations (pressure, temperature,
121 % heat flow, superficial velocity and component mass fractions) in
122 % axial direction for each radial discretised point.
123
124 options = odeset('Mass', massmatrix, 'RelTol',1e-6, 'AbsTol',1e-6);
125 [z,x] = ode15s(@deriv, zspan, x0, options);
126
127 % x-variable placing:
128 w_CH4 = x(:,(1-1)*RP+1:RP*1); % (ZP, 0:10)
129 w_CO = x(:,(2-1)*RP+1:RP*2); % (ZP, 11:20)
130 w_H2 = x(:,(3-1)*RP+1:RP*3); % (ZP, 21:30)
131 w_H2O = x(:,(4-1)*RP+1:RP*4); % (ZP, 31:40)
132 w_N2 = x(:,(5-1)*RP+1:RP*5); % (ZP, 41:50)
133 uz = x(:,(6-1)*RP+1:RP*6); % (ZP, 51:60)
134 T = x(:,(7-1)*RP+1:RP*7); % (ZP, 61:70)
135 p = x(:,(8-1)*RP+1); % (ZP, 71)
136 Q = x(:,(8-1)*RP+2); % (ZP, 72)
137
138 toc
139
140
141 %% MODEL CALCULATIONS FOR PLOTTING
142 % -----
143
144 w_CO2 = 1 - (w_CH4 + w_CO + w_H2 + w_H2O + w_N2); % CO2 solved separately
145
146 % Mass fraction to Mole fraction
147 % y(i) = w(i)/Mw(i)/(sum(w(i)/Mw(i)))
148 w = cat(3, w_CH4, w_CO, w_CO2, w_H2, w_H2O, w_N2); % 3D matrix
149 y = zeros(size(w)); % Preallocation
150 for i = 1:Ncomp
151     y(:,i) = w(:,i)/MMASS(i)/( ...
152         w(:,1)/MMASS(1) + ... % w(ZP,RP,CH4)
153         w(:,2)/MMASS(2) + ... % w(ZP,RP,CO)
154         w(:,3)/MMASS(3) + ... % w(ZP,RP,CO2)
155         w(:,4)/MMASS(4) + ... % w(ZP,RP,H2)
156         w(:,5)/MMASS(5) + ... % w(ZP,RP,H2O)
157         w(:,6)/MMASS(6) ); % w(ZP,RP,N2)
158 end %for
159
160 % Inlet and outlet specifications printing in command window
161 % Assuming that the radial change is not present at inlet/outlet
162 y_CH4 = [y(1,1,1)*100 y(end,1,1)*100] % percentage
163 y_CO = [y(1,1,2)*100 y(end,1,2)*100] % percentage
164 y_CO2 = [y(1,1,3)*100 y(end,1,3)*100] % percentage
165 y_H2 = [y(1,1,4)*100 y(end,1,4)*100] % percentage
166 y_H2O = [y(1,1,5)*100 y(end,1,5)*100] % percentage
167 y_N2 = [y(1,1,6)*100 y(end,1,6)*100] % percentage
168 velocity = [uz(1,1) uz(end,1)] % m/s
169 Temperature = [T(1,1)-273.15 T(end,1)-273.15] % dC
170 Pressure = [p(1)/1e5 p(end)/1e5] % bar
171 Heatflow = Q(end)/1000 % kW
```

```

172 X_CO2      = (1 - (y(end,1,3)/y(1,1,3)))*100 % percentage
173 T_max      = max(max(T))-273.15 % Maximum temperature [dC]
174 v_min      = min(min(uz)) % Minimum temperature [m/s]
175 v_max      = max(max(uz)) % Maximum temperature [m/s]
176
177 % Sizing of reactor (excluding coolant space)
178 InnerTubeArea = pi/4*(2*RADIUSi)^2; % Tube cross-sectional area [m2]
179 ReactorAcs = Tubes*(2*RADIUSo+Dit)^2*(sqrt(3)/2); % Reactor cs area [m2]
180 ReactorVolume = ReactorAcs*LENGTH; % Reactor volume [m3]
181 ReactorDiameter = sqrt(4*ReactorAcs/pi); % Reactor diameter [m]
182
183 % Flowrate over the reactor (not for each tube)
184 MWg(:, :) = 1./(... % Molar mass of gas mixture [kg/kmol]
185     w(:, :, 1) ./MMASS(1) + ... % w(ZP,RP,CH4)
186     w(:, :, 2) ./MMASS(2) + ... % w(ZP,RP,CO)
187     w(:, :, 3) ./MMASS(3) + ... % w(ZP,RP,CO2)
188     w(:, :, 4) ./MMASS(4) + ... % w(ZP,RP,H2)
189     w(:, :, 5) ./MMASS(5) + ... % w(ZP,RP,H2O)
190     w(:, :, 6) ./MMASS(6) ); % w(ZP,RP,N2)
191 rhog = (p.*MWg)/(GASCONST.*T); % Mixture density [kg/m3]
192 VolumetricFlow = uz.*3600*InnerTubeArea*Tubes; % Volumetric flowrate [m3/h]
193 MassFlow = rhog.*VolumetricFlow; % Mass flowrate [kg/h]
194 MolarFlow = MassFlow./MWg; % Molar flowrate [kmol/h]
195
196 % Rate of reaction and Reaction heat
197 Rcomp = zeros(length(z),RP,Ncomp); % pre-allocation
198 DELTAHr = zeros(length(z),RP); % pre-allocation
199 eta = zeros(length(z),RP); % pre-allocation
200 ymatrix = zeros(RP,Ncomp); % pre-allocation
201 wmatrix = zeros(RP,Ncomp); % pre-allocation
202 for i = 1:length(z)
203     for j = 1:Ncomp
204         ymatrix(:,j) = y(i,:,j); % 2D matrices in z for mole fraction
205         wmatrix(:,j) = w(i,:,j); % 2D matrices in z for mass fraction
206     end %for
207     [Rcomp(i,:, :), DELTAHr(i, :)] = reaction(T(i, :)', ymatrix, p(i));
208     eta(i, :) = effectiveness(T(i, :)', ymatrix, wmatrix, p(i), Rcomp(i, :, :));
209 end %for
210 % eta
211 Rrxn = Rcomp(:, :, 1)*zeta*RHOcat*(1-EPS).*eta; % [kmolCH4/m^3b/s]
212 DELTAHr = -DELTAHr(:, :)/1000.*Rcomp(:, :, 1).*zeta.*RHOcat*(1-EPS).*eta; % [kW/m^3b]
213
214
215 %% 3D PLOTTING OF VARIABLES
216
217 az = 135; % Azimuth angle for setting viewpoint in figures
218 el = 9; % Elevation height for setting viewpoint in figures
219
220 % Choose which x-variable to plot
221 dataplots = 0;
222 % 0 = all plots below from 8
223 % 1 = CH4 mole fraction (y_CH4)
224 % 2 = CO mole fraction (y_CO)
225 % 3 = CO2 mole fraction (y_CO2)
226 % 4 = H2 mole fraction (y_H2)
227 % 5 = H2O mole fraction (y_H2O)
228 % 6 = N2 mole fraction (y_N2)
229 % 7 = Gas mixture molar mass (MWg)
230 % 8 = Component mole fractions in 2D
231 % 9 = Effectiveness factor (eta) in 2D
232 % 10 = Reaction rate (Rrxn) in 3D
233 % 11 = Superficial velocity (uz) in 3D
234 % 12 = Temperature (T) in 3D
235 % 13 = Pressure (P) in 2D
236 % 14 = Heat flowrate (Q) in 2D

```

```

237 % 15 = Mass/Molar/Volumetric flowrate in 2D
238
239 run('plotting.m') % Run plotting file
240
241
242 %% MODEL OUTPUT
243 % -----
244 % Radial change at outlet is neglectable assumed for all below
245 % Might want to do a area averaging???
246
247 fout = MolarFlow(end,1)*1000/3600; % [mol/s]
248 yout = [y(end,1,1) y(end,1,5) y(end,1,4) y(end,1,3) abs(y(end,1,2)) y(end,1,6) yin(7)]; % [-]
249 Tout = T(end,1); % [K]
250 pout = p(end); % [Pa]
251
252 setProduct(1,fout,yout,'temperature',Tout,'pressure',pout)
253
254 setParameter('Heat flow',Heatflow)
255 setParameter('CO2 conversion',X.CO2)
256 setParameter('Reactor diameter',ReactorDiameter)
257 setParameter('Reactor volume',ReactorVolume)
258 setParameter('Maximum temperature',T_max)
259 setParameter('Minimum velocity',v_min)
260 setParameter('Maximum velocity',v_max)
261
262 toc % end timer for simulation

```

Model Declaration

The Model declaration function, `deriv.m`, contains the derivatives together with implemented boundary conditions for the radial coordinates and contains several chemical properties. This function communicates directly with the `main.m` script where the algebraic-differential equations are integrated over z .

```

1 % deriv.m
2 % This function specifies the axial derivatives to be solved in the main.m
3 % script by calculating the first and second order radial derivatives of
4 % the components mass fractions, temperature, superficial velocity in the
5 % discretisation points using specified chemical and physical properties
6 % as well as radial boundary conditions.
7
8 function dxdz = deriv(~, x)
9
10 global GASCONST Ncomp RP RHOcat EPS Dp Tcoolant RADIUSi MMASS CP B S zeta Tubes
11
12 r = linspace(0, RADIUSi, RP)'; % Creates an evenly distributed grid
13 % in the radial direction
14
15 comps = [1 2 4 5 6]; % Not integrate CO2 component
16
17 % Splitting the x variable
18 w = [x(1:RP) ... % Combined mass fraction
19 x(RP+1:RP*2) ... % variable for use in for loops
20 zeros(RP,1) ... % where component CO2 is excluded
21 x(2*RP+1:RP*3) ... % since it has the highest overall
22 x(3*RP+1:RP*4) ... % mass fraction (to minimise errors).
23 x(4*RP+1:RP*5)];
24
25 w(:,3) = 1 - ( w(:,1) + w(:,2) + w(:,4)+ w(:,5) + w(:,6) ); % CO2 placed
26
27 uz = x(5*RP+1:RP*6);
28 T = x(6*RP+1:RP*7);

```

```

29 p = x(7*RP+1);
30 Q = x(7*RP+2);
31
32 %% Chemical- and Physical Properties
33
34 % Mole fractions (y) from mass fractions (w)
35 %  $y(i) = w(i)/Mw(i)/(\sum(w(i)/Mw(i)))$ 
36 %-----
37 y = zeros(RP,Ncomp); % Preallocation
38 for i = 1:Ncomp
39     y(:,i) = w(:,i)/MMASS(i)/( ...
40         w(:,1)/MMASS(1) + ... % w(RP,CH4)
41         w(:,2)/MMASS(2) + ... % w(RP,CO)
42         w(:,3)/MMASS(3) + ... % w(RP,CO2)
43         w(:,4)/MMASS(4) + ... % w(RP,H2)
44         w(:,5)/MMASS(5) + ... % w(RP,H2O)
45         w(:,6)/MMASS(6) ); % w(RP,N2)
46 end %for
47
48 % Average Molar Mass of Gas Mixture [kg/kmole]
49 %  $MWg = \sum(yi*MMASSi)$  or  $MWg = 1/\sum(wi/MMASSi)$ 
50 %-----
51 MWg = y*MMASS'; % or  $MWg = 1./(w*(1./MMASS)')$ ;
52
53 % Gas Mixture Viscosity from component viscosities [kg/m.s]
54 % assuming a linear dependency of mixture VISg and component VISi
55 %-----
56 VISi = zeros(RP,Ncomp); % preallocation
57 VISg = zeros(RP,1); % preallocation
58 for i = 1:RP
59     for j = 1:Ncomp
60         VISi(i,j) = B(j)*T(i)^(1.5)/(T(i)+S(j)); % Component
61         VISg(i) = y(i,:) * VISi(i,:)'; % Gas Mixture
62     end %for
63 end %for
64
65 % Gas Mixture Heat Capacity from component heat capacities [J/kg.K]
66 % assuming a linear dependency of mixture CPg and component CPi
67 %-----
68 CPi = zeros(RP,Ncomp); % preallocation
69 CPg = zeros(RP,1); % preallocation
70 for i = 1:RP
71     for j = 1:Ncomp
72         CPi(i,j) = CP(j,1) + CP(j,2)*T(i) + CP(j,3)*T(i)^2 + CP(j,4)*T(i)^3;
73         CPg(i) = y(i,:) * CPi(i,:)'/MWg(i); % Gas Mixture
74     end %for
75 end %for
76
77 % Gas mixture density and Reynolds numbers
78 %-----
79 rhog = p.*MWg./(GASCONST.*T); % Gas Mixture Density [kg/m^3]
80 Rep = rhog.*uz.*Dp./VISg; % Particle Reynolds Number [-]
81 Re = rhog.*uz.*2*RADIUSi./VISg; % Fluid Reynolds number [-]
82
83 % Radial mass dispersion coefficient
84 %-----
85 Pe = 1.1*8*(2-(1-Dp/RADIUSi)^2); % Peclet number [-]
86 Dr = uz*RADIUSi/Pe; % Radial Dispersion Coef. [m^2/s]
87
88 % Heat transfer and reaction properties, calculated by functions
89 %-----
90 [Ur,LAMBDAer] = heatcoef(Rep,Re,T,y,VISg,CPg); % Heat Transfer Coefficient
91 % and Effective Radial Conductivity
92
93 [Rcomp,DELTAHr] = reaction(T,y,p); % Component reaction rates

```

APPENDIX E. METHANATION MODEL

```
94                                     % and Heat of Reaction
95
96 eta = effectiveness(T,y,w,p,Rcomp); % Interparticle mass transport
97
98 %% Radial 1st order derivatives
99 % The file dss020.m uses a forward finite difference to calculate the
100 % derivative of the function f with respect to the independent variable r.
101 % The function head: dss020(r(1), r(n), n, f, 1);
102
103 % Temperature (dT/dr)
104 dTdr = dss020(r(1), r(RP), RP, T, 1)';
105
106 % Superficial velocity (duz/dr)
107 duzdr = dss020(r(1), r(RP), RP, uz, 1)';
108
109 % Mass fractions (dwi/dr)
110 dwdr = zeros(RP,Ncomp-1); % preallocation
111 for j = 1:Ncomp-1
112     i = comps(j);
113     dwdr(:,j) = dss020(r(1), r(RP), RP, w(:,i), 1)';
114 end %for
115
116 %% Radial 2nd order derivatives
117 % The file dss042.m uses a central finite difference to calculate the
118 % second derivative of f with respect to the independent variable r.
119 % The function head: dss042(r(1), r(n), n, f, dldr1, BC1(1), BC2(RP));
120 % Insert 2 for boundary condition type to specify use of Newmann boundary
121 % conditions or insert 1 for Dirichlet boundary conditions.
122
123 % Temperature (d2T/dr2)
124 d2Tdr2 = dss042(r(1), r(RP), RP, T, dTdr, 2, 2)';
125
126 % Component mass fractions (d2wi/dr2)
127 d2wdr2 = zeros(RP, Ncomp-1); % preallocation
128 for j = 1:Ncomp-1
129     i = comps(j);
130     d2wdr2(:,j) = dss042(r(1), r(RP), RP, w(:,i), dwdr(:,j), 2, 2)';
131 end %for
132
133 %% Axial derivatives
134
135 % Pressure (dP/dz) – Ergun equation
136 dpdz = ergun(rhog,uz,Rep,r);
137
138 % Temperature (dT/dz)
139 dTdz = 1./(rhog.*CPg.*uz) .* (LAMBDAer.*((1./r).*dTdr + d2Tdr2) + ...
140     (-DELTAHr.*Rcomp(:,1).*zeta*RHOcat*(1-EPS).*eta));
141
142 % Component mass fractions (dwi/dz)
143 dwdz = zeros(RP, Ncomp); % preallocation
144 for j = 1:Ncomp-1
145     i = comps(j);
146     dwdz(:,i) = Dr./uz.*( 1./r.*dwdr(:,j) + d2wdr2(:,j) ...
147         -1./T.*dTdr.*dwdr(:,j)) ...
148         +Rcomp(:,i)*MMASS(i)*zeta*RHOcat*(1-EPS).*eta./(rhog.*uz);
149 end %for
150 dwdz(:,3) = -(dwdz(:,1)+dwdz(:,2)+dwdz(:,4)+dwdz(:,5)+dwdz(:,6));
151
152 % Molar mass of gas mixture (dMWg/dz)
153 dMWgdz = -MWg.^2 .* (dwdz*(1./MMASS)');
154
155 % Superficial velocity (duz/dz)
156 duzdz = (uz./T).*dTdz -(uz./p).*dpdz -(uz./MWg).*dMWgdz;
157
158 % Heat flow (dQ/dz)
```

```

159 dQdz = Ur.*(T(RP)-Tcoolant).*2*pi*RADIUSi*Tubes;
160
161 %% Radial boundary conditions
162
163 % Temperature at centre (1) and wall (RP)
164 dTdz(1) = dTdr(1); % = 0 at r = 0
165 dTdz(RP) = dTdr(RP) + Ur/LAMBDAer(RP)*(T(RP)-Tcoolant); % eq. at r = RP
166
167 % Superficial Velocity at centre (1) and wall (RP)
168 duzdz(1) = duzdr(1); % = 0 at r = 0
169 duzdz(RP) = duzdr(RP); % = 0 at r = RP
170
171 % Component Mass fraction at centre (1) and wall (RP)
172 for j = 1:Ncomp-1
173     i = comps(j);
174     dwdz(1,i) = dwdr(1,j); % = 0 at r = 0
175     dwdz(RP,i) = dwdr(RP,j); % = 0 at r = RP
176 end %for
177 dwdz(1,3) = 0; % for CO2 % = 0 at r = 0
178 dwdz(RP,3) = 0; % for CO2 % = 0 at r = RP
179
180 %% Returned vector of derivatives
181
182 dxdz = [ dwdz(:,1);
183          dwdz(:,2);
184          dwdz(:,4);
185          dwdz(:,5);
186          dwdz(:,6);
187          duzdz;
188          dTdz;
189          dpdz;
190          dQdz;      ];
191
192 end %function

```

Constants

The constant script, `constant.m`, contains the constants used to solve the model and the variables stated in this script are made global for calculations in each of the model its scripts/functions.

```

1 % constant.m
2 % This script states the constants used to solve the model.
3
4 % Global constant variables that are used in different scripts/functions
5 global GASCONST Ncomp MMASS Aq Eq beta Tref Hr kref ...
6     EA AXref dHX CP LAMBDA B S sunny
7
8 % General constants
9 %-----
10 GASCONST = 8.3145e3; % Gas constant [J/kmole.K]
11 Ncomp = 6; % Number of components [-]
12
13 % Component molar mass (from HYSYS) [kg/kmole]
14 %-----
15 MMASS(1) = 16.0429000854492; % Molar mass of CH4
16 MMASS(2) = 28.0109004974365; % Molar mass of CO
17 MMASS(3) = 44.0097007751465; % Molar mass of CO2
18 MMASS(4) = 2.01600003242493; % Molar mass of H2
19 MMASS(5) = 18.0151004791260; % Molar mass of H2O
20 MMASS(6) = 28.0130004882813; % Molar mass of N2
21
22 % Equilibrium constant coefficients

```

APPENDIX E. METHANATION MODEL

```

23 %-----
24 Aq = 11.2561956932934; % Pre-exp. factor coef. [bar^-2 K^-1]
25 Eq = 18530.1820006599; % Activation energy coef. [kJ/kmol]
26 beta = -4.84168695852905; % Temperature coef. [-]
27
28 % Pre-exponential factor for the rate constant
29 %-----
30 Tref = 555; % Reference temperature [K]
31 kref = 3.46e-4; % Rate constant factor [kmole/bar.kgcat.s]
32
33 % Activation energy coefficient for reaction [J/kmole]
34 %-----
35 EA = 77.5e6; % Activation energy
36
37 % Pre-exponential factor for the adsorption constant [bar^-0.5]
38 %-----
39 AXref(1) = 0.50; % Factor of OH
40 AXref(2) = 0.44; % Factor of H2
41 AXref(3) = 0.88; % Factor of MIX
42
43 % Adsorption enthalpy coefficients [J/kmole]
44 %-----
45 dHX(1) = 22.4e6; % Adsorption enthalpy of OH
46 dHX(2) = -6.2e6; % Adsorption enthalpy of H2
47 dHX(3) = -10.0e6; % Adsorption enthalpy of MIX
48
49 % Reaction enthalpy coefficients
50 %-----
51 Hr(1) = -1.47040e2; % 1st coefficient [J/kmole]
52 Hr(2) = -6.59812e-2; % 2nd coefficient [J/kmole.K]
53 Hr(3) = 2.31450e-5; % 3rd coefficient [J/kmole.K^2]
54 Hr(4) = 1.51675e-10; % 4th coefficient [J/kmole.K^3]
55
56 % Component heat capacity coefficients
57 %-----
58 CP(1,1) = 1.925e4; % 1st coefficient for CH4 [J/kmole.K]
59 CP(1,2) = 5.213e1; % 2nd coefficient for CH4 [J/kmole.K^2]
60 CP(1,3) = 1.197e-2; % 3rd coefficient for CH4 [J/kmole.K^3]
61 CP(1,4) = -1.132e-5; % 4th coefficient for CH4 [J/kmole.K^4]
62
63 CP(2,1) = 3.087e4; % 1st coefficient for CO [J/kmole.K]
64 CP(2,2) = -1.285e1; % 2nd coefficient for CO [J/kmole.K^2]
65 CP(2,3) = 2.789e-2; % 3rd coefficient for CO [J/kmole.K^3]
66 CP(2,4) = -1.272e-5; % 4th coefficient for CO [J/kmole.K^4]
67
68 CP(3,1) = 1.980e4; % 1st coefficient for CO2 [J/kmole.K]
69 CP(3,2) = 7.344e1; % 2nd coefficient for CO2 [J/kmole.K^2]
70 CP(3,3) = -5.602e-2; % 3rd coefficient for CO2 [J/kmole.K^3]
71 CP(3,4) = 1.715e-5; % 4th coefficient for CO2 [J/kmole.K^4]
72
73 CP(4,1) = 2.714e4; % 1st coefficient for H2 [J/kmole.K]
74 CP(4,2) = 0.9274e1; % 2nd coefficient for H2 [J/kmole.K^2]
75 CP(4,3) = -1.381e-2; % 3rd coefficient for H2 [J/kmole.K^3]
76 CP(4,4) = 0.7645e-5; % 4th coefficient for H2 [J/kmole.K^4]
77
78 CP(5,1) = 3.224e4; % 1st coefficient for H2O [J/kmole.K]
79 CP(5,2) = 0.1924e1; % 2nd coefficient for H2O [J/kmole.K^2]
80 CP(5,3) = 1.055e-2; % 3rd coefficient for H2O [J/kmole.K^3]
81 CP(5,4) = 0.3596e-5; % 4th coefficient for H2O [J/kmole.K^4]
82
83 CP(6,1) = 3.115e4; % 1st coefficient for N2 [J/kmole.K]
84 CP(6,2) = -1.357e1; % 2nd coefficient for N2 [J/kmole.K^2]
85 CP(6,3) = 2.680e-2; % 3rd coefficient for N2 [J/kmole.K^3]
86 CP(6,4) = -1.168e-5; % 4th coefficient for N2 [J/kmole.K^4]
87

```

```

88 % Component conductivity coefficients
89 %-----
90 LAMBDA(1,1) = -1.869e-3;    % 1st coefficient for CH4    [W/m.K]
91 LAMBDA(1,2) = 8.727e-5;    % 2nd coefficient for CH4    [W/m.K^2]
92 LAMBDA(1,3) = 1.179e-7;    % 3rd coefficient for CH4    [W/m.K^3]
93 LAMBDA(1,4) = -3.614e-11;  % 4th coefficient for CH4    [W/m.K^4]
94
95 LAMBDA(2,1) = 5.067e-4;    % 1st coefficient for CO     [W/m.K]
96 LAMBDA(2,2) = 9.1025e-5;   % 2nd coefficient for CO     [W/m.K^2]
97 LAMBDA(2,3) = -3.524e-8;   % 3rd coefficient for CO     [W/m.K^3]
98 LAMBDA(2,4) = 8.199e-12;   % 4th coefficient for CO     [W/m.K^4]
99
100 LAMBDA(3,1) = -7.215e-3;   % 1st coefficient for CO2    [W/m.K]
101 LAMBDA(3,2) = 8.015e-5;    % 2nd coefficient for CO2    [W/m.K^2]
102 LAMBDA(3,3) = 5.477e-9;    % 3rd coefficient for CO2    [W/m.K^3]
103 LAMBDA(3,4) = -1.053e-11;  % 4th coefficient for CO2    [W/m.K^4]
104
105 LAMBDA(4,1) = 8.099e-3;    % 1st coefficient for H2     [W/m.K]
106 LAMBDA(4,2) = 6.689e-4;    % 2nd coefficient for H2     [W/m.K^2]
107 LAMBDA(4,3) = -4.158e-7;   % 3rd coefficient for H2     [W/m.K^3]
108 LAMBDA(4,4) = 1.562e-10;   % 4th coefficient for H2     [W/m.K^4]
109
110 LAMBDA(5,1) = 7.341e-3;    % 1st coefficient for H2O    [W/m.K]
111 LAMBDA(5,2) = -1.013e-5;   % 2nd coefficient for H2O    [W/m.K^2]
112 LAMBDA(5,3) = 1.801e-7;    % 3rd coefficient for H2O    [W/m.K^3]
113 LAMBDA(5,4) = -9.100e-11;  % 4th coefficient for H2O    [W/m.K^4]
114
115 LAMBDA(6,1) = 3.919e-4;    % 1st coefficient for N2     [W/m.K]
116 LAMBDA(6,2) = 9.966e-5;    % 2nd coefficient for N2     [W/m.K^2]
117 LAMBDA(6,3) = -5.067e-8;   % 3rd coefficient for N2     [W/m.K^3]
118 LAMBDA(6,4) = 1.504e-11;   % 4th coefficient for N2     [W/m.K^4]
119
120 % Component viscosity coefficients
121 %-----
122 B(1) = 1.00e-6;            % Coefficient for CH4        [kg/m.s.K^0.5]
123 B(2) = 1.50e-6;            % Coefficient for CO          [kg/m.s.K^0.5]
124 B(3) = 1.50e-6;            % Coefficient for CO2         [kg/m.s.K^0.5]
125 B(4) = 0.65e-6;            % Coefficient for H2          [kg/m.s.K^0.5]
126 B(5) = 1.74e-6;            % Coefficient for H2O         [kg/m.s.K^0.5]
127 B(6) = 1.40e-6;            % Coefficient for N2          [kg/m.s.K^0.5]
128
129 S(1) = 168;                 % Coefficient for CH4        [K]
130 S(2) = 220;                 % Coefficient for CO          [K]
131 S(3) = 220;                 % Coefficient for CO2         [K]
132 S(4) = 67;                  % Coefficient for H2          [K]
133 S(5) = 625;                 % Coefficient for H2O         [K]
134 S(6) = 108;                 % Coefficient for N2          [K]
135
136 % Special diffusion volumes coefficients (from Sinnott2009)    [-]
137 %-----
138 sumny(1) = 24.42;           % Coefficient for CH4
139 sumny(2) = 18.90;           % Coefficient for CO
140 sumny(3) = 26.90;           % Coefficient for CO2
141 sumny(4) = 7.07;            % Coefficient for H2
142 sumny(5) = 12.70;           % Coefficient for H2O
143 sumny(6) = 17.90;           % Coefficient for N2

```

CO₂ Methanation Reaction

The reaction function, `reaction.m`, contains implemented kinetics from Koschany (2016) for the CO₂ methanation reaction. It calculates both the rate of reaction and the heat of reaction.

APPENDIX E. METHANATION MODEL

```

1 % reaction.m
2 % This function calculates the reaction rates for all the components
3 % and the heat of the reaction in all the discretication points.
4 %
5 % INPUT:
6 % T      [=] K      Temperature
7 % y      [=] -      Mole fraction
8 % p      [=] Pa     Total pressure
9 %
10 % OUTPUT:
11 % Rcomp  [=] kmol/kgcat.s  Component reaction rate
12 % DELTAHr [=] J/kmol      Total reaction heat
13
14 function [Rcomp,DELTAHr] = reaction(T,y,p)
15
16 global GASCONST Ncomp RP Aq Eq beta Tref kref EA AXref dHX Hr
17
18 % Component partial pressures [bar]
19 Pcomp = zeros(RP,Ncomp); % Preallocating
20 for i=1:Ncomp
21     Pcomp(:,i) = y(:,i).*p/1e5;
22 end %for
23
24 Rcomp = zeros(RP,Ncomp); % Preallocating
25 DELTAHr = zeros(RP,1); % Preallocating
26 for i=1:RP
27
28     % Equilibrium constant [bar^-2]
29     % from HSC chemistry database
30     Keq = exp(Aq)*T(i)^beta*exp(Eq/T(i));
31
32     % Rate constant [kmol/bar.kgcat.s]
33     % Krxn = kref.*exp(-EA./(GASCONST*T(i)));
34     Krxn = kref.*exp(EA./GASCONST*(1/Tref-1/T(i)));
35
36     % Adsorption constant [bar^-0.5]
37     % Kads = AXref.*exp(-dHX./(GASCONST*T(i)));
38     Kads = AXref.*exp(dHX./GASCONST*(1/Tref-1/T(i)));
39
40     % Denominator of rate equation [-]
41     DEN = 1 + Kads(1)*Pcomp(i,5)*Pcomp(i,4)^(-0.5) ...
42           + Kads(2)*Pcomp(i,4)^(0.5) ...
43           + Kads(3)*Pcomp(i,3)^(0.5);
44
45     % Reaction rate equation [kmol/kgcat.s]
46     Rrxn = ( Krxn * Pcomp(i,4)^(0.5) * Pcomp(i,3)^(0.5) ...
47             * ( 1 - (Pcomp(i,1) * Pcomp(i,5)^(2)) ...
48               / ((Pcomp(i,3) * Pcomp(i,4)^(4) * Keq) ) ) ) / (DEN)^2;
49
50     % Production/consumption rates of the individual components
51     % [kmol/kgcat.s], which needs conversion to reactor volume basis and
52     % mass basis for mass balance. Reaction: CO2 + 4 H2 = CH4 + 2 H2O
53     Rcomp(i,1) = +1*Rrxn; % CH4
54     Rcomp(i,2) = 0; % CO
55     Rcomp(i,3) = -1*Rrxn; % CO2
56     Rcomp(i,4) = -4*Rrxn; % H2
57     Rcomp(i,5) = +2*Rrxn; % H2O
58     Rcomp(i,6) = 0; % N2
59
60     % Heat of reaction [J/kmol] from HSC chemistry database
61     % needs conversion to mass basis in mass balance.
62     DELTAHr(i) = ( Hr(1) +Hr(2)*T(i) +Hr(3)*T(i).^2 +Hr(4)*T(i).^3 )*1e6;
63
64 end %for
65

```

```
66 end %function
```

Effectiveness Factor

The effectiveness function, `effectiveness.m`, contains the determined effectiveness factor to take the interparticle mass transport limitations in account, as was described previously in this appendix.

```
1 % factor.m
2 % This function calculates the effectiveness factor in two dimensions.
3 % The effectiveness factor takes intraparticle mass transport limitations
4 % into consideration to correct for the reaction rate and reaction heat.
5 % The expressions used are extracted from article: Bremer, Sundmacher(2019)
6 % "Operation range extension via hot-spot control for catalytic CO2
7 % methanation reactors" and book: Kee (2003) "Chemically reacting flow".
8 %
9 % ASSUMPTIONS APPLIED:
10 % - CO2 methanation proceeds as a first order reaction.
11 % - CO2 is the limiting compound to diffuse to the reaction site and is
12 % therefore the key component for determining the effectiveness factor.
13 % - The catalyst particles are spherical with 100% sphericity.
14 % - Steady state, equimolar counterdiffusion and isothermal process.
15 %
16 % INPUT:
17 % T      [=] K           Temperature
18 % y      [=] -           Mole fraction
19 % w      [=] -           Mass fraction
20 % p      [=] Pa          Total pressure
21 % Rcomp  [=] kmol/kg(cat).s Reaction rate
22 %
23 % OUTPUT:
24 % eta    [=] none        Effectiveness factor
25
26 function eta = effectiveness(T,y,w,p,Rcomp)
27
28 global GASCONST RP Dp MMASS Dpore tau EPSp sumny Ncomp RHOfat EPS zeta
29
30 comps = [1 2 4 5 6];
31
32 % Binary diffusion coefficients [-]
33 % only for CO2,CH4; CO2,CO; CO2,H2; CO2,H2O; CO2,N2
34 Dij = zeros(RP,Ncomp-1);
35 Mv = zeros(RP,1);
36 for j = 1:Ncomp-1
37     i = comps(j);
38     Mv(i) = 2*(1/MMASS(i)+1/MMASS(3))^( -1);
39     Dij(:,j) = 1e-4*0.00143*T.^1.75./...
40         (p*1e-5*sqrt(Mv(i))*(sumny(i)^(1/3)+sumny(3)^(1/3))^2);
41 end %for
42
43 % Molecular diffusivity [m2/s]
44 % Mixture-averaged coefficient for CO2
45 SUMmole = 0;
46 SUMmass = 0;
47 for j = 1:Ncomp-1
48     i = comps(j);
49     SUMmole = SUMmole + y(:,i)./Dij(:,j);
50     SUMmass = SUMmass + w(:,i)./Dij(:,j);
51 end %for
52 Dm = 1./ (SUMmole + y(:,3)/(1-w(:,3))*SUMmass);
53
54 % Knudsen diffusivity [m2/s]
55 Dk = Dpore/3 *sqrt( 8*GASCONST*T/(pi*MMASS(3)) );
```

```

56
57 % Effective diffusivity [m2/s]
58 De = 1./ ( tau/EPSP* (1./Dm + 1./Dk) );
59
60 % Thiele modulus [-]
61 phi = Dp/2*( sqrt((abs(Rcomp(:,3))*MMASS(3)*zeta*RHOcat*(1-EPS)*GASCONST.*T) ...
62     ./(De.*p.*y(:,3))));
63
64 % Effectiveness factor [-]
65 eta = 3./phi.*(1./tanh(phi) - 1./phi);
66
67 end

```

Ergun Equation

The Ergun function, `ergun.m`, calculates the pressure drop over the axial direction where the Reynolds number, velocity and mixture density are area averaged.

```

1 % ergun.m
2 % This function computes the 1D pressure gradient in the system by using
3 % the area averaged superficial velocity, gas density and Reynolds number
4 % (Radial change is averaged since the change in r is neglectable for P)
5 %
6 % INPUT:
7 % rhog      [=] kg/m^3      Gas density
8 % uz        [=] m/s        Superficial velocity
9 % Rep       [=] -          Particle reynolds number
10 % r         [=] m          Radial coordinate
11 %
12 % OUTPUT:
13 % dpdz      [=] Pa/m       Pressure gradient
14
15 function dpdz = ergun(rhog,uz,Rep,r)
16
17 global EPS Dp RP
18
19 % Area averaged density, velocity and Reynolds number for Ergun equation
20 %-----
21 SUMrhog = 0;
22 SUMuz   = 0;
23 SUMRep  = 0;
24 SUMrhog = SUMrhog + rhog(1)*r(1)^2;
25 SUMuz   = SUMuz + uz(1)*r(1)^2;
26 SUMRep  = SUMRep + Rep(1)*r(1)^2;
27
28 for i=2:RP
29     SUMrhog = SUMrhog + rhog(i)*(r(i)^2-r(i-1)^2);
30     SUMuz   = SUMuz + uz(i)*(r(i)^2-r(i-1)^2);
31     SUMRep  = SUMRep + Rep(i)*(r(i)^2-r(i-1)^2);
32 end %for
33
34 rhog_avg = SUMrhog/r(RP)^2;
35 uz_avg   = SUMuz/r(RP)^2;
36 Rep_avg  = SUMRep/r(RP)^2;
37
38 % Friction factor according to parameterisation by Tallmadge [-]
39 % b = 150 for Ergun parameterisation
40 %-----
41 a = 1.75;
42 b = 4.2*Rep_avg.^(5/6);
43 f = (1-EPS)/EPS^3*(a+b*(1-EPS)/Rep_avg);
44

```



```

45 % The Ergun equation to be solved
46 %-----
47 dpdz = -f*rhog_avg*uz_avg^2/Dp;
48
49 end %function

```

Heat Coefficient

The Heat coefficient function, `heatcoef.m`, determines the effective radial conductivity (λ_{er}) and overall heat coefficient (U) which are used to solve the temperature and heat balances.

```

1 % heatcoef.m
2 % This function computes the heat transfer coefficient for radial transport
3 % of heat from the bed to the surrounding coolant as well as the effective
4 % radial conductivity that is used in the temperature boundary condition.
5 % INPUT:
6 % Rep      [=] -      Particle Reynolds number
7 % Re       [=] -      Reynolds number
8 % T        [=] K      Temperature
9 % y        [=] -      Mole fraction
10 % VISgas   [=] kg/m.s Gas viscosity
11 % CPgas    [=] J/kg.K Gas heat capacity
12 %
13 % OUTPUT:
14 % Ur       [=] J/m^2.s.K Heat coefficient
15 % LAMBDAer [=] J/m.s.K   Effective radial conductivity
16
17 function [Ur,LAMBDAer] = heatcoef(Rep,Re,T,y,VISg,CPg)
18
19 global Ncomp RP EPS Dp kwall RADIUSi RADIUSo LAMBDA LAMBDAcat
20
21 % Calculates the gas heat conductivity [W/m.K]
22 % assumed linear dependency of mixture LAMBDAg and pure LAMBDAi
23 Tmatrix = [ones(RP,1) T T.^2 T.^3]; % Design matrix
24 LAMBDAi = zeros(RP,Ncomp); % preallocation
25 for i=1:Ncomp
26     LAMBDAi(:,i) = Tmatrix*LAMBDA(i,:)';
27 end %for
28 LAMBDAg=diag(y*LAMBDAi');
29
30 % Prandtl number [-]
31 Pr = VISg.*CPg./LAMBDAg;
32
33 % Nusselt number [-]
34 % Nu = 1.6*Rep(RP).^0.5.*Pr(RP).^0.3333; % From HYSYS based on Rep
35 Nu = 0.683*Re(RP).^0.466.*Pr(RP).^0.3333; % cylinder for Re = 40-4000 from Cengel p443
36
37 % Heat transfer coefficient inside tube [W/m2.K]
38 hgas = Nu.*LAMBDAg(RP)./Dp; % characteristic length for particle
39
40 % Heat transfer coefficient for coolant [W/m2.K]
41 % for Boiling Water: 3.000 - 100.000 (engineeringtoolbox)
42 hcoolant = 5000;
43
44 % Overall heat transfer coefficient [W/m2.K]
45 Ur = ( 1/hgas +RADIUSi/kwall*log(RADIUSo/RADIUSi) ...
46       +RADIUSi/(hcoolant*RADIUSo) )^(-1);
47
48 % Prefactors
49 P = 1.0;
50 BETA = 1.0; % between 0.9 - 1.0
51 PHI = 0.3; % read from graph

```

```
52
53 % Radial effective static conduction
54 ALPHArv = 0.227e-3/(1+EPS/(2*(1-EPS)))*(1-P)/P)*(T/100).^3;
55 ALPHArs = 0.227e-3*P/(2-P)*(T/100).^3;
56 LAMBDAer0 = LAMBDAg.*(EPS*(1+BETA*Dp*ALPHArv./LAMBDAg) + ...
57             BETA*(1-EPS)./(1./((1/PHI+ALPHArs*Dp./LAMBDAg)) + ...
58             2/3*LAMBDAg/LAMBDAcat));
59
60 % Effective radial conductivity
61 LAMBDAer = LAMBDAer0 + 0.14.*LAMBDAg.*Rep.*Pr;
62
63 end %function
```

Plotting of Profiles

The plotting script, `plotting.m`, plots the profiles of several important parameters to compare results with the methanation HYSYS model to check for validity. The switch statement can be used to plot the requested profile only instead of having to plot all the profiles for each simulation.

```
1 % plotting.m
2 % This script is imported in the main.m script for plotting the parameters:
3 % temperature, velocity, pressure, flowrate, component mole fractions,
4 % reaction rate, heat flowrate and heat of reaction.
5
6 switch dataplots
7
8     case 1 % CH4 molefraction
9         surf(r*100,z,y(:,:,1)*100)
10        view(az, el);
11        xlabel('Tube radius, $R$ [cm]', 'interpreter','latex', 'fontsize',12)
12        xticks(0:0.25:RADIUSi*100)
13        xtickformat('%0.2f')
14        ylabel('Reactor length, $L$ [m]', 'interpreter','latex', 'fontsize',12)
15        ylim([0, LENGTH+0.5])
16        yticks(0:1:LENGTH)
17        zlabel('CH4 mole fraction, $y_{CH4}$ [$\%$]', 'interpreter','latex', 'fontsize',12)
18        ztickformat('%0f')
19        filename = 'MoleFractionProfileCH4';
20        fname = 'C:\Users\Sander Wijnsma\OneDrive - NINU\Master\Courses S4\MATLAB\Methanation\Profiles';
21        saveas(gca, fullfile(fname, filename), 'png');
22
23     case 2 % CO molefraction
24        surf(r*100,z,y(:,:,2)*100)
25        view(az, el);
26        xlabel('Tube radius, $R$ [cm]', 'interpreter','latex', 'fontsize',12)
27        xticks(0:0.25:RADIUSi*100)
28        xtickformat('%0.2f')
29        ylabel('Reactor length, $L$ [m]', 'interpreter','latex', 'fontsize',12)
30        ylim([0, LENGTH+0.5])
31        yticks(0:1:LENGTH)
32        zlabel('CO mole fraction, $y_{CO}$ [$\%$]', 'interpreter','latex', 'fontsize',12)
33        zlim([-0.05, 0.1])
34        ztickformat('%0.1f')
35        filename = 'MoleFractionProfileCO';
36        fname = 'C:\Users\Sander Wijnsma\OneDrive - NINU\Master\Courses S4\MATLAB\Methanation\Profiles';
37        saveas(gca, fullfile(fname, filename), 'png');
38
39     case 3 % CO2 molefraction
40        surf(r*100,z,y(:,:,3)*100)
41        view(az, el);
42        xlabel('Tube radius, $R$ [cm]', 'interpreter','latex', 'fontsize',12)
```

```
43     xticks(0:0.25:RADIUSi*100)
44     xtickformat('%0.2f')
45     ylabel('Reactor length, $L$ [m]', 'interpreter','latex', 'fontsize',12)
46     ylim([0, LENGTH+0.5])
47     yticks(0:1:LENGTH)
48     xlabel('CO2 mole fraction, $y_{CO_2}$ [%]', 'interpreter','latex', 'fontsize',12)
49     ztickformat('%0f')
50     filename = 'MoleFractionProfileCO2';
51     fname = 'C:\Users\Sander Wijnsma\OneDrive - NINU\Master\Courses S4\MATLAB\Methanation\Profiles';
52     saveas(gca, fullfile(fname, filename), 'png');
53
54 case 4 % H2 molefraction
55     surf(r*100,z,y(:, :, 4)*100)
56     view(az, el);
57     xlabel('Tube radius, $R$ [cm]', 'interpreter','latex', 'fontsize',12)
58     xticks(0:0.25:RADIUSi*100)
59     xtickformat('%0.2f')
60     ylabel('Reactor length, $L$ [m]', 'interpreter','latex', 'fontsize',12)
61     ylim([0, LENGTH+0.5])
62     yticks(0:1:LENGTH)
63     xlabel('H2 mole fraction, $y_{H_2}$ [%]', 'interpreter','latex', 'fontsize',12)
64     ztickformat('%0f')
65     filename = 'MoleFractionProfileH2';
66     fname = 'C:\Users\Sander Wijnsma\OneDrive - NINU\Master\Courses S4\MATLAB\Methanation\Profiles';
67     saveas(gca, fullfile(fname, filename), 'png');
68
69 case 5 % H2O molefraction
70     surf(r*100,z,y(:, :, 5)*100)
71     view(az, el);
72     xlabel('Tube radius, $R$ [cm]', 'interpreter','latex', 'fontsize',12)
73     xticks(0:0.25:RADIUSi*100)
74     xtickformat('%0.2f')
75     ylabel('Reactor length, $L$ [m]', 'interpreter','latex', 'fontsize',12)
76     ylim([0, LENGTH+0.5])
77     yticks(0:1:LENGTH)
78     xlabel('H2O mole fraction, $y_{H_2O}$ [%]', 'interpreter','latex', 'fontsize',12)
79     ztickformat('%0f')
80     filename = 'MoleFractionProfileH2O';
81     fname = 'C:\Users\Sander Wijnsma\OneDrive - NINU\Master\Courses S4\MATLAB\Methanation\Profiles';
82     saveas(gca, fullfile(fname, filename), 'png');
83
84 case 6 % N2 molefraction
85     surf(r*100,z,y(:, :, 6)*100)
86     view(az, el);
87     xlabel('Tube radius, $R$ [cm]', 'interpreter','latex', 'fontsize',12)
88     xticks(0:0.25:RADIUSi*100)
89     xtickformat('%0.2f')
90     ylabel('Reactor length, $L$ [m]', 'interpreter','latex', 'fontsize',12)
91     ylim([0, LENGTH+0.5])
92     yticks(0:1:LENGTH)
93     xlabel('N2 mole fraction, $y_{N_2}$ [%]', 'interpreter','latex', 'fontsize',12)
94     ztickformat('%0.3f')
95     filename = 'MoleFractionProfileN2';
96     fname = 'C:\Users\Sander Wijnsma\OneDrive - NINU\Master\Courses S4\MATLAB\Methanation\Profiles';
97     saveas(gca, fullfile(fname, filename), 'png');
98
99 case 7 % MWg
100     surf(r*100,z,MWg)
101     view(az, el);
102     xlabel('Tube radius, $R$ [cm]', 'interpreter','latex', 'fontsize',12)
103     xticks(0:0.25:RADIUSi*100)
104     xtickformat('%0.2f')
105     ylabel('Reactor length, $L$ [m]', 'interpreter','latex', 'fontsize',12)
106     ylim([0, LENGTH+0.5])
107     yticks(0:1:LENGTH)
```

APPENDIX E. METHANATION MODEL

```
108     xlabel('Molar mass, $MW_g$ [$kg/kmol$]', 'interpreter','latex', 'fontsize',12)
109     zlim([min(MWg(:,1)) 18])
110     ztickformat('%0.1f')
111     filename = 'MWg';
112     fname = 'C:\Users\Sander Wijnsma\OneDrive - NTNU\Master\Courses S4\MATLAB\Methanation\Profiles';
113     saveas(gca, fullfile(fname, filename), 'png');
114
115 case 8 % Component mole fractions
116     figure
117     hold on
118     plot(z, y(:,1,1)*100, ':', 'color','#A2142F', 'LineWidth',2)
119     plot(z, y(:,1,2)*100, ':', 'color','#D95319', 'LineWidth',2)
120     plot(z, y(:,1,3)*100, ':', 'color','#EDB120', 'LineWidth',2)
121     plot(z, y(:,1,4)*100, ':', 'color','#7E2F8E', 'LineWidth',2)
122     plot(z, y(:,1,5)*100, ':', 'color','#77AC30', 'LineWidth',2)
123     plot(z, y(:,1,6)*100, ':', 'color','#0072BD', 'LineWidth',2)
124     lgd = legend('CH_4$ mole fraction, $y_{CH_4}$', 'CO mole fraction, $y_{CO}$', ...
125         'CO_2$ mole fraction, $y_{CO_2}$', 'H_2$ mole fraction, $y_{H_2}$', ...
126         'H_2$O mole fraction, $y_{H_2O}$', 'N_2$ mole fraction, $y_{N_2}$', ...
127         'interpreter','latex', 'location','northoutside', ...
128         'Orientation','horizontal', 'Box','off', 'fontsize',10);
129     lgd.NumColumns = 2;
130     xlabel('Reactor length, $L$ [m]', 'interpreter','latex', 'fontsize',12)
131     ylabel('Mole fraction, $y_i$ ', 'interpreter','latex', 'fontsize', 12)
132     ylim([0 80])
133     filename = 'Molefractions';
134     fname = 'C:\Users\Sander Wijnsma\OneDrive - NTNU\Master\Courses S4\MATLAB\Methanation\Profiles';
135     saveas(gca, fullfile(fname, filename), 'png');
136
137 case 9 % Effectiveness factor (eta)
138     plot(z, eta(:,1), 'LineWidth', 2);
139     xlabel('Reactor length, $z$ [m]', 'interpreter', 'latex', 'fontsize',12)
140     ylabel('Effectiveness factor, $\eta$ [$-]$', 'interpreter', 'latex', 'fontsize',12)
141     ytickformat('%0.2f')
142     filename = 'Effectiveness';
143     fname = 'C:\Users\Sander Wijnsma\OneDrive - NTNU\Master\Courses S4\MATLAB\Methanation\Profiles';
144     saveas(gca, fullfile(fname, filename), 'png');
145
146 case 10 % Reaction rate (Rrxn)
147     surf(r*100,z,Rrxn)
148     view(az, el);
149     xlabel('Tube radius, $R$ [cm]', 'interpreter','latex', 'fontsize',12)
150     xticks(0:0.25:RADIUSi*100)
151     xtickformat('%0.2f')
152     ylabel('Reactor length, $L$ [m]', 'interpreter','latex', 'fontsize',12)
153     ylim([0, LENGTH+0.5])
154     yticks(0:1:LENGTH)
155     xlabel('Reaction rate, $R_{CH_4}$ [$kmol/m^3_{bulk}/s$]', 'interpreter','latex', 'fontsize',12)
156     ztickformat('%0.2f')
157     filename = 'Reactionrate';
158     fname = 'C:\Users\Sander Wijnsma\OneDrive - NTNU\Master\Courses S4\MATLAB\Methanation\Profiles';
159     saveas(gca, fullfile(fname, filename), 'png');
160
161 case 11 % Superficial velocity (uz)
162     surf(r*100,z,uz)
163     view(az, el);
164     xlabel('Tube radius, $R$ [cm]', 'interpreter','latex', 'fontsize',12)
165     xticks(0:0.25:RADIUSi*100)
166     xtickformat('%0.2f')
167     ylabel('Reactor length, $L$ [m]', 'interpreter','latex', 'fontsize',12)
168     ylim([0, LENGTH+0.5])
169     yticks(0:1:LENGTH)
170     xlabel('Superficial velocity, $u_z$ [m/s]', 'interpreter','latex', 'fontsize',12)
171     ztickformat('%0.2f')
172     filename = 'SuperficialVelocity';
```

```

173     fname = 'C:\Users\Sander Wijnsma\OneDrive – NTNU\Master\Courses S4\MATLAB\Methanation\Profiles';
174     saveas(gca, fullfile(fname, filename), 'png');
175
176 case 12 % Temperature (T)
177     surf(r*100,z,T-273.15)
178     view(az, el);
179     xlabel('Tube radius, $R$ [cm]', 'interpreter','latex', 'fontsize',12)
180     xticks(0:0.25:RADIUSi*100)
181     xtickformat('%0.2f')
182     ylabel('Reactor length, $L$ [m]', 'interpreter','latex', 'fontsize',12)
183     ylim([0, LENGTH+0.5])
184     yticks(0:1:LENGTH)
185     zlabel('Temperature, $T$ [$^\circ$C]', 'interpreter','latex', 'fontsize',12)
186     ztickformat('%0.f')
187     filename = 'Temperature';
188     fname = 'C:\Users\Sander Wijnsma\OneDrive – NTNU\Master\Courses S4\MATLAB\Methanation\Profiles';
189     saveas(gca, fullfile(fname, filename), 'png');
190
191 case 13 % Pressure (P)
192     plot(z,p/100000, 'LineWidth', 2);
193     xlabel('Reactor length, $z$ [m]', 'interpreter', 'latex', 'fontsize',12)
194     ylabel('Pressure, $p$ [bar]', 'interpreter', 'latex', 'fontsize',12)
195     ytickformat('%0.2f')
196     filename = 'Pressure';
197     fname = 'C:\Users\Sander Wijnsma\OneDrive – NTNU\Master\Courses S4\MATLAB\Methanation\Profiles';
198     saveas(gca, fullfile(fname, filename), 'png');
199
200 case 14 % Heat flow (Q)
201     plot(z, Q/1000, 'LineWidth', 2);
202     xlabel('Reactor length, $z$ [m]', 'interpreter', 'latex', 'fontsize',12)
203     ylabel('Heat flow, $Q$ [kW]', 'interpreter', 'latex', 'fontsize',12)
204     ytickformat('%0.f')
205     filename = 'Heatflow';
206     fname = 'C:\Users\Sander Wijnsma\OneDrive – NTNU\Master\Courses S4\MATLAB\Methanation\Profiles';
207     saveas(gca, fullfile(fname, filename), 'png');
208
209 case 15 % Mass/Molar/Volumetric flowrate [kmol/h – kg/h – m3/h]
210     figure
211     subplot(3,1,1)
212     plot(z, MassFlow(:,1), ':', 'color','#7E2F8E', 'LineWidth',2)
213     legend('Mass flowrate, $\phi_m$' ,...
214           'interpreter','latex', 'location','northeast', ...
215           'Orientation','horizontal', 'Box','off', 'fontsize',10);
216     ytickformat('%0.1f')
217     ylim([3980 3981])
218     hold on
219     subplot(3,1,2)
220     plot(z, MolarFlow(:,1), ':', 'color','#A2142F', 'LineWidth',2)
221     legend('Molar flowrate, $\phi_M$' ,...
222           'interpreter','latex', 'location','northeast', ...
223           'Orientation','horizontal', 'Box','off', 'fontsize',10);
224     ytickformat('%0.1f')
225     ylim([220 400])
226     hold on
227     subplot(3,1,3)
228     plot(z, VolumetricFlow(:,1), ':', 'color','#0072BD', 'LineWidth',2)
229     legend('Volumetric flowrate, $\phi_v$' ,...
230           'interpreter','latex', 'location','northeast', ...
231           'Orientation','horizontal', 'Box','off', 'fontsize',10);
232     xlabel('Reactor length, $L$ [m]', 'interpreter','latex', 'fontsize',12)
233     ytickformat('%0.1f')
234     ylim([700 1500])
235     filename = 'Flowrates';
236     fname = 'C:\Users\Sander Wijnsma\OneDrive – NTNU\Master\Courses S4\MATLAB\Methanation\Profiles';
237     saveas(gca, fullfile(fname, filename), 'png');

```

```

238
239 case 0 % all plots below
240 figure % molefractions
241 hold on
242 plot(z, y(:,1,1)*100, ':', 'color','#A2142F', 'LineWidth',2)
243 plot(z, y(:,1,2)*100, ':', 'color','#D95319', 'LineWidth',2)
244 plot(z, y(:,1,3)*100, ':', 'color','#EDB120', 'LineWidth',2)
245 plot(z, y(:,1,4)*100, ':', 'color','#7E2F8E', 'LineWidth',2)
246 plot(z, y(:,1,5)*100, ':', 'color','#77AC30', 'LineWidth',2)
247 plot(z, y(:,1,6)*100, ':', 'color','#0072BD', 'LineWidth',2)
248 lgd = legend('~~CH$_4$ mole fraction, $y_{CH_4}$~~~~', '~~CO mole fraction, $y_{CO}$~~~~', ...
249             '~~CO$_2$ mole fraction, $y_{CO_2}$~~~~', '~~H$_2$ mole fraction, $y_{H_2}$~~~~', ...
250             '~~H$_2$O mole fraction, $y_{H_2O}$~~~~', '~~N$_2$ mole fraction, $y_{N_2}$~~~~', ...
251             'interpreter','latex', 'location','northoutside', ...
252             'Orientation','horizontal', 'Box','off', 'fontsize',10);
253 lgd.NumColumns = 2;
254 xlabel('Reactor length, $L$ [m]', 'interpreter','latex', 'fontsize',12)
255 ylabel('Mole fraction, $y_i$ ', 'interpreter', 'latex', 'fontsize', 12)
256 ylim([0 80])
257 filename = 'Molefractions';
258 fname = 'C:\Users\Sander Wijnsma\OneDrive - NINU\Master\Courses S4\MATLAB\Methanation\Profiles';
259 saveas(gca, fullfile(fname, filename), 'png');
260 figure % Effectiveness factor
261 plot(z, eta(:,1), 'LineWidth', 2);
262 xlabel('Reactor length, $z$ [m]', 'interpreter', 'latex', 'fontsize',12)
263 ylabel('Effectiveness factor, $\eta$ [$-]$', 'interpreter', 'latex', 'fontsize',12)
264 ytickformat('%0.2f')
265 filename = 'Effectiveness';
266 fname = 'C:\Users\Sander Wijnsma\OneDrive - NINU\Master\Courses S4\MATLAB\Methanation\Profiles';
267 saveas(gca, fullfile(fname, filename), 'png');
268 figure % Reaction rate
269 surf(r*100,z,Rrxn)
270 view(az, el);
271 xlabel('Tube radius, $R$ [cm]', 'interpreter','latex', 'fontsize',12)
272 xticks(0:0.25:RADIUSi*100)
273 xtickformat('%0.2f')
274 ylabel('Reactor length, $L$ [m]', 'interpreter','latex', 'fontsize',12)
275 ylim([0, LENGTH+0.5])
276 yticks(0:1:LENGTH)
277 zlabel('Reaction rate, $R_{CH_4}$ [$mol/m^3_{bulk}/s$]', 'interpreter','latex', 'fontsize',12)
278 ztickformat('%0.2f')
279 filename = 'Reactionrate';
280 fname = 'C:\Users\Sander Wijnsma\OneDrive - NINU\Master\Courses S4\MATLAB\Methanation\Profiles';
281 saveas(gca, fullfile(fname, filename), 'png');
282 figure % uz
283 surf(r*100,z,uz)
284 view(az, el);
285 xlabel('Tube radius, $R$ [cm]', 'interpreter','latex', 'fontsize',12)
286 xticks(0:0.25:RADIUSi*100)
287 xtickformat('%0.2f')
288 ylabel('Reactor length, $L$ [m]', 'interpreter','latex', 'fontsize',12)
289 ylim([0, LENGTH+0.5])
290 yticks(0:1:LENGTH)
291 zlabel('Superficial velocity, $u_z$ [m/s]', 'interpreter','latex', 'fontsize',12)
292 ztickformat('%0.2f')
293 filename = 'SuperficialVelocity';
294 fname = 'C:\Users\Sander Wijnsma\OneDrive - NINU\Master\Courses S4\MATLAB\Methanation\Profiles';
295 saveas(gca, fullfile(fname, filename), 'png');
296 figure % T
297 surf(r*100,z,T-273.15)
298 view(az, el);
299 xlabel('Tube radius, $R$ [cm]', 'interpreter','latex', 'fontsize',12)
300 xticks(0:0.25:RADIUSi*100)
301 xtickformat('%0.2f')
302 ylabel('Reactor length, $L$ [m]', 'interpreter','latex', 'fontsize',12)

```

```

303     ylim([0, LENGTH+0.5])
304     yticks(0:1:LENGTH)
305     xlabel('Temperature, $T$ [K]', 'interpreter','latex', 'fontsize',12)
306     ztickformat('%0f')
307     filename = 'Temperature';
308     fname = 'C:\Users\Sander Wijnsma\OneDrive - NTNU\Master\Courses S4\MATLAB\Methanation\Profiles';
309     saveas(gca, fullfile(fname, filename), 'png');
310 figure % P
311 plot(z,p/100000, 'LineWidth', 2);
312 xlabel('Reactor length, $z$ [m]', 'interpreter', 'latex', 'fontsize',12)
313 ylabel('Pressure, $p$ [bar]', 'interpreter', 'latex', 'fontsize',12)
314 ytickformat('%0.2f')
315 filename = 'Pressure';
316 fname = 'C:\Users\Sander Wijnsma\OneDrive - NTNU\Master\Courses S4\MATLAB\Methanation\Profiles';
317 saveas(gca, fullfile(fname, filename), 'png');
318 figure % Q
319 plot(z, Q/1000, 'LineWidth', 2);
320 xlabel('Reactor length, $z$ [m]', 'interpreter', 'latex', 'fontsize',12)
321 ylabel('Heat flow, $Q$ [kW]', 'interpreter', 'latex', 'fontsize',12)
322 ytickformat('%0f')
323 filename = 'Heatflow';
324 fname = 'C:\Users\Sander Wijnsma\OneDrive - NTNU\Master\Courses S4\MATLAB\Methanation\Profiles';
325 saveas(gca, fullfile(fname, filename), 'png');
326 figure % flowrates
327 subplot(3,1,1)
328 plot(z, MassFlow(:,1), ':', 'color','#7E2F8E', 'LineWidth',2)
329 legend('Mass flowrate, $\phi_m$', ...
330         'interpreter','latex', 'location','northeast', ...
331         'Orientation','horizontal', 'Box','off', 'fontsize',10);
332 ytickformat('%0.1f')
333 ylim([3980 3981])
334 hold on
335 subplot(3,1,2)
336 plot(z, MolarFlow(:,1), ':', 'color','#A2142F', 'LineWidth',2)
337 legend('Molar flowrate, $\phi_M$', ...
338         'interpreter','latex', 'location','northeast', ...
339         'Orientation','horizontal', 'Box','off', 'fontsize',10);
340 ytickformat('%0.1f')
341 ylim([220 400])
342 hold on
343 subplot(3,1,3)
344 plot(z, VolumetricFlow(:,1), ':', 'color','#0072BD', 'LineWidth',2)
345 legend('Volumetric flowrate, $\phi_v$', ...
346         'interpreter','latex', 'location','northeast', ...
347         'Orientation','horizontal', 'Box','off', 'fontsize',10);
348 xlabel('Reactor length, $L$ [m]', 'interpreter','latex', 'fontsize',12)
349 ytickformat('%0.1f')
350 ylim([700 1500])
351 filename = 'Flowrates';
352 fname = 'C:\Users\Sander Wijnsma\OneDrive - NTNU\Master\Courses S4\MATLAB\Methanation\Profiles';
353 saveas(gca, fullfile(fname, filename), 'png');
354
355 end %switch

```

Finite Difference Method

The finite difference functions, `dss020.m` and `dss042.m`, are implemented to discretise the radial derivatives so that the `ode15s` solver only has the axial coordination to solve for. The `dss020` function discretises the first order derivatives (d/dr) by applying the forward differences scheme while the `dss042` function discretises the second order derivatives (d^2/dr^2) by applying the central

differences scheme.

$$\frac{df(x_i)}{dx} = \frac{f_{i+1} - f_i}{x_{i+1} - x_i} \quad (\text{forward}) \quad \frac{d^2f(x_i)}{dx^2} = \frac{f_{i+1} - 2f_i + f_{i-1}}{(x_{i+1} - x_i)^2} \quad (\text{central}) \quad (\text{E.72})$$

```

1 % dss020.m
2 % ...
3 %... SUBROUTINE DSS020 IS AN APPLICATION OF FOURTH-ORDER DIRECTIONAL
4 %... DIFFERENCING IN THE NUMERICAL METHOD OF LINES.
5 %...
6 %... IT IS INTENDED SPECIFICALLY FOR THE ANALYSIS OF CONVECTIVE SYSTEMS
7 %... MODELLED BY FIRST-ORDER HYPERBOLIC PARTIAL DIFFERENTIAL EQUATIONS,
8 %... BEING:
9 %...
10 %...      U + v*U = 0
11 %...      t      x
12 %...
13 %... POSITIVE v FOR MEDIUM FLOWING IN DIRECTION OF HIGHER x.
14 %...
15 %... BASED ON A SUBROUTINE CALLED DSS020 IN BOOK BY W.E.SCHIESSER CALLED
16 %... THE NUMERICAL METHOD OF LINES AND ALSO FOUND ON INTERNET AT:
17 %... https://www.lehigh.edu/~wes1/apci/28apr00.pdf
18 %...
19 %...
20 %... ARGUMENT LIST
21 %...
22 %... r(1) LEFT VALUE OF THE SPATIAL INDEPENDENT VARIABLE (INPUT)
23 %...
24 %... r(n) RIGHT VALUE OF THE SPATIAL INDEPENDENT VARIABLE (INPUT)
25 %...
26 %... n NUMBER OF SPATIAL GRID POINTS, INCLUDING THE END POINTS (INPUT)
27 %...
28 %... f ONE-DIMENSIONAL ARRAY OF THE DEPENDENT VARIABLE TO BE
29 %... DIFFERENTIATED (INPUT)
30 %...
31 %... fx ONE-DIMENSIONAL ARRAY OF THE FIRST DERIVATIVE OF f (OUTPUT)
32 %...
33 %... v INTEGER INDEX FOR THE TYPE OF BOUNDARY CONDITION, WITH VALUE:
34 %...      1 - FOR A DIRICHLET BOUNDARY CONDITION
35 %...      2 - FOR A NEUMANN BOUNDARY CONDITION
36
37 function fx = dss020(r1, rn, n, f, v)
38
39 %... GRID SPACING
40 dx = (rn-r1)/(n-1);
41 rdx = 1/(12*dx);
42
43 %... (1) FINITE DIFFERENCE APPROXIMATION FOR POSITIVE V
44 if (v > 0)
45     fx(1) = rdx*(-25*f(1) +48*f(2) -36*f(3) +16*f(4) -3*f(5));
46     fx(2) = rdx*(-3*f(1) -10*f(2) +18*f(3) -6*f(4) +1*f(5));
47     fx(3) = rdx*( 1*f(1) -8*f(2) +0*f(3) +8*f(4) -1*f(5));
48     fx(n) = rdx*( 3*f(n-4) -16*f(n-3) +36*f(n-2) -48*f(n-1) +25*f(n));
49     for i=4:(n-1)
50         fx(i) = rdx*( -1*f(i-3) +6*f(i-2) -18*f(i-1) +10*f(i) ...
51             +3*f(i+1));
52     end %for
53
54 %... (2) FINITE DIFFERENCE APPROXIMATION FOR NEGATIVE V
55 else %if
56     fx(1) = rdx*(-25*f(1)+48*f(2)-36*f(3)+16*f(4)- 3*f(5));
57     fx(n) = rdx*( 3*f(n-4) -16*f(n-3) +36*f(n-2) -48*f(n-1) +25*f(n));
58     fx(n-1) = rdx*(-1*f(n-4) + 6*f(n-3) -18*f(n-2) +10*f(n-1) + 3*f(n));
59     fx(n-2) = rdx*( 1*f(n-4) - 8*f(n-3) + 0*f(n-2) + 8*f(n-1) - 1*f(n));

```



```

60         for i=2:(n-3)
61             fx(i) = rdx*(-1*f(i-1) +6*f(i) -18*f(i+1) +10*f(i+2) ...
62                 +3*f(i+3));
63         end %for
64     end %if
65
66 end %function

1 % dss042.m
2 %...
3 %... FUNCTION DSS042 COMPUTES A SECOND-ORDER APPROXIMATION OF A
4 %... SECOND-ORDER DERIVATIVE, WITH OR WITHOUT THE NORMAL DERIVATIVE
5 %... AT THE BOUNDARY.
6 %...
7 %... BASED ON A SUBROUTINE CALLED DSS042 IN BOOK BY W.E.SCHIESSER AND CAN
8 %... ALSO FOUND AT https://www.lehigh.edu/~wes1/apci/28apr00.pdf
9 %...
10 %... ARGUMENT LIST
11 %...
12 %... x(1) LEFT VALUE OF THE SPATIAL INDEPENDENT VARIABLE (INPUT)
13 %...
14 %... x(n) RIGHT VALUE OF THE SPATIAL INDEPENDENT VARIABLE (INPUT)
15 %...
16 %... n NUMBER OF SPATIAL GRID POINTS, INCLUDING THE END POINTS (INPUT)
17 %...
18 %... f ONE-DIMENSIONAL ARRAY OF THE DEPENDENT VARIABLE TO BE
19 %... DIFFERENTIATED (INPUT)
20 %...
21 %... fx ONE-DIMENSIONAL ARRAY OF THE FIRST DERIVATIVE OF f.
22 %... THE END VALUES OF fx, fx(1) AND fx(N), ARE USED IN
23 %... NEUMANN BOUNDARY CONDITIONS AT X = f(1) AND X = f(n),
24 %... DEPENDING ON THE ARGUMENTS NL AND NU
25 %...
26 %... fxx ONE-DIMENSIONAL ARRAY OF THE SECOND DERIVATIVE OF f (OUTPUT)
27 %...
28 %... NL INTEGER INDEX FOR THE TYPE OF BOUNDARY CONDITION AT
29 %... X = XL (INPUT). THE ALLOWABLE VALUES ARE:
30 %...
31 %... 1 - DIRICHLET BOUNDARY CONDITION AT X = f(1)
32 %... (fx(1) IS NOT USED)
33 %...
34 %... 2 - NEUMANN BOUNDARY CONDITION AT X = f(1)
35 %... (fx(1) IS USED)
36 %...
37 %... NU INTEGER INDEX FOR THE TYPE OF BOUNDARY CONDITION AT
38 %... X = f(n) (INPUT). THE ALLOWABLE VALUES ARE
39 %...
40 %... 1 - DIRICHLET BOUNDARY CONDITION AT X = XU
41 %... (UX(N) IS NOT USED)
42 %...
43 %... 2 - NEUMANN BOUNDARY CONDITION AT X = XU
44 %... (UX(N) IS USED)
45
46 function fxx = dss042(x1, xn, n, f, fx, v1, vn)
47
48 %... GRID SPACING
49     dx = (xn-x1)/(n-1);
50
51 %... CALCULATE UXX AT THE LEFT BOUNDARY, WITHOUT UX
52     if v1==1
53         fxx(1) = ( (2.)*f(1) +(-5.)*f(2) +(4.)*f(3) +(-1.)*f(4) ) / (dx^2);
54
55 %... CALCULATE UXX AT THE LEFT BOUNDARY, INCLUDING UX
56     elseif v1==2
57         fxx(1) = ( (-7.)*f(1) +(8.)*f(2) +(-1.)*f(3) ) / (2.*dx^2) ...

```

APPENDIX E. METHANATION MODEL

```
58         +(-6.)*fx(1) / (2.*dx);
59     end %if
60
61 %... CALCULATE UXX AT THE RIGHT BOUNDARY, WITHOUT UX
62     if vn==1
63         fxx(n) = ( (2.)*f(n) +(-5.)*f(n-1) +(4.)*f(n-2) +(-1.)*f(n-3) ) ...
64             /(dx^2);
65
66 %... CALCULATE UXX AT THE RIGHT BOUNDARY, INCLUDING UX
67     elseif vn==2
68         fxx(n)=( (-7.)*f(n) +(8.)*f(n-1) +(-1.)*f(n-2))/(2.*dx^2) ...
69             +(6.)*fx(n) / (2.*dx);
70     end %if
71
72 %... CALCULATE UXX AT THE INTERIOR GRID POINTS
73     fxx(2:n-1) = ( f(3:n) -2*f(2:n-1) +f(1:n-2) ) / dx^2;
74
75 end %function
```

Appendix F

Operating Manual

To operate the final HYSYS model, it is required to install the CAPE-OPEN fluid package. In addition, several tips are given on how to perform case-studies with the HYSYS model to make the convergence faster and solve convergence challenges.

F.1 Open the HYSYS simulation from Hand-in Files

The code to solve the polyimide membrane and multi-tubular methanation reactor is incorporated into the HYSYS model itself and does not need to be opened externally to open the simulation files. However, the HYSYS model consists of a CAPE-OPEN unit operation where the inlet and outlet material streams attached need to have a CAPE-OPEN based fluid. Therefore, a CAPE-OPEN fluid package has been prepared manually consisting of the well-known Peng Robinson thermodynamic properties for both liquid and gas phases and the specific gas components in our model. The CAPE-OPEN fluid package and other files have been attached digitally to thesis in the zipped folder.

First, extract the CAPE-OPEN fluid package files called:

- CapeOpenFluidPackage.ctf
- CapeOpenFluidPackageCC.XML
- CapeOpenFluidPackagePM.XML

and place these files into the HYSYS folder called CTFFiles that can be found in:

- C:\ProgramFiles(x86)\CommonFiles\Hyprotech\COMThermo\CTFFiles

After doing this it is possible to open the HYSYS file, but the CAPE-OPEN unit operation is "unable to load extension server". Now, it is required to install the MATLAB CAPE-OPEN unit operation to this computer (also attached digitally) called:

- MatlabCapeOpenUnitOperation.2.0.0.11.exe

Newer versions or the file itself can be found at <https://www.amsterchem.com/downloads.html>.

After installing the MATLAB CAPE-OPEN unit operation, opening HYSYS prompts to fill in a "Registration code". This registration code can be requested for free and send to email within one working day for academic purposes. Follow link: <https://www.amsterchem.com/matlabunitop.html>.

Once the CAPE-OPEN fluid package and unit operation have been configured it should be possible to run the model. If it does not work, try to reload the fluid package in HYSYS.

F.2 Create CAPE-OPEN Fluid Package in HYSYS

The CAPE-OPEN fluid package can be configured in HYSYS. It is specific for the components present in the *Component list* and needs to be done only once if the same components are used in the simulations. The method is extracted from Ostadi [43].

First, add the wanted components to the *Component list* in the *Properties* window. Then add a COMThermo based fluid package by pressing the arrow next to *add* to find *COMThermo*. In here it is required to select the thermodynamic model that is wanted for the system. In this case, press *Peng-Robinson* for both the *Vapour* and *Liquid* phases with *HYSYSFlash*. Export the created fluid package, give it a name and save it as "COMThermo Property Package (.ctf)" in the following folder:

- C:\ProgramFiles(x86)\CommonFiles\Hyprotech\COMThermo\CTFFiles

Now the CAPE-OPEN fluid package is created and can be used in HYSYS. To do this, go back to the *Fluid Packages* item in the *Properties* window and add a COMThermo fluid package. Here, select *CAPE-OPEN 1.1* as a model selection for both the vapour and liquid phase with *CAPE-OPEN 1.1 Flash*. This should open the *Property Component Manager* tab in which it is possible to find the before created CAPE-OPEN Fluid package. Select it. After the tab is closed, press *Extended PropPkg Setup..* and select *Finish Setup..* as a final step. After these steps it should be possible to use the MATLAB CAPE-OPEN unit operation in HYSYS from the *Model Palette*.

F.3 Operate the CAPE-OPEN Unit Operation

When the CAPE-OPEN unit operation is placed in the *Flowsheet* from the *Model Palette*, it is possible to open its environment by double clicking the unit. In the MATLAB CAPE-OPEN unit operation select *Show Unit GUI* to open the setup tab. In here, it is possible to see the *main.m* MATLAB script and additional functions/scripts, find the model report and linked input/output parameter between the HYSYS simulation and MATLAB code (which can also be adjusted in the *Methanation* spreadsheet in HYSYS). This should be fairly straightforward to operate.

To find more information press *help* in the Unit GUI. Alternatively, the online version of Help On Matlab CAPE-OPEN Unit Operation can be found on <https://www.amsterchem.com/matlabunitophelp.php>.

One tip for the specific model would be to press the *Matlab* tab to find the *main.m* code and remove/add the % symbol before the *run('plotting.m')* line of the script. This makes it possible to (not) get MATLAB figures for the *methanation* unit for a specific case study.

